A PHOTOMETRIC AND SPECTROSCOPIC SURVEY OF AGB STARS IN M31

By

James P. Brewer

B.Sc. (Physics with Astrophysics) University of Leeds, 1988

M.Sc. (Astronomy) University of British Columbia, 1991

A THESIS SUBMITTED IN PARTIAL FULFILLMENT OF

THE REQUIREMENTS FOR THE DEGREE OF

DOCTOR OF PHILOSOPHY

in

THE FACULTY OF GRADUATE STUDIES

DEPARTMENT OF GEOPHYSICS AND ASTRONOMY

We accept this thesis as conforming

to the required standard

THE UNIVERSITY OF BRITISH COLUMBIA

December 1995

In presenting this thesis in partial fulfilment of the requirements for an advanced degree at the University of British Columbia, I agree that the Library shall make it freely available for reference and study. I further agree that permission for extensive copying of this thesis for scholarly purposes may be granted by the head of my department or by his or her representatives. It is understood that copying or publication of this thesis for financial gain shall not be allowed without my written permission.

Department of Geophysics and Astronomy
The University of British Columbia
129-2219 Main Mall
Vancouver, Canada
V6T 1Z4

Date: 29 December 1995.

Abstract

Asymptotic giant-branch (AGB) stars are identified and classified in five $7' \times 7'$ fields spaced along M31's SW semi-major axis using a four band photometric system. An investigation of the AGB luminosity functions and red giant-branch widths reveals significant differences between the star forming histories of the five fields. The distance modulus of M31 is derived using carbon stars (C-stars) and found to be consistent with both a value obtained from Cepheids and with values in the literature.

The ratio of AGB C- to M-stars (C/M ratio) in the five fields is found to increase with galactocentric distance and it is shown that photometric incompleteness is not responsible for this effect. This is the first clear demonstration of a varying C/M ratio in an external galaxy. The C/M ratios appear to be insensitive to star-forming history differences but sensitive to metallicity differences between the fields. Previous observations are used to define a relationship between the C/M ratio and metallicity, and this is used to obtain estimates of the field metallicities. These estimates are found to be consistent with a previous measurement of M31's metallicity gradient. The C/M ratios measured in M31 indicate that the composition of M31's interstellar medium may be position dependent, and evidence is cited in favour of this.

Follow up spectroscopy was obtained in two of the five fields, and is used to show that the photometric system did an excellent job of discriminating between M-, S- and C-stars. Of the 48 C-stars for which spectra were obtained, 7 have strongly enhanced ^{13}C bands (J-stars), 2 have strong Hα emission, while 3 are found to exhibit enhanced Li absorption (Li-stars). Both the J- and Li-stars are fainter than predicted by current theoretical models, while the colours of the Hα stars suggest they may be in the terminal

phases of their evolution. The C_2 and CN bandstrengths of the C-stars are measured, and no correlation between these bandstrengths and either $M_{\rm bol}$ or $(V-I)$ is found. It is suggested that this lack of correlation is due to an age spread. The spectra of the first confirmed S-star in M31 is presented, and two evolutionary pathways are suggested to account for this star's high luminosity.

Table of Contents

List of Tables

List of Figures

Publications

In keeping with the guidelines described in the Faculty of Graduate Studies Publication *"Instructions for the Preparation of Graduate Theses"*, this preface is intended to notify the reader of publications in which work from this thesis appears. The majority of the work pertaining to the photometry (Chapters 2 to 5) was published in Brewer, Richer, & Crabtree 1995, AJ, **109**, 2480–2502. The work on the the spectroscopic observations (mainly Chapters 6 to 9) is not yet published, but is in the process of being submitted to the Astronomical Journal. In addition to these, I have presented work in the form of poster papers at three conferences. The preliminary photometry results were presented at the 24$^{\text{th}}$ CASCA Meeting (Victoria, B.C. May 1993) and the 182$^{\text{nd}}$ AAS Meeting (Berkeley, Ca. June 1993), while the work on diffuse interstellar bands (§5.1) was presented at the 26$^{\text{th}}$ CASCA Meeting (Penticton, B.C. May 1995). In November 1994 I gave a talk at the Dominion Astrophysical Observatory on various facets of the thesis, while finally parts of Chapter 11 first appeared in a review paper I wrote for the 1995 CFHT User's Meeting in Lyon.

Description of Accompanying CD-ROM

Contents

A CD-ROM containing supplemental data accompanies this thesis. The CD-ROM contains:

- `0ReadMe`: A file describing the contents of the CD-ROM, similar to this preface in its contents.
- `Images`: This is a directory containing *I*-band images of the five fields observed in M31. The files are in FITS[1] format, and each file is around 7.8 megabytes. More details on the images can be found on page 10.
- `Spectra`: This is a directory, and contains the sub-directories "Galactic" and "M31". The Galactic sub-directory contains spectra of Galactic C-stars, while the M31 sub-directory contains spectra of stars in M31. Both the Galactic and M31 sub-directories contain the directories "PS", "fits", and "text" which contain the spectra as PostScript[2] files, FITS files, and as wavelength/flux text files respectively.
- `Tables`: This is a directory containing Tables 2.2 (see page 12), 4.1 (see page 48), and 4.2 (see page 48) as LaTeX files ("latex" sub-directory), PostScript files ("PS" sub-directory), and as text files ("text" sub-directory).
- `Thesis.ps`: A PostScript file of this Ph.D. thesis.

Technical Information

This CD-ROM was produced at the Canadian Astronomy Data Centre, using a Phillips 522 CD-ROM recorder. The format of the CD-ROM conforms to ISO 9660.

[1] FITS: Flexible Image Transport System (Wells *et al.* 1981).
[2] A trademark of Adobe Systems Incorporated).

Glossary of Abbreviations

The parlance of astronomers is littered with abbreviations and terminology, and this thesis is no exception. So that the reader may quickly find the meaning of abbreviations used in this work, below I provide a glossary listing them along with their definitions.

Abbreviations and Terminology	
AGB	Asymptotic Giant-Branch
BC	Bolometric Correction
BC_{I_C}	BC to Cousins I magnitude
BF I	Baade's Field 1 (also 2, 3, and 4)
CCD	Charge-Coupled Device
CFHT	Canada-France-Hawai'i Telescope
CMD(s)	Colour-Magnitude Diagram(s)
DAO	Dominion Astrophysical Observatory
DIB(s)	Diffuse Interstellar Band(s)
EAGB	Early AGB
E_{B-V}	Interstellar reddening in $(B-V)$
E_{V-I}	Interstellar reddening in $(V-I)$
FBPS	Four-Band Photometric System
FWHM	Full-Width at Half Maximum
HBCE	Hot Bottom Convective Envelope
IMF	Initial Mass-Function
ISM	Interstellar Medium
LF	Luminosity Function
$M_{\rm bol}$	Bolometric Magnitude
MOS	Multi-Object Spectrometer
PN(e)	Planetary Nebula(e)
PSF	Point-Spread Function
RGB	Red Giant-Branch
$R_{\rm M31}$	Galactocentric distance in M31
$R_{\rm MW}$	Galactocentric distance in the Milky Way
SFR	Star Formation Rate
SNR(s)	Supernova Remnant(s)
SRL	Superrich Li
TCD(s)	Two-Colour Diagram(s)
T_{ce}	T at base of convective envelope
T_{eff}	Effective Temperature
TPAGB	Thermally Pulsing AGB
ZSSK	Zero-Sum Sobel Kernel

Acknowledgements

I owe a great debt of thanks to my parents for nurturing my childhood curiosity and encouraging me to pursue my interests well beyond the realm of the norm. My parents have always had confidence in my abilities, and I hope this thesis shows their belief in me to be well founded.

This thesis owes its existence to the endless encouragement I received from my supervisor and friend, Dr. Harvey Richer. Thanks Harvey! I would also like to thank my collaborator, Dr. Dennis Crabtree, for his assistance and friendship throughout the course of this work.

My friends in Vancouver have helped to make graduate school a smooth and enjoyable journey. Special thanks go to Adrian & Heather, Chris & Donna, Gen & Jim, Jaymie Matthews, John & Sue, Paul Deman, Phil Murphy, Roger & Judy, and Tak Sato.

I would like to extend my appreciation to the third-floor residents (both past and present) of the Geophysics & Astronomy building for their comradeship during my time at UBC. Special mention goes to Dave Bohlender, Greg Burley, Sally Craven, Gordon Drukier, Brad Gibson, Phil Hodder, Dave Hogg, Steve Holland, Rodrigo Ibata, Yiman Jiang, Ted Kennelly, Chris König, Cláudia Mendes de Oliveira, Alex Razoumov, Sandra Scott, Andrew Walker and last (and most definitely least) Dave Woods.

Finally, I would like to thank Helen WP for making it all worthwhile, and for agreeing to marry me.

Chapter 1

INTRODUCTION

"We are all in the gutter, but some of us are looking at the stars"

Oscar Wilde (1854 – 1900)

1.1 Nature of the AGB

The asymptotic giant branch (AGB) is the final luminous phase of stellar evolution for low- and medium-mass stars ($0.8\mathcal{M}_{\odot} \lesssim M \lesssim 10\mathcal{M}_{\odot}$) and, apart from the red giant and horizontal branches, is the only way in which low mass stars can be directly studied in other galaxies. A star's journey up to the luminous excesses of the AGB starts when it exhausts its central reserves of hydrogen and evolves away from the main-sequence and onto the red giant-branch (RGB). During its sojourn on the RGB the star burns hydrogen in a shell around its helium core. This state of affairs lasts until the central helium core, which grows in mass, ignites. The star moves off the RGB and, after exhausting its helium core, starts burning helium in a shell. This phase of a star's life is known as the early AGB (EAGB). When the helium shell is exhausted, a hydrogen shell is reignited. The hydrogen shell increases the mass of the helium shell until the helium shell ignites with a flash. The helium shell burns until exhausted, and then the cycle repeats. This stage of the star's life is known as the thermal-pulsing AGB (TPAGB). It is believed that the AGB is terminated by catastrophic mass-loss in which the expelled envelope becomes a planetary nebula (PN) and the remnant core evolves rapidly to a white dwarf.

Schwarzschild and Härm (1965) showed the double shell source to be thermally unstable, and speculated that the thermal instabilities could lead to the formation of C-stars.

Ten years later Iben (1975), using improved computing power, was able to demonstrate that the thermal instabilities lead to processed material being deposited in the stellar atmosphere, a process known as "third dredge-up". The third dredge-up can alter the surface composition of an AGB M-star (in which oxygen is more abundant than carbon, i.e. C/O < 1), transforming it to either an S-star (in which C/O $\simeq 1$) or a C-star (in which C/O > 1). In this thesis, unless otherwise stated, M, S, and C refer to the spectral types of AGB stars. For more details than those provided by this brief outline, I refer the reader to the review articles by Iben & Renzini (1983, hereafter referred to as IR83) and Iben (1995).

1.2 Interest of the AGB

An understanding of AGB evolution is important in many areas of astronomy. Below I provide a list (not intended to be comprehensive) of areas in which a knowledge of the AGB plays an important role.

- **Spectral Evolution:** Stars on the AGB can make a significant contribution to the integrated light of a galaxy. Renzini (1981) estimated that the AGB is responsible for around 50% of the integrated luminosity of a system which is approximately 2×10^8 years old (although in a system as old as a Galactic globular cluster this contribution will have dropped to around 10%). At cosmological distances only the integrated colour and spectrum of a galaxy are observed, and any interpretation of these observations will require an understanding of the AGB. For example, incorporating AGB evolution into galactic models allowed Lilly (1987) to explain the locus of galaxies in the $(U-V,\ V-H)$ plane.

- **Mass Loss:** A recent review of mass loss from AGB stars is given by Knapp (1991). It appears that AGB stars are losing mass at a rate of 10^{-8} to $10^{-4}\mathcal{M}_{\odot}$ yr^{-1}. Indeed, the high mass-loss rate of C-stars and their low temperatures have caused them to be likened to "smoking candles". Knapp (1991) states that it appears that AGB stars can account for the bulk of material returned to the interstellar medium (ISM) by stellar evolutionary processes. The returned material contributes to the radiative cooling of dense interstellar clouds and will expedite their collapse and subsequent star formation. An AGB star with a high mass-loss rate can avoid becoming a supernova by ejecting its outer envelope before its core mass grows above the Chandrasekhar limit. The fate of a star (PN or supernova) has strong consequences for both the composition and the blast-wave energy input of the ISM.

- **Dynamical Probes:** Aaronson *et al.* (1989) discussed the properties of C-stars which make them useful as probes of Galactic structure. They mention the observational evidence of a narrow C-star luminosity function, the high luminosity of C-stars which allows them to be observed at the edge of the Galaxy through several magnitudes of absorption, and the fact that they are relatively abundant. Also discussed by Aaronson *et al.* (1989) are: the ease with which C-stars can be detected at low Galactic latitudes on objective prism plates; their rich spectra allowing velocity determinations from low signal-to-noise exposures; and their age (1-5 Gyrs) which means they have lost memory of their formation velocities. To take full advantage of these features of C-stars as possible probes of Galactic structure, any dependence (or lack thereof) of the C-star luminosity function on metallicity must be determined. Comprehensive study of C-stars in a nearby spiral galaxy like M31 is a step toward this goal.

1.3 Aims of Thesis

To try and write a thesis that encompassed the many facets of AGB stars and their evolution would be an exercise in futility. I instead have two observational aims, the goals of which I hope will shed light on the bigger picture of AGB evolution and the interaction of AGB stars with their environment. The first observational aim of this thesis is to take a "census" of AGB stars in fields along the SW semi-major axis of M31. The census is used to study the interplay between properties of M31's AGB population, such as C-star luminosity functions and C- to M-star ratios, and differences in local properties, such as metallicity and star-forming history. Having identified the AGB stars, the second observational aim of this thesis is to identify those AGB stars with spectral peculiarities and to try and understand, through comparison with theory, the processes occurring inside these stars. In this thesis I investigate *faint* AGB stars in M31 rather than *bright* Galactic AGB stars. For my study the many advantages offered by observing faint AGB stars in M31 outweigh the disadvantages, a point I now take up in §1.4.

1.4 M31: An Ideal Candidate

An ideal candidate for a study of AGB stars is M31 (which commonly goes under the aliases of both NGC 224 and the Andromeda Galaxy). The relative proximity of M31 allows its AGB population to be easily observed with a four-meter class telescope, while it is sufficiently distant that: (1) a large number of stars can be observed in a single field; and (2) for all intents and purposes, the stars in M31 are at the same distance. Observing M31 also offers the advantages that: (1) by investigating the interplay between the AGB population and the local properties of a single system, the need to take into consideration the effects of galactic morphological type is eliminated; (2) the fields observed have

differing star-forming histories, allowing an investigation of the impact of this on M31's AGB population; (3) an abundance gradient has been previously observed along the major-axis of M31, allowing the effect of this on the AGB populations to be studied; and (4) there is evidence that in M31 the extinction law is correlated with galactocentric distance, and it is of interest to see how such differences correlate with AGB properties. In the conclusions of his Ph.D. thesis *"AGB Populations in Composite Systems"*, Cook (1987) suggests that M31 should be surveyed for AGB stars, citing the last two reasons I give. Indeed, Cook did secure observations of AGB stars along a semi-major axis of M31, but has never published the results (Cook 1993).

So that the reader may become more acquainted with M31, in Table 1.1 I provide a summary of some of its physical properties, while I highly recommend *The Andromeda Galaxy* (Hodge 1992) for a recent in-depth review of this system.

Table 1.1: Basic Properties of M31.[a]

Property	Value
Right Ascension (1950)	$00^h40^m00^s.3$
Declination (1950)	$41°00'03''$
Angular diameter (optical)	$240'$
Apparent magnitude (V)	3.58
Colour ($B-V$) and ($U-B$)	0.91, 0.50
Foreground reddening, E_{B-V}	0.08
Distance modulus, true	24.3
Distance, kpc	725
Absolute magnitude, M_V	–21.0
Diameter, kpc	51
Angle of plane to line of sight	$12^\circ.5$
Position angle of major axis	$37^\circ.7$
Radial velocity (w.r.t. $\odot$), km/sec	–310
Mass (total, $\mathcal{M}_\odot$)	$> 4.1 \times 10^{11}$
Mass (neutral hydrogen, $\mathcal{M}_\odot$)	3.9×10^9

[a]Adapted from Hodge (1992).

Chapter 2

PHOTOMETRIC DATA

"It is a capital mistake to theorize before one has data. Insensibly one begins to twist facts to suit theories, instead of theories to suit facts."

Sir Arthur Conan Doyle (1859 – 1930)

2.1 A Four-Band Photometric System

To further the knowledge of the AGB, groups led by Richer (Richer *et al.* 1984, hereafter referred to as RCP84; Richer & Crabtree 1985, hereafter referred to as RC85; Richer *et al.* 1985; Pritchet *et al.* 1987; Hudon *et al.* 1989; and Richer *et al.* 1990, hereafter referred to as RCP90) and the late Marc Aaronson (Aaronson *et al.* 1984; Cook *et al.* 1986; Cook 1987) developed and refined a technique, similar to one originally suggested by Palmer & Wing (1982), to identify C- and M-stars in crowded fields. The technique involves imaging a field through four filters. Two narrowband filters, the CN and TiO filters, provide low-resolution spectral information on CN and TiO molecular band strengths, while the $(V-I)$ colour provides a temperature discriminator. Richer's CN and TiO narrowband filters have a width of $\Delta\lambda \sim 140$Å and are centred on the CN ($\Delta\nu = +2$, 8100Å) and TiO ($\Delta\nu = -1$, 7800Å) absorption bands respectively.[1] In Fig. 2.1 I have plotted spectra of an A-, C- and an M-star and included on this figure the bandpasses of the narrowband filters. Figure 2.1 shows that: (1) the hot A-star will have a $(CN-TiO)$ colour of around zero; (2) the C-star will have a positive $(CN-TiO)$ colour; and (3) the M-star will have a negative $(CN-TiO)$ colour. Additionally, I note that Figs. 66 and 68 of

[1]Throughout this thesis I adopt a convention whereby CN and TiO refer to molecules, while CN and TiO refer to the filters whose bandpasses lie on the mentioned CN and TiO absorption features.

Turnshek *et al.* (1985, henceforth referred to as TTCB) indicate that S-stars will have $(CN-TiO)$ colours around zero. In Fig. 2.2 I reproduce a plot from Richer *et al.* (1985) which shows photoelectric standards and LMC stars of known spectral type plotted in a $(CN-TiO,\ V-I)$ two-colour diagram (TCD). Figure 2.2 clearly demonstrates the relative insensitivity of the $(CN-TiO)$ colour to hotter spectral types (which lack molecular features), and the bifurcation into C- and M-spectral types at cooler temperatures.

The appeal of the four-band photometric system (henceforth referred to as the FBPS) is that it allows surveys to be made in fields otherwise too crowded for grism or grens methods while, unlike spectroscopy of individual stars, still offering a multiplex advantage. Use of this method has pushed surveys of AGB stars beyond the Milky Way and its dwarf companions; the most distant C-stars currently known, with a true distance modulus of around 27.4, were identified by Hudon *et al.* (1989) in NGC 2403 using Richer's FBPS.

In combination with the FBPS, charge-coupled devices (CCDs), with their high quantum efficiency and linearity, make ideal detectors for surveys of AGB stars in Local-Group galaxies. The small field size of a CCD still enables a significant fraction of a Local-Group galaxy to be observed, while the data obtained from a CCD is easily reduced in a standard manner using custom software.

Using a CCD detector along with a three band version of the FBPS, Green *et al.* (1994) recently conducted a search for faint high-latitude C-stars. I would point out to the reader that in uncrowded fields the FBPS will work with photographic plates and plate scanners, and despite the disadvantages of these over CCDs, the use of photographic plates has the potential to greatly increase sky coverage.

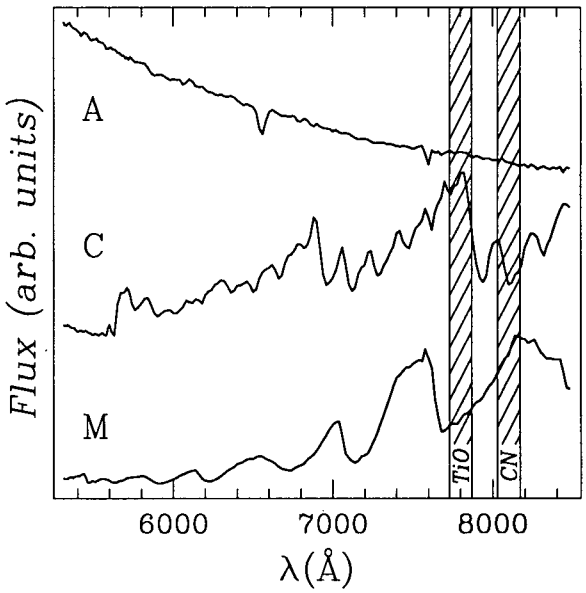

Figure 2.1: The upper spectrum is that of an A-star, the middle spectrum a C-star and the lower spectrum an M giant. Superimposed on these spectra are the bandpasses of the CN and TiO filters. Notice how the TiO filter lies on a TiO absorption band in the M-star, while the CN filter lies on a CN absorption band in the C-star. (Data courtesy of the Canadian Astronomical Data Centre.)

2.2 Observations

The photometric observations were made with the FOCAM camera at the prime focus of the CFHT (3.6-m) by myself and Dennis Crabtree. The detector used was Lick2, a 2048^2 thick CCD coated with a laser dye to improve its blue efficiency. The CCD is cosmetically good and has a quantum efficiency which rises from 30% to 60% between 5000Å and 8000Å. The pixel size on the CCD is 15 μm^2, which gives a plate scale of $0\farcs205$/pixel and a field size of approximately $7' \times 7'$.

The five fields observed were all located along M31's SW semi-major axis. The locations of the fields are easily identified using features marked in Hodge's (1981) *Atlas of the Andromeda Galaxy.* Field 1, the innermost field, is approximately centred on the

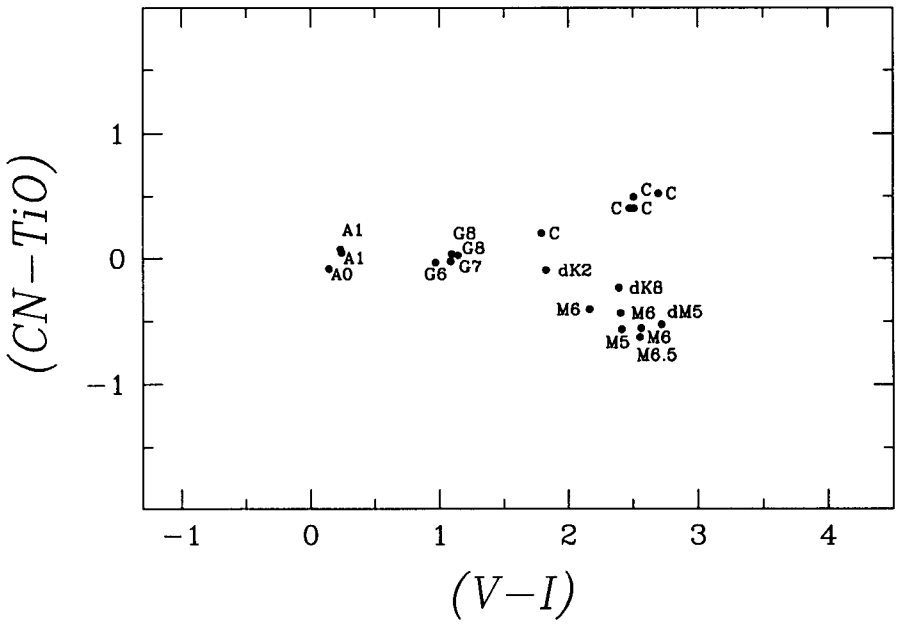

Figure 2.2: A plot of the $(CN-TiO)$ narrowband colour versus $(V-I)$ broadband colour for a sample of photoelectric standards and LMC stars. The data for this plot are taken from Richer *et al.* 1985, and have been calibrated in $(CN-TiO)$ as described in §2.4.

dust cloud D152, while Fields 2, 3 and 4 are roughly centred on the dust cloud D61 and the globular clusters G53 and G31 respectively. No distinctive features are located in Field 5, though the centre of this field has the coordinates $\alpha = 0^{\rm h}33^{\rm m}00^{\rm s}$, $\delta = 39°12\farcm5$ (equinox 1950.0) on Hodge's (1981) Chart 16. Coordinates (equinox 2000.0) for all 5 field centres are given in Table 2.1, while I-band images of each field can be found on the accompanying CD-ROM. The approximate sizes, orientations and locations of the five M31 fields are shown in Fig. 2.3 which is a montage of 2 plates, E–398 and E–851, from the Palomar Sky Survey. Figure 2.3 gives a good indication of both the fraction of M31 that was imaged and the radial extent of the fields.

In Table 2.2 I present a list of stars from the Guide Star Catalog[2], variable stars

[2]The Guide Star Catalog was prepared by the STScI operated by the Association of Universities for Research in Astronomy, Inc., for the National Aeronautics and Space Administration.

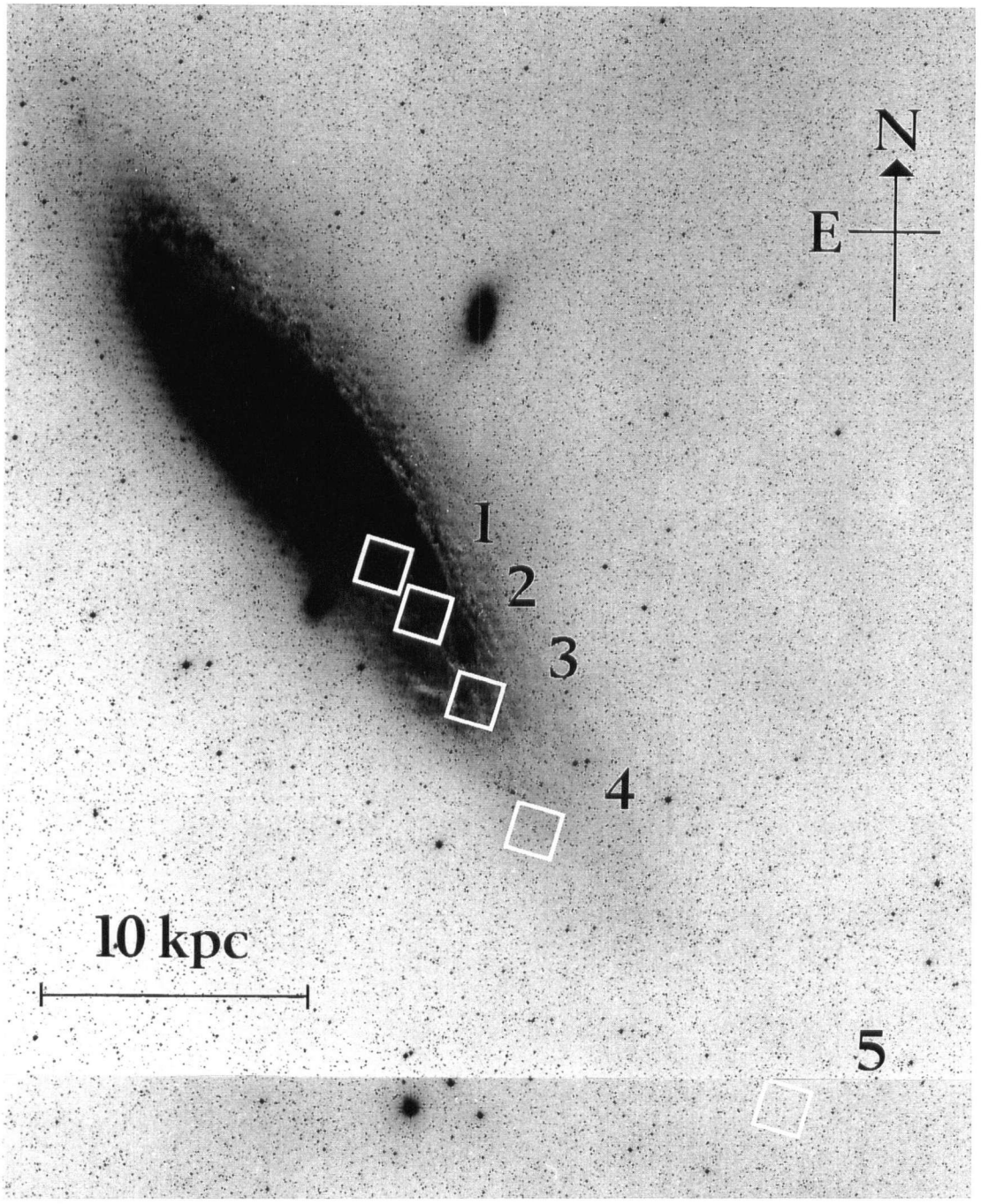

Figure 2.3: A montage of 2 Palomar Sky Survey E–plates showing the positions of the five M31 fields. The fields are approximately contained within the square outlines. The scale bar indicates a length of 10 kpc at a distance of 762 kpc, the assumed distance to M31 (see ahead to §3.3.1).

(Baade & Swope 1965), and clusters in M31 (Hodge 1981) that I re-identified in my fields. The version of Table 2.2 in this thesis is for guidance regarding form and content only, it is presented in its complete form on the CD-ROM which accompanies this thesis. Table 2.2 contains: in column (1) the field in which the star/cluster was identified; in column (2) the X,Y coordinates which can be used to identify the star/cluster using the appropriate I-band image on the accompanying CD-ROM; in column (3) the type of star/cluster; in column (4) a name from the literature; and in column (5) the reference for this name.

The five fields were observed through filters that approximated the Johnson V and Cousins I filters, as well as the CN and TiO filters that were described in §2.1. Individual exposure times were 600 seconds (V) and 300 seconds (I) for the broadband filters, and 1200 seconds for the narrowband filters. Three or more frames were secured in each filter for each field. The seeing conditions throughout the four night CFHT run were superb; the mean seeing, defined as the full-width at half-maximum (FWHM) of the point-spread function (PSF), on the combined frames was $0\farcs76$, and all but the last night were deemed photometric. Table 2.1 is a condensed observing log and contains: in column (1) the coordinates of the field centres; in column (2) the filter ID; in column (3) the combined exposure time; in column (4) the mean seeing on the combined frame; in column (5) the number of stars fitted on the combined frame; and in column (6) the nights on which the fields were observed.

Table 2.1: Observing Log for M31 Program Fields.

α_{2000}, δ_{2000}	Filter	Exp. (s)	FWHM	Fitted[a]	Night[b]
		Field 1			
$\alpha = 0^h41^m41^s$	CN	3×1200	0.″78	59742	1 2[c]
$\delta = 40°59'00''$	TiO	3×1200	0.″78	23909	1[c]
	V	3×600	0.″68	40398	1 4[c]
	I	3×300	0.″66	158952	1 4[c]
		Field 2			
$\alpha = 0^h41^m08^s$	CN	3×1200	0.″82	35626	3[c]4[c]
$\delta = 40°50'41''$	TiO	3×1200	0.″76	36427	3[c]
	V	4×600	0.″82	9841	2[c]4[c]
	I	4×300	0.″74	69809	2[c]3
		Field 3			
$\alpha = 0^h40^m22^s$	CN	3×1200	0.″78	21141	3[c]
$\delta = 40°36'24''$	TiO	3×1200	0.″78	21629	3[c]
	V	5×600	0.″80	21737	2[c]4[c]
	I	4×300	0.″78	44935	2[c]4[c]
		Field 4			
$\alpha = 0^h39^m24^s$	CN	4×1200	0.″82	15794	3[c]
$\delta = 40°14'32''$	TiO	3×1200	0.″76	14830	3[c]
	V	2×600	0.″72	8948	2 4[c]
	I	3×300	0.″80	14043	2[c]
		Field 5			
$\alpha = 0^h35^m42^s$	CN	3×1200	0.″80	1291	4[c]
$\delta = 39°29'03''$	TiO	3×1200	0.″66	925	4[c]
	V	4×600	0.″76	2226	4[c]
	I	4×300	0.″68	950	2[c]

[a]Number of stars fitted by ALLSTAR.
[b]1-4 refer to the nights of 27/09/91 to 30/09/91 respectively.
[c]Frames from these nights combined to make program frames.

Table 2.2: Serendipitous Objects Identified in the Five M31 Fields.[a]

Field	X,Y	Type[a]	Name	Ref.
		Field 1		
1	444, 316	OC:	C204	1
1	648, 408	GC	G117	1
		Field 2		
2	264, 624	OC	C177	1
2	332, 1150	GSC	0738-2057	2
2	1680, 860	GSC	0738-2041	2
2	1108, 508	OC	C162	1
2	1882, 1874	OC	C164	1
		Field 3		
3	655, 820	OC	C107	1
3	694, 1280	OC	C112	1

[a]Table 2.2 is presented in its complete form on the accompanying CD-ROM (see page xiii).

[a]OC: Open cluster; GC: Globular cluster; GSC: Star from HST Guide Star Catalog; Ceph: Cepheid variable; Irreg: Irregular variable; Eclip: Eclipsing variable; Short: Short period variable.

References: (1) Hodge (1981); (2) Guide Star Catalog; (3) Baade & Swope (1965).

2.3 Reductions

Using standard routines in IRAF[3] the raw frames were bias-subtracted and divided by flat fields which were made from images of the sky and the inside of the dome. Vignetting was apparent in the corners of some frames, the level of which was small enough that it could be ignored. Owing to crowding, the combined CN, TiO, V, and I frames for each field were made using only those frames with the best seeing. The frames were averaged together using the IMCOMBINE task in IRAF, with either AVSIGCLIP or CRREJECT used to eliminate cosmic ray[4] events. The total exposure of the combined frames is given in column 3 of Table 2.1, while in column 4 I give the measured FWHM of the stellar images on these frames.

All subsequent photometric measurements on the combined frames were made using the photometry reduction packages DAOPHOT II and ALLSTAR (Stetson *et al.* 1990; Stetson 1992), both of which have been extensively discussed in the literature. After building a PSF from typically 20 to 30 stars on each frame, I used a "double pass" of FIND/PHOT/ALLSTAR to reduce the frames. Briefly, the steps involved in a double pass of FIND/PHOT/ALLSTAR are: (1) search the frame for stars using a finding threshold of 4σ (where σ is the standard deviation of the sky noise); (2) use the frame's PSF along with ALLSTAR to produce a frame on which the stars from step 1 have been fitted and then subtracted out; (3) search the subtracted frame (finding threshold of 4σ) for stars which had been missed in step 1; (4) combine the list of subtracted stars with the list of stars from step 3; and finally (5) rereduce the original frame using ALLSTAR and the

[3]Image Reduction and Analysis Facility (IRAF), a software system distributed by the National Optical Astronomy Observatories (NOAO).

[4]There are both primary and secondary cosmic rays. High-energy primary cosmic rays impinge on the Earth's atmosphere and produce showers of secondary cosmic rays, and it is these which are detected by a CCD.

combined list of stars. Because of the CCD frame size (2048^2) and the large number of stars found on some frames, I had to increase the dimensions of certain arrays in DAOPHOT II and ALLSTAR. The number of stars fitted on each of the 20 combined frames is given in column 5 of Table 2.1. To match the stars between the CN, TiO, V, and I frames of each field I used the program DAOMASTER (Stetson 1993), saving only those stars that were found on at least two of the four frames.

2.4 Calibration

Standards were secured through V and I filters on nights 1 and 2 of the run and I summarize these observations in Table 2.3, listing: in column (1) the name of the standard field; in column (2) the airmass(es) at which the field was observed; and in column (3) a reference. The NGC 2419 and NGC 7006 frames were reduced with a double pass of FIND/PHOT/ALLSTAR (see §2.3), and I produced a frame containing only photometric standards. The aperture magnitudes of the standards were measured using DAOGROW (Stetson 1990), and were corrected for exposure time. Extinction coefficients for V (which is commonly referred to as Q_y) and $(V-I)$ (which is commonly referred to as k_9) were derived from observations of NGC 7006 at various airmasses and found to be $Q_y = 0.40 \pm 0.05$ mag/airmass and $k_9 = 0.17 \pm 0.06$ mag/airmass. Krisciunas (1994) states that the mean value of Q_y at the Mauna Kea summit is 0.125 mag/airmass, though also mentions that volcanic dust can cause extinction coefficients to vary by over a factor of 3 in the optical. I believe that my higher-than-normal values can be attributed to the eruption of Mount Pinatubo in the Philippines which occurred three months prior to my observations. Having calculated the extinction coefficients, I proceeded to correct the aperture magnitudes for atmospheric extinction.

The transformation equations between aperture magnitudes and standard magnitudes

had colour terms consistent with zero, indicating that both the V and I filters were good approximations to the standard Johnson-Cousins filters. The zero points on nights 1 and 2 were, within their errors, the same. The data for both nights were combined and new zero points determined. Secondary standards were chosen on single program frames from nights 1 and 2 and had their aperture magnitudes measured with DAOGROW in the same manner as the standards. As with the crowded standard frames, the secondary standard frames were processed in such a way that only the standards were left in the frame. After correction for exposure and airmass, the standard magnitudes of the secondary standards were determined and the offset between PSF and standard magnitudes applied to the PSF magnitudes of all the stars on the frame in question. I was unable to calibrate the Field 5 V frame as this was only observed on night 4 of the run (see column 6 of Table 2.1 and Table 2.3). In lieu of calibration, I used the (I, $V-I$) CMDs to choose an offset (by eye) for the Field 5 V magnitude such that the colour of its AGB/RGB branch coincided with the AGB/RGB branches of the other fields. This *ad hoc* calibration must be considered insecure.

No photometric standards were observed with the CN or TiO filters, instead I added an offset to the instrumental $(CN-TiO)$ colours such that the mean colour of stars bluer than $(V-I) = 1$ was zero. My reasoning here is that hot stars are expected to have featureless spectra in the CN and TiO filter bandpasses (see Fig. 2.1), and consequently to have $(CN-TiO)$ colours of around zero. On account of the paucity of hot stars in Fields 1, 4 and 5, the mean $(CN-TiO)$ value of stars bluer than $(V-I) = 1$ is poorly defined, and subsequently the $(CN-TiO)$ "calibration" of these fields is less certain.

Table 2.3: Observing Log of Standard Fields Used for Calibration of Photometric Data.

Field	Airmass	Ref.
Night 1 (27/09/91)		
SA110 364, 365	1.45	1
NGC 7006	1.03, 1.40	2
NGC 2419	1.30	2
Night 2 (28/09/91)		
SA111-1969	1.07	1
SA110	1.08	1
NGC 7006	1.03, 1.05, 1.35	2
NGC 2419	1.27	2
GD71	1.01	1

References: (1) Landolt 1992; (2) Davis 1994.

Chapter 3

COLOUR-MAGNITUDE DIAGRAMS

"After a year's research, one realises that it could have been done in a week."

Sir William H. Bragg (1862 – 1942)

3.1 General Features

In Fig. 3.1 I present calibrated (I, $V-I$) CMDs for the five fields observed in M31. The number of stars in each plot, those matched between the V and I frames and with average (ALLSTAR) χ^2 values (returned by DAOMASTER) less than 4, is indicated in each panel. The bottom right panel of Fig. 3.1 shows the expected position of some features in the M31 CMDs. These features were placed using reddening and absorption values appropriate for Fields 1 to 4 (see ahead to §3.2) and a true distance modulus of $(m-M)_0 = 24.41$ (see ahead to §3.3.1). The features shown are: (1) fiducial sequences of a metal-poor (M15) and a metal-rich (47 Tuc) globular cluster (DaCosta & Armandroff 1990); (2) the Cepheid instability strip (RCP84, Kraft 1963); (3) supergiants with spectral types M0Ib, M2Ib, M3Ib and M4Ib (RCP84, Lee 1970); and (4) giants with spectral types M0II, M2II, M3II and M4II (RCP84, Lee 1970). I have plotted the globular cluster fiducials to give an idea of the luminosity of the RGB tip, while the Cepheid instability strip shows that I can expect many Cepheids in the fields, especially in Field 3.

The most striking feature of Fig. 3.1 is the strong blue component seen in Field 3. This comes as no surprise as this field lies in a spiral arm and is currently undergoing star formation, as evidenced by the presence of (relatively young) Cepheids. Field 2 also has a blue component, though at a somewhat reduced level. These features are further

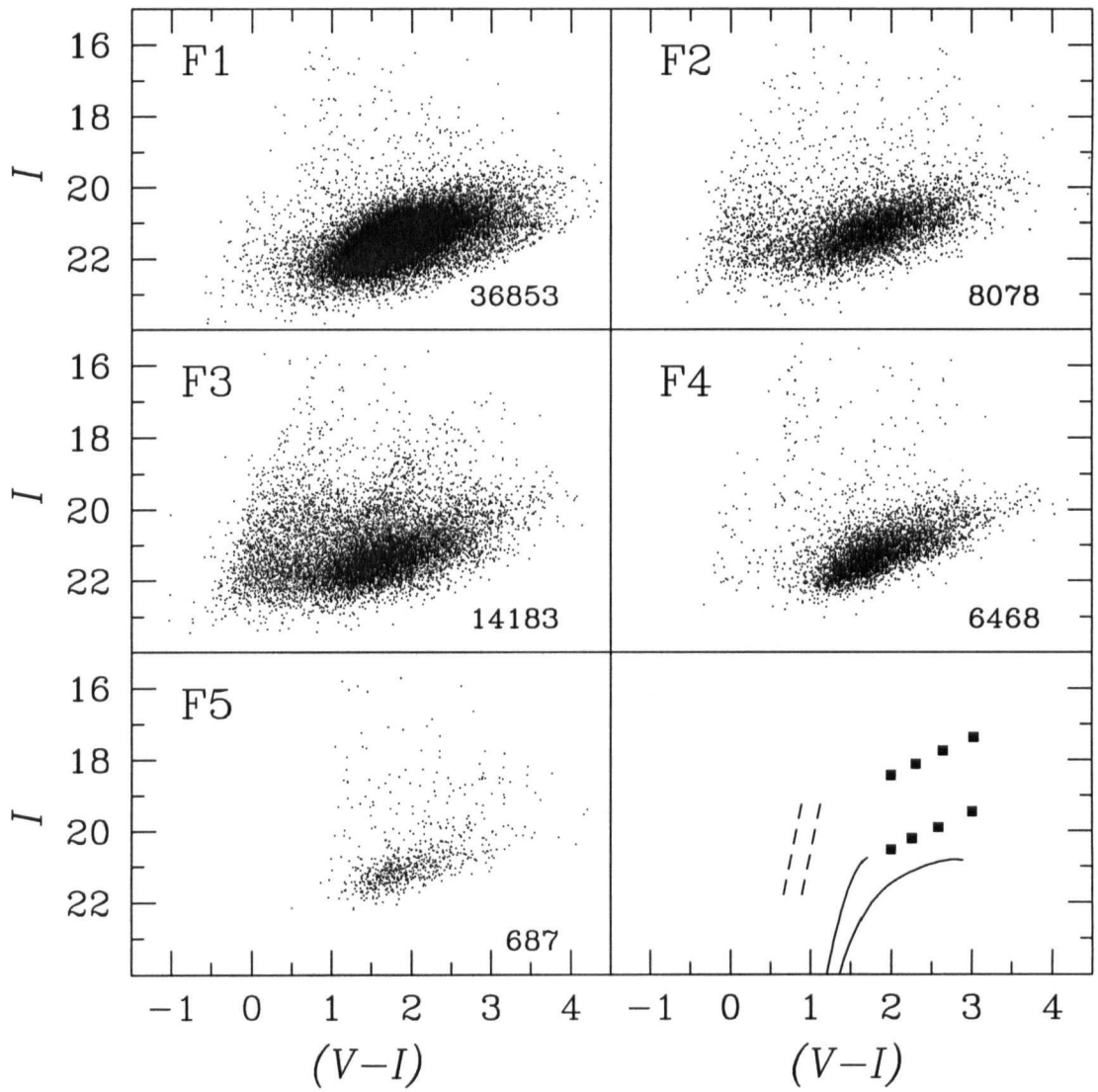

Figure 3.1: The (I, $V-I$) CMDs for the five M31 fields. The data are calibrated, although no reddening corrections have been applied. In the lower right panel parallel dashed lines show the region occupied by Galactic Cepheids, while the redder solid line is the 47 Tuc fiducial and the bluer solid line the M15 fiducial. The upper sequence of points shows the positions of supergiants with spectral types M0Ib, M2Ib, M3Ib and M4Ib, while the lower sequence of points shows the positions of giants with spectral types M0II, M2II, M3II and M4II. These features have been located in the CMD as described in §3.1.

discussed in §4.5.5 where I compare a census of AGB stars with star-forming histories.

3.2 Reddening

Knowledge of the reddening is important as it affects many of the measurements made in this thesis. For example, in Chapter 4 I count stars redder than a certain colour which leads to the counts being dependent on the adopted value of reddening. The reddening (or more precisely the absorption associated with it) also affects the mean magnitudes of luminosity functions (LFs), and consequently affects distance estimates and comparisons between the LFs in different fields.

The stars I observed in M31 suffer from both internal and foreground reddening. The scale on Fig. 2.3 shows the physical size of my M31 fields to be ~1.6kpc×1.6kpc (with no correction for the inclination of M31's axis). Within such large fields, the internal reddening will vary because of irregularities in the dust distribution. For example, an inspection of the Field 3 location in Hodge (1981) clearly shows dust lanes superimposed on the background. A field with a uniform dust distribution may also have variable reddening on account of the relative positions of the stars and dust along our line of sight. In conclusion, I can legitimately adopt no single reddening value for any of my fields, and the values I do use should be considered as mean values.

My data affords me only crude estimates of the reddening, and so I turn to previous studies as a guide. Hodge & Lee (1988) used UBV photometry to investigate reddening as a function of galactocentric distance in the plane of M31 (henceforth, referred to as $R_{\rm M31}$). An inspection of their Fig. 17 suggests that the reddening in Fields 1, 2, and 4 (located at $R_{\rm M31}$= 4.6, 7.2, and 16.8 kpc) is around $E_{B-V} \sim 0.23$, while the reddening in Field 3 (located at $R_{\rm M31}$= 10.8 kpc) is higher ($E_{B-V} \sim 0.4$) and in Field 5 (located at $R_{\rm M31}$= 31.5 kpc) lower ($E_{B-V} \sim 0.1$). I believe that the high reddening value in Field

3 indicated by Hodge & Lee's (1988) data might be inappropriate. The evidence I cite in favour of this is: (1) As shown in Fig. 3.1, the blue edges of the CMDs of Fields 2 and 3 both lie at similar colours, indicating that these fields have similar reddening values. (2) In their study of the star cluster C107 (Hodge 1979), which lies in Field 3, Bohlin *et al.* (1988) estimated the reddening of the cluster as $E_{B-V} = 0.20$. (3) A $BVRI$ investigation of Cepheids by Freedman & Madore (1990, hereafter referred to as FM90) indicated that the visual absorption in Baade's Field I (henceforth referred to as BF I, and likewise for Baade's other M31 fields), in which Field 1 mostly lies, and BF III, in which Field 3 entirely lies, was 0.60 and 0.75 respectively. Adopting a value of 3.1 for the ratio of A_V/E_{B-V} (Savage & Mathis 1979) leads to reddening values of $E_{B-V} = 0.19$ and $E_{B-V} = 0.24$, suggesting that the reddening in Field 3 is similar to that in Field 1. (4) In §3.3 I show good agreement between the position of the Cepheids and the instability strip in the (I, $V-I$) CMD when a lower value of the reddening is adopted. Taking the above into consideration, I adopt a reddening of $E_{B-V} = 0.23$ for Fields 1, 2, 3, and 4. Beyond 10 kpc, Fig. 17 of Hodge & Lee (1988) shows that the reddening drops, the last point on their Fig. 17 indicates a reddening of $E_{B-V} = 0.13$ at a distance of approximately 20 kpc. The minimum reddening that Field 5 can possibly have is the foreground reddening of $E_{B-V} = 0.08$ (Burstein & Heiles 1984) and, as a compromise between the minimum reddening value and the reddening value at 20 kpc, I adopt a reddening value of $E_{B-V} = 0.10$ in Field 5.

I obtain E_{V-I} from E_{B-V} using the relationship, $E_{V-I} = 1.25E_{B-V}$, given by Bessell & Brett (1988). The absorption in V is derived by adopting a value of 3.1 for the ratio of A_V/E_{B-V} (Savage & Mathis 1979), and the absorption in I (Cousins) is obtained from $A_I = 0.6A_V$ (Cohen *et al.* 1981).

Reddening is unimportant for the $(CN-TiO)$ colour for two reasons: (1) because

of the small (300Å) separation between the central wavelengths of the CN and TiO filters, low levels of reddening have little effect on the $(CN-TiO)$ colour; and (2) the "calibration" of $(CN-TiO)$ (see §2.4) corrects for any reddening.

3.3 Cepheid Distance Modulus

Three of the M31 fields have regions in common with fields observed by Baade in which variable stars were identified. Variable stars in BF II were identified by Baade (unpublished by Baade, though see Gaposchkin 1962), while variable stars in BF I and BF III were identified by Baade & Swope (1965). Field 1 is mostly contained in BF I, while Fields 2 and 3 lie within BF II and BF III respectively. The outer two fields do not coincide with any of Baade's fields. An inspection of the $(I,\ V-I)$ CMDs in Fig. 3.1 shows that Field 4 may contain a handful of Cepheids, while Field 5 probably contains no Cepheids.

By locating the position of Field 1 on Plate I of Baade & Swope (1965) I found that Field 1 contains ten variable stars, five of which are Cepheids. Of these five Cepheids, Baade & Swope's identification of three was uncertain. I located the position of Field 2 in Fig. 1 of Gaposchkin (1962) and counted 38 variable stars within its bounds, 15 of which had been identified as Cepheids. In the case of both Fields 1 and 2, I was unable to re-identify the *individual* stars in my fields due to insufficient detail on the plate/figure.

In Field 3 I re-identified the individual variable stars using the more detailed finding charts (Plates IV and V) given by Baade & Swope (1965). Of the 80 variable stars I was able to re-identify, 60 were Cepheids. These 80 variable stars can be located using the Field 3 image along with the frame coordinates given in Table 2.2, both of which are included on the accompanying CD-ROM. Using my calibrated photometry, I plot in Fig. 3.2 an $(I,\ V-I)$ CMD of the re-identified Field 3 Cepheids, along with the features

described in §3.1. One can see that, with the occasional exception, the Cepheids lie where expected. The scatter in $(V-I)$ of the Cepheids may, in part, be due to differential reddening and misidentifications.

To obtain a Cepheid distance modulus I first exclude those Cepheids which, from their position in Fig. 3.2, I believe to be mis-identified. I have circled these stars in Fig. 3.2. Using the Cousins I-band Cepheid period-luminosity (P-L) relationship given by Madore & Freedman (1991, hereafter referred to as MF91),

$$M_I = -3.06(\pm 0.07)(\log P - 1.00) - 4.87(\pm 0.03)\ [\pm 0.18], \tag{3.1}$$

along with the periods from Baade & Swope (1965) and my I-band photometry, I calculated a true distance modulus of 24.42 ± 0.05 for the Cepheids in Field 3. The P-L data for the Cepheids, along with the fit, are shown in Fig. 3.3. The fit was achieved by rejecting those stars, shown as open squares, which deviated from the initial fit by more than 3σ. The I magnitudes shown have been corrected for 0.43 magnitudes of absorption in I (see §3.2).

3.3.1 Adopted Distance Modulus

The value I derive for the true distance modulus of M31 (24.42 ± 0.05) from Cepheids in Field 3 is in *superb* agreement with the value of 24.41 ± 0.09 derived (from Cepheids) by FM90 in BF III. The value I adopt for true distance modulus in this thesis is the established value from FM90 in preference to my own. I point out to the reader that the findings in this thesis are insensitive to the small difference between these distant moduli.

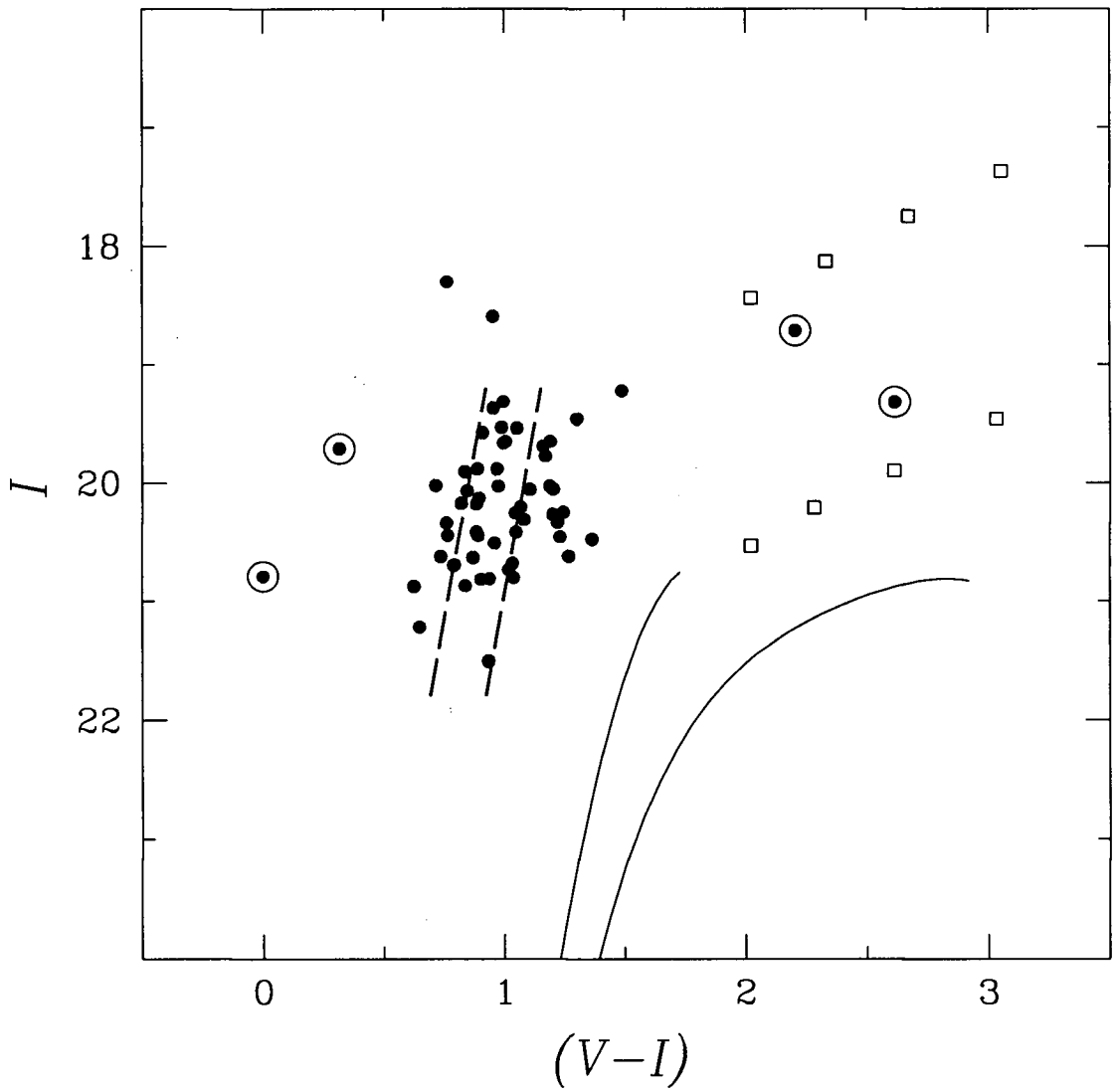

Figure 3.2: An (I, $V-I$) CMD of the Cepheids from Baade & Swope (1965) that I re-identified in Field 3. Included on the CMD are the features previously described in the Fig. 3.1 caption and in §3.1. Of special note is the expected position of the Cepheid instability strip, shown by parallel dashed lines. The circled points are Cepheids which I considered to lie outside the instability region, these are likely to be misidentifications.

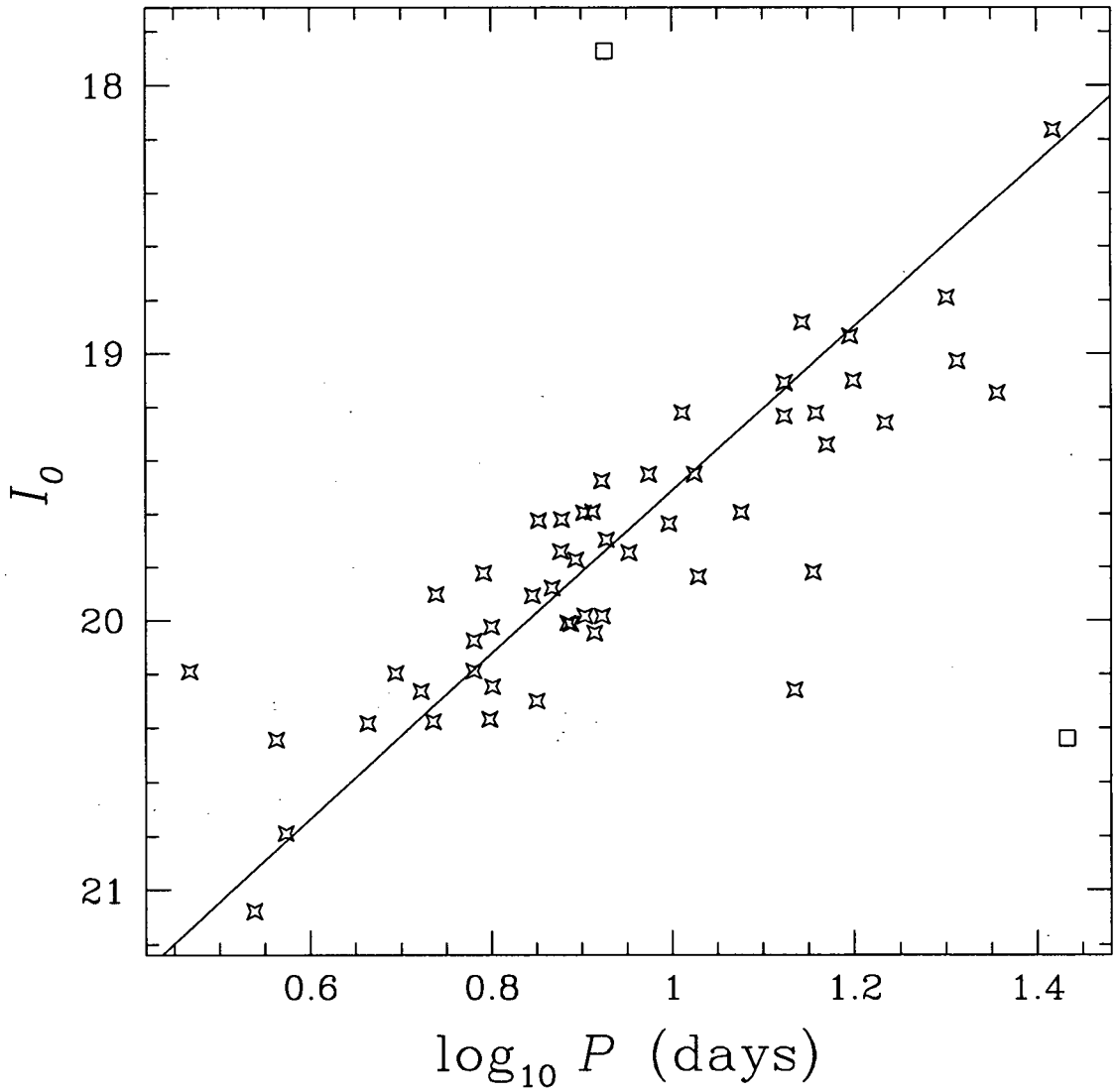

Figure 3.3: An unphased P-L diagram for Cepheids in Field 3. The periods are from Baade & Swope (1965), while the I magnitudes, corrected for absorption, are from this study. The solid line is a fit of MF91's P-L relationship given in eq. (3.1). The circled points from Fig. 3.2 are excluded from this plot, while open squares indicate those stars which deviated from the initial fit by more than 3σ. The errors in the I magnitudes returned by ALLSTAR were approximately 0.02 for the brighter Cepheids and 0.04 for the fainter Cepheids.

3.4 Red Giant-Branch Widths

The observed $(V-I)$ width of the RGBs in Fig. 3.1 is a combination of four factors. Two of the factors, age and abundance spread of the stars in the field, are "intrinsic" properties of the stellar population. The other two factors, differential reddening and photometric error, are "extrinsic" to the stars. If I correct the observed RGB width for contributions from the extrinsic parameters, I can use the intrinsic RGB width to investigate (albeit in a crude manner) the age and abundance spread of the field's stellar population.

In the $(I,\ V-I)$ CMDs of Fig. 3.1 the RGB blends in with the AGB. To disentangle the RGB from the AGB I take advantage of the longer evolutionary timescale of RGB stars which causes them to "pile-up". This causes an "edge" in the CMD at the RGB-AGB transition magnitude which, following Lee *et al.* (1993), I find by use of the Zero-Sum Sobel Kernel (ZSSK) edge detection algorithm. I provide no details of the ZSSK here, but instead refer the interested reader to Lee *et al.* (1993). After rejecting stars which were clearly RGB or AGB outliers, I employed the ZSSK to determine the I magnitude of the RGB tip in the five fields. The robustness of the ZSSK on the data was tested by using the ZSSK with bin widths of 0.20, 0.10 and 0.05 magnitudes, and the results of these tests are summarized in Table 3.1. In Table 3.1 column 1 gives the field number, while columns 2, 3 and 4 are the measured RGB tip magnitudes (maximum value of the convolution of the field's stellar I-magnitude histogram with the ZSSK) for bin widths of 0.20, 0.10 and 0.05 magnitudes respectively, and column 5 is the average of these values. The resolution of the technique is determined by the bin width, though the technique will fail if the bins are so narrow that small number statistics dominate. Assuming the bin width to be an error estimator, I see from Table 3.1 that in Fields 1 and

Table 3.1: The *I* Magnitudes of the RGB Tips as Determined by the ZSSK.

Field	——Bin Width——			Avg.
	0.20	0.10	0.05	
1	20.7	20.65	20.725	20.69
2	20.7	20.75	20.725	20.73
3	20.7	20.95	21.175	20.94
4	20.7	20.75	20.975	20.81
5	20.9	20.95	21.225	21.03

2 consistent values are obtained. The measured RGB tip magnitudes for Fields 3, 4, and 5 disagree between the 0.10 and 0.05 bins. When I use the 0.05 bins I find that in Field 5 there are 30 stars in the bins close to the maximum value of the convolution and for Field 4 this number increases to 200. With as few as 30 stars in the bins, small number statistics will play a role in determining the RGB tip, especially if the edge is ill-defined, as would be caused by an age or abundance spread in the RGB stars. As the exact value adopted for the RGB tip has little effect on my measured RGB width, I simply adopt the average values given in column 5 of Table 3.1. I note that Lee *et al.* (1993) employ the tip of the RGB as a distance indicator, but warn that the calibration they use is valid only in the metallicity range $-2.2 < [\mathrm{Fe/H}] < -0.7$ and is unlikely to be applicable to a metal-rich population such as that found in M31's disk. Having the RGB tips, I note that the data in Fig. 3.1 is insufficiently deep to reach the main-sequence turn-off. This being the case, I define the RGBs as reaching from the magnitude limit of the data to the RGB tip. Knowing the location of the RGBs, I now consider the factors that contribute to their widths.

An idea of one of the extrinsic factors which influences the width of the observed RGB, differential reddening, can be arrived at by examining Hodge's (1981) *Atlas of the*

Andromeda Galaxy. In Fields 4 and 5 there is no evidence of differential reddening: the background shows no patchiness and no dust clouds are apparent. In contrast, Fields 1, 2 and 3 appear patchy and have dust clouds outlined. I proceed by assuming that, unlike the inner three fields, Fields 4 and 5 have negligible differential reddening. Without knowledge of the level of differential reddening in the inner three fields, any attempt to interpret the RGB width in terms of the intrinsic parameters will be limited.

The contribution to the RGB widths from the other extrinsic parameter, photometric error, was measured using Monte Carlo simulations. I defined a "dispersionless" RGB by rejecting stars (by eye) on the (I, $V-I$) CMDs which were RGB or AGB outliers, and then making a least-squares fit to the remaining RGB and AGB stars. Artificial stars were generated along the "dispersionless RGB" (the least-squares fit), and these were "broken down" into unique V and I magnitudes. The artificial stars were assigned random frame coordinates and added into the V and I frames using Stetson's (1987) ADDSTAR program. The ADDSTAR frames were reduced with a double pass of FIND/PHOT/ALLSTAR (see §2.3), and the resulting V and I ALLSTAR files matched with the V and I ADDSTAR files using DAOMASTER, imposing the condition that a star had to be found in all four of these files to count as a recovery. The recovered RGB width indicates the contribution of photometric errors to the observed RGB width. I point out to the reader that a similar method is often used to obtain photometric error estimates which can be compared to the analytical errors returned by ALLSTAR (e.g. Stetson & Harris 1988).

Results from the Field 4 RGB ADDSTAR tests are shown in Fig. 3.4. The leftmost panel in Fig. 3.4 shows the dispersionless relationship along which the stars were added, while the middle panel shows the added stars that were recovered and matched on both the V and I frames. The rightmost panel of Fig. 3.4 shows the real RGB, as recovered from the frame on which the ADDSTAR tests were conducted. A measure of the standard deviation

Table 3.2: Observed, 'Photometric' and Intrinsic $(V-I)$ Widths of RGBs.

Field	R_{M31}	σ_{obs}	σ_{phot}	σ_{int}	FWHM$_{int}$
1	4.6 kpc	0.35	0.28	0.21	0.49
2	7.2 kpc	0.36	0.25	0.26	0.61
3	10.8 kpc	0.47	0.22	0.42	0.99
4	16.8 kpc	0.25	0.15	0.20	0.47
5	31.5 kpc	0.24	0.11	0.21	0.49

(σ) of the colour distribution of the RGB stars is given above each panel. To measure σ, I first dropped from consideration any stars brighter than the measured RGB tips (as given in column 5, Table 3.1) or fainter than an I magnitude of 22.0 (the approximate I magnitude limit of the data). Those stars satisfying these magnitude criteria were split into ten bins in I magnitude (binning in magnitude is necessary as the mean colour changes with magnitude) and the mean and σ of the $(V-I)$ colour distribution were calculated for each bin. Outliers and non-AGB stars were rejected by excluding stars which lay more than 2σ from the mean colour, and then σ was recalculated. To ensure that this rejection scheme was reasonable, the colour bounds (2σ, all stars) for each bin were plotted for all the fields. These are shown in Fig. 3.4 for the Field 4 data, where it can be seen that only outliers are being rejected. The σ values shown above each panel in Fig. 3.4 are the average of the σ measured in the ten magnitude bins. Measurements of the observed and photometric σ measured in the five fields using the above techniques are given in columns 3 and 4 of Table 3.2. It is of interest to note that the value of σ_{phot} (Column 4, Table 3.2) decreases with increasing R_{M31}. This result comes as no surprise, as larger photometric errors are expected in the more crowded inner fields.

If I assume that the observed RGB $(V-I)$ distribution is a convolution of the intrinsic RGB distribution (which would be caused by metallicity and age spreads) and the

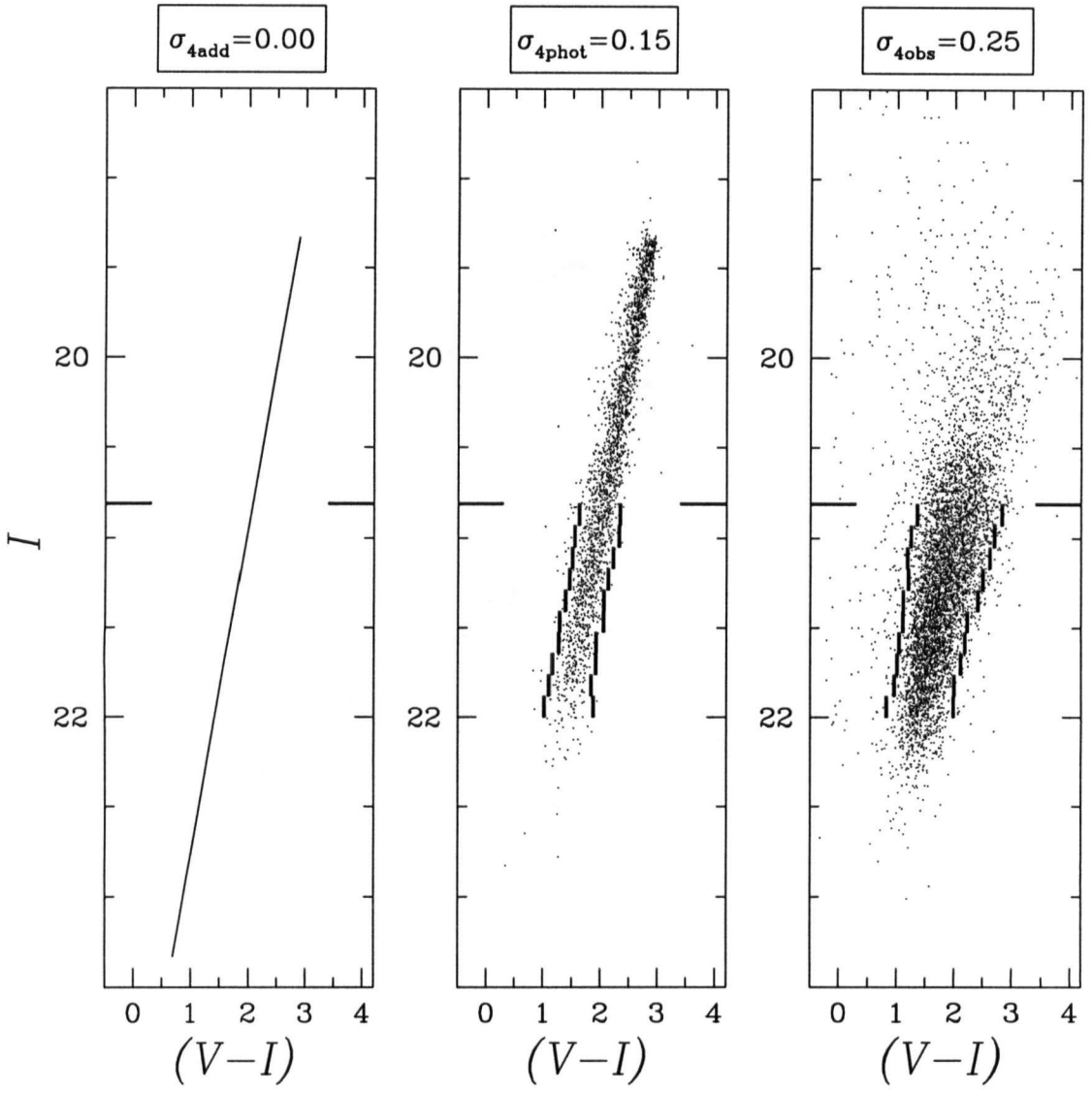

Figure 3.4: The leftmost panel shows the dispersionless RGB along which the artificial stars added to the Field 4 V and I frames lay. The middle panel shows the artificial stars which were recovered from the V and I frames and successfully matched, while the rightmost panel shows real stars which were recovered from the same V and I frames and successfully matched. The stars contained between the thick vertical lines in the right two panels are the stars from which σ was measured, while the thick horizontal lines indicate the RGB tip as given in Table 3.1.

distribution arising from photometric errors, I can calculate σ for the intrinsic distribution using $\sigma^2_{obs} = \sigma^2_{int} + \sigma^2_{phot}$. This is obviously invalid for Fields 1, 2 and 3 where the contribution from differential reddening needs to be considered. I include in Table 3.2 the calculated σ of the intrinsic RGB distribution (column 5) as well as the FWHM that corresponds to this σ if a gaussian distribution is assumed (column 6).

In calculating the intrinsic FWHM values the effect of differential reddening in the inner-three fields was ignored. The level of differential reddening needed to account for the observed RGB widths is large. For example, in Field 3 I measure the intrinsic FWHM of stars on the RGB as $\sim$ 1 magnitude in $(V-I)$, while the reddening, in $(V-I)$, is approximately 0.3 (§3.2). This suggests that differential reddening is only a small factor contributing to the RGB widths seen in these fields. As I have no way of dealing with the effects of differential reddening I (cautiously) drop it from consideration and interpret the intrinsic RGB widths in terms of metallicity and mass variations of RGB stars in my fields, noting that any estimated variations will be upper limits.

What is the metallicity dispersion in the fields? I note that the metal-poor spheroidal component in M31 dominates the light (in B) for distances less than 4 kpc along the major axis (de Vaucouleurs 1958) meaning that it only makes a significant contribution in Field 1. The other fields are dominated by the disk, and for these fields I adopt a dispersion of 0.165 dex. This is the value for the metallicity dispersion in the solar neighbourhood, based on observations of 38 clusters in the solar vicinity by Cameron (1987). To see what effect metallicity dispersion has on the RGB width I plot Z = 0.05, 0.02, and 0.008 isochrones from Bertelli *et al.* (1994) for ages between 1 and 5 Gyr. In Fig. 3.5a I show these three isochrones for an age of $\sim$5 Gyr. The range in Z is equivalent to a range of 0.8 dex in metallicity, and I find that, regardless of age, the $(V-I)$ colour difference between the Z = 0.05 and the Z = 0.008 isochrones is approximately 0.4 magnitudes. From this

I conclude that a large variation in metallicity in Field 1 (presumably arising from the superposition of spheroidal and disk stars) is a plausible explanation for the width of its RGB. In the outer four fields I can expect metallicity variations to cause an RGB width of around 0.08 magnitudes and, as this is considerably smaller than the observed RGB widths, I now see whether age can provide an explanation.

In a field which has had continuous star formation, the stars currently ascending the RGB will be both the younger, more-massive, and the older, less-massive, stars. Regardless of metallicity, the loci of the RGBs for the lower- and higher-mass stars will be different, leading to a dispersion of the RGB in the field. In Field 3, and to a lesser extent Field 2, the intrinsic width of the RGB is greater than in the other fields. Both of these fields have strong blue components indicative of ongoing star formation. The obvious interpretation of the observed RGB widths in these fields is that stars of different masses are "funnelling" onto the RGB, their combined loci giving rise to the RGB width. To estimate the mass range needed to account for the intrinsic RGB widths in terms of mass funnelling, I use the solar metallicity (Z = 0.02) isochrones of Bertelli *et al.* (1994). I find that for stars in the age range 1×10^{10} yrs to 3.2×10^{8} yrs (corresponding to turn-off masses of approximately 1 to $3\mathcal{M}_{\odot}$) the locus of the RGB moves by around 0.6 magnitudes in $(V-I)$, which I illustrate in Fig. 3.5b by plotting solar metallicity isochrones in this age range. Comparing this value to the FWHM values given in Table 3.2 it can be seen that, if this is the dominant source of RGB width, Field 2 is dominated by stars in the mass range 1 to $3\mathcal{M}_{\odot}$ while Field 3, with its vigorous star formation, has a significant component of RGB stars with masses greater than $3\mathcal{M}_{\odot}$. Fields 4 and 5, with their narrower RGBs, probably ceased star formation some time ago and now their RGBs are dominated by lower-mass stars than those of Fields 2 and 3.

I stress again that these results must be used as a guide only. A more detailed analysis

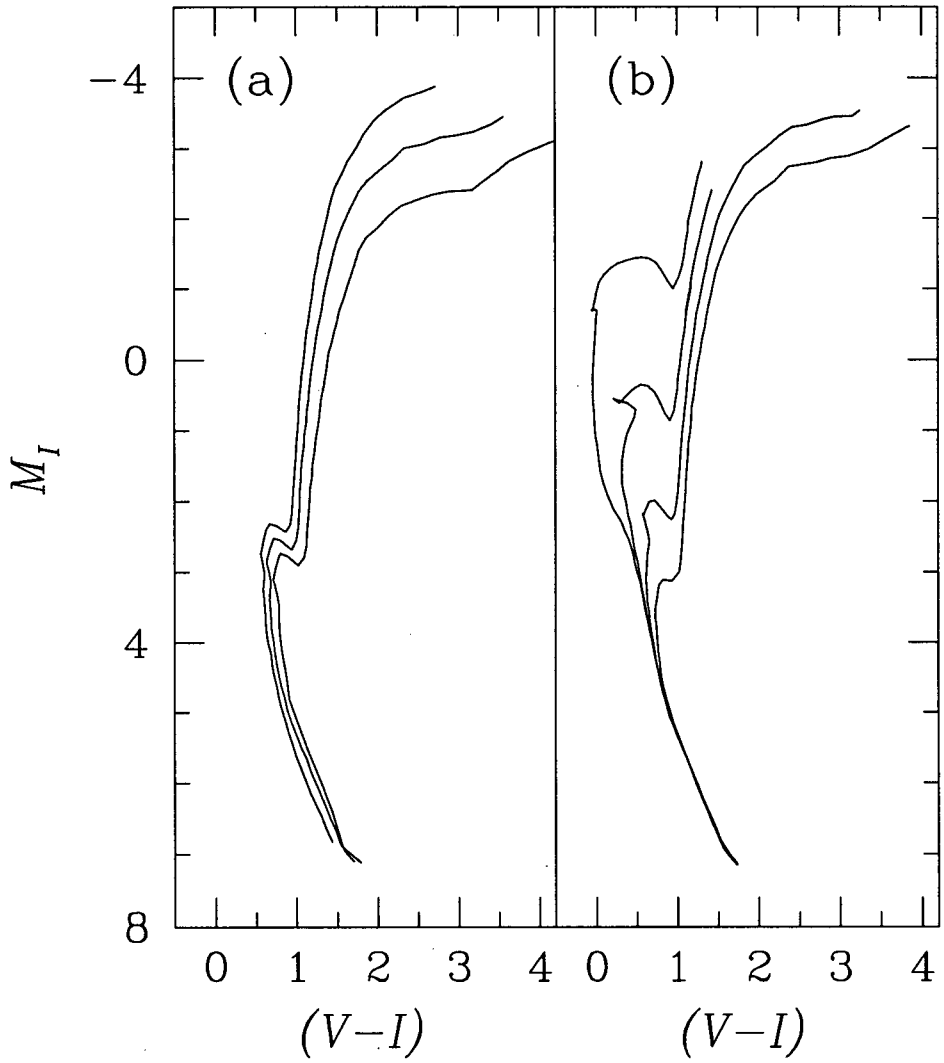

Figure 3.5: Isochrones from Bertelli *et al.* (1994). In the left panel I have plotted 5 Gyr isochrones for Z values (from left to right) of 0.008, 0.02, and 0.05. The other panel shows isochrones with Z = 0.02, and ages (from left to right) of 3.2×10^8, 1×10^9, 3.2×10^9, and 1×10^{10} years.

would include factors such as differential reddening, RGB morphology and completeness. For example, with continuous star formation I would expect the RGB colour distribution to have an extended tail to the blue, the details of which would depend on the initial mass-function (IMF) in the field.

3.5 AGB Luminosity Functions

The AGB LF is of interest as it provides insight into the formation and evolution of stars. For example, observations of the LMC showed there to be a lack of bright AGB stars when compared to theoretical predictions (see Iben 1981 and references therein). This discrepancy, known as the bright C-star mystery, led theorists to either adopt revised mass-loss laws in their models for the more massive AGB stars or to include effects such as semiconvection and convective overshooting. AGB evolution theory (Iben & Truran 1978, Renzini & Voli 1981) predicts that the luminosity at the tip of the AGB is a monotonic increasing function of mass, a result verified by Aaronson & Mould (1982). As pointed out by Reid & Mould (1984) this means that any point on the AGB LF will have contributions only from stars younger than a certain age. In summary, observations of the AGB LFs allow us to get an estimate of the star formation rate, the IMF and the mass-loss rate.

Assuming similar IMFs in the five M31 fields, a comparison of their AGB LFs will allow a comparison of the different star formation histories in these fields. For example, in a field that had ceased star formation a long time ago, I would expect a lack of brighter AGB stars, and would thus expect a steep LF. On the other hand, a field in which there has been continuous star formation will contain luminous AGB stars, and will consequently have a shallower AGB LF.

Calculating a single AGB star model is computationally expensive, while calculating

an AGB LF for an ensemble of stars is unrealistic. Much of the computational expense involved in calculating an AGB LF can be circumvented through the use of empirical relationships, a method known as synthetic AGB evolution. The AGB LFs produced by such models are in terms of bolometric magnitude, and observers often derive bolometric AGB LFs to allow comparison with synthetic models. To allow easy comparison between synthetic models and previous studies, I also derive bolometric AGB LFs. To obtain the bolometric magnitude of a (late-type) M31 star, a bolometric correction is applied to the (Cousins) I magnitude (henceforth BC_{I_C}). Adopting $(m-M)_0 = 24.41$ (see §3.3.1), and applying the BC_{I_C} that Bessell & Wood (1984) derived from oxygen-rich stars gives

$$M_{\rm bol} = I_0 + 0.3 + 0.38(V-I)_0 - 0.14(V-I)_0^2 - 24.41. \qquad (3.2)$$

Bessell & Wood (1984) do not derive a BC_{I_C} for C-stars, though I note that in their Fig. 1 the 3 C-stars with $(V-I)_0 \lesssim 2.6$ deviate by only a few tenths of a magnitude from the BC_{I_C} for the oxygen-rich stars. As this error in BC_{I_C} is minimal for the purposes of deriving AGB LFs, I proceed by using eq. 3.2 on all the AGB stars. The BC_{I_C} for C-stars is further discussed in §9.2 where I attempt a comparison of the bolometric magnitudes of C-stars with theoretical models.

The completeness in the ($M_{\rm bol}$, $V-I)_0$ CMD was determined by Monte-Carlo methods. I follow Reid & Mould (1984) who, by consideration of the M92 RGB tip, defined an AGB star as having $(V-I)_0 > 1.48$. Stars (points) were randomly placed in the ($M_{\rm bol}$, $V-I)_0$ CMD in the region defined by $1.48 < (V-I)_0 < 3.98$ and $-6 < M_{\rm bol} < -1$. The stars are mapped to unique V and I instrumental magnitudes and, after assigning random frame coordinates, added into the V and I frames using the ADDSTAR program. The V and I frames are reduced with a double pass of FIND/PHOT/ALLSTAR (see §2.3). The completeness corrections can be determined by matching the ADDSTAR

and ALLSTAR files to find those added stars which were recovered. The region to which stars were added in the $(M_{\rm bol},\ V-I)_0$ CMD was split into a 10×10 grid and I determined the completeness in each element of this grid. Fields 5 and 4 had 4000 stars added over 4 tests, while Fields 3, 2 and 1 had 4000 stars added over 2 tests. Adding stars at this level produced only a slight increase in the crowding.

To correct the LFs for non M31 stars, stars from the background field of NGC 205 (RCP84, Fig. 6) were mapped into the $(M_{\rm bol},\ V-I)_0$ CMD. No mention of the completeness of the NGC 205 background CMD is made by RCP84, though their I magnitude limit appears to be around 21. As I am only interested in stars brighter than $M_{\rm bol}=-3.5$ ($I_0\sim20.5$), I proceed by assuming their background CMD to be complete. After scaling the background counts to allow for the relative field sizes, I subtract the background counts from the completeness corrected counts. In Fig. 3.6 I show the corrected counts in Field 4 after subtraction of background stars. Some of the elements in Fig. 3.6 have negative counts, this is simply due to scaling the background counts, and is compensated for when the counts are summed in $M_{\rm bol}$ over the colour bins.

In Fig. 3.7 I show the bolometric LFs for the five M31 fields before (triangles, dashed lines) and after (squares, solid lines) corrections for completeness and background counts. The errors shown for the uncorrected LFs are Poisson[1] errors, while the errors for the corrected LFs have both errors from the incompleteness and the background corrections folded in. In Fig. 3.7 I only plot bins with more than 10 real stars (before background corrections), and plot open squares for the bins in which the completeness was less than 50%. The turnover in the LFs is expected as: (1) at faint magnitudes the stars are too blue

[1]The field in which the counts are made will contain fluctuations in its distribution of stars. I count stars in a frame in this field, and consequently the number of stars counted on this frame will vary depending on its exact location. It is usually assumed that the star counts follow a Poisson distribution, and consequently that the error in the counts is simply $\sqrt{n}$ (in photon terms, this is known as "shot noise").

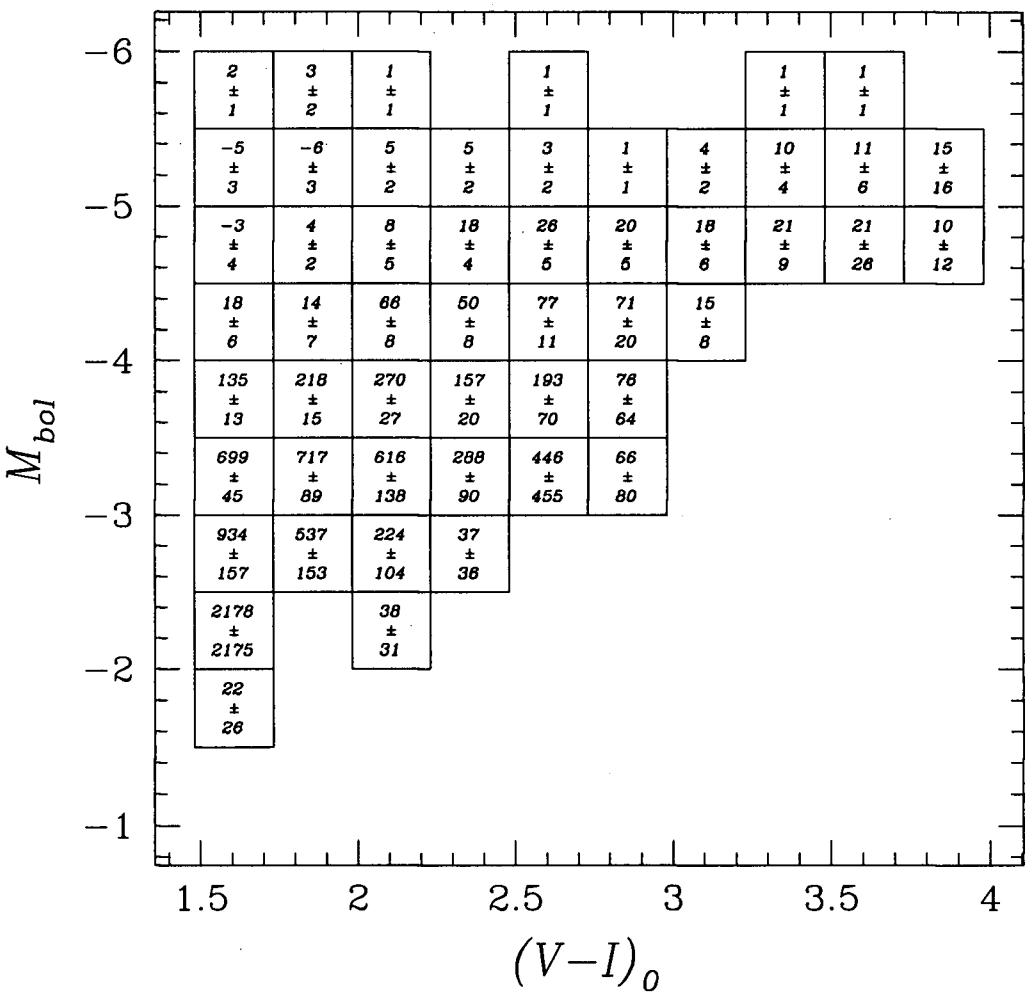

Figure 3.6: In this figure I show the corrected counts for Field 4 stars on the $(M_{\rm bol},\ V-I)_0$ CMD. Stars were added to a 10×10 grid, though bins are only shown if real stars existed in the bins and completeness corrections were finite (at least one added star was recovered). The upper number in the bins is the completeness and background corrected count, while the lower number is the error in the corrected count.

to meet the aforementioned colour criteria; and (2) the data suffer from incompleteness at fainter magnitudes. Figure 3.7 shows that the Field 5 LF has very few stars and is strongly affected by corrections for background counts. I note that in all but the Field 2 LF, the bins with $M_{\rm bol} < -3.5$ have a completeness level greater than 50%, and that completeness corrections are of little concern for the AGB stars.

I now consider how the AGB LFs differ in the fields. In the following comparison I drop Field 5 from consideration due to its lack of stars and ill-defined LF. The corrected LFs in Fig. 3.7 for Fields 1 through 4 were normalised such that they all contained the same number of stars in the magnitude range $-5 < M_{\rm bol} < -3$. In Fig. 3.8 these LFs are plotted in the range $-6 < M_{\rm bol} < -3$. For each of the fields in Fig. 3.8, I make a weighted least-squares fit to the LFs in the magnitude range $-6 < M_{\rm bol} < -3$, and in Table 3.3 I present a comparison of the gradients of the AGB LFs, giving: in column (1) the field numbers; in column (2) the value of $R_{\rm M31}$; in column (3) the gradients of the fits; and in column (4) the errors in the gradients. Inspection of Table 3.3 reveals that Fields 3 and 4 have shallow AGB LF gradients, whereas Fields 1 and 2 have significantly steeper AGB LF gradients. Field 3 contains many luminous blue stars and Cepheids (see Fig. 3.1) indicating that it is currently undergoing star formation. The shallower AGB LF gradient in Field 3 then suggests that in this field star formation has been ongoing for *at least a few Gyr.* Field 4 has a similar AGB LF gradient to Field 3, but has a reduced blue component compared with both Fields 2 and 3 (again, see Fig. 3.1). This suggests that Field 4 may have had more active star formation in the past. The AGB LFs of Fields 1 and 2 look similar, despite Field 2 having a moderate blue component which Field 1 lacks. This suggests that the star formation in Field 2 has been sporadic. To understand the AGB LFs more fully, synthetic AGB models need to be generated, which was beyond the scope of this thesis. In the study of M31 by RCP90 a similar trend

Table 3.3: Gradients of AGB LFs.

Field	R_{M31}	Gradient	Error
1	4.6 kpc	0.88	0.02
2	7.2 kpc	0.90	0.04
3	10.8 kpc	0.60	0.03
4	16.8 kpc	0.62	0.04

was seen, with a field at $R_{M31} = 4$ kpc having an older component than fields at 11 and 20 kpc.

In §3.4 an investigation of RGB widths led me to suggest that the mass range of stars ascending the RGB was different in the five fields. I showed that after correcting for photometric errors, and putting aside the possibility of differential reddening, Field 3 had the widest RGB. Using the isochrones of Bertelli *et al.* (1994) I then demonstrated that the width could be due to "mass funnelling" onto the RGB. This result is in agreement with the shallower AGB LF observed in Field 3. Given this result, it is then unexpected that Field 2, with a RGB wider than all but the Field 3 RGB, does not have the next shallowest AGB LF. It may be that in Field 2 the AGB LF is dominated by lower-mass stars, and the brighter AGB stars provide insufficient "leverage" to give the field a shallower LF. Field 4 has a RGB width narrower than that of Fields 2 and 3, though its AGB LF has a gradient consistent with that found in Field 3. This result would seem in accord with the previous suggestion that Field 4 has a large, intermediate aged, population. As the RGB width of Field 1 is difficult to interpret because of the possibility of large metallicity effects, and the AGB LF of Field 5 suffers from small number statistics I present no comparison of AGB LFs and RGB widths in these fields.

In conclusion, *there are different AGB LFs in the different fields, indicative of different star formation histories.* The AGB LFs will be further discussed in §4.5.5 where I

compare AGB LFs and a census of AGB spectral types.

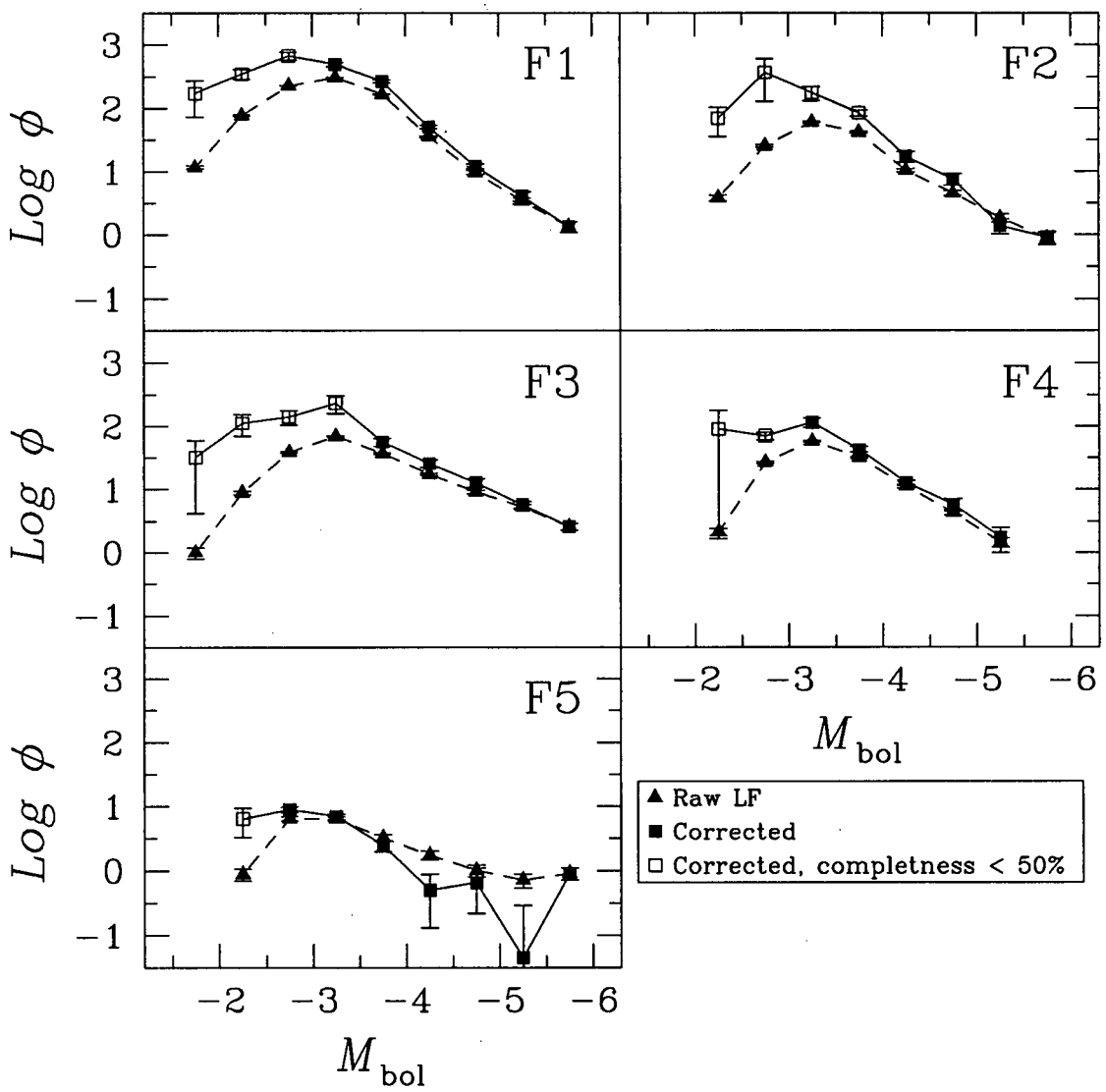

Figure 3.7: In this diagram I show bolometric LFs for stars with $1.48 < (V-I)_0 < 3.98$ in the five M31 fields. The units of ϕ are number mag^{-1} $arcmin^{-2}$. Solid triangles indicate the LFs before corrections for background stars and completeness, whereas squares indicate the LFs after correction for these two effects. An open square indicates that the applied completeness correction was greater than 2.

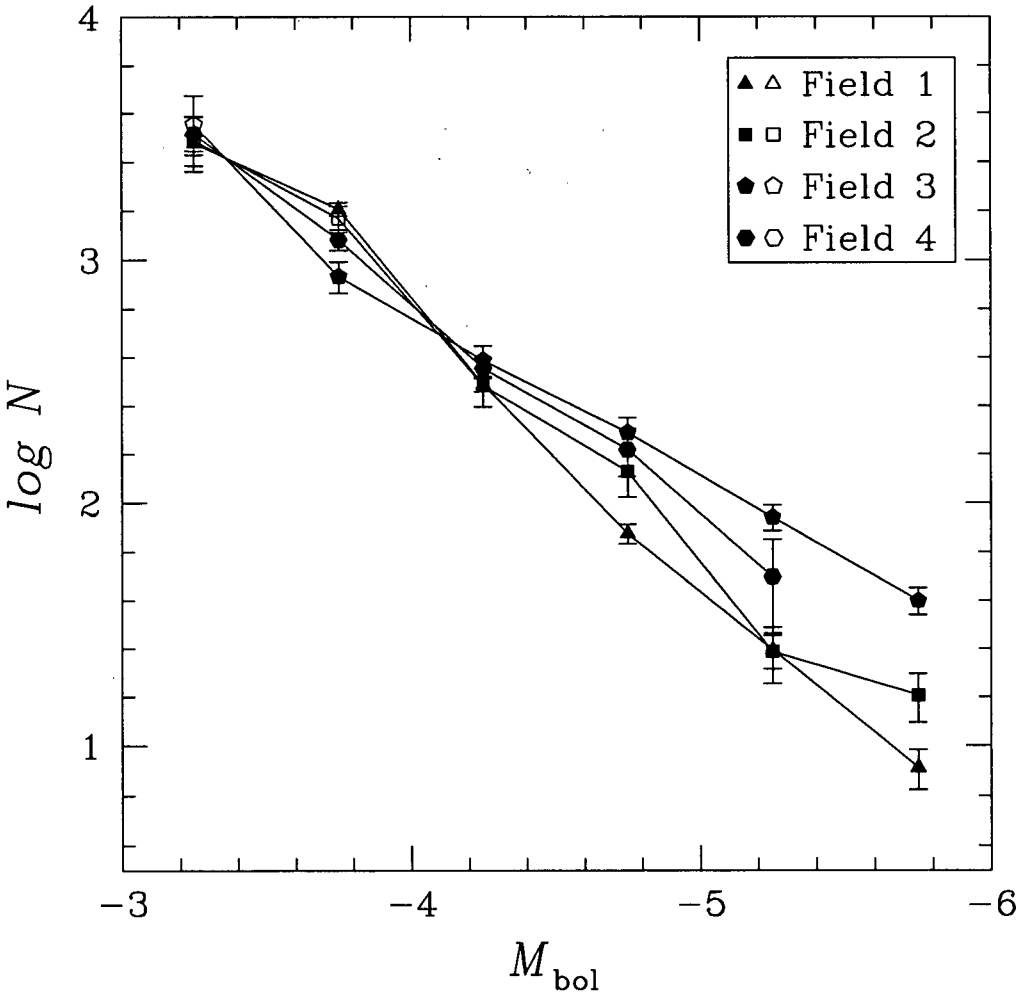

Figure 3.8: This plot contains the AGB LFs for Fields 1 through 4 from Fig. 3.7. The LFs were normalised such that they all contained 5000 stars in the magnitude range $-5 < M_{\rm bol} < -3$. The lines are to guide the eye only.

Chapter 4

THE $(CN-TiO,\ V-I)$ TCD: AN AGB CENSUS

"The whole is more than the sum of the parts."

Aristotle (384 – 322 B.C.E.)

4.1 General Features

In this chapter I combine the broadband photometry with the narrowband photometry to identify AGB stars in the five fields. I discussed the FBPS in §2.1, and gave an example of its ability to discriminate between spectral types in Fig. 2.2. In Fig. 4.1 I have plotted $(CN-TiO,\ V-I)$ TCDs for the five M31 fields. A comparison of Figs. 2.2 and 4.1 will give the reader an indication of the stars present in each of the five M31 fields, while a relative comparison of the $(CN-TiO,\ V-I)$ TCDs in Fig. 4.1 shows that: Field 1 has both very few C-stars and hot stars; Field 2 has a handful of C-stars along with a strong population of hot stars; Field 3 has many C-stars and many hot stars; Field 4 has many C-stars, though only a few hot stars; and Field 5 appears to have no hot stars and possibly a few C-stars. Figure 4.1 also shows the power of the FBPS to distinguish between spectral types; in Fields 3 and 4, where there are many C-stars, it can be seen that the separation between the C-stars and the M-stars is *around a magnitude* in $(CN-TiO)$.

In §4.2 of this chapter I define criteria for selecting C- and M-stars from Fig. 4.1. Having "recovered" the C-stars in the fields, I consider both their LF (§4.3) and space density (§4.4). The final section of this chapter (§4.5) is devoted to an investigation of the ratio of C- and M-stars in the five M31 fields.

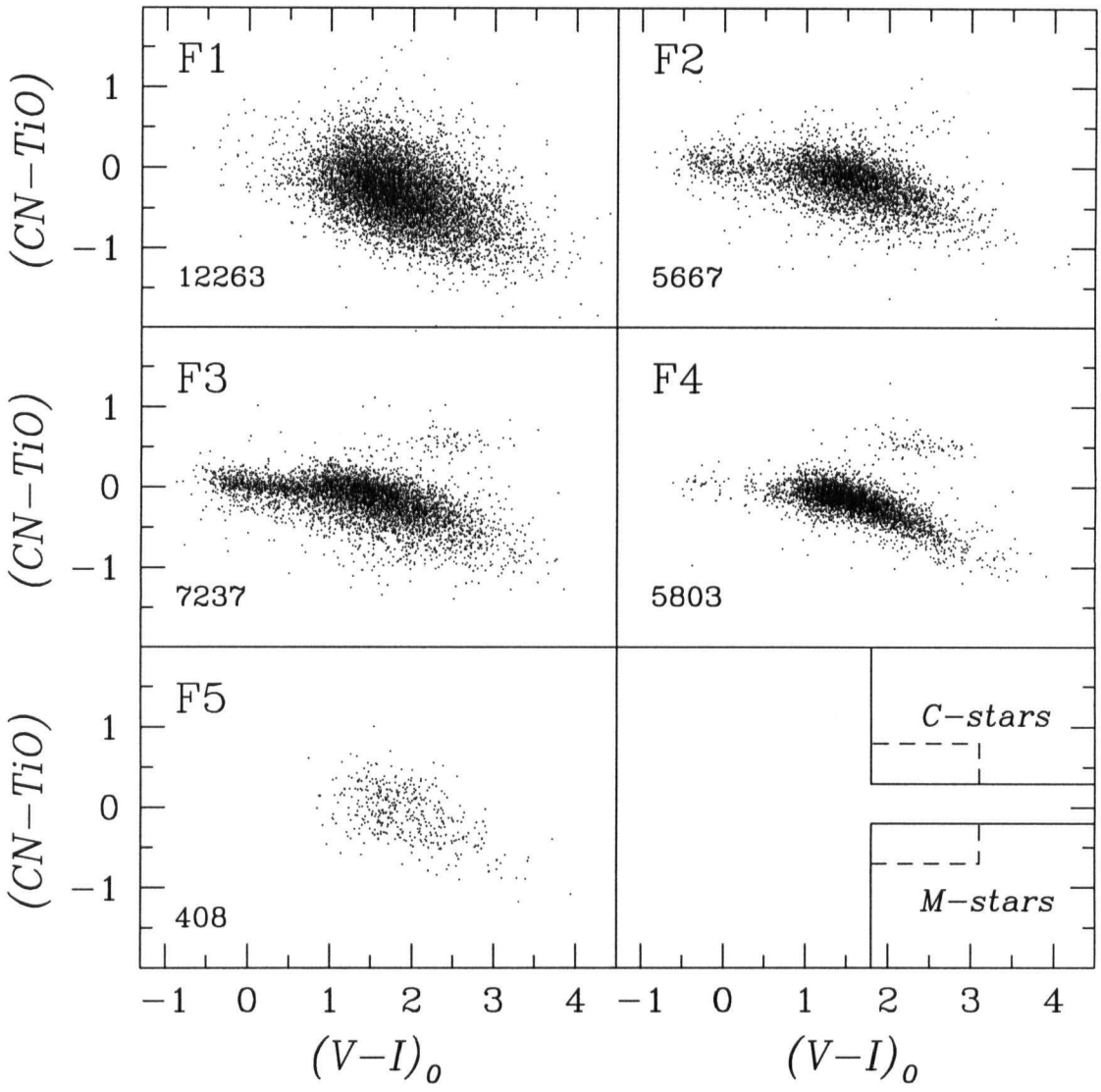

Figure 4.1: The labeled panels show the $(CN-TiO,\ V-I)$ TCDs for the five M31 fields and include the number of stars plotted in each panel. The $(V-I)$ colour has been calibrated onto the Johnson-Cousins system and corrected for reddening (§3.2), while the $(CN-TiO)$ colour has been shifted such that the mean value of $(CN-TiO)$ for stars bluer than $(V-I) = 1$ is zero. In the above labeled panels, stars with $I_0 < 18.5$ are excluded (see §4.2.2). The lower right panel shows the boundaries used to define the C- and M-stars, as discussed in the text (§§4.2.1 and 4.5.2).

4.2 Selection Criteria

4.2.1 Colour

In §7.2 I examine spectra of stars from Fields 3 and 4. Using my spectral classifications along with the colours of these stars, I define both C- and M-type stars as having $(V-I)_0 > 1.8$. Additionally, I define C-stars as those stars with $(CN-TiO) > 0.3$, while M-stars I define as having $(CN-TiO) < -0.2$. I ask the reader to refer to Chapter 7 of this thesis for justification of these values. The M- and C-star colour limits are shown as solid lines in the lower right panel of Fig. 4.1 (The dashed lines on Fig. 4.1 will be discussed in §4.5.2). Though my definitions of what constitutes C- and M-stars differ slightly from other studies, I point out that I use a consistent definition throughout this thesis.

4.2.2 Magnitude

The M-star region on the ($CN-TiO$, $V-I$) TCD can suffer contamination from both M31 M-supergiants and Galactic M-stars. The brighter of the M-type stars can be eliminated by applying a magnitude criterion. In their study of M31, RCP90 found that the number of stars brighter than $I = 19.0$ in their program field was similar to the number in the background field of RCP84. This suggests that the stars I observed with $I < 19.0$ are either foreground stars or M31 supergiants. Given this, I have excluded stars with $I_0 < 18.5$ from Fig. 4.1.

The exclusion of the brighter stars fails to address the problem of contamination from Galactic M-dwarfs. At a Galactic latitude of $b = -21.^{\circ}6$, M31 suffers from modest foreground contamination. The number of stars in the background field CMD from RCP84 redder than $(V-I) = 1.8$ and fainter than $I = 19.0$ is 12 which, when scaled

to allow for the relative field sizes in RCP84 and the present work, becomes 100 ± 30. Counting stars redder than $(V-I) = 1.8$ and fainter than $I = 19.0$ in the CMDs I find 19371, 3311, 4214, 8086, and 372 stars in Fields 1 to 5 respectively. It is clearly seen that M31's stars dominate the sample in all but Field 5 where I estimate that approximately 25% of the stars satisfying the aforementioned colour and magnitude criteria are field stars.

Contamination in the C-star region of the ($CN-TiO$, $V-I$) TCD from dwarf C-stars in the Galactic halo is of no concern as their low surface density ($0.019^{+0.044}_{-0.016}$ deg^{-2} to a limit of $V = 18$, Green 1992) renders them statistically unimportant. Any Galactic C-stars will be excluded by the aforementioned magnitude criterion.

We are interested in the C- and M-stars found on the AGB. IR83 state that for a star to develop its own peculiar abundances it has to be brighter than $M_{\rm bol} \sim -3.5$. Using the BC_{I_C} from Bessell & Wood (1984, see eq. 3.2) I calculated the bolometric magnitudes of the M-stars, and excluded those fainter than $M_{\rm bol} = -3.5$. Bessell & Wood (1984) point out that their BC_{I_C} is inapplicable to C-stars. The magnitude criterion I adopt for C-stars was $I_0 < 20.6$. This was chosen after noting that the ($CN-TiO$, $V-I$) TCDs of Fields 3 and 4 had well discriminated C-stars, and none of these were fainter than $I_0 = 20.6$. Additionally, I note that of 64 C-stars (with good photometry) observed in the LMC by Richer (1981a), only one of the stars was fainter than $I_0 = 20.6$ (see ahead to §4.3 and Fig. 4.3). An inspection of Fig. 4.1 suggests that many of the Field 1 C-star candidates are interlopers, as there is a blueward skew in the colour distribution compared to the other fields and many of the candidate C-stars in Field 1 fail the magnitude criterion (see ahead to §4.5.1). Although the C-star magnitude criterion is only partially effective at eliminating blue interlopers, it does eliminate the more obvious ones.

The candidate C-stars in each field (stars with $(V-I)_0 > 1.8$, $(CN-TiO) > 0.3$, and

Table 4.1: Coordinates and Photometry of Candidate C-Stars.[a]

ID	X,Y	I	$(V-I)$	$(CN-TiO)$
		Field 1		
f1C.1	153, 898	19.15(0.02)	2.42(0.03)	0.62(0.03)
f1C.2	564, 240	19.43(0.01)	3.15(0.03)	0.38(0.04)
f1C.3	823, 1132	19.63(0.02)	2.90(0.03)	0.34(0.03)
f1C.4	250, 1146	19.83(0.03)	5.08(0.38)	0.65(0.05)
f1C.5	1272, 605	19.87(0.04)	3.92(0.14)	0.34(0.05)
f1C.6	578, 153	19.98(0.02)	3.55(0.07)	1.04(0.04)
f1C.7	943, 322	19.99(0.03)	2.52(0.05)	0.59(0.05)
f1C.8	322, 1994	20.00(0.02)	2.81(0.04)	0.57(0.04)
f1C.9	72, 1330	20.04(0.02)	2.56(0.04)	0.32(0.05)
f1C.10	1343, 1038	20.06(0.02)	3.02(0.06)	0.61(0.05)

[a]Table 4.1 is presented in its complete form on the accompanying CD-ROM (see page xiii).

$18.5 < I_0 < 20.6$) are listed in Table 4.1 which is presented in its complete form on the accompanying CD-ROM. The following data appear for each C-star candidate: in column (1) an ID number, ordered by magnitude; in column (2) X-Y coordinates (these can be used to identify the candidates on the I-band images, included on the accompanying CD-ROM); in column (3) the I magnitude along with its ALLSTAR error; and in columns (4) and (5) the $(V-I)$ and $(CN-TiO)$ colours, along with their errors derived by the addition of ALLSTAR errors in quadrature. In Table 4.2 (again, presented in its complete form on the accompanying CD-ROM) I list the M-stars (stars with $(V-I)_0 > 1.8$, $(CN-TiO) < -0.2$, $I_0 > 18.5$, and $M_{\rm bol} < -3.5$). The layout of Table 4.2 is identical to that of Table 4.1.

In Fig. 4.2 I plot the CMDs of those stars with $(V-I)_0 > 1.8$, $(CN-TiO) > 0.3$, and $18.5 < I_0 < 20.6$; the candidate C-stars. A comparison of Figs. 3.1 and 4.2 shows the C-stars to be among the brightest and reddest stars in the fields. Also included in

Table 4.2: Coordinates and Photometry of Candidate M-Stars.[a]

ID	X,Y	I	$(V-I)$	$(CN-TiO)$
		Field 1		
f1M.1	705, 862	18.95(0.02)	3.79(0.05)	−1.13(0.04)
f1M.2	1816, 421	19.04(0.02)	2.62(0.06)	−0.46(0.02)
f1M.3	1419, 1151	19.06(0.02)	2.26(0.02)	−0.51(0.04)
f1M.4	1517, 508	19.07(0.03)	3.33(0.05)	−0.50(0.04)
f1M.5	576, 1667	19.11(0.03)	3.86(0.05)	−1.37(0.04)
f1M.6	309, 798	19.21(0.01)	2.59(0.03)	−0.24(0.03)
f1M.7	823, 1210	19.23(0.02)	2.38(0.03)	−0.40(0.03)
f1M.8	1252, 1682	19.25(0.01)	3.44(0.04)	−1.17(0.03)
f1M.9	447, 1772	19.26(0.01)	3.13(0.05)	−0.83(0.03)
f1M.10	693, 1973	19.26(0.03)	2.92(0.06)	−0.45(0.04)

[a]Table 4.2 is presented in its complete form on the accompanying CD-ROM (see page xiii).

Fig. 4.2 are the Field 3 Cepheids which I re-identified. A comparison of the Field 3 C-stars and Cepheids shows them to have similar I magnitudes, suggesting that C-stars are potentially useful distance indicators, a point I now take up in §4.3.

4.3 C-Stars: Smoky Standard Candles?

Due to their high luminosity, very red colour and strong spectral characteristics, C-stars are potentially good distance indicators. One of their advantages over Cepheids, for example, is that they can be identified and used as a distance indicator in a single epoch of observation. Other advantages are the reduced effect of interstellar reddening when observing at longer wavelengths where C-stars are brightest and, unlike M-stars, there is only a remote chance of contamination from dwarf field stars. One possible caveat of using C-star LFs as standard candles is the need to adopt a universal C-star LF which assumes a common IMF and star-formation rate (SFR). This aside, there is strong

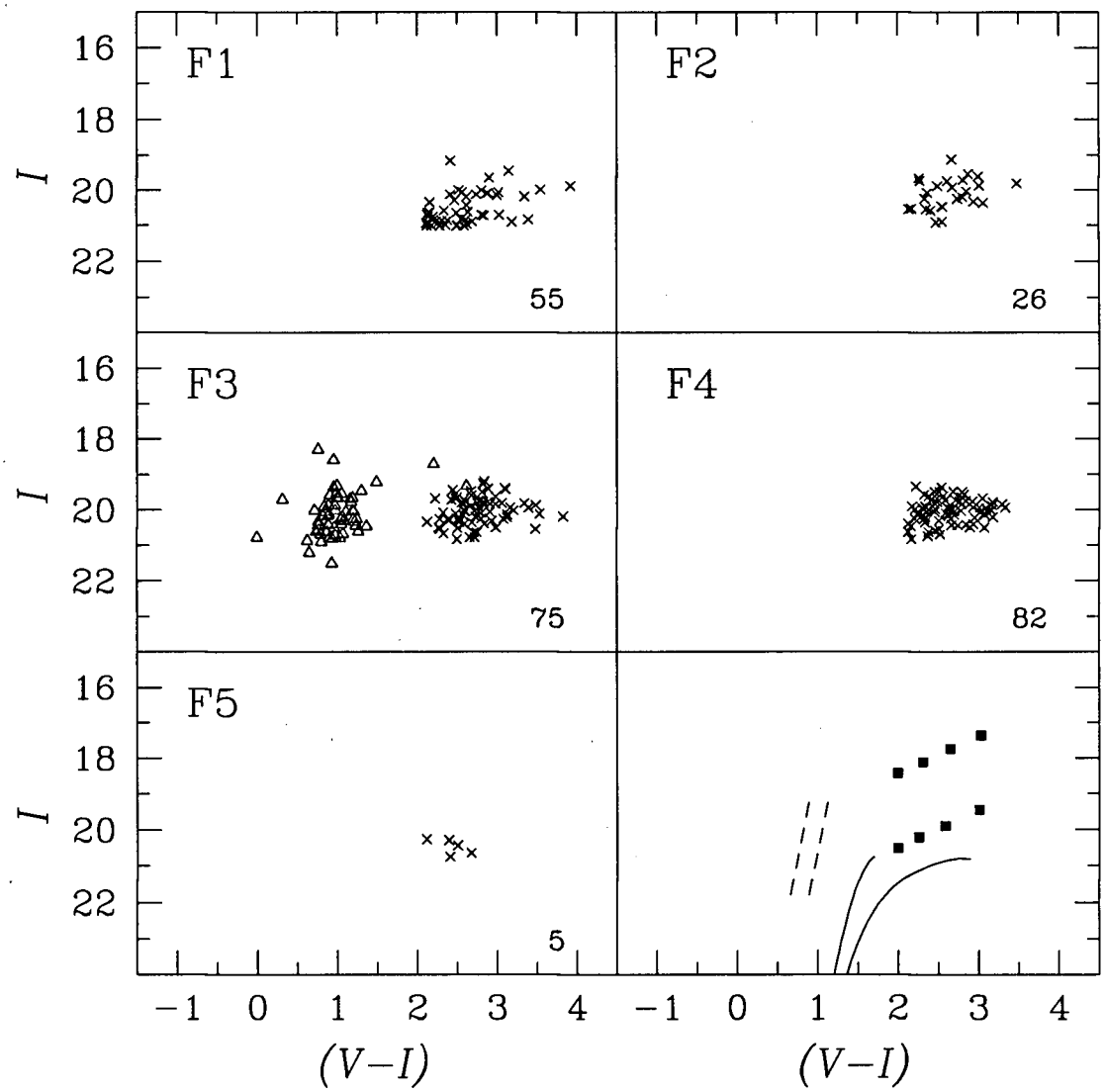

Figure 4.2: Calibrated (I, $V-I$) CMDs for the C-stars identified in the five M31 fields. The C-stars (shown as crosses) were selected according to photometric criteria described in §4.2. The bottom right panel shows features previously described in the Fig. 3.1 caption and §3.1. The Baade & Swope (1965) Cepheids which I re-identified in Field 3 are shown as open triangles.

observational evidence that there is a universal C-star LF for certain types of systems. Richer, Pritchet and Crabtree (1985) concluded that if a galaxy is sufficiently metal-rich ([Fe/H] > -1.8) and sufficiently bright ($M_V < -12.9$), then its C-stars will have the same luminosity as those in Fornax, the Magellanic Clouds, the Milky Way, M31 and NGC 205.

The FBPS is limited by seeing and crowding conditions; enough positive identifications of C-stars are needed to build a LF that allows a reasonable estimate of the mean to be obtained. For example, the innermost field in this study is of little value for determining the distance modulus of M31 as the crowding causes photometric errors which lead to many misidentifications and a deviant C-star LF. Taking this effect into account, I estimate that the current technique may be workable out to the Virgo cluster galaxies. I back up this claim by noting that in Fig. 4.2 the Field 3 C-stars and Cepheids have similar I magnitudes, and that Cepheids have recently been identified in the Virgo cluster with both ground-based (Pierce *et al.* 1994) and HST (Freedman *et al.* 1994) observations.

In earlier work by the Richer group, a mean absolute Cousins I magnitude of -4.75 was adopted for C-stars. This value was derived by transforming Richer's (1981a) photometry of 70 C-stars on the Johnson system in the LMC Bar-West (BW) field (originally identified in the survey of Blanco *et al.* 1978) to the Cousins photometric system using the transformation given by Bessell (1979). After allowing for reddening and absorption in their LMC BW field (Richer *et al.* 1985, and references therein), and adopting a distance modulus for the LMC of 18.45 (Welch *et al.* 1986) a mean absolute Cousins I magnitude of -4.75 ($\sigma = 0.40$) was derived. The transformation given by Bessell (1979), $(V-I_C)_0 = 0.835(V-I_J)_0 - 0.13$, is valid for stars with $2.0 < (V-I_J)_0 < 3.0$. The mean $(V-I_J)_0$ colour of Richer's (1981a) stars was 3.0 with a standard deviation of $\sigma = 0.6$ meaning that extrapolation of Bessell's (1979) transformation equation was used in many

cases. To verify that the extrapolation is valid, I made a comparison with Cousins I photometry of the same 70 stars made by Blanco *et al.* (1980). After correcting the mean Cousins I magnitude of Blanco *et al.* (1980) for the previously mentioned absorption and distance modulus, a value for the mean absolute magnitude of the LMC BW C-star sample of –4.79 ($\sigma = 0.35$) is derived. The agreement between the values shows that the extrapolation of Bessell's (1979) transformation was valid. For consistency with previous studies, I adopt the value of –4.75 for the mean absolute magnitude of the LMC BW C-stars.

Figure 4.3 shows I_0 LFs for the C-stars from all five M31 fields, a combined sample from Fields 2, 3 and 4 (henceforth, referred to as Field 234), and the LMC BW C-stars (with good photometry) from Richer (1981a). The stars in the M31 LFs pass the photometric criteria described in §4.2, and have been corrected for absorption as outlined in §3.2. The LMC BW C-star magnitudes were corrected for absorption, converted to the Cousins system, and moved to the M31 distance modulus by adding the difference between the M31 and LMC true distance moduli (FM90, Welch *et al.* 1986). In Fig. 4.3 I exclude those stars from Richer (1981a) which had poor photometry. For the M31 C-star LFs in Fig. 4.3 I give $\langle I_0 \rangle$, the number of stars, the standard deviation and the standard error for each distribution.

In the following analysis I assume the C-star LFs to be gaussian. How good is this assumption? In Fig. 4.4 I have plotted cumulative distributions for the C-stars in the five M31 fields as well as for Field 234. To compare these distributions to gaussian distributions I include in Fig. 4.4 cumulative gaussians that have the same mean and σ as the appropriate C-star LF. To see whether the C-star LFs are gaussian, I calculate the Kolmogorov-Smirnov (K-S) statistic and the significance level (which I include in Fig. 4.4) for the two distributions. The significance level lies between 0 and 1, with a

small significance indicating that the distribution is significantly different from a gaussian. Inspection of Fig. 4.4 shows that the Field 1 C-star LF is very poorly fit by a gaussian distribution. This is no surprise given the tail of faint stars, which I believe is due to photometric scatter. All the other distributions are reasonably well fit by gaussians. Note that the Field 5 C-star LF does not "look" gaussian though has a high significance. This result is not unexpected as Field 5 has few C-stars, and the high significance level is saying that it is likely that the Field 5 distribution was drawn from a parent gaussian distribution.

As previously discussed, it is apparent that Field 1 is contaminated by stars scattering into the C-star region. As this is hard to disentangle, I drop Field 1 from further discussion. I also drop Field 5 from consideration due to the paucity of C-stars and, again, problems with non-C-stars scattering into the region. For the Field 234 sample, a mean value of 19.61 ± 0.03 (error in the mean) is obtained. Taking the mean absolute I magnitude of C-stars to be –4.75 (justified previously) gives a true distance modulus of 24.36 ± 0.03 for M31, in agreement with the value of 24.45 ± 0.15 which RCP90 similarly derived. The value of 24.36 ± 0.03 is also in accord with the true distance modulus (24.42 ± 0.05) derived from the Field 3 Cepheids in §3.3. I note that the distance modulus derived from the Field 3 C-star LF is in agreement with the Cepheid distance modulus *regardless* of the Field 3 reddening value (see §3.2).

I note that the mean magnitudes of the Field 2, 3 and 4 C-stars are consistent within their standard errors. This is a remarkable result given that: (1) Field 3 is in spiral arm and, comparatively, has undergone much recent star formation; (2) the AGB LF of Field 2 was found to be dissimilar to those of Fields 3 and 4; and (3) the observations of Blair *et al.* (1982) indicate that the difference in metallicity between Fields 2 and 4 is ~ 0.3 dex. From these results I conclude that *the C-star LF provides a robust standard candle.*

As discussed briefly in §1.2, this then implies that C-stars are useful as probes of Galactic structure, as it appears that neither star formation history nor metallicity gradient in the disk of the Milky Way strongly affect the C-star LF.

Figure 4.3 also supports the hypothesis that higher mass stars avoid becoming C-stars (IR83). IR83 mention that Cepheids are the progenitors of bright ($M_{\rm bol} < -6$) AGB stars, and that the lifetimes of Cepheids and bright AGB C-stars are similar ($\sim 10^6$ years). This suggests that I should find comparable numbers of bright C-stars and Cepheids in my fields. In fact, the C-star LFs of Fields 3 and 4 are alike despite Field 4 having fewer Cepheids than Field 3 (see Fig. 3.1). This argues that the lack of bright C-stars (the "bright C-star discrepancy") is not due to a lack of massive progenitors (the "old age solution") and that either the theoretical models are somehow incomplete or the bright C-stars are very red and are being missed by surveys such as this. A strong argument against the second of these possibilities (incompleteness) was provided by Frogel & Richer (1983) who showed, from infrared observations, a lack of luminous AGB stars in the Bar West field of the LMC.

4.4 Surface Density of C-Stars in M31

Of interest is a comparison of the surface densities of Galactic and M31 C-stars. The Galactic C-star density was estimated by Richer (1981a) who used the Galactic N-star[1] volume density estimates of Westerlund (1965) and Scalo & Miller (1979), along with an estimate for the scale height of red giants from Blaauw (1965), to derive a value of between 6.7×10^{-5} and 1.3×10^{-5} N stars pc^{-2}.

How does this density compare with my observations in M31? To address this question, the de-projected areas of my fields are needed. I assume that one side of the (square)

[1]Recall, an N-type C-star is an AGB C-star.

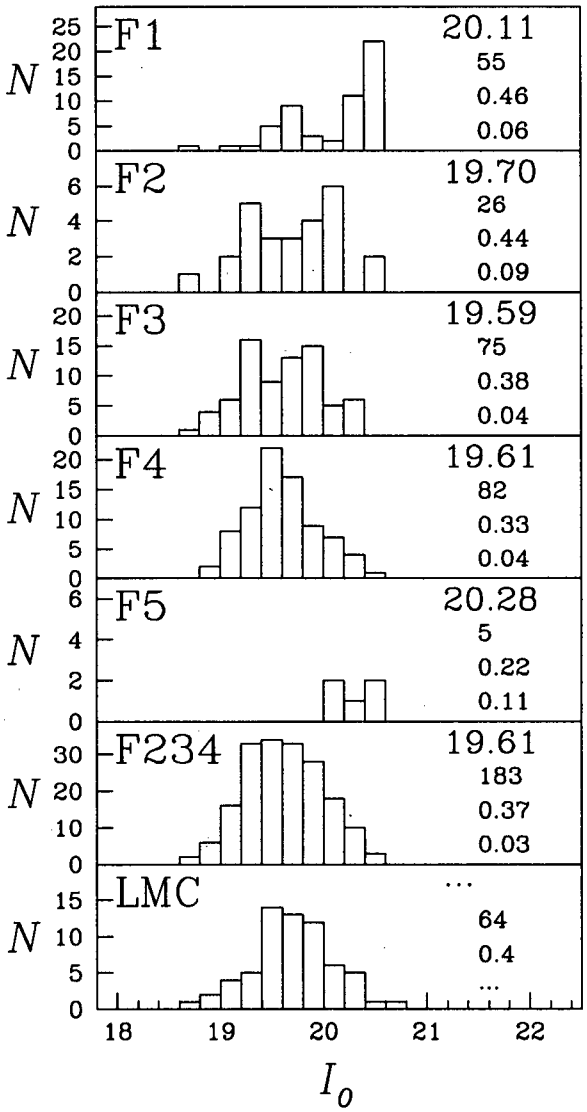

Figure 4.3: C-star LFs for the five M31 fields, Field 234, and the LMC Bar West field (Richer 1981a). The C-stars were selected according to the photometric criteria described in §4.2. The mean magnitude is given in the upper right hand corner of the panels, followed by the number of stars in the distribution, the standard deviation of the distribution and the error in the mean. To obtain ϕ (number of C-stars mag^{-1} arcmin^{-2}), N can be divided by 9.8 for Fields 1 to 5, and by 29.4 for Field 234.

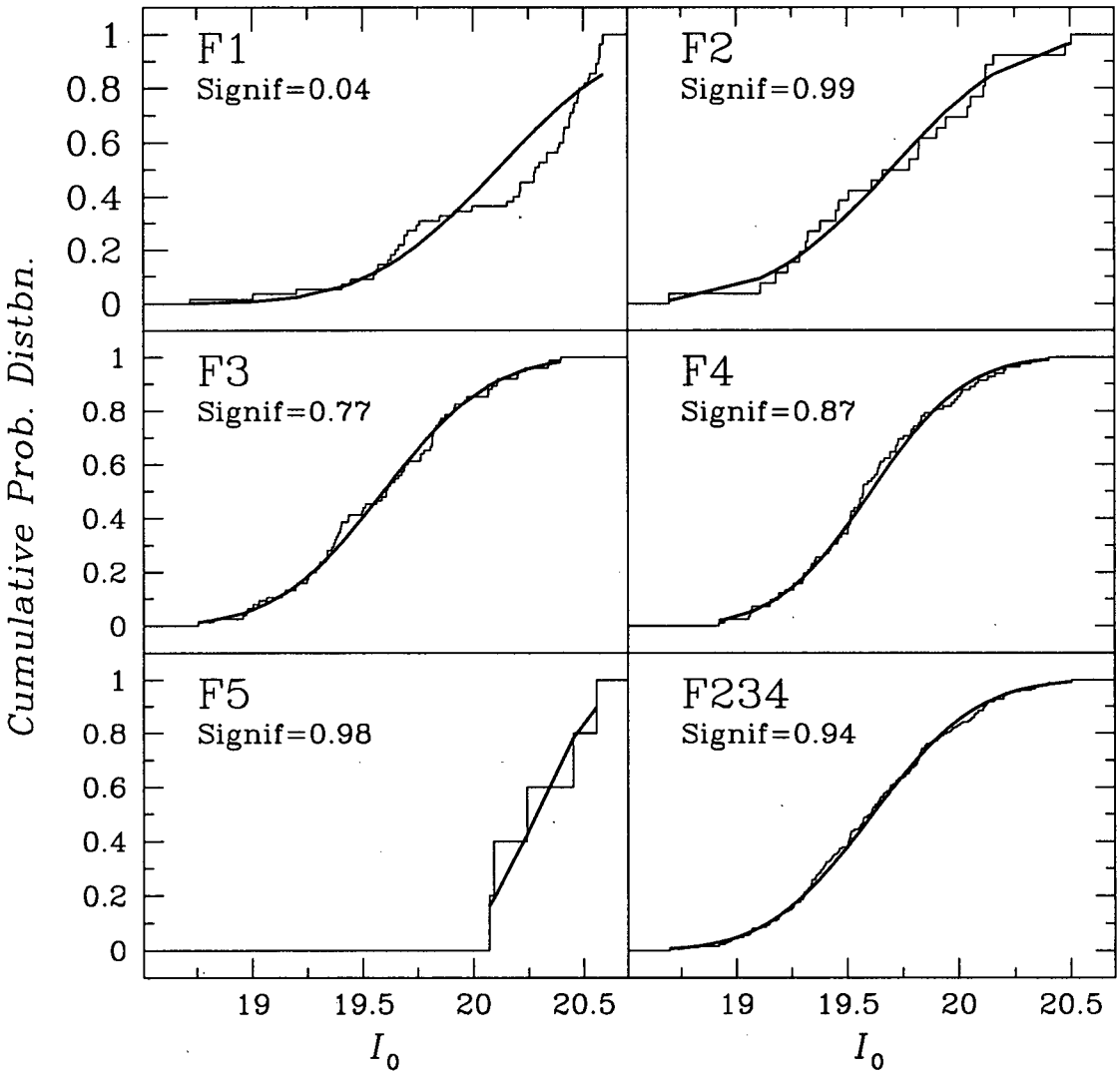

Figure 4.4: In the above diagram I plot the cumulative distributions of C-stars in the five M31 fields and Field 234 (light lines). Included with each of these distributions is a cumulative gaussian (thick line) with the same mean and σ as the C-star LF from which the distribution was derived. The value of "Signif" in each panel is the significance level of D, the K-S statistic. Small values of "Signif" indicate that the cumulative gaussian is significantly different from the cumulative data.

fields is aligned with, while the other is perpendicular to, the SW semi-major axis of M31. That this is a reasonable assumption can be seen from inspection of Fig. 2.3. The side of the field that is parallel with the axis suffers from no projection effects, while the side of the field perpendicular to the SW semi-major axis has a true size of $1.6 \times \sec(77.^{\circ}5)$ kpc, where $77.^{\circ}5$ is the inclination of M31's disk (van den Bergh 1991b) and the field size perpendicular to the SW semi-major axis is 1.6 kpc. The de-projected field size thus becomes 1.6×7.4 kpc^2. To make a comparison with the value of Richer (1981a) I use Fields 3 and 4, as these have approximately solar abundance (see §4.5.5) and should provide the best comparison with the solar neighbourhood. The numbers of C-stars found in Fields 3 and 4 are 75 and 82, which leads to a surface density of around 0.7×10^{-5} N stars pc^{-2} in M31. From these results it appears that, for the same metallicity, the surface density of C-stars in the Galaxy is between 2 and 10 times greater than in M31. Given the large range in Richer's (1981a) estimate for the Galactic surface density of C-stars, it is conceivable that the values are in agreement. If the surface density of C-stars is greater in the Galaxy than in M31, then either: (1) the Galactic sample is from a region of the Milky Way with a higher stellar density than found in the M31 regions; or (2) there is a relatively higher density of C-star progenitors in the Galaxy. It would be interesting to "normalise" the C-star surface density against, for example, the density of RGB stars. Such an investigation, however, is beyond the scope of this thesis.

4.5 The C/M Ratio: A Significant Statistic

Blanco *et al.* (1978) noted that the number ratio of C-stars to M-stars (hereafter referred to as the C/M ratio) was much greater in the metal-poor Magellanic Clouds than it was in the metal-rich Galactic Nuclear Bulge. They attributed the different C/M ratios to differences in metallicity or age, or both metallicity and age. Presently, the mechanism

controlling the C/M ratio is believed to be the metallicity of the gas from which the stars condensed, though it remains unclear what effect parent galaxy morphology, star formation history, and age play (Pritchet *et al.* 1987). In systems such as globular clusters and giant elliptical galaxies the C/M ratio is undefined as it is believed that stars with masses $\lesssim 0.9\mathcal{M}_{\odot}$ evolve off the AGB (their envelopes "evaporating") before undergoing helium shell flashing (Renzini 1977).

4.5.1 The "Raw" C/M Ratio

In Fig. 4.1 I presented ($CN-TiO$, $V-I$) TCDs for the five M31 fields in which it was apparent that the C/M ratio increased with $R_{\rm M31}$. To get a more quantitative picture of this increase I count the C- and M-stars in the five fields using the photometric criteria described in §4.2. The resulting counts are presented in Table 4.3. The first two columns in Table 4.3 give field number and $R_{\rm M31}$, columns 3 and 4 give the counts when the C- and M-stars are selected by colour criteria only, and columns 5 and 6 contain counts when the C- and M-stars are selected using both the colour and magnitude criteria. A comparison of columns 3 and 5 of Table 4.3 suggests that Fields 1 and 5 have comparatively more photometric scatter than Fields 2, 3 and 4.

Before determining the C/M ratios I multiply the M-star counts in Field 5 by 0.75 (see §4.2.2) to correct for foreground stars. In Fig. 4.5 I plot the C/M ratios as a function of $R_{\rm M31}$. The error bars in Fig. 4.5 are propagated from the Poisson errors associated with the C- and M-star counts. I note that the C/M ratio of Field 1 is likely to be an upper limit as its C-star LF (Fig. 4.3) is skewed to fainter magnitudes suggesting that many of the C-star candidates in Field 1 may be spurious.

The correlation seen between C/M and $R_{\rm M31}$ in Fig. 4.5 will be discussed in §4.5.5 after I have considered what effects incompleteness may have on the data.

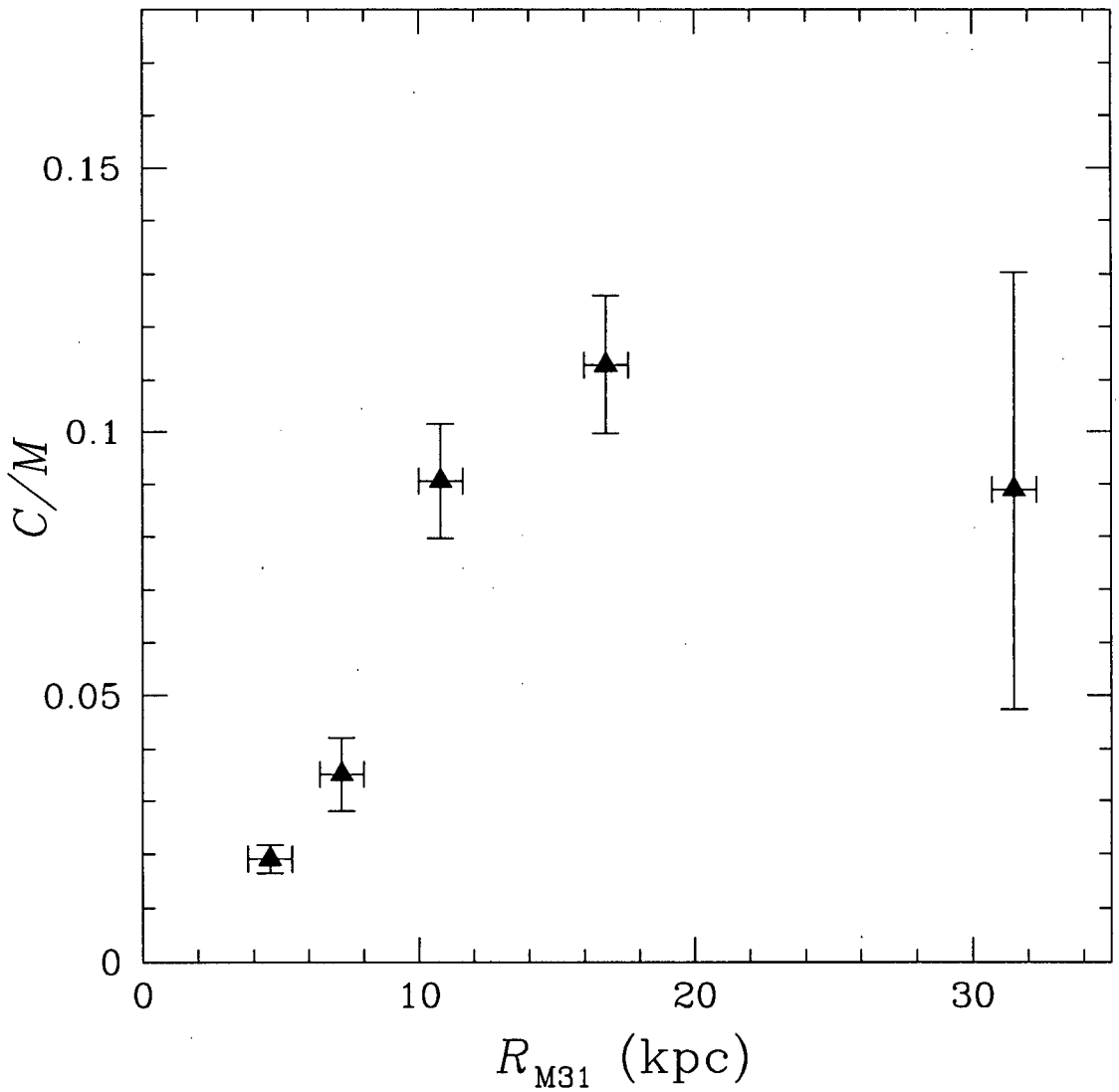

Figure 4.5: The measured C/M ratios in the five M31 fields as a function of R_{M31}, with no completeness corrections. The C- and M-stars were selected according to the photometric criteria described in §4.2. Vertical error bars show the Poissonian errors in the counts of the C- and M-stars, while horizontal error bars (±0.8kpc) indicate the field size at the distance of M31.

Table 4.3: C- and M-star Counts in M31.

Field	R_{M31}	C[a]	M[a]	C[b]	M[b]
1	4.6 kpc	108	4514	55	2886
2	7.2 kpc	29	1092	26	740
3	10.8 kpc	75	1334	75	829
4	16.8 kpc	82	1225	82	726
5	31.5 kpc	14	108	5	75

[a]Colour criteria only.
[b]Colour and magnitude criteria.

4.5.2 Effects of Incompleteness on the C/M Ratio

What are the potential effects of incompleteness on the measured C/M ratio? This question was briefly discussed by Cook *et al.* (1986) who showed, using data from Blanco *et al.* (1980), that the C/M ratio measured in the LMC Bar West and Radio Centre fields changed with sample depth in I. In this section I consider the effects of incompleteness on my data in more detail.

Theory predicts that an M-star (of appropriate mass and metallicity) will evolve into an S-star and then a C-star as it ascends the AGB. As a star ascends the AGB it becomes cooler and more luminous. As C-stars are generally expected to be bolometrically brighter than M-stars it might be naïvely expected that the C-stars are more complete in the data. This is not necessarily the case. The reddest C-stars may suffer from incompleteness on the V frame despite their high bolometric luminosity. Indeed, bolometrically bright infrared C-stars may fail to be detected at all! The CN and TiO filters further complicate the issue as these were designed to exploit the fact that molecular opacities make C-stars brighter in TiO than CN and M-stars brighter in CN than TiO. Indeed, the difference between the ($CN-TiO$) colour for C- and M-stars can be as great as a magnitude (see

Fig. 4.1). As a star has to be found on the CN, TiO, V and I frames to be identified, the completeness on all four of these frames needs to be simultaneously considered.

As a demonstration that completeness can have a significant effect I present in Fig. 4.6a the I-band LFs for the C- and M-stars in Field 3 that were selected according to the photometric criteria given in §4.2. The bin width used to produce these LFs is 0.2 magnitudes, and the M-star counts have been multiplied by 0.1 to make easier a comparison of the two LFs. Figure 4.6a shows that the C-star LF has a brighter mean I magnitude than does the M-star LF. This result is predicted by the third dredge-up theory for the formation of AGB stars which predicts that, under some circumstances, M-stars evolve into C-stars as they ascend the AGB (IR83).

As the C- and M-star LFs are different, completeness will affect the measured C/M ratio. This is shown in Fig. 4.6b where I have plotted the logarithm of the cumulative counts of C- and M-stars that are brighter than the abscissa magnitude. In Fig. 4.6b the logarithm of the C/M ratio at a limiting I magnitude is the (negative) "gap" between the distributions. If the C- and M-stars had identical LFs, though different scaling factors, the lines in Fig. 4.6b would have a constant separation, this separation being dependent on the scaling factors of their LFs. For the Field 3 C- and M-stars shown in Fig. 4.6b the gap (and hence the C/M ratio) between the distributions varies as a function of limiting magnitude. The variation of the C/M ratio as a function of limiting magnitude is shown in Fig. 4.6c where it is seen (from right to left) that initially the C/M ratio increases as fainter stars are excluded. This increase is expected as the C-star LF in I is brighter than the M-star LF, as shown in Fig. 4.6a. At even brighter magnitudes ($I_0 < 19.5$) the C/M ratio decreases. This is explained by the tail of the M-star distribution at brighter magnitudes.

To summarize, I have shown that the measured C/M ratio from Field 3 is sensitive to

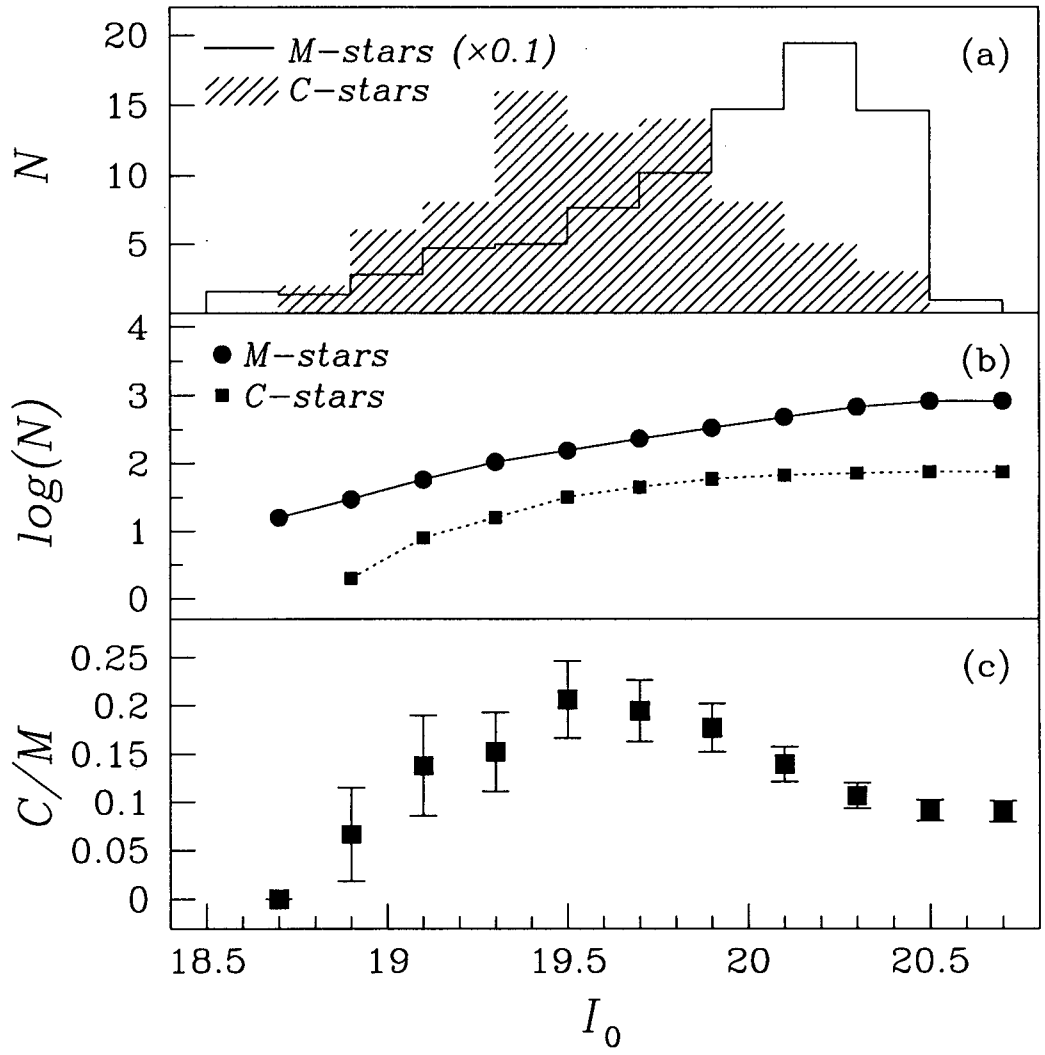

Figure 4.6: The upper panel shows the LFs of the C- and M-stars that were counted to derive the Field 3 C/M ratio. The M-star counts were multiplied by 0.1 to fit on the same scale as the C-stars. Panel (b) shows the logarithm of the cumulative counts of these stars with increasing magnitude. The final panel shows the measured C/M ratios derived when only those stars brighter than the abscissa magnitude are counted. The error bars in panel (c) are Poisson counting errors.

the I magnitude limit of the data. As completeness can potentially affect the measured C/M ratio, it needs be taken into consideration when counting the C- and M-stars.

Every star which appears in the ($CN-TiO$, $V-I$) TCDs of Fig. 4.1 has been found and fitted on the CN, TiO, V and I frames, and subsequently successfully matched. To measure the completeness of the stars in the ($CN-TiO$, $V-I$) TCD, artificial stars are added to, and recovered from, the CN, TiO, V and I frames. Using this Monte-Carlo method allows completeness to be measured without consideration of the many (often unknown) parameters needed for an analytical method to succeed. The Monte-Carlo method of adding artificial stars has been extensively used in the past to investigate monochromatic LFs (e.g. Brewer *et al.* 1993, and references therein) and bolometric LFs (Hudon *et al.* 1989, §3.5). Unlike these previous studies, the present study suffers from a degeneracy of stars in the ($CN-TiO$, $V-I$) TCD, i.e. a point in the ($CN-TiO$, $V-I$) TCD does not represent unique CN, TiO, V and I magnitudes. To obtain the magnitude of a star in a ($CN-TiO$, $V-I$) TCD, a relationship between colour and magnitude is needed. This can be provided by a CMD of the stars in question. As this is the first time that completeness in ($CN-TiO$, $V-I$) TCDs has been investigated, I detail below my approach to this problem.

In §4.2.1 I defined C- and M-star "regions" in the ($CN-TiO$, $V-I$) TCD using unbounded inequalities in ($V-I$) and ($CN-TiO$). As it is impossible (and also unnecessary) to measure the completeness on the (infinite) C- and M-star regions defined in this way, I used further colour criteria to constrain the C- and M-star regions to finite sizes in the ($CN-TiO$, $V-I$) TCD.

To the criteria from §4.2.1 I added a red limit (for both C- and M-stars) from the reddest, $(V-I)_0 = 3.1$, C-star for which a spectrum was obtained (F3–19.1, see ahead to Table 6.1). The upper ($CN-TiO$) bound for C-stars was chosen to encompass all C-stars

apart from obvious outliers. The lower ($CN-TiO$) bound for M-stars was set to -0.7, to give the M-star region the same ($CN-TiO$) width as the C-star region. Although not all M-stars lie within this region, enough do for a statistically significant comparison, and it is the relative numbers from field-to-field that are important. The finite C- and M-star regions are shown in Fig. 4.1 as the areas bounded by the solid and dashed lines in the lower right panel. I point out to the reader that changing the definition of what constitutes C- and M-stars, will cause the C/M ratios to be different to those previously calculated.

Artificial C- and M-stars were generated by randomly placing points in the (finite) C- and M-star regions in a ($CN-TiO$, $V-I$) TCD. The ($V-I$) and ($CN-TiO$) colours of these artificial stars are broken down into representative magnitudes using the (I, $V-I)_0$ and (TiO, $CN-TiO$) CMDs of the real C- and M-stars from these regions. The stars in the C-star region of the Field 1 ($CN-TiO$, $V-I$) TCD were found to be fainter than the other candidate C-stars, so a sample representative of the C-stars from Fields 3 and 4 was used. In Field 5 the paucity of C- and M-stars caused me to adopt mean colour-magnitude relationships from other fields. When the artificial colours were broken down into magnitudes, I ensured that the dispersion of the artificial data matched that of the real data. The artificial stars were assigned random frame coordinates and added into the CN, TiO, V and I frames using Stetson's (1987) ADDSTAR program.

The CN, TiO, V, and I frames with the added stars were reduced with a double pass of FIND/PHOT/ALLSTAR (see §2.3) and the resulting four ALLSTAR files matched with the four ADDSTAR files using DAOMASTER. By imposing the condition that a star had to be found in *at least* four of the eight matched files resulted in the rejection of real stars that were found on less than four frames. The file of matched stars from DAOMASTER was filtered to produce files containing the added stars, the added stars that were recovered,

and the real stars.

For each field I ran two completeness tests, and on each I added 500 C-stars and 500 M-stars. Adding these stars to each frame resulted in approximately 1 star being added to every 60×60 pixel section of the frame. Visual inspection showed this to be a reasonable level; there was generally no overlap between the added stars and stars of a similar magnitude. Further confirmation that the crowding characteristics of the frames were unaffected came from noting that the numbers of C- and M-stars recovered from those frames without added stars were similar to the numbers recovered from the frames with added stars.

The files produced by filtering the DAOMASTER match file can be used to determine completeness corrections. As the colours and magnitudes of stars have a dependence on position in the ($CN-TiO$, $V-I$) TCD, I binned the C- and M-star regions into 4 bins in ($V-I$) and 3 in ($CN-TiO$). For each of these 24 bins the completeness was calculated by counting the number of stars added to, and recovered from, the bin. A star added in one bin may be recovered in a different bin, an effect known as "bin jumping" (Drukier *et al.* 1988). In matching the added and recovered stars I imposed no colour criteria on the recovered stars. This is reasonable as I found the scatter around the bins to be approximately symmetrical, with as many stars jumping into a bin as jumping out. Having obtained the completeness, I next applied the completeness corrections to the real stars in the bin. I applied the corrections to the real stars from the ADDSTAR frames as the corrections apply *only* to the frames from which they were calculated. All of the added, recovered and real stars were only considered if they passed the photometric criteria (§4.2) to be C- or M-stars.

The results of the incompleteness tests in Field 3 are summarized in Fig. 4.7. In the bins in Fig. 4.7, the upper two numbers are the number of real stars and the measured

completeness in the bin while the lower two are the corrected number of stars in the bin and its associated error. The error in the corrected counts includes contributions from both Poisson errors in the number of real stars and the error in the completeness correction (Bolte 1989). Figure 4.7 shows that the C-stars in Field 3 with $(V-I)_0 < 3.1$ are highly complete, while Fig. 4.1 shows that there are few C-stars with $(V-I) > 3.1$. From this I conclude that the lack of very red C-stars is real. Figure 4.7 also shows that the redder M-stars are more incomplete than the bluer M-stars. This result is contrary to what might be expected; as an M-star evolves up the AGB it is generally expected to become redder and more luminous. An explanation of this result may be that the cooler M-stars have stronger TiO bands and are fainter in the TiO frames and subsequently less complete.

In Fig. 4.8 I plot C/M ratios that are both corrected (squares) and uncorrected (triangles) for completeness. The C- and M-stars used to derive the C/M ratios in Fig. 4.8 were within the bounded regions in the ($CN-TiO$, $V-I$) TCD. I remind the reader that the uncorrected C/M ratios in Figs. 4.8 and 4.5 are different as additional colour criteria were used to define the C- and M-stars in Fig. 4.8. Figure 4.8 shows that, after completeness corrections, the C/M ratios in Fields 1 and 5 increased slightly, while they decreased slightly in Fields 2, 3 and 4. In Fields 1 and 5 I found that the C-stars were less complete than in the other fields. Though the cause of this is unknown, it may be due to reasons such as the CN frames being shallower (poorer seeing, brighter sky) or problems with the ($CN-TiO$) calibration in these fields.

To conclude, I have shown that the completeness has an effect on the measured C/M ratios, but in the case of my data, the effect is small and the trend seen between C/M and $R_{\rm M31}$ persists. This shows that the observed increase of the C/M ratio with $R_{\rm M31}$ is a *true physical effect*, and not due to some obscure effect related to the crowding statistics

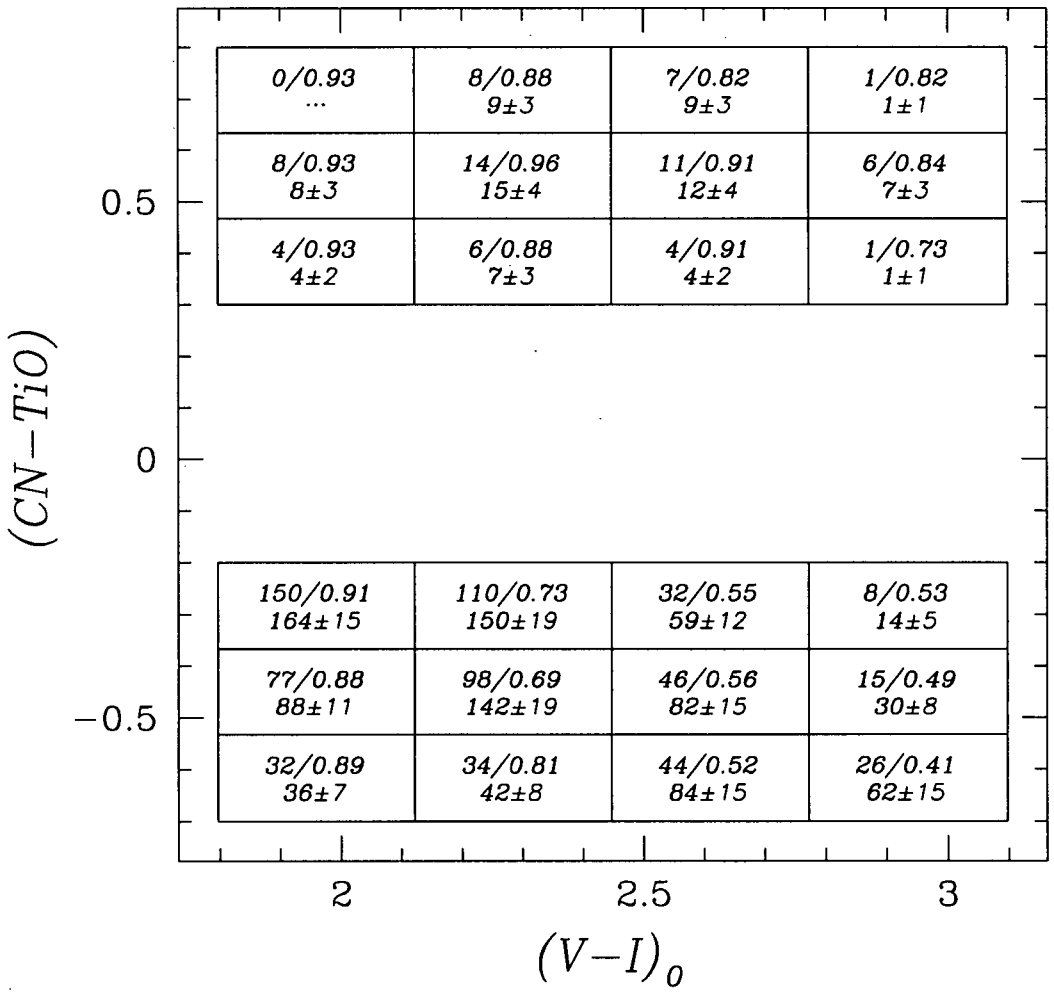

Figure 4.7: A summary of the results from the CN, TiO, V, and I ADDSTAR tests in Field 3. The upper 12 bins in the ($CN-TiO$, $V-I$) TCD encompass the region in which a star is defined as a C-star, and the bottom 12 cover the M-star region. The first number on the top row gives the number of real stars found in this bin together with incompleteness correction. The lower line gives the corrected counts along with their errors. An ellipsis indicates that no real stars were found in the bin.

in the fields. For the rest of this thesis I consider the "raw" C/M ratios shown in Fig. 4.5. The reasons for this are: (1) as previously mentioned, in Fields 1 and 5 I adopted a mean colour-magnitude relationship for the C-stars which may be invalid; (2) some bona fide C- and M-star candidates are excluded from the "corrected" counts as they lay outside the finite C- and M-star regions; and (3) the conclusions arrived at using the "raw" ratios are similar if the "corrected" C/M ratios are used instead.

4.5.3 Comparison with Previous Studies

The C/M ratio in M31 has been previously investigated by RC85, Cook *et al.* (1986) and RCP90. Below I briefly discuss and comment on each of these previous FBPS in M31.

- RC85 investigated a disk field in BF II at $R_{\rm M31}$ = 11 kpc. Using the FBPS they identified 5 C-stars and 41 stars later than type M5 in a 1.′2 ×2′ field. The ratio of 5/41 was, at the time, the smallest C/M ratio found in any extragalactic system. Interpreting this ratio as a metallicity effect led RC85 to conclude that the metallicity of their field was approximately solar. RC85 used different criteria to those used in this thesis to obtain their C/M ratio of 0.12 ± 0.06. In Field 3 (at $R_{\rm M31}$= 10.8 kpc) I obtained a C/M ratio (using C- and M-stars selected using the photometric criteria described in §4.2) of 0.09 ± 0.01 which, despite the differences in selection criteria, is consistent with the RC85 value.

- Cook *et al.* (1986) investigated two 1.′5 ×2.′5 fields located in BF II ($R_{\rm M31}$ = 7 kpc) and BF III ($R_{\rm M31}$ = 10 kpc). They found only one C-star in each of these fields and as the fields were located in arm and inter-arm regions concluded that they were measuring primarily an old disk population which was being unaffected by the presence of extreme population I. A comparison with my C-star counts (see

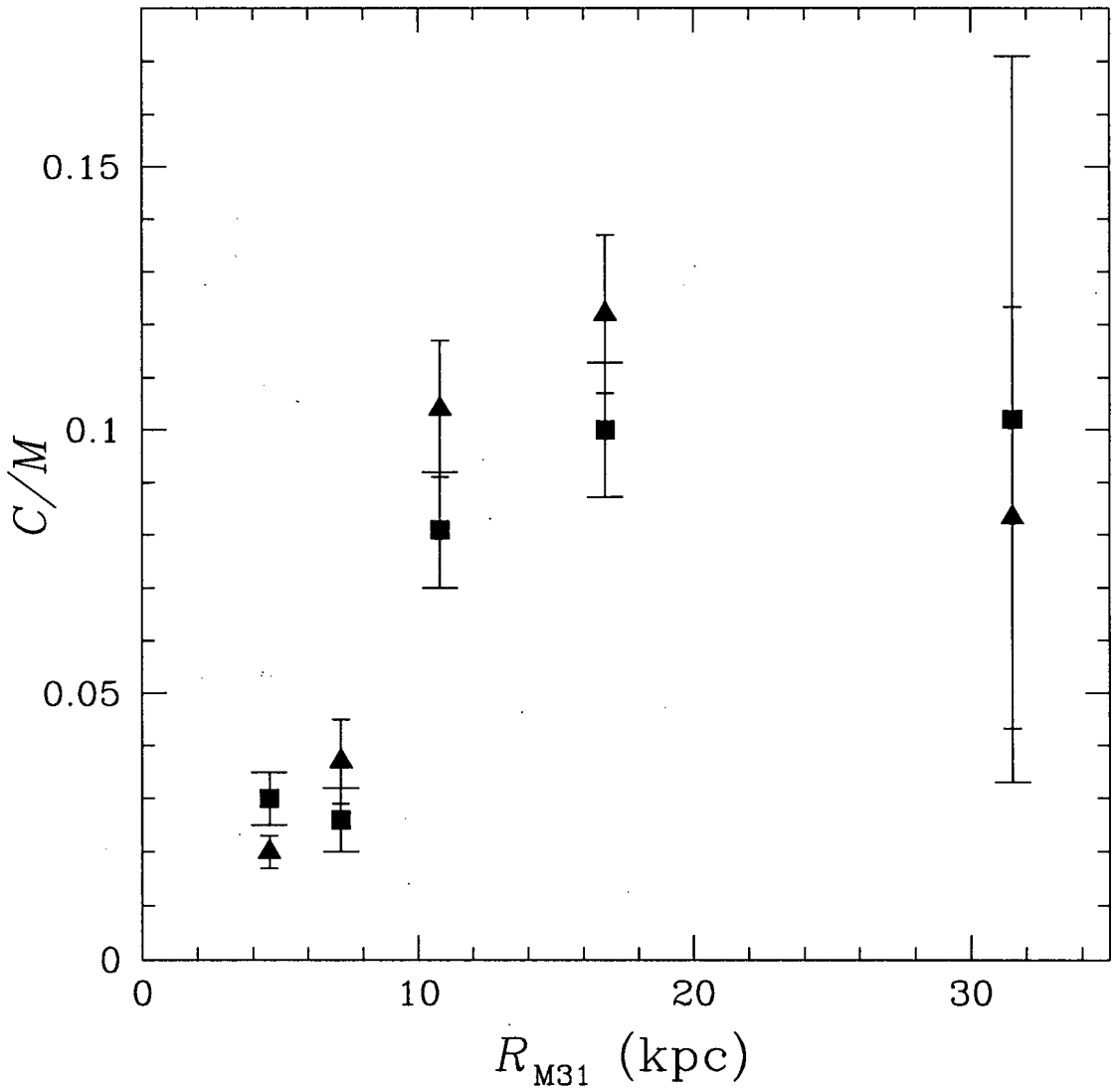

Figure 4.8: The measured C/M ratios in the five M31 fields as a function of R_{M31}. The C- and M-stars were selected according to the photometric criteria described in §4.2, and the further colour criteria given in §4.5.2. Triangles are uncorrected ratios, while squares indicate ratios corrected for incompleteness.

Table 4.3) shows that I would have expected them to have found $\sim$ 2 C-stars in their inner, and $\sim$ 6 C-stars in their outer field. Given this, I am surprised that Cook *et al.* (1986) found only one C-star in their outer field. Cook *et al.* (1986) state that the magnitude limit of their survey is $M_I = -4.4$ while as discussed in §4.3 the mean magnitude of C-stars is around $M_I = -4.75$. It appears that the low C-star surface density found by Cook *et al.* (1986) is not a result of an I magnitude limit, and I instead suggest that it is a result of a magnitude limit in one of the other bands.

- RCP90 looked at two 2.'2 $\times$3.'5 disk fields; one in BF IV at $R_{\rm M31} = 20$ kpc was observed through CN, TiO, V and I filters, while the other, at $R_{\rm M31} = 4$ kpc, was observed through V and I filters only. After correcting for field stars, RCP90 obtained a C/M ratio for their field at 20 kpc of 6/39, which was identical, within the errors, to the ratio found in the field at 11 kpc by RC85. This result was unanticipated by RCP90; if the C/M ratio depended solely on metallicity a much higher ratio ($\sim$0.3) would have been expected in the outer field if the metallicity gradient of Blair *et al.* (1982) was extrapolated out to the field at 20 kpc. This result was attributed by RCP90 to either small number statistics, a flattening out of the metallicity gradient or to star formation differences.

I note in passing that the total area covered by all previous FBPS surveys in M31 was 17 $\Box'$, while in my study I have surveyed an area of 245 $\Box'$.

4.5.4 The C/M Ratio and Star Formation History

In Fig. 4.1 I plotted ($CN-TiO$, $V-I$) TCDs for the five M31 fields. The panels for Fields 1 and 5 show that it is possible that the C-star candidates in these two fields are

being misidentified due to photometric errors. If this is the case, and there are no C-stars in Fields 1 and 5, then it appears that these fields are either very metal-rich or ceased star formation sufficiently long ago that stars now ascending the AGB fail to undergo thermal pulsing. The latter possibility seems unlikely in Field 1 as it does contain bright AGB stars (see Fig. 3.7). Field 5 also contains bright AGB stars (Fig. 3.7) though, after correction for foreground stars, at low levels. Spectroscopic confirmation of C-stars in Field 5 will rule out the possibility that this field has an old population which is incapable of undergoing thermal pulsing. As I have no spectra of the C-star candidates in Field 5, I use the data *primae facie*, assuming the C/M ratios measured in Fields 1 and 5 to be correct.

In §3.5 I derived AGB LFs for the five fields and was able to show that significant differences existed between them. Comparing these (Fig. 3.8) with the C/M ratios in Fig. 4.5 I see no simple correlation. For example, Field 3 has the shallowest AGB LF and a strong blue component, indicative of ongoing star formation, though has a lower C/M ratio than Field 4. I conclude that if star-forming history plays a role in determining the C/M ratio in M31, then it is a secondary factor. Consequently, I can say that age, and hence mass, is of secondary importance in determining the C/M ratio in M31.

4.5.5 The C/M Ratio: An Alternative Abundance Indicator?

The increase in the C/M ratio with $R_{\rm M31}$ is as expected if: (1) the C/M ratio is inversely correlated with metallicity; and (2) if the metallicity in M31 is inversely correlated with $R_{\rm M31}$. An anticorrelation between metallicity and galactocentric distance has been previously observed in many spiral galaxies (see Dinerstein 1990 for a review), including M31.

Before pursuing the correlation between C/M ratio and metallicity any further, I

first dismiss an alternative interpretation of the data presented in Fig. 4.5. The data in Fig. 4.5 could be construed as showing that there are two values for the C/M ratio in M31, one for the bulge (inner two data) and one for the disk (outer three data). I note however that the effective radius of the bulge of M31 is around 2 kpc (Walterbos & Kennicutt 1988) whereas the inner two fields lie at $R_{\rm M31} = 4.6$ and 7.2 kpc respectively.

The metallicity gradient in M31 has been investigated by Dennefeld & Kunth (1981) and Blair *et al.* (1981, 1982). As pointed out by Blair *et al.* (1982, hereafter referred to as BKC82) M31 has often been neglected for abundance studies due to its inclination and relative lack of large, bright, H II regions. In the most recent study (BKC82) abundances were derived using both supernova remnants (SNRs) and H II regions. BKC82 measured a consistent gradient for N using both SNRs and H II regions, but found that whereas H II regions showed an O gradient, SNRs did not. BKC82 attributed the inconsistency to problems with the SNR shock model. This result aside, they found that in M31 both N and O abundances decreased by a factor of 4 between $4 \lesssim R_{\rm M31} \lesssim 23$ kpc.

How well do estimates of the metallicity in the fields (derived from the C/M ratios) compare with the (O/H) measurements of BKC82? I obtain estimates for [m/H][2] in the fields from an unweighted least-squares fit to data from Table 5 of Pritchet *et al.* (1987), which I show in Fig. 4.9. The fit gives the expression

$$[\mathrm{m/H}] = -0.53 \log(\mathrm{C/M}) - 0.49 \qquad (4.1)$$

for [m/H] in terms of the C/M ratio. Assuming that in the fields [m/H] = [O/H][3] (note my nomenclature: (O/H) is the number ratio, while [O/H] is the logarithm of

[2]In the following discussion I use [m/H] in a very general sense to mean enrichment.

[3]It is known that the solar composition of elements *is not* found in all stars. For example, population II stars are enhanced in α-elements such as oxygen. However, as I have mentioned, BKC82 found a similar abundance gradient for both O (an α-element) and N (not an α-element) in the disk of M31, indicating α-element enhancement is not a strong function of $R_{\rm M31}$. For the purposes of my work, I simply assume that the gas from which the stars in M31 formed had solar abundance ratios.

the abundance relative to solar values), and adopting a value of 6.6×10^{-4} for the solar number ratio of (O/H) (Allen 1976), I have

$$(\mathrm{O/H}) = 6.6 \times 10^{-4}(10^{[\mathrm{m/H}]}) \tag{4.2}$$

for (O/H) in the fields. In Fig. 4.10 I show a comparison between the (O/H) gradient derived by BKC82 and that using the C/M ratio as derived above. As can be seen, reasonable agreement is seen up to the limit of the BKC82 data. Beyond the limit of the BKC82 data, *the Field 5 datum suggests that the metallicity gradient flattens out.* Indeed, the BKC82 data does show evidence of flattening for $R_{\mathrm{M31}} > 15$ kpc. I strengthen the suggestion made by RCP90 that the metallicity gradient in M31 flattens out.

The above result is of importance for two reasons. Firstly, the C/M ratios show the metallicity *gradient* in the disk of M31 as it was a few Gyr ago when the AGB stars formed, in contrast to H II regions which shows the metallicity gradient at the present epoch. (N.B. Figure 4.9 provides a calibration of the C/M ratio against present-epoch abundance. This figure shows that all the galaxies in Fig. 4.9 have undergone similar, possibly zero, chemical evolution during the last few Gyr.) The agreement between (O/H) ratios derived from H II regions and C/M ratios implies that no significant evolution of the metallicity gradient (such as a flattening or reversal) has occurred in M31's disk during the last few Gyr. As discussed by Peimbert (1995), PNe can provide information about past abundances. Observations of PNe will allow the question of whether the abundance in M31's disk has evolved over the last few Gyr to be addressed.[4] Secondly, knowledge of the abundance gradient can be used to constrain models of galaxy formation. For example, using a star-forming viscous disk model for spiral galaxy disks, Zaritsky (1992)

[4]Maciel & Köppen (1994) have determined the radial abundance gradients of O/H, Ne/H, S/H, and Ar/H for Galactic disk PNe and shown them to be generally similar and of the same order of magnitude as the O/H gradient displayed by Galactic H II regions.

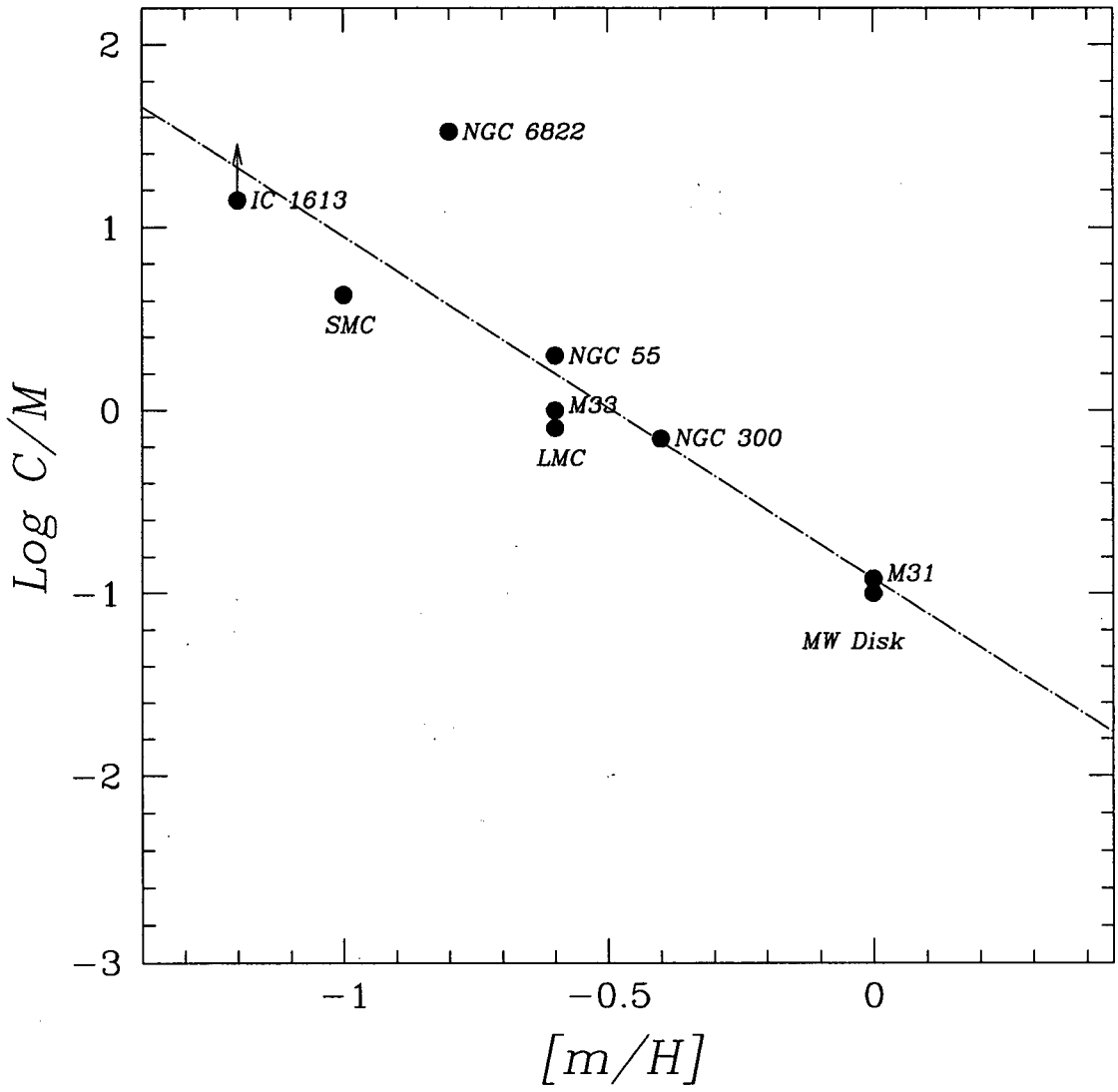

Figure 4.9: Circles show data from Table 5 of Pritchet *et al.* (1987). The broken line shows the least-squares fit to the data used to derive (O/H) in Fig. 4.10.

predicts that the radial abundance profile of a non-interacting unbarred spiral galaxy changes slope at a radius where the rotation curve changes from linearly rising to flat. In M31 this happens at 30′-40′ (Rubin & Ford 1970) which corresponds to $R_{\rm M31} = 6$ to 8 kpc. The steep rise in the C/M ratio from Field 2 to Field 3 and the slower rise from Field 3 to Field 4 provides tantalizing evidence that a manifestation of such an effect is being seen in M31.

Turning some of the above arguments around, I can use the BKC82 data to obtain metallicity estimates in the fields and see how well the data fit the trend from Pritchet *et al.* (1987) shown in Fig. 4.9. In Fig. 6 of BKC82 a fit is given to the (O/H) ratio measured in M31 which I include in my reproduction of this figure in Fig. 4.10. Using this fit I derive the expression

$$[\mathrm{O/H}] = \log(-0.076 R_{\rm M31} + 2.1) \tag{4.3}$$

for the abundance in the disk of M31 relative to solar. This equation is only valid for the range of BKC82's data ($23 > R_{\rm M31} > 4$ kpc). In Fig. 4.11 I plot data from Table 5 of Pritchet *et al.* (1987) as well as data from my inner four fields. In Fig. 4.11 the Field 5 datum is excluded as a metallicity value cannot be derived for this field by extrapolation of BKC82's fit to their data. As pointed out by Pritchet *et al.* (1987), the data in their Table 5 were derived using varying definitions of both M-stars and metallicity. Nonetheless, Fig. 4.11 clearly shows that the new, internally consistent, measurements of C/M ratio in M31 follow the relationship that is seen to hold over *4 dex* in (C/M) and *1.5 dex* in [m/H] for the many types of galaxies in Fig. 4.11. From this I conclude that *it is metallicity and not galactic morphological type that determines the C/M ratio.*

Reid & Mould (1985) found evidence for variations in the C/M ratio between LMC

fields.[5] Although their statistics were poor, their data suggest that the C/M ratio *decreases* with distance from the LMC's bar. If the decrease in the C/M ratio is attributed to a metallicity gradient, then the C/M ratios indicate that the LMC's bar is less enriched than its outer regions. This is contrary to the findings of Pagel *et al.* (1978) who found, from a study of H II regions, marginal evidence for a metallicity gradient in the opposite sense to this. As Reid & Mould (1985) point out, it is hard to envisage a mechanism that selectively enhances the metallicity in regions well away from the main site of star formation. This led Reid & Mould (1985) to suggest that the differences in the C/M ratio were independent of metallicity and that differing star formation histories were a plausible way of accounting for the observed ratios. My M31 observations lend little support to this suggestion; as previously discussed the star forming history in my fields appears to have *no bearing* on the C/M ratios measured in those fields. To resolve whether the C/M ratio in the LMC is really driven by star formation differences, an extensive survey of C- and M-stars in the LMC is needed to eliminate the effects of small number statistics.

4.5.6 Reasons for the Correlation

Why is the C/M ratio correlated with metallicity? The C/M ratio data from this and other surveys can be explained if either: (1) the number of M-stars decreases with metallicity; (2) the number of C-stars increases with metallicity; or (3) a combination of (1) and (2). A physical reason for the first of these possibilities is that in a metal-poor environment the colour of the AGB will be shifted bluewards and hence fewer stars will appear as M-types. Under this hypothesis, it is expected that the number of C-stars will

[5] Owing to its slight metallicity gradient, the LMC is far from being the ideal system in which to look for variations in the C/M ratio induced by differing metallicities. However, as I discuss in §11.1, M33 has a strong metallicity gradient and makes an ideal candidate for future observation.

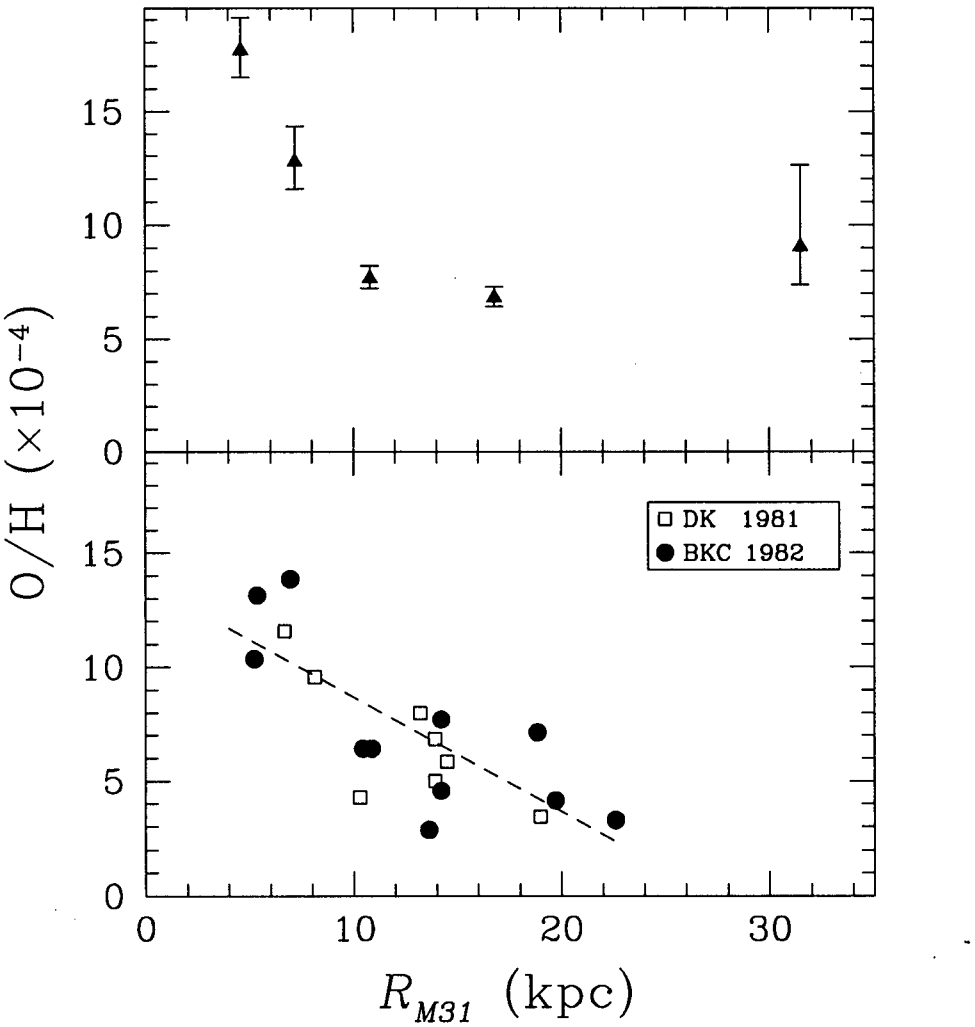

Figure 4.10: The data in the lower panel are from Fig. 6 of BKC82. The solid circles are measurements made by BKC82, while the open squares are data from Dennefeld & Kunth (1981). The dashed line is the fit of BKC82 to their (solid circles) data. The upper panel shows the number ratio of (O/H) derived from the C/M measurements. A full description of how these abundances were derived is given in the text. The errors shown in the upper panel were derived by propagation of the Poisson errors in the C/M ratio through eqs. (4.1) and (4.2).

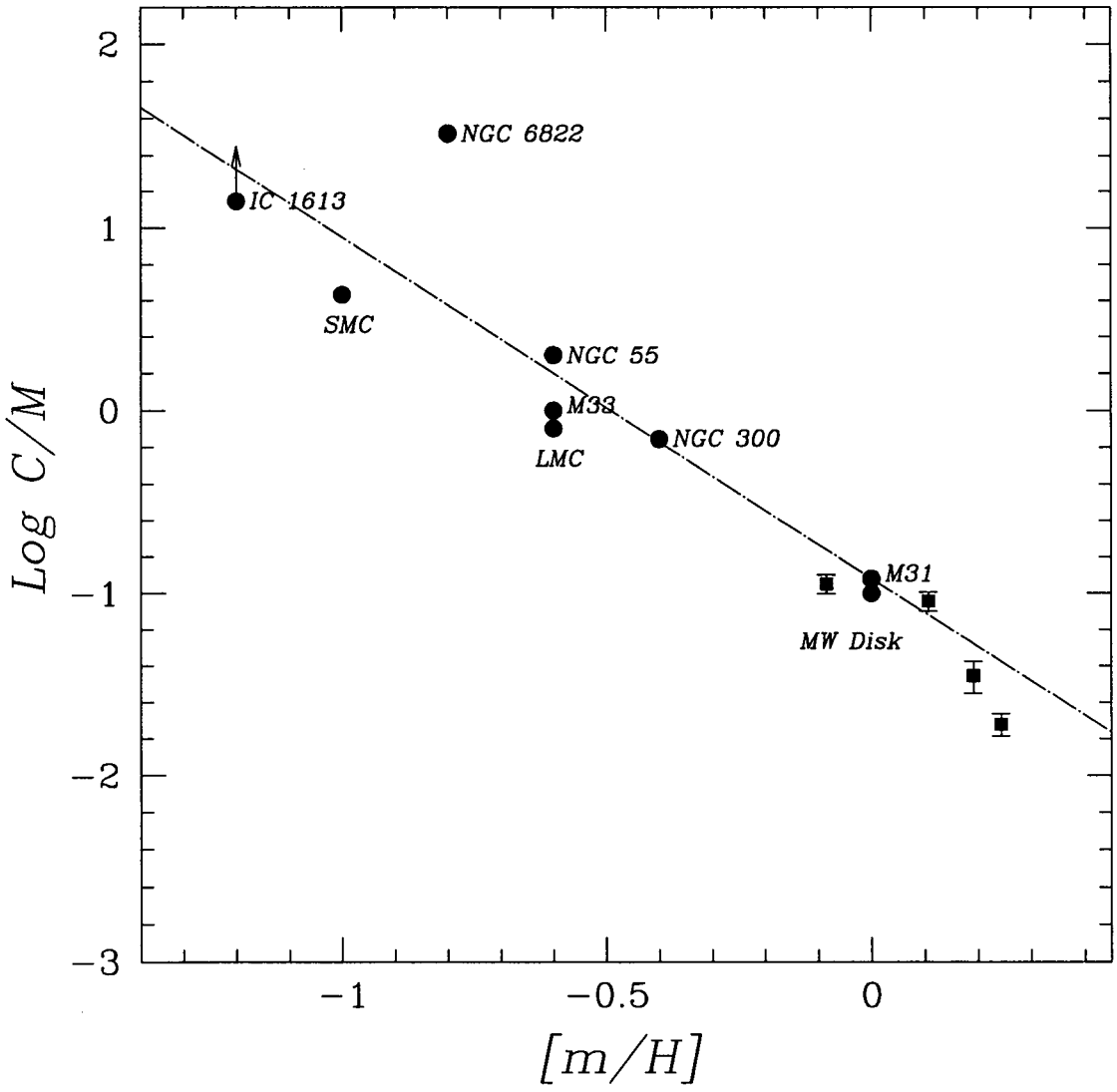

Figure 4.11: Circles are data from Table 5 of Pritchet *et al.* (1987) and squares are data from this study. From left to right the squares are data for Fields 4 to 1 and have been placed using my C/M ratios and metallicity estimates from BKC82 (see eq. 4.3). The vertical error bars on the solid squares are Poisson errors associated with the C- and M-star counts. The broken line shows the least-squares fit to the data from Fig. 4.9.

be proportional to the integrated luminosity of the field (there being a constant proportion of AGB stars which are C-stars). This hypothesis is clearly ruled out by the C-star counts from Fields 1 and 2. As the AGB colour has, at most, only a minor effect on the observed C/M ratio, I look to an increase in the number of C-stars with decreasing metallicity as an explanation for the correlation.

From the data it appears that C-stars have an affinity for metal-poor environments, and I introduce the neologism *mepephiles* (lovers of MEtal-Poor Environments) to describe them. That C-stars are mepephiles may be explained by it being easier to turn a metal-poor AGB star into a C-star, since (1) a metal-poor star will have a less extended envelope and so a shallower convection envelope will cause third dredge-up, and (2), in a metal-poor star, less C needs to be dredged up to drive C > O. As discussed by Scalo (1981) preliminary theoretical models *do* produce a variation of C/M in the right direction, though the variations are *too small by orders of magnitude* when compared to observations.

A competing explanation for why C-stars are mepephiles is that metal-rich C-stars have high mass-loss rates, leading to them either: (1) being short lived compared to their metal-poor counterparts; or (2) evolving into infrared C-stars which remain undetected in my survey. In a recent review of mass-loss on the AGB, Jørgensen (1992) mentions that:

> "An estimate of the corresponding molecular levitation effect for stars of lower metallicity has shown that a decrease in the metallicity by an order of magnitude, relative to the solar value, also decreases the radiative force by an order of magnitude. If levitation by radiative force on molecules is (one of) the triggering mechanism(s) for high-efficiency mass loss in red giants, it

> follows that much higher values of C/O will be reached by carbon stars in low-metallicity galaxies than in the solar neighbourhood (and hence that the relative impact on chemical evolution was even greater in the past). This fact may be part of the explanation of why the number ratio of carbon stars to M-type giants is a decreasing function of metallicity, as observed, for example, by Richer and Westerlund (1983)."

Theory should help guide us here. For example, if it can be shown that the time taken for third dredge-up to turn a metal-rich AGB star into a C-star is only slightly longer (compared with the lifetime of the C-stars) than the time taken to turn a metal-poor AGB star into a C-star, then the mass-loss explanation is more likely. Two observational studies which may help cast light on the matter are: (1) a search for infrared C-stars in the M31 fields. Frogel & Richer (1983) found a lack of luminous infrared C-stars in an LMC field, suggesting that luminous AGB stars undergo high mass-loss rates and are consequently short lived. A similar study in M31 will allow the role of metallicity in mass-loss rates to be better understood. For example, it would be of interest to investigate how the C/M ratio changed with $R_{\rm M31}$ when infrared C-stars were included; and (2) an investigation of how the ratio of C- to O-rich PNe varies with $R_{\rm M31}$. If the C/O PNe ratio tracks the C/M star ratio then the variation is a metallicity effect, whereas if the ratios are uncorrelated (for example the C/O PNe ratio remains constant) other causes such as lifetimes are involved in determining the C/M ratio. An extensive catalog of PNe in M31 already exists (Ford & Jacoby 1978), although obtaining carbon abundances for PNe is difficult, requiring ultraviolet spectra and HST observations (Jacoby 1994). In the following section I discuss some evidence which suggests that the ratio of C-rich to O-rich PNe *does* track the C/M ratio.

4.5.7 The Post-AGB Connexion

What becomes of AGB stars? The standard picture of stellar evolution suggests that an AGB star will expel an envelope of material which becomes a PN, and leave behind a remnant core which quickly evolves to a white dwarf.[6] Given this, it is interesting to enquire about carbon abundances in PNe to see if they can tell us anything about the evolutionary status of the AGB stars from which they formed.

Kingsburgh & Barlow (1994, hereafter referred to as KB94) present spectrophotometric observations for a sample of 80 southern Galactic PNe. Some of their optical observations were supplemented with UV data, and for 20 PNe KB94 were able to derive both carbon and oxygen abundances. Figure 9 of KB94 is a plot of log(C/O) versus log(O/H) for the 20 PNe with carbon abundances. I reproduce this plot in Fig. 4.12 and include on it a dashed line which separates the C-rich (C/O > 1) PNe from the O-rich (C/O < 1) PNe. As I have indicated by the labels on Fig. 4.12, PNe with C/O > 1 are expected to be the progeny of C-stars, while conversely PNe with C/O < 1 are expected to be the progeny of M-stars. The solid points in Fig. 4.12 represent "Type-I" PNe in which dredged-up carbon has been converted to nitrogen by envelope burning. Envelope burning is believed only to occur in the more massive of AGB stars. The Type I PNe confuse the issue somewhat, as they may have evolved from M-stars to C-stars and then back to M-stars. In the following discussion I ignore the Type I PNe, noting that this makes little difference to my conclusions. Why is Fig. 4.12 of any interest? Below I discuss what I feel are two important conclusions that can be drawn from Fig. 4.12.

How does the ratio of C-rich to O-rich PNe compare to the C/M ratio? To answer this question I note that the mean value of log(O/H) for the PNe in Fig. 4.12 is –3.35,

[6]Here I have painted a very simple picture of a very complicated subject. I recommend to the reader Iben (1995) as an excellent review on the origin and evolution of PNe.

which is 0.3 dex more metal-poor than the solar value given by KB94 in their Table 13. Using Fig. 4.9 it is found that this metallicity corresponds to a C/M ratio of around 0.40. Excluding Type I PNe, the ratio of C-rich to O-rich PNe is $7/9 = 0.77 \pm 0.38$ (error from the propagation of Poisson errors). One can see that there is agreement (albeit very marginal) between the estimated C/M ratio and the ratio of C-rich to O-rich PNe. Further evidence that the C/M ratio is in agreement with the ratio of C-rich to O-rich PNe comes from the observations of Walton *et al.* (unpublished) who found that all of the PNe they observed in the Magellanic Clouds (excluding Type I PNe) have $C/O > 1$. That the relatively metal-poor LMC has a greater proportion of C-rich PNe than the Galaxy strongly suggests that *the reason the C/M ratio changes is unassociated with the relative lifetimes of C- and M-stars, but is due to a physical mechanism that prevents metal-rich stars from evolving to C-stars.*

As pointed out by KB94, oxygen is neither created nor destroyed by nucleosynthesis reactions during the lifetime of the PN progenitor star, and so is a good indicator of the progenitor star's metallicity. Considering the abscissa of Fig. 4.12 as a measure of metallicity, one might then assume to find more C-rich PNe at lower metallicities. No such trend is apparent in the data and, if anything, an opposite trend is seen. The range covered by log(O/H) is rather small ($\sim$ 0.3 dex) and it is feasible that such a trend may be lost in the scatter. Taking the observations of Walton *et al.* (unpublished) into account, I make the prediction that as more data are added to Fig. 4.12 a trend will be seen where the C-rich PNe are found at lower values of log(O/H).

If the differing C/M ratios were due to a lifetime effect, it might be expected that the material returned to the ISM by AGB stars is similar in all parts of M31. The PNe indicate that the C/M ratios are caused by a physical mechanism that prevents the formation of C-stars in metal-rich environments, and consequently that the C/M ratio

will have an effect on the composition of the ISM, a point I take up in Chapter 5.

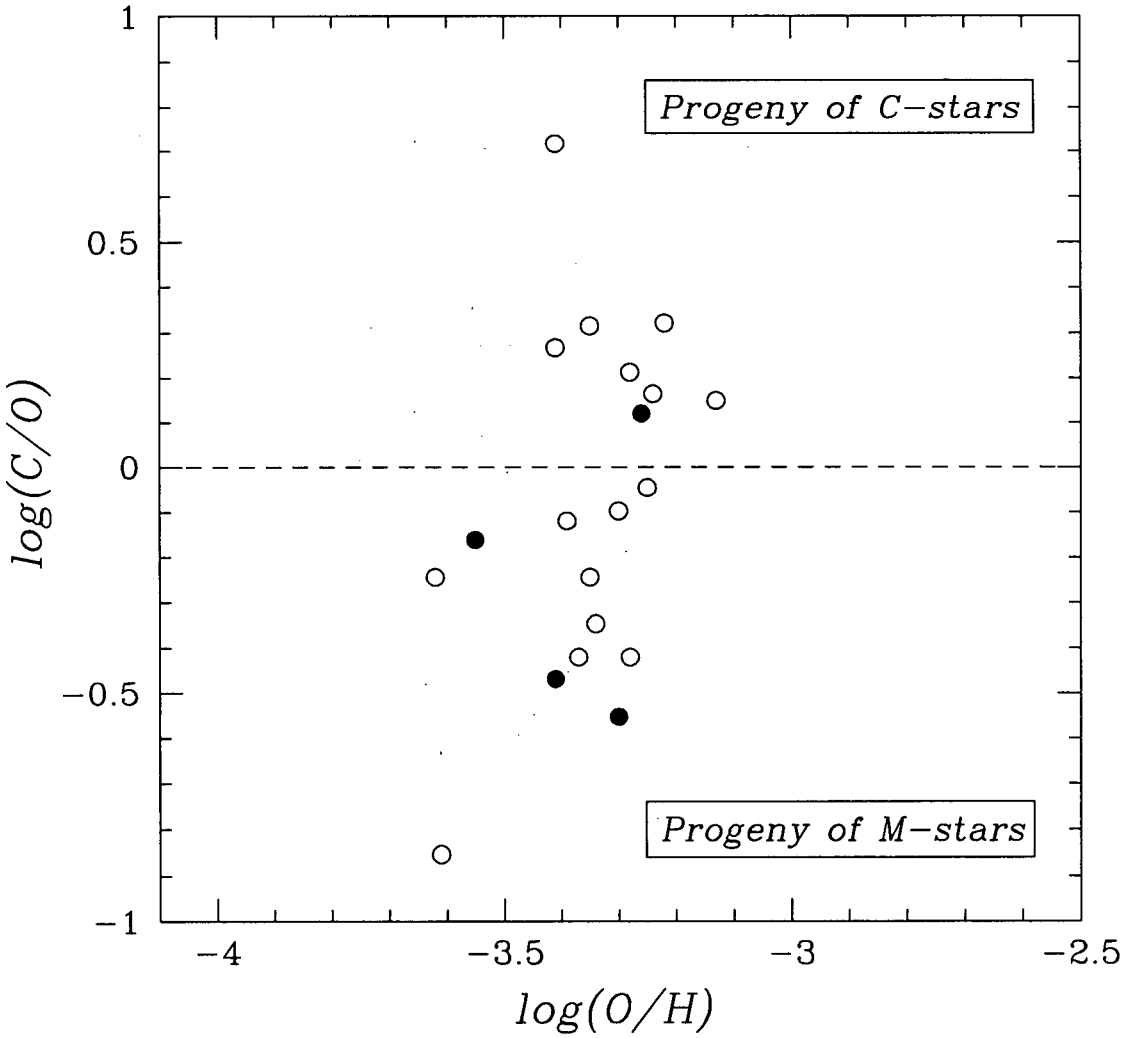

Figure 4.12: This figure is a plot of log(C/O) versus log(O/H) for Galactic PNe from KB94. The plot is identical to Fig. 9 of KB94 with the exception of the horizontal dashed line which I have added to discriminate between the C-rich (C/O > 1) PNe and the O-rich (C/O < 1) PNe, and the labels indicating the likely progenitors of the PNe.

Chapter 5

MANIFESTATIONS OF THE C/M RATIO ON THE ISM

"There is something fascinating about science. One gets such wholesale returns of conjecture out of such a trifling investment of fact."

Mark Twain (1835 – 1910)

Using IRAS data, Thronson *et al.* (1987) demonstrated that the highly-evolved C-rich and O-rich stars in the Galaxy have different surface densities as a function of Galactocentric distance (see their Fig. 6). The sense of this relationship is an increasing ratio of C-rich to O-rich stars with Galactocentric distance, in the same sense as the variation of the C/M ratio in M31. Thronson *et al.* (1987) note that O-rich stars will be siliceous-grain generators whereas C-rich stars will produce carbonaceous grains.[1] They note that though the change in elemental abundances may be modest (depending on the poorly understood roles of novae and supernovae in ISM enrichment), the grain composition will have a strong radial variation in the Galaxy. Thronson *et al.* (1987) mention three areas in which the varying grain composition might be expected to have an effect. Briefly, these are:

1. temperature regulation of dense molecular clouds. This will affect star formation and lead to the IMF being position-dependent.

2. extinction laws. As the grain composition varies as a function of position in the Galaxy, there would be no universal interstellar extinction law.

[1]Indeed, C-star atmospheres may be veritable laboratories for the production of carbon compounds. Barnbaum (1994) mentions that as well as carbonaceous grains and chains, exotic molecules such as buckminsterfullerenes may be formed. Also, as noted by Anders & Zinner (1993) the laboratory conditions needed to form diamonds by chemical vapour deposition are remarkably similar to the conditions found in C-star atmospheres!

3. molecular cloud chemistry.

To these I add a fourth area in which I believe grain composition may have an effect:

4. the ratio of diffuse interstellar band (DIB) strength to interstellar reddening. Such a correlation may arise if DIBs are caused by carbonaceous grains, which I expect to be more dominant at greater galactocentric distances in both M31 and the Milky Way Galaxy.

Having shown that the C/M ratio varies in M31, I expect the phenomena described above to be present in M31. In §5.1 I look for a connexion between DIBs, reddening, and Galactocentric distance, while in §5.2 I cite evidence in favour of a connexion between the C/M ratio and extinction laws in M31.

5.1 DIBs and C-stars: A Cosmic Connexion?

DIBs are broad absorption features seen in the spectra of stars. From observations of binary stars these absorption features have been shown to have their origins in the ISM. It is found that, to first order, DIB strength is correlated with interstellar reddening. However, the large dispersion in plots of DIB strength against interstellar reddening has been shown to be intrinsic, and not caused by random errors. This suggests that the DIB strength depends on dust properties which have little bearing on the dust's gross absorption properties. I direct readers interested in more than my basic outline to the excellent review article by Herbig (1995).

Recently, as discussed by Herbig (1995), DIBs have been produced in the laboratory by containing complex carbon based compounds in a matrix of neon. If, as this suggests, at least some of the DIBs are due to organic compounds, then an increase in the ratio

of DIB strength to interstellar reddening (hereafter referred to as DIB/E_{B-V}) may be expected with $R_{\rm M31}$, owing to the C/M ratio increasing with $R_{\rm M31}$.

I propose that if the C/M ratio plays a significant role in determining the content and morphology of carbon in the ISM, and (some) DIBs are caused by carbon compounds, the strength of (some) DIBs in M31 relative to interstellar reddening will be correlated with $R_{\rm M31}$.

Unfortunately no investigation of DIBs in M31 has ever been undertaken. Indeed, extragalactic DIBs have only been observed in the Magellanic Clouds and NGC 5128, and these data are very limited (Herbig 1995). Nonetheless, I can use the varying C/M ratio in the Galaxy to test this idea. Blanco & McCarthy (1981) were the first to point out the enormous change in the C/M ratio in the Galaxy. They found the C/M ratio in the bulge to be 0.002, compared to a value of 0.01 in the solar neighbourhood.[2] Such a variation of C/M ratio is expected in the Galaxy given that it has a metallicity gradient of around -0.05 dex kpc^{-1} in the solar neighbourhood (Pagel & Edmunds 1981). As the C/M ratio in the Galaxy increases with Galactocentric distance (hereafter, in analogy with $R_{\rm M31}$, referred to as $R_{\rm MW}$) we may expect the ISM at greater $R_{\rm MW}$ to have a relatively greater carbon content, and hence produce a larger DIB/E_{B-V} ratio.

To test the above idea, I combined measurements of the 4430Å DIB, E_{B-V}, and spectral type from Walker (1963) with Galactic coordinates and apparent magnitudes from Snow *et al.* (1977). Spectroscopic parallax was used to calculate heliocentric distances to the stars on whose spectra the DIBs were superimposed and, assuming the absorbing material responsible for the DIBs to lie midway between us and the star, simple geometry provided values of $R_{\rm MW}$ for the absorbing material. Walker's (1963) measurements of

[2]RC85 claim a value of about 0.1 for the C/M ratio in the solar neighbourhood, and from an inspection of Blanco (1965) it appears the value of 0.01 may be a typo. Indeed, a C/M ratio of 0.1 would be expected from the metallicity C/M ratio relationship presented in Fig. 4.9.

the DIBs were all converted to his "Cambridge" system, and values of DIB/E_{B-V} were calculated for those stars with $E_{B-V} > 0.20$. Figure 5.1 is a plot of DIB/E_{B-V} against $R_{\rm MW}$ for these stars and shows no evidence of a correlation (correlation coefficient of 0.21) between $R_{\rm MW}$ and DIB/E_{B-V}. Visually, a "lower envelope" of points can be seen in Fig. 5.1. However, given the few stars observed at $R_{\rm MW} > 10$kpc, I attach little significance to this.

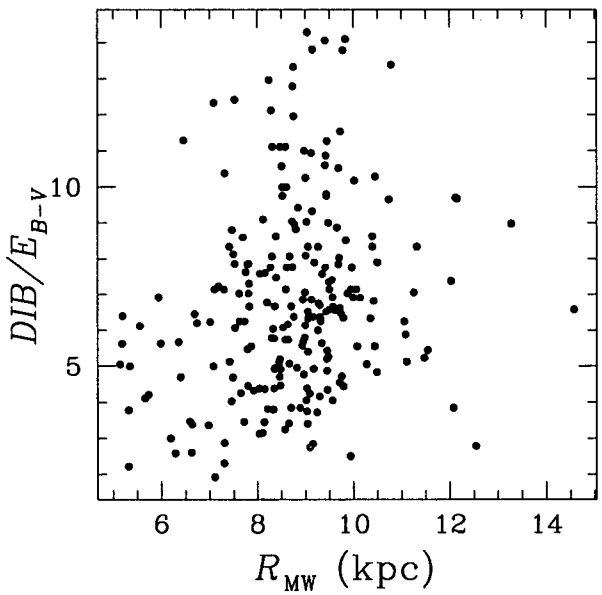

Figure 5.1: In the above plot I show DIB/E_{B-V} as a function of $R_{\rm MW}$. The stars are from Walker's (1963) sample and have $E_{B-V} > 0.20$.

There may be no correlation between DIB/E_{B-V} and $R_{\rm MW}$ for two reasons. Firstly, it may be that the $R_{\rm MW}$ range of the data is too small for the effect to show up, and secondly the 4430Å DIB has not yet been verified as being caused by a carbon compound, leading to the possibility that there is no correlation for this particular DIB. It may also be that there is intrinsically no correlation, as would be caused if the metal-rich C-stars have shorter lifetimes, and the C/M ratio had no bearing on the ISM composition.

An investigation of DIB/E_{B-V} as a function of $R_{\rm M31}$ (observational difficulties aside) would be of interest as it would allow the effect of a greater range of C/M ratio to be assessed. My hypothesis could also be tested by undertaking a Galactic survey, which encompassed a large range of $R_{\rm MW}$, of a DIB which is strongly suspected of being caused by a carbon compound.

5.2 The C/M Ratio and Interstellar Extinction in M31

As noted by IR83, the different proportions of C-stars in the SMC, LMC and Milky Way should translate into different relative proportions of carbonaceous- and siliceous-grains in the interstellar medium (ISM) of these galaxies. They mention that the differences between the UV extinction curves of these three galaxies correlate with their C-star abundances. If extinction laws are affected by the grain composition, as this suggests, then a correlation between C/M ratio and extinction laws would be expected. In M31, the radial dependence of the C/M ratio would lead to the extinction law varying with $R_{\rm M31}$.[3]

Leonard Searle (1982) studied globular clusters in M31 and, using reddening free parameters, showed that the reddening law varied systematically with $R_{\rm M31}$. In a later review of this work (Searle & Thompson 1985) it is stated that the extinction in the violet (for a given $(V-K)$ reddening) decreases with $R_{\rm M31}$, and the following speculation is given for the origin of this relationship:

> "The dust responsible for interstellar reddening is thought to have been formed in, and then ejected from, the atmospheres of cool evolved giant stars.

[3] *Caveat emptor:* Cardelli (1994) attributes deviations in ultraviolet extinction laws to changes in the ISM such as grain growth, destruction and changes in grain size distribution and *not* to variations in composition.

> There are two common types of such stars, Carbon stars and M stars, whose atmospheres contain free carbon and free oxygen respectively. In the Galaxy, the ratio of these two types of stars is known to vary systematically with distance from the centre of the Galaxy. It seems likely that the radial variation in the dust properties of M31 has its origin in a similar change in the populations of dust producing stars."

Before this study it was known that both the extinction law in M31 and the C/M ratio in the Galaxy varied with galactocentric distance. I can now pull together evidence in favour of a connexion between the C/M ratio and extinction laws by stating that in M31 *both the extinction law and C/M ratio vary with galactocentric distance.* It is interesting to note that Searle (1982) finds a similar reddening law to that in the solar neighbourhood at $R_{\rm M31} = 12$ kpc, while a comparison of the cosmic O/H ratio (Allen 1976) with Fig. 4.10 shows that at $R_{\rm M31} = 15$ kpc the abundance is approximately solar. As mentioned by Searle (1982), it is no surprise that an extinction law gradient in the Galaxy has escaped detection as remote regions in the plane of the Galaxy are heavily obscured and cannot easily be observed. Observational difficulties aside, it would be of great interest to demonstrate that the Galactic extinction law behaves similarly to that of M31.

In their investigation of M31 Cepheids, the variation in M31's extinction law was discussed by FM90. This was of concern to them as an inappropriate extinction law would lead to an erroneous Cepheid distance modulus. Such an error would ultimately be propagated into measurements of the Hubble constant. FM90 mention that the sense of Searle's measured colour excesses is such that the ratio of A_V/E_{B-V} increases with $R_{\rm M31}$, and that such a trend is consistent with the findings of van den Bergh (1968) and

Kron & Mayall (1960). Using realistic estimates of A_V/E_{B-V}, FM90 found the effects of a varying extinction law to lie within the noise of their data.

How can the dust composition physically affect the extinction laws? Thronson *et al.* (1987) mention that a common description of interstellar extinction has carbonaceous grains dominating visual and near-infrared extinction, while siliceous grains, with their large mantles, dominate mid- and far-infrared extinction (Draine & Lee 1984). The ratio of A_V/E_{B-V} appears to increase with $R_{\rm M31}$ (FM90 and references within), as would be expected if the C/M ratio, and consequently the abundance of carbonaceous grains, increases with $R_{\rm M31}$.

It would be of great interest to investigate whether M31's extinction law remains unchanged beyond where the C/M ratio flattens out.[4] If the extinction law were found to track the C/M ratio, this would be strong evidence in favour of the C/M ratio determining the grain composition, and the grain composition determining the extinction law.

[4]John Hutchings (presently at the DAO) is working on UV observations of M31 fields taken with the HST (Hutchings 1995). This work will be a powerful lever in studying extinction differences, superseding the unpublished work of Searle. Unfortunately, Hutchings is unlikely to detect my predicted extinction-law "flattening" as he needs observations of young hot stars, and these are not homogeneously scattered throughout the disk of M31.

Chapter 6

SPECTROSCOPIC DATA

"I ask you to look both ways. For the road to a knowledge of the stars leads through the atom; and important knowledge of the atom has been reached through the stars."

Sir Arthur S. Eddington (1882 – 1944)

6.1 Motivation

With the exception of neutrino astronomy, no direct observation of *any* nuclear processes in stars can be made. Although no direct observation of their nuclear processes can be made, AGB stars, like careless criminals, leave behind evidence of their activities. Whereas criminals leave behind fingerprints, AGB stars have spectra which, when read properly, provide indelible evidence of their activities. The evidence left in the spectra of AGB stars can be used to better understand the stars themselves and consequently the areas of astronomy, such as the ISM and the colour evolution of galaxies, where AGB stars play a role.

As noted by IR83, the compositional peculiarities of red giants can basically be split into three types: (1) nonsolar C/O ratios, sometimes accompanied by a low ratio of $^{12}C/^{13}C$; (2) enhancement of *s*-process isotopes; and (3) very large Li overabundances. Current AGB models are capable of producing all of these spectral peculiarities. The AGB models suggest that there is a threshold luminosity (which is both mass and initial-composition-dependent) for each of the processes that leads to a certain spectral peculiarity. Consequently, nuclear processes in AGB stars can be investigated by identifying spectral peculiarities in stars of known bolometric magnitude.

Using Galactic AGB stars to investigate spectral peculiarities has the major drawback that the distance to, and consequently the absolute magnitude of, many of these stars is poorly known. On the other hand, AGB stars in a Local-Group galaxy are, for all intents and purposes, at the same distance and $M_{\rm bol}$ can be obtained for these stars provided their magnitude, colour, the distance to the parent galaxy, and an appropriate bolometric correction are known. Having already identified AGB stars in M31, it is now a natural step to obtain spectra of these; firstly to confirm the validity of the FBPS, and secondly to investigate the evolution of spectral peculiarities.

The M31 C-star spectra I present in this thesis are unique. Indeed, prior to my observations, only one star in M31 had been spectroscopically confirmed as C-type (Mould & Aaronson 1986). The only other similar data to my spectra is that of Richer *et al.* (1979, hereafter referred to as ROW79) who, *over 4 observing seasons*, were able to obtain photometry for 126 stars and spectroscopy for 54 stars in the LMC. The present M31 spectral survey took two nights to obtain and is comparable in size to the ROW79 survey in the comparatively metal-poor LMC.

Two sets of spectral observations were made for this thesis: the CFHT (3.6-m) was used to obtain the spectra in M31, while the 1.85-m Plaskett Telescope at the DAO was used to obtain spectra of C-stars from the compilations of Yamashita (1972, 1975) for comparison. In the following two sections I describe the data obtained from the CFHT (§6.2) and the DAO (§6.3).

6.2 CFHT Data

6.2.1 Instrumentation (CFHT)

The spectroscopic observations were made with the Multi-Object Spectrograph (MOS) at the f/8 Cassegrain focus of the CFHT by myself and Dennis Crabtree. The MOS is designed for multi-aperture spectroscopy over a $10' \times 10'$ field, and achieves its multiplex advantage by using a mask with appropriately cut slits to isolate the stars for which spectra are to be obtained. The detector used was the Loral3 2048^2 CCD, which is a thick device with a blue coating and 15μm pixels. The Loral3 CCD has a quantum efficiency that drops from approximately 45% at 6000Å to 40% at 8000Å. For the observations I used the O600 grism which has a zero deviation[1] of 6010Å and an efficiency that drops from approximately 58% at 5000Å to 37% at 7000Å. The spectra had a 2 pixel resolution of 3.1Å, or $R = \lambda/\Delta\lambda = 2000$ at 6150Å.

A slit length of $11''$ was chosen as a compromise between a larger length, that would improve the fitting of the sky, and a smaller length, that would allow more spectra to be imaged on the CCD. The slit width was $1''.2$, which is suited to the good seeing at CFHT.

To further the multiplex advantage of MOS, I commissioned a filter to be built which truncated the spectra such that two spectra could be 'stacked' along the dispersion axis of the CCD. The bandpass of the filter (5450Å to 6850Å) isolated the yellow-red part of the spectrum and encompassed the diagnostic features I was interested in. The filter (hereafter referred to as the YR filter) had a high transmittance (~95%), and a sharp cut-off with a blocking of 10^{-4} outside its bandpass. With a bandwidth of ~1400Å and a dispersion of 1.55Å/pix, the spectra have lengths of ~900 pixels. To stack 2 spectra,

[1]The zero deviation is the wavelength of light that ends up where white light would end up if no grism was in place.

candidate stars had to be found which were sufficiently separated along the dispersion axis that there was no overlap between the spectra. Finding such pairs of stars proved a difficult task, and the YR filter led only to an extra six spectra being obtained out of a maximum possible of $\sim$70. Of the extra spectra, two were truncated while two overlapped to some extent with their "partner" spectra along the dispersion axis. The YR filter failed to increase the multiplex advantage of the MOS as much as hoped and, with hindsight, is more suited to a fibre fed spectrograph where the relative positions of the stars on the field are unimportant.

To construct the MOS mask, an image of the field was obtained using MOS (with no grism or mask in place) and displayed. An IRAF script was used which, given a star's coordinates and the observational set-up, drew an outline on the field of where the slit would be cut and where the spectrum would fall. My design goal with the masks was to minimize both overlap and unused areas. After selecting those stars for which spectra would be obtained, two bright stars were chosen as references for mask alignment.

6.2.2 Selection (CFHT)

My primary selection criterion was to maximize the number of C-star spectra. The magnitude of the C-stars in M31 ($19 \lesssim I \lesssim 20.8$) meant that to obtain spectra with a reasonable S/N level, an entire night's (6 hours) integration was required for each mask. The two-night run consequently allowed for two masks. By choosing to observe Fields 3 and 4, which have the highest surface density of C-stars (see Table 4.3), I increased the chances of finding C-stars to fill in the unused areas of the CCD. The spectra from Fields 3 and 4 also make an interesting comparison as differences might be expected between their AGB stars owing to the differing star forming histories in these fields. As previously noted, Fields 3 and 4 are both disk fields, though Field 3 has a strong blue component

which Field 4 lacks.

Candidate C-, S-, and M-stars had been previously identified in Fields 3 and 4, though preselection of stars for which spectra would be obtained was impractical due to differences in field size and rotation between the FOCAM and MOS fields. Instead, the stars were selected while at the CFHT. Although I used no rigid selection criteria, I first selected C-stars with a large range in magnitude. The reasoning here is that one of my aims is to investigate spectral peculiarities as a star evolves up the AGB, increasing its core mass and bolometric luminosity. After the C-stars, the next priority went to the few S-star candidates, and the remaining gaps were filled by the ubiquitous M-star candidates. In Figs. 6.1 and 6.2 I show the ($CN-TiO$, $V-I$) TCDs and (I, $V-I$) CMDs of the stars for which spectra were obtained. In some cases, the slit placed on the candidate star encompassed other "serendipitous" stars in the field. Some of the serendipitous stars had incomplete photometry, and are excluded from Fig. 6.1, while serendipitous stars lacking either V or I-band photometry are excluded from Fig. 6.2.

Photometry for all the stars for which I obtained spectra is presented in Tables 6.1 (Field 3) and 6.2 (Field 4). The first five columns of Tables 6.1 and 6.2 contain: in column (1) the slit number; in column (2) the X,Y coordinates of the star (these coordinates can be used in conjunction with the the images on the accompanying CD-ROM to identify the stars); in column (3) the I_0 magnitude; in column (4) the $(V-I)_0$ colour; and in column (5) the ($CN-TiO$) colour. The remaining columns of Tables 6.1 and 6.2 are described in Chapter 8.

6.2.3 Observations (CFHT)

Observations were made on the Moonless nights of September 14/15 and 15/16 1993. An observing log is given in Table 6.3 in which I list: in column (1) the object; in

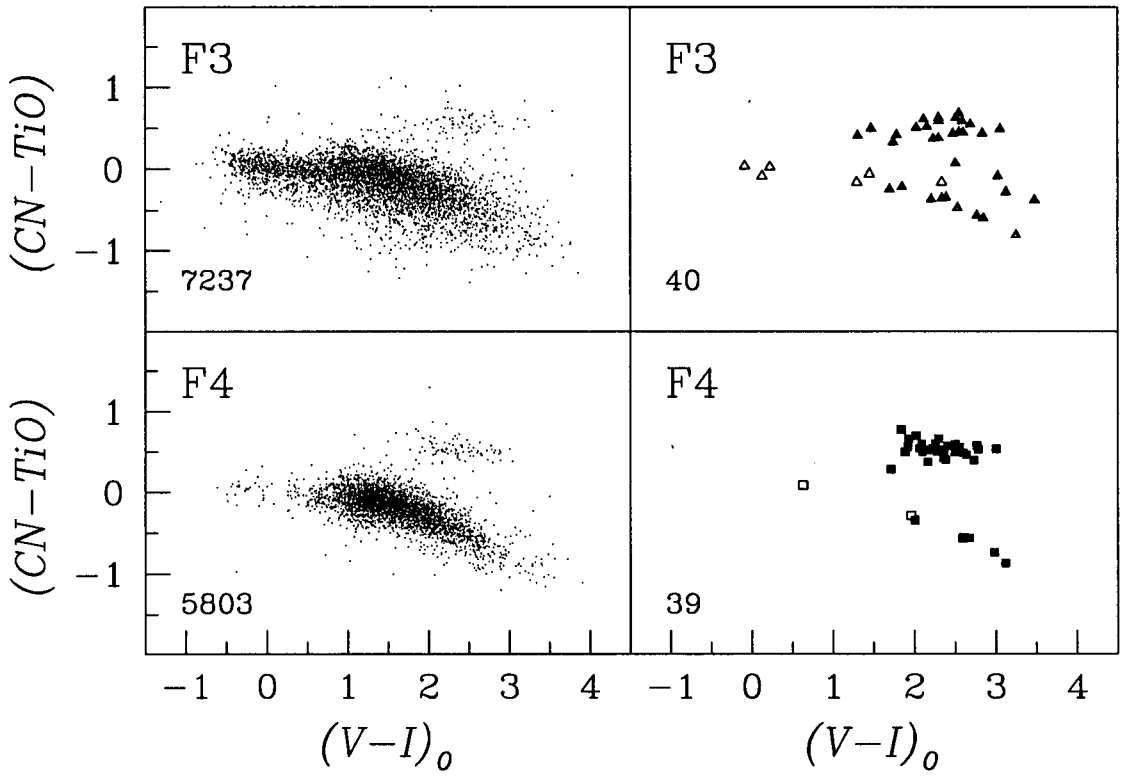

Figure 6.1: The panels on the left are ($CN-TiO$, $V-I$) TCDs for Fields 3 and 4 (cf. Fig. 4.1), while the panels on the right are ($CN-TiO$, $V-I$) TCDs of the stars for which spectra were obtained. Solid points show stars for which I intentionally obtained spectra, while open points are serendipitous stars that happened to lie on the slits. Some of the serendipitous stars had incomplete photometry and are consequently excluded from these diagrams. The numbers in the lower left of each panel indicate the number of stars plotted.

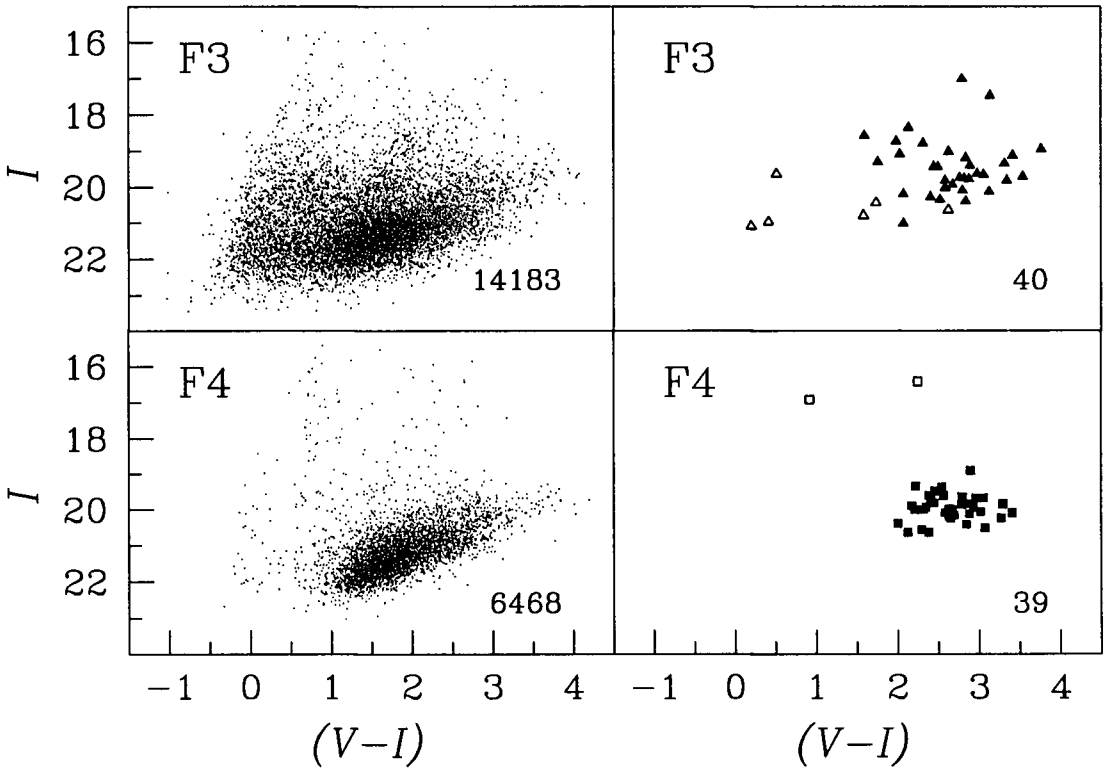

Figure 6.2: The panels on the left are (I, $V-I$) CMDs for Fields 3 and 4 (cf. Fig. 3.1), while the panels on the right are (I, $V-I$) CMDs of the stars for which spectra were obtained. Solid points show stars for which I intentionally obtained spectra, while open points are serendipitous stars that happened to lie on the slits. Some of the serendipitous stars lacked photometry in V or I, and are consequently excluded from these diagrams. The numbers in the lower right of each panel indicate the number of stars plotted.

Table 6.1: Spectral Classification of Field 3 Stars.

Slit/ID	X,Y	I_0	$(V-I)_0$	$(C-T)$	Sp.[a]	FBPS[b]	C_2^{5635}	CN^{5730}	J[c]	Hα[c]	Li[c]
F3–1.1	74, 195	19.76	1.79	0.42	C	?	1.03	0.40	×	×	×
F3–2.1	647, 798	18.86	1.47	0.50	M	?	···	···	···	···	···
F3–3.1	992, 312	20.60	1.79	0.42	M:	?	···	···	···	···	···
F3–4.1	927, 638	19.61	2.30	0.63	C	C	1.02	0.48	:	✓	×
F3–5.1	993, 656	20.41	···	–0.51	?	···	···	···	···	···	···
F3–5.2	1012, 660	19.20	2.69	0.55	C	C	···	···	×	×	×
F3–7.1	1428, 144	19.91	2.24	0.38	C	C	···	···	✓	×	:
F3–8.1	1524, 171	19.20	0.23	0.03	Hot	?	···	···	···	···	···
F3–8.2	1532, 175	19.31	2.48	0.44	C	C	0.75	0.83	×	:	×
F3–9.1	1682, 426	19.96	2.55	0.45	C	C	···	···	×	×	×
F3–10.1	2002, 470	18.35	2.03	0.51	C	?	0.47	0.15	×	:	×
F3–11.1	1955, 803	20.53	···	···	Hot	···	···	···	···	···	···
F3–11.2	1974, 810	18.76	2.55	0.69	C	C	···	···	×	×	×
F3–12.1	1832, 1271	19.66	2.51	0.63	C	C	0.75	0.41	:	×	×
F3–13.1	1817, 1739	19.34	2.59	0.59	C	C	1.19	0.47	×	×	×
F3–13.2	1842, 1752	20.00	1.45	–0.06	M	?	···	···	···	···	···
F3–14.1	1800, 1667	20.36	1.30	–0.16	?	?	···	···	···	···	···
F3–14.2	1824, 1673	19.39	2.30	0.38	C	C	0.91	0.38	×	×	×
F3–15.1	1530, 1450	18.65	1.74	0.33	M	?	···	···	···	···	···
F3–15.2	1561, 1464	20.22	···	–0.46	?	···	···	···	···	···	···
F3–16.1	1262, 1339	19.69	2.84	0.44	C	C	···	···	×	×	×
F3–17.1	1017, 1740	18.97	2.60	0.45	C	C	0.75	0.99	✓	×	×
F3–18.1	832, 1672	19.56	2.30	0.59	C	C	···	···	:	×	×
F3–18.2	848, 1676	19.36	···	–1.05	Hot	···	···	···	···	···	···
F3–19.1	164, 1642	19.38	3.06	0.49	C	C	1.19	0.44	×	:	···
F3–20.1	140, 826	19.84	2.12	0.61	C	C	0.88	0.85	:	×	×
F3–20.2	148, 834	20.56	0.13	–0.08	Hot	?	···	···	···	···	···
F3–21.1	526, 853	18.14	1.31	0.41	M	?	···	···	···	···	···
F3–22.1	137, 609	18.52	3.48	–0.38	M	M	···	···	···	···	···
F3–23.1	108, 561	18.30	1.70	–0.24	Hot	?	···	···	···	···	···
F3–24.2	867, 479	18.92	3.03	–0.08	S	S	···	···	···	···	···
F3–25.1	297, 1904	18.70	3.13	–0.28	M	M	···	···	···	···	···
F3–26.1	464, 117	17.04	2.85	–0.60	M	?	···	···	···	···	···
F3–27.1	96, 1281	16.58	2.51	0.07	M	?	···	···	···	···	···
F3–28.1	237, 1181	19.00	2.16	0.52	C	C	0.95	0.59	:	×	×
F3–29.1	485, 373	19.01	2.21	–0.36	M	M	···	···	···	···	···
F3–31.1	1197, 1859	17.92	1.85	–0.22	M	?	···	···	···	···	···
F3–32.1	1239, 1871	20.73	···	–0.18	M:	···	···	···	···	···	···
F3–32.2	1254, 1875	19.28	3.25	–0.81	M	M	···	···	···	···	···
F3–33.1	839, 1370	19.50	2.39	–0.34	M	M	···	···	···	···	···
F3–33.2	856, 1373	20.67	–0.08	0.04	Hot	?	···	···	···	···	···
F3–34.1	258, 37	19.32	2.53	–0.47	M:	M	···	···	···	···	···
F3–35.1	1453, 658	19.23	2.77	–0.57	M	M	···	···	···	···	···
F3–36.1	1049, 1260	18.59	2.34	–0.35	M	M	···	···	···	···	···
F3–36.2	1060, 1264	20.22	2.34	–0.16	?	S	···	···	···	···	···

[a,b,c] See footnotes on page 101.

Table 6.2: Spectral Classification of Field 4 Stars.

Slit/ID	X,Y	I_0	$(V-I)_0$	$(C-T)$	Sp.[a]	FBPS[b]	C_2^{5635}	CN^{5730}	J[c]	Hα[c]	Li[c]
F4–1.1	114, 474	18.95	2.25	0.60	C	C	1.34	0.87	×	×	×
F4–2.1	487, 762	18.92	1.93	0.67	C	C	0.75	0.44	×	:	×
F4–3.1	363, 696	19.19	2.09	0.60	C	C	2.14	0.65	×	×	×
F4–4.1	412, 665	20.86	···	–0.15	?	···	···	···	···	···	···
F4–4.2	443, 676	19.99	2.56	0.56	C	C	···	···	×	×	×
F4–5.1	638, 539	19.26	2.76	0.58	C	C	···	···	×	×	×
F4–6.1	1044, 208	19.55	2.36	0.43	C	C	0.75	0.20	×	×	×
F4–7.1	1747, 769	16.48	0.63	0.09	Hot	?	···	···	···	···	···
F4–7.2	1762, 776	15.98	1.96	–0.28	M	?	···	···	···	···	···
F4–7.3	1777, 789	19.82	2.37	0.49	C:	C	···	···	×	:	×
F4–8.1	1850, 666	20.09	2.78	0.53	C	C	···	···	×	×	×
F4–9.1	1805, 297	19.39	2.16	0.53	C	C	1.95	1.06	✓	×	×
F4–10.1	1843, 939	19.06	2.22	0.55	C	C	0.42	0.32	×	×	×
F4–11.1	2006, 941	20.20	1.84	0.78	C	C	1.58	0.41	✓	×	:
F4–12.1	2016, 879	19.43	2.50	0.50	C	C	2.11	0.71	×	:	×
F4–13.1	1978, 1223	19.57	2.38	0.41	C	C	···	···	×	:	×
F4–14.1	1890, 1680	19.42	2.60	0.49	C	C	1.22	0.82	×	:	×
F4–15.1	1943, 1606	20.65	···	–0.42	?	···	···	···	···	···	···
F4–15.2	1981, 1626	20.21	2.10	0.51	C	C	1.19	0.58	✓	×	×
F4–16.1	1592, 1755	19.56	2.34	0.54	C	C	1.75	0.75	×	×	×
F4–17.1	1306, 1783	19.75	2.34	0.52	C	C	1.06	0.67	×	✓	×
F4–18.1	1233, 1720	19.48	1.89	0.50	C	C	0.75	0.31	×	:	×
F4–19.1	1116, 1698	19.06	2.17	0.38	C	C	0.75	0.40	:	:	×
F4–20.1	1043, 1412	19.19	2.28	0.51	C	C	1.79	0.44	×	×	×
F4–21.1	902, 1681	20.77	···	–0.40	M	···	···	···	···	···	···
F4–21.2	913, 1684	19.52	2.65	0.47	C	C	···	···	×	:	×
F4–22.1	957, 1085	19.57	1.92	0.56	C	C	1.26	0.44	×	×	×
F4–23.1	997, 899	19.30	2.12	0.53	C	C	1.39	0.77	✓	×	×
F4–24.1	811, 1139	19.64	2.73	0.40	C	C	···	···	×	×	×
F4–25.2	943, 723	19.50	2.06	0.55	C	C	1.62	0.50	:	:	×
F4–26.1	710, 1907	19.97	1.72	0.28	C	?	0.40	0.58	×	×	···
F4–27.1	492, 1504	19.22	2.50	0.59	C	C	0.82	0.51	×	:	×
F4–28.2	413, 1561	19.57	2.02	0.70	C	C	0.81	0.35	✓	×	✓
F4–29.1	354, 1456	19.73	2.41	0.58	C	C	1.51	0.71	×	×	×
F4–30.1	232, 1589	19.67	2.30	0.66	C	C	1.36	0.99	:	×	×
F4–31.1	195, 1046	19.43	3.00	0.54	C	C	···	···	×	×	×
F4–32.1	274, 166	19.27	2.67	–0.56	M	M	···	···	···	···	···
F4–33.1	801, 292	19.67	3.12	–0.87	M:	M	···	···	···	···	···
F4–34.1	829, 289	18.48	2.61	–0.55	M	?	···	···	···	···	···
F4–35.1	1885, 303	19.70	2.59	–0.57	M	M	···	···	···	···	···
F4–36.1	456, 1830	19.81	2.99	–0.73	M:	M	···	···	···	···	···
F4–37.1	40, 1265	20.13	2.01	–0.34	M	M	···	···	···	···	···

[a,b,c] See footnotes on page 101.

Footnotes for Tables 6.1 and 6.2.

[a]C, S, and M refer to spectral type obtained directly from the stellar spectrum, Hot indicates the spectrum was of a star hotter than an M-type. A colon (:) indicates an uncertain assessment, while a question mark (?) indicates that I was unable to classify the spectrum with any confidence.

[b]C, S, and M refer to spectral type, as determined by the FBPS, an ellipsis (...) indicates incomplete photometry while a question mark (?) indicates the star is unclassified by the FBPS.

[c]A tick (✓) indicates that the feature is present, a colon (:) indicates a marginal detection, while a cross (×) indicates an absence of the feature. An ellipsis (...) means that either the star was not C-type, or I was unable to measure the feature.

column (2) the exposure time (in seconds); in column (3) the filter used, if any; and in column (4) the mask used, if any. For each mask I integrated for a total time of 6×3600 seconds. Observations of He/Ne arcs were made for wavelength calibration, and the spectrophotometric standards Wolf 1346 and LDS 749B were also observed. To enable the frames to be debiassed and flat fielded, bias frames and the spectrum of a quartz lamp were obtained.

6.2.4 Reductions (CFHT)

The six star+sky frames obtained in each of the two fields were bias subtracted and, using a sigma clipping routine in IRAF, medianed together to produce a combined star+sky frame for each field. The quartz lamp frames for both fields were similarly combined, as were the He/Ne arc frames. The combined frames, in addition to the individual star+sky frames containing the spectra, were corrected for distortion in the telescope optics by using the GEOTRAN task in IRAF with a distortion file provided by Olivier Le Fèvre.

The spectra were extracted and wavelength calibrated using the high level CL script,

Table 6.3: Log of Spectral Observations at the CFHT.

Object	Exp. (s)	Filter	Mask
	Sept. 13/14 1993		
M31, F4[a,b]	300	*I*	...
	Sept. 14/15 1993		
Bias frames	3×0	...	...
Wolf 1346	120	*YR*	F4
LDS 749B	300	*YR*	F4
M31, F3[a,b]	500	*I*	...
M31, F4	6×3600	*YR*	F4
Dome[a]	0.2	*YR*	F4
Bias frames	11×0	...	...
Quartz lamps	7×120	*YR*	F4
He/Ne arcs	3×1	*YR*	F4
He/Ne arcs	3×1	*YR*	F3
	Sept. 15/16 1993		
M31, F3	6×3600	*YR*	F3
Quartz lamps	7×120	*YR*	F3
Dome[a]	0.2	*YR*	F3

[a]No grism in place.
[b]No mask in place.

MULTIALL, in the MULTIRED package (Le Fèvre *et al.* 1995). The MULTIALL script was written to expedite the reduction of data from multi-object spectrometers and is based on the IRAF tasks ONEDSPEC and TWODSPEC.

The spectra from the slits are reduced by MULTIALL one at a time. Given the dimensions and coordinates of the slit, the dispersion of the grism, and the bandpass of the YR filter, MULTIALL identifies a "sub-frame" where the slit produced a star+sky spectrum. To obtain a wavelength calibrated stellar spectrum from the sub-frame, MULTIALL takes the user through the following steps: (1) Define fitting parameters for flat field correction. The lamp sub-frame is binned perpendicular to the dispersion axis and plotted. An interactive fit is made and the large-scale variations subtracted off, leaving a pixel-to-pixel flat field. (2) Define sky fitting parameters. The star+sky sub-frame is binned along its dispersion axis, displayed, and used to define sky fitting parameters. (3) Extract individual spectra and combine. The star+sky sub-frames from each exposure are extracted, flat field corrected, and sky subtracted, and after this the resulting stellar spectra are combined into a single image. (4) Wavelength calibrate the spectrum. The arc sub-frame is extracted and used to derive a dispersion solution. (5) Extract a digital stellar spectrum from the (flat field and sky subtracted) combined image. The spectrum is summed along its dispersion axis, and extraction apertures defined for the star/stars that lies/lie along the slit. The spectrum/spectra is/are extracted and plotted, and finally MULTIALL moves on to reduce the data from the next slit.

The spectrophotometric flux standards LDS 749B and Wolf 1346 were observed on the night of September 14/15, and their spectra extracted using MULTIALL. The IRAF task STANDARD was used to integrate the standards in the bandpasses needed for comparison and normalize the flux to an exposure of 1 second. To build the sensitivity function, the integrated flux measurements from STANDARD were interactively fitted using SENSFUNC.

The mean airmass of the combined star+sky frame was calculated, and a file containing atmospheric extinction data for Mauna Kea generated. Finally, the sensitivity function was applied to the data using the task CALIBRATE, which also corrected for extinction.

6.2.5 The Spectra (CFHT)

The spectra obtained at CFHT are presented in Appendix A. The spectra have been smoothed using a bin size of 7 pixels, have various spectral features labeled on them, and in some cases include comments. The spectra in Appendix A have been "normalised" by dividing through by the maximum flux level, *without* subtraction of a DC level. Some of the spectra contain negative flux values due to sky oversubtraction. This is likely to happen if there is more than one star on a slit, as this makes it difficult to find a "clear" piece of sky.

The radial motions of the stars in M31 arise from a combination of the Sun's motion toward M31, the rotation of the stars in M31, the bulk motion of M31 towards the Galaxy, and the individual velocity of M31's stars. Rubin & Ford (1970) used emission regions in M31 to obtain radial velocities and translated these into rotational velocities. In Fig. 3 of Rubin & Ford (1970) M31's rotation curve is plotted and it can be seen that the curve flattens out around 20′ from the centre. Fields 3 and 4 are further out than this and, using Rubin & Ford's (1970) Fig. 3, I estimate that the rotational velocities in these fields are around –250 km/s. The radial velocities in these fields are obtained by using Equation (2) of Rubin & Ford (1970) which, as Fields 3 and 4 are along M31's SW semi-major axis, can be written as

$$V_{obs} = V(R)\sin 77^\circ - 300 \text{ km/s}. \tag{6.1}$$

Adopting a value of –250 km/s for $V(R)$ leads to a value of ~ -545 km/s for the radial

velocity (V_{obs}) in Fields 3 and 4. In the spectral region 5000Å to 7000Å this corresponds to a blueshift of 9Å to 13Å. The CFHT spectra presented in Appendix A and all other figures in this thesis have been shifted to a zero radial velocity frame.

Inspection of the spectra showed that a slight misalignment of the grism had caused the telluric lines to be not quite perpendicular to the dispersion axis of the CCD. When the sky was subtracted from the spectra the grism misalignment caused poor subtraction of these lines, and this effect was particularly noticeable on the fainter spectra. The strong [OI] 5577Å line was noticeable in all the CFHT spectra, and I have cut this out of all the spectra I present. In many of the spectra it is obvious that the [NaI] telluric lines at 5890Å and 5896Å have been poorly subtracted. The stellar NaD lines are $\sim$ 10Å bluer than the telluric NaD lines, making it hard to identify the stellar NaD line. For this reason, I present no analysis of stellar NaD lines. The other telluric line that is sometimes noticeable in the sky subtracted spectra is the [OI] line at 6300Å. I have marked the position of these telluric lines on the spectra in Appendix A (N.B. as previously mentioned, the spectra have been shifted to a zero velocity frame, and I have shifted the marks indicating the positions of the telluric lines appropriately).

6.3 DAO Data

6.3.1 Instrumentation (DAO)

The Galactic C-star spectra were obtained with the DAO 1.85-m Plaskett Telescope using the Cassegrain Spectrograph. I used the 2131R grating, which has a dispersion of 60Å/mm, and a SITe 2 CCD with 24μm pixels. The CCD has a quantum efficiency that rises from 81% at 4000Å to 87% at 7000Å. The spectra had a 2 pixel resolution of 2.88Å, or R = $\lambda/\Delta\lambda$ = 2100 at 6150Å. The wavelength coverage of the DAO spectra (5430Å to

6870Å) encompassed that of the CFHT spectra.

6.3.2 Selection (DAO)

The stars observed at the DAO are a subset of those observed by Yamashita (1972, 1975). In Table 6.4 I summarize the relevant information for the stars observed listing: in column (1) the proper name of the star; in column (2) the number of the star from Yamashita (1972, 1975); in columns (3) and (4) the 1900.0 coordinates; in column (5) the apparent V magnitude; in column (6) the radial velocity (in km/s); in column (7) the exposure time, in seconds; in column (8) the classification from the *Henry Draper Catalogue*; in column (9) the classification from the Keenan & Morgan (1941) system (The classifications in brackets in columns 6 and 7 are from different catalogues.); and in column (10) the C-types obtained by Yamashita (1972, 1975). All of the data in Table 6.4 (with the obvious exception of column 6) are taken from the compilations of Yamashita (1972, 1975). In Fig. 6.3 I plot a diagram to show the coverage I managed to achieve in the KM (Keenan & Morgan 1941) plane.

6.3.3 Observations (DAO)

The DAO observations were made by myself and Ted Kennelly on the nights of May 25/26 and 26/27 1994. Bias and quartz lamp frames were obtained as well as Cd/Ne arcs for calibration. The Moon was full on May 25 1994, though the stars were sufficiently bright ($m_V \sim$ 4.8 to 12.0) that this was no worry. Spectra were obtained of 13 N-type C-stars during the two nights of observations.

Table 6.4: Galactic Carbon Stars Observed at the DAO.

Name	Yam[a]	α_{1900}	δ_{1900}	m_v	V_r[b]	Exp. (s)	HD[c]	KM[d]	Ok[e]
AW Cyg	156	$19^h25\overset{m}{.}8$	$+45°50'$	8.0-10.2	−12	5×420	(N3)	(C5,5)	C4,5
HK Lyr	150	$18^h39\overset{m}{.}4$	$+36°51'$	8.1	−5	5×180	Nb	C6,4	C7,4
RS Cyg	163	$20^h09\overset{m}{.}8$	$+38°26'$	6.5-9.3	−50	5×600	N0pe	C8,2	C8,2e
RY Dra	126	$12^h52\overset{m}{.}5$	$+66°32'$	6.1-7.1	−20	3×180	N4	C4,4	C4,5J
SS Vir	123	$12^h20\overset{m}{.}1$	$+1°20'$	6.0-9.6	+2	5×600	Np	C6,3	C5,3e
T Lyn	226	$08^h16\overset{m}{.}4$	$+33°50'$	8.0-12.0	+31	3×600	N0e	C6,3e	C7,1e
T Lyr	148	$18^h28\overset{m}{.}9$	$+36°54'$	7.8-9.6	−12	5×360	(N3)	C6,5	C6,5J
UX Dra	258	$19^h25\overset{m}{.}1$	$+76°23'$	6.1-7.1	+6	5×90	N0	C7,3	C7,3
U Cyg	268	$20^h16\overset{m}{.}5$	$+47°35'$	6.7-11.4	+13	5×480	Np	C7,2	C8,2e
V Aql	152	$18^h59\overset{m}{.}1$	$-5°50'$	6.7-8.2	+37	5×180	N6	C6,4	C5,4
V Oph	138	$16^h21\overset{m}{.}2$	$-12°12'$	7.0-10.5	−40	4×600	(N3e)	C7,4	C7,3e
X Cnc	100	$08^h49\overset{m}{.}8$	$+17°37'$	5.9-7.5	−1	5×240	N3	C5,4	C5,4
Y CVn	124	$12^h40\overset{m}{.}4$	$+45°59'$	4.8-6.0	+12	5×120	N3	C5,4	C5,5J

[a]Yamashita number, see Yamashita 1972, 1975.
[b]Units: km/s.
[c]HD Classification, see §6.3.2 for details.
[d]Keenan-Morgan classification, see §6.3.2 for details.
[e]Okayama, see §6.3.2 for details.

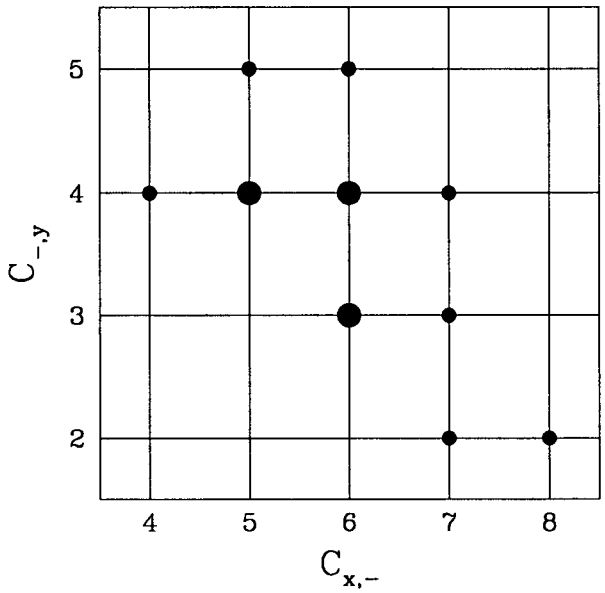

Figure 6.3: This figure shows the KM classification of the Galactic C-stars observed. On the abscissa I plot the KM temperature index ($C_{x,-}$), while on the ordinate I plot the KM C_2 strength index ($C_{-,y}$). The larger points indicate that two stars with the spectral classification were observed.

6.3.4 Reductions (DAO)

Both the bias frames and the lamp frames had their overscan values subtracted and were combined to make "master" bias and "master" lamp frames. The master lamp frame was used to make a flat field, and then the frames of the spectra were debiassed (by subtracting their overscan values and the master bias frame) and divided by this flat field. I found that the position of the star on the slit deviated only slightly between exposures, and so combined the frames together with IMCOMBINE, using the AVSIGCLIP option to eliminate cosmic rays.

The spectra and Cd/Ne arcs were extracted using APALL; this was an easy procedure as the spectra were well exposed. The lines from the Cd/Ne arcs were identified and a dispersion solution obtained which was applied to the spectra using DISPCOR. More

details of this whole procedure can be found in *A User's Guide to Reducing Slit Spectra with IRAF* (Massey *et al.* 1992).

6.3.5 The Spectra (DAO)

The spectra obtained at the DAO are presented in Appendix B. The Galactic C-star spectra were not contaminated by telluric lines, and I have not marked the position of these lines on the spectra. Also, none of the Galactic C-stars suffered from problems with sky oversubtraction. The same features have been marked on the Galactic C-stars as the M31 C-stars, and they have been normalised in the same way as the CFHT spectra (see §6.2.5).

The radial velocities of the Galactic C-stars are given in column 6 of Table 6.4. It can be seen that the radial velocities of these stars will cause a wavelength shift in the spectral region 5000Å to 7000Å of $\sim$ 1Å (I can expect similar wavelength shifts in the M31 spectra on account of the stars' peculiar velocities). For the purposes of my thesis the wavelength shift is minimal, and I plot the Galactic C-star spectra (both in Appendix B and in all subsequent plots) without any radial velocity corrections.

Chapter 7

RELIABILITY OF THE FOUR-BAND PHOTOMETRIC SYSTEM

"If a man will begin with certainties, he shall end in doubts; but if he will be content to begin with doubts, he shall end in certainties."

Sir Francis Bacon (1561 – 1626)

7.1 Recognition of the Spectra

How well does the FBPS work as a photometric spectral classifier? To answer this question the spectra need first to be classified. In the spectral range of the data (5450Å to 6850Å) a C-star is recognized by its closely spaced molecular absorption lines of CN and C_2. Barnbaum (1994) points out that in C-stars the spectral region from 5600Å to 7850Å is dominated by the vibration-rotation transitions of CN, specifically by the Red System ($A^2\Pi - X^2\Sigma$), while the Swan bands of C_2 ($A^3\Pi_g - X^3\Pi_u$) dominate the blue region, and extend out to 6600Å. The bandheads of CN and C_2 are easily distinguished as the CN branches of the red system degrade to the red and have more diffuse bandheads than the Swan bands which degrade to the blue. I chose the spectral range to include the C_2 band at 5635Å and this is my key diagnostic for recognizing C-star spectra. Included on the C-star spectra in Appendices A (M31) and B (Galactic) are the positions of the diagnostic C_2 and CN bandheads.

M-stars have an envelope chemistry dominated by oxygen, and their spectral "fingerprints" are the bandheads of TiO which degrade to the red. S-stars have C $\sim$ O, and the "smoking guns" for these stars are ZrO bandheads. A good reference that shows digital spectra of late-type stars, and points out many of the features I discuss is *An Atlas of*

Digital Spectra of Cool Stars (TTCB).

I visually examined the CFHT spectra and classified them as either M, M:, S, S:, C, C:, Hot or "?". The M, S and C refer to spectral type, and when followed by a colon indicate a marginal identification. The classification of "Hot" is given to stars which I classified as being of a spectral type earlier than M, while a question mark indicates that I was unable to classify the spectrum with any confidence. My classifications are included on the spectra in Appendix A and also in column 6 of Tables 6.1 and 6.2. Slit 6 of Field 3 had three stars on it which caused severe problems with the sky fit. The spectra from this slit appear confused, and so I drop these three spectra from any further consideration.

7.2 Justification of Colour Boundaries

In §4.2.1 I used boundaries in a $(CN-TiO,\ V-I)$ TCD and magnitude criteria (§4.2.2) to identify M-, S-, and C-stars. I refer the reader to §4.2 for details of the magnitude criteria, while I now justify the colour criteria given in §4.2.1.

In Fig. 7.1 I symbolically plot my spectral classifications in $(CN-TiO,\ V-I)$ TCDs for the Field 3 and 4 spectra. In Fig. 7.1 the solid points are stars which are brighter than $I_0 > 18.5$ (none of the stars meeting the C-star colour criteria were fainter than $I_0 = 20.6$), while the solid lines show my colour criteria for C- and M-stars. Figure 7.1 immediately shows that the FBPS has been highly successful at separating the C- and M-stars. Where on the $(CN-TiO,\ V-I)$ TCD should the M-, S-, and C-stars regions be defined? In Field 3 the bluest C-star (with $(V-I)_0 = 1.79$) has the same $(V-I)$ colour as F3–3.1, a star I classified as marginal M. To avoid inclusion of this non C-star I defined C-stars as having $(V-I)_0 > 1.8$. In choosing this criterion I eliminate two of the spectroscopically confirmed C-stars (stars F3–1.1 and F4–26.1). The $(CN-TiO)$

colour criterion for C-stars was chosen as $(CN-TiO) > 0.3$ by noting that, with the exception of F4–26.1, this limit comfortably embraces all the C-stars in both Fields 3 and 4. I notice that F4–26.1 lies on the non C-star side of both the $(V-I)$ and $(CN-TiO)$ colour limits. My classification of F4–26.1 as a C-star was based mainly on it having a strong C_2 band at 6191Å (it has a relatively weak C_2 band at 5635Å). I note that F4–26.1 is one of the fainter C-stars in the sample, and consider this star to be a pathological case.

I defined the M-star $(V-I)_0$ colour criterion by noting that in Field 3 I classified F3–31.1, with $(V-I)_0 = 1.85$, as an M-star, while classifying F3–23.1, with $(V-I)_0 = 1.70$, as "Hot", it looking similar to a K-star spectrum. Given this, I chose the same $(V-I)_0$ colour limit for the M-stars as the C-stars. The $(CN-TiO)$ bound was chosen as $(CN-TiO) < -0.2$ to avoid the inclusion of F3–24.2 which I had spectroscopically identified as an S-star, and F3–36.2, which I was unable to classify with any confidence.

The colour boundaries chosen for S-stars were $(V-I)_0 > 1.8$ and $-0.2 < (CN-TiO) < 0.3$, this being the 'gap' between the C- and M-stars. This is justified as firstly I identified an S-star in this region (F3–24.2), and secondly, the $(CN-TiO)$ "colour" of stars in this region suggests that they have neither strong CN or TiO bands, as would be expected of S-stars. I point out that the aforementioned limits are still rather arbitrary and should only be used as an approximate guide by future practitioners of the FBPS.[1]

In column 7 of Tables 6.1 and 6.2 I present the FBPS classification of the stars. The classifications are either M, S, C for spectral types, a question mark if the star lies out of the colour *and/or* magnitude bounds, and an ellipsis if the photometry was incomplete,

[1]The colour of the AGB will depend on the metallicity, with metal-rich AGB stars appearing redder. An improvement could be made to my $(V-I)$ colour criterion by incorporating a metallicity dependence. Note that, as discussed in §4.5.6, the colour dependence of the AGB on metallicity at most plays only a minor role in the variation of the C/M ratio with metallicity. I also note that at constant temperature, the strength of the TiO band will depend on metallicity.

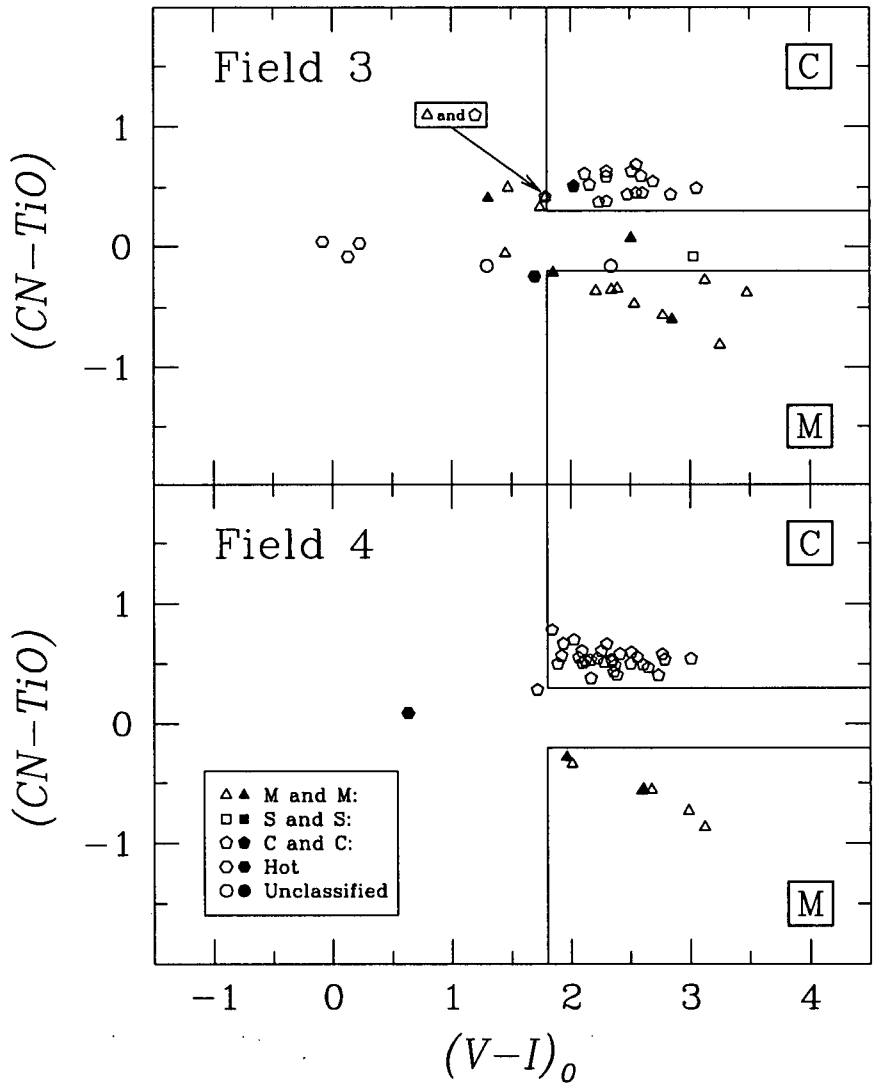

Figure 7.1: Above I plot ($CN-TiO$, $V-I$) TCDs for the M31 stars for which spectra were obtained and which *also* had CN, TiO, V and I photometry. My classification of the spectra is represented by points with differing numbers of sides, a key to which is provided in the lower panel. Solid points represent stars brighter than $I_0 = 18.5$. The solid lines represent the colour-bounds used, along with magnitude criteria, to identify C- and M-stars. The letters show the regions where C- and M-stars are expected to be found.

making FBPS classification impossible.

7.3 The "Gang of Four"

Inspection of Fig. 7.1 shows a "gang of 4" stars (stars F3–2.1, F3–3.1, F3–15.1, and F3–21.1) in Field 3 which are bluer than the C-stars though have similar $(CN-TiO)$ colours. What are these stars? I identified the spectra of stars F3–2.1, F3–15.1, and F3–21.1 as M supergiants, while classing F3–3.1 as marginal M.

In Fig. 7.2 I plot my spectral classifications of Field 3 stars in an $(I,\ V-I)_0$ CMD, providing a legend in the lower panel to identify the spectral types. I have encased the gang of 4 with large circles, and included solid squares to show the expected positions of (from blue to red) M0Ib, M2Ib, M3Ib, and M4Ib stars (RCP84, Lee 1970). A supplementary axis in M_I (assuming a true distance modulus of 24.41, see §3.3.1) is included on the right ordinate. The positions of F3–2.1, F3–15.1, and F3–21.1 in the CMD are approximately as expected if they are indeed early M-supergiants. The other gang member, F3–3.1, is one of the faintest stars for which a spectrum was obtained, and I propose that it's gang membership is a result of photometric scatter. In the CMD, I noticed four other supergiants, namely F3–26.1, F3–27.1, F3–31.1, and F3–23.1. I classed the first three of these as M supergiants, while the spectrum of F3–23.1 looked earlier than an M-type. Looking again at Fig. 7.1, it is apparent that these supergiants, with the exception of F3–27.1 which lies in the S-star region, lie where expected in the $(CN-TiO,\ V-I)$ TCD.

Why do the earlier type supergiants have $(CN-TiO)$ colours similar to C-stars? As noted by Sharpless (1956) in spectral types M0–M3 the infrared CN bands are extremely weak or absent in luminosity class III, though increase with luminosity. Sharpless (1956) also notes that luminosity effects are less apparent in M4 and later stars. I propose that

the gang of 4 (less F3–3.1) is due to the infrared CN bands being luminosity indicators in earlier M-stars.

I notice that the supergiants form a band in the $(CN-TiO,\ V-I)$ TCD, extending from the blue of C-stars down into the M-star region. With my chosen colour boundaries, I skirt around these M-supergiants. Indeed, no supergiants were found in the C-star region on the $(CN-TiO,\ V-I)$ TCD.

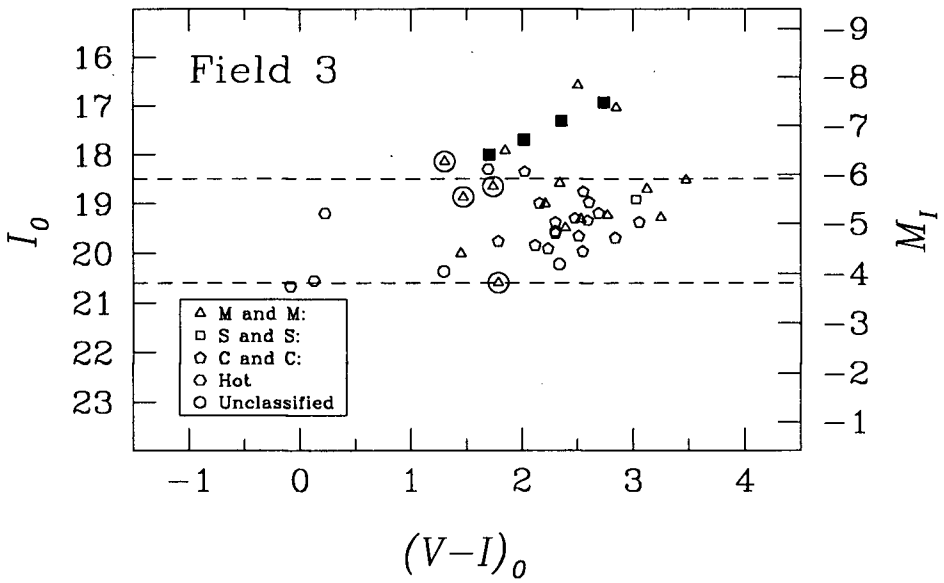

Figure 7.2: In the above figure I plot an $(I,\ V-I)_0$ CMD for the Field 3 stars for which spectra were obtained and which *also* had V and I photometry. My classification of the spectra is represented by points with differing numbers of sides, a key to which is provided. The dashed lines show magnitudes of $I_0 = 18.5$ and $I_0 = 20.6$, the magnitude range of C-stars as defined in §4.2. The 4 stars encased by large circles are the M-stars which had $(CN-TiO)$ colours similar to C-stars, while the solid squares show the expected position of supergiants with spectral types M0Ib, M2Ib, M3Ib, and M4Ib (RCP84, Lee 1970). The supplementary axis on the right shows M_I, assuming a true distance modulus of 24.41 (see §3.3.1) to M31.

7.4 A Figure of Merit

How well does the FBPS work? I must be cautious in answering this question as I chose my colour limits based on the spectra. However, I can state that: (1) In the C-star region of the ($CN-TiO$, $V-I$) TCD, I found only C-stars. Of all the C-stars I identified, I felt that only F4–7.3 was a marginal identification. I note however that F4–7.3 was on a slit with two other stars which probably caused problems in fitting the sky and consequently led to a poor spectrum. (2) Three stars that I identified as C-stars from the spectra would fail to be classified as C-stars by the FBPS. Two of these stars were too blue, though I note that had I chosen a $(V-I)_0$ limit to encompass these two stars then I would have included a few non C-stars. Given the paucity of C-stars bluer than $(V-I)_0 = 1.8$, the C/M statistics, discussed in Chapter 4, will be unaffected. One of the stars in Field 3, F3–10.1, met the colour criteria to be a C-star, but would be rejected based on its magnitude ($I_0 < 18.5$). I point out that that the magnitude criterion was rather arbitrary, and C-stars this bright must be relatively scarce given that F3–10.1 is the only star brighter than $I_0 = 18.5$ from the 157 stars in Fields 3 and 4 that met the *colour criteria* to be C-stars.

Chapter 8

RECOGNITION OF SPECTRAL CHARACTERISTICS

Twinkle, twinkle little star,
I don't wonder what you are,
For by spectroscopic ken
I know that you are hydrogen

Anonymous

In this chapter I describe my measurements of C_2 and CN band strengths in the C-stars, and summarize the criteria that I used to recognize spectral peculiarities.

8.1 Measurement of C_2 Band Strength at 5635Å

Mould & Aaronson (1979) defined the strength of the C_2 band at 5635Å as the flux ratio in magnitudes of $F_\nu(5615)/F_\nu(5690)$. I similarly measured the 5635Å C_2 bandstrength (hereafter referred to as C_2^{5635}), estimating by eye the flux level to the red and blue of the C_2 band.

As discussed in §6.2.5, some of the M31 C-star spectra have negative flux levels blueward of 5635Å caused by oversubtraction of the sky. Sky oversubtraction is likely to happen if there are multiple stars on a slit, making it hard to find a "clear" piece of sky. In the M31 C-star spectra, the oversubtraction becomes particularly noticeable blueward of 5635Å as this is where the C-stars are particularly faint. Of my 48 M31 C-star spectra, 12 had negative flux values blueward of 5635Å and, as I measure the band strength as a ratio, I avoided using these to measure C_2^{5635}. With the exclusion of these stars, it is still possible that my other measurements of C_2^{5635} are erroneous if they have a flux offset introduced by sky subtraction. Two other C-stars, F3–9.1 and F4–7.3, were

excluded from bandstrength measurement due to poor spectra making the measurement uncertain. The values for C_2^{5635} measured from the M31 C-stars are given in column 8 of Tables 6.1 and 6.2. My estimates of the flux level to the blue and red of the C_2 band at 5635Å are included as an "error bar" on the spectra in Appendices A (M31) and B (Galactic). In Fig. 8.1 I give examples of M31 C-star spectra in which I measured weak, medium and strong C_2^{5635}.

How do my values of C_2^{5635} compare with the KM measure of C_2 band strength? As I can make no comparison using the M31 spectra, I instead use my C_2^{5635} measurements of the Galactic C-star spectra. In Fig. 8.2 I plot C_2^{5635} versus the KM measure of C_2 strength (Yamashita 1972, 1975 and references therein). Figure 8.2 shows a reasonable correlation (correlation coefficient of 0.81) between C_2^{5635} and the KM classification, suggesting that my approach to measurement of C_2 bandstrength is reasonably valid. An estimate of the KM class of the M31 C-stars can be obtained from C_2^{5635} by using Fig. 8.2.

8.2 Measurement of CN Band Strength at 5730Å

The strength of the CN band at 5730Å (hereafter referred to as CN^{5730}) was measured in a similar way to the C_2 band at 5635Å (see §8.1) with the difference that the ratio of the flux to the red to flux to the blue was used (these bands degrade in opposite directions). Those C-stars that had negative flux values were discarded for the reasons cited in §8.1, while the two aforementioned stars with poor spectra were discarded. The values for CN^{5730} measured from the C-stars are given in column 9 of Tables 6.1 and 6.2. My estimates of the flux to the blue and red of the CN^{5730} band are included as an "error bar" on the spectra in Appendices A (M31) and B (Galactic). In Fig. 8.3 I give examples of M31 C-star spectra in which I measured weak, medium and strong CN^{5730}.

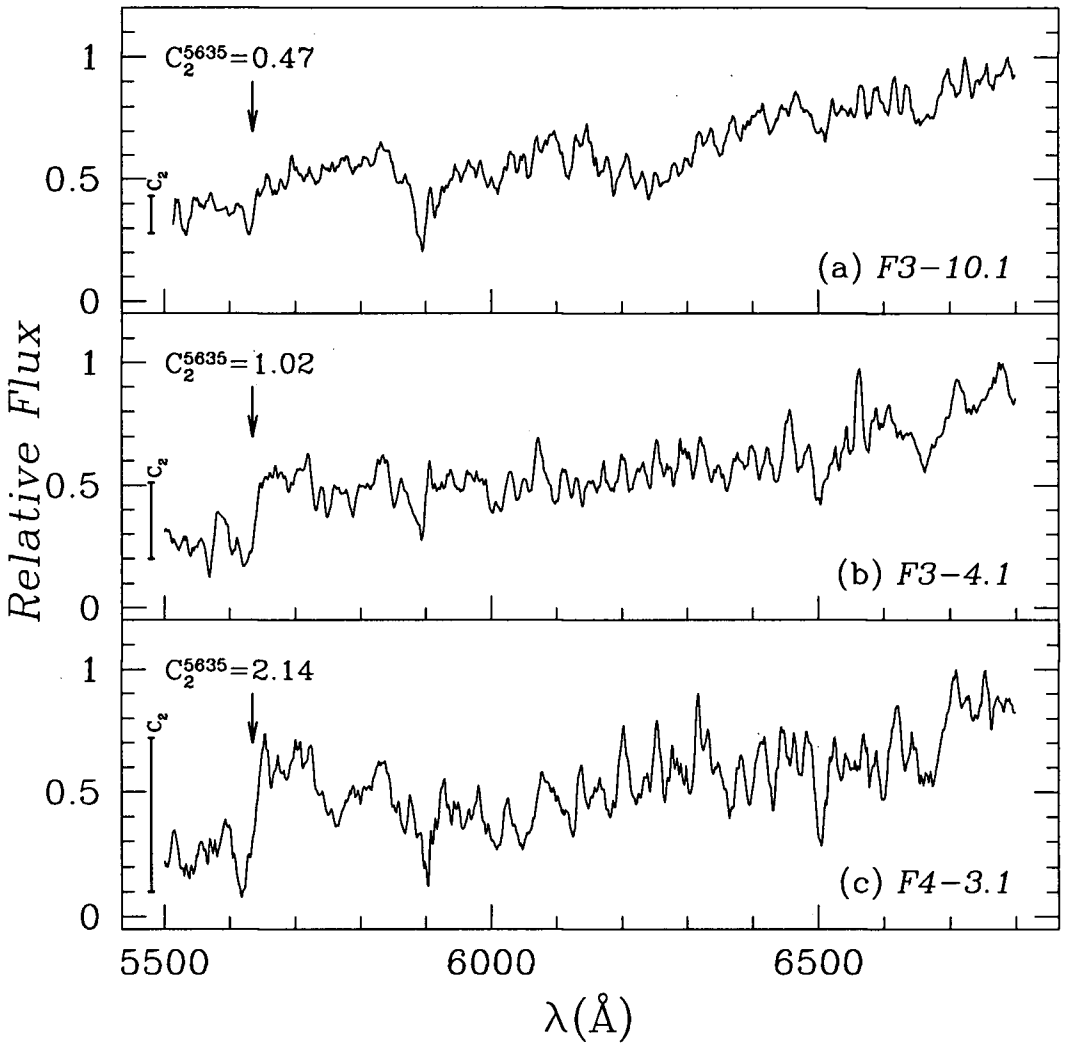

Figure 8.1: From top to bottom, the three panels contain spectra of M31 C-stars which show progressively stronger C_2^{5635} bands. Included in each panel is: (1) a vertical arrow showing the wavelength of the band head; (2) an "error bar" indicating where I measured the red and blue side of the C_2^{5635} band to lie; and (3) the value of C_2^{5635}, as defined in §8.1. All three spectra have been wavelength shifted to lie in a zero velocity frame (see §6.2.5) and smoothed using a bin size of 7 pixels.

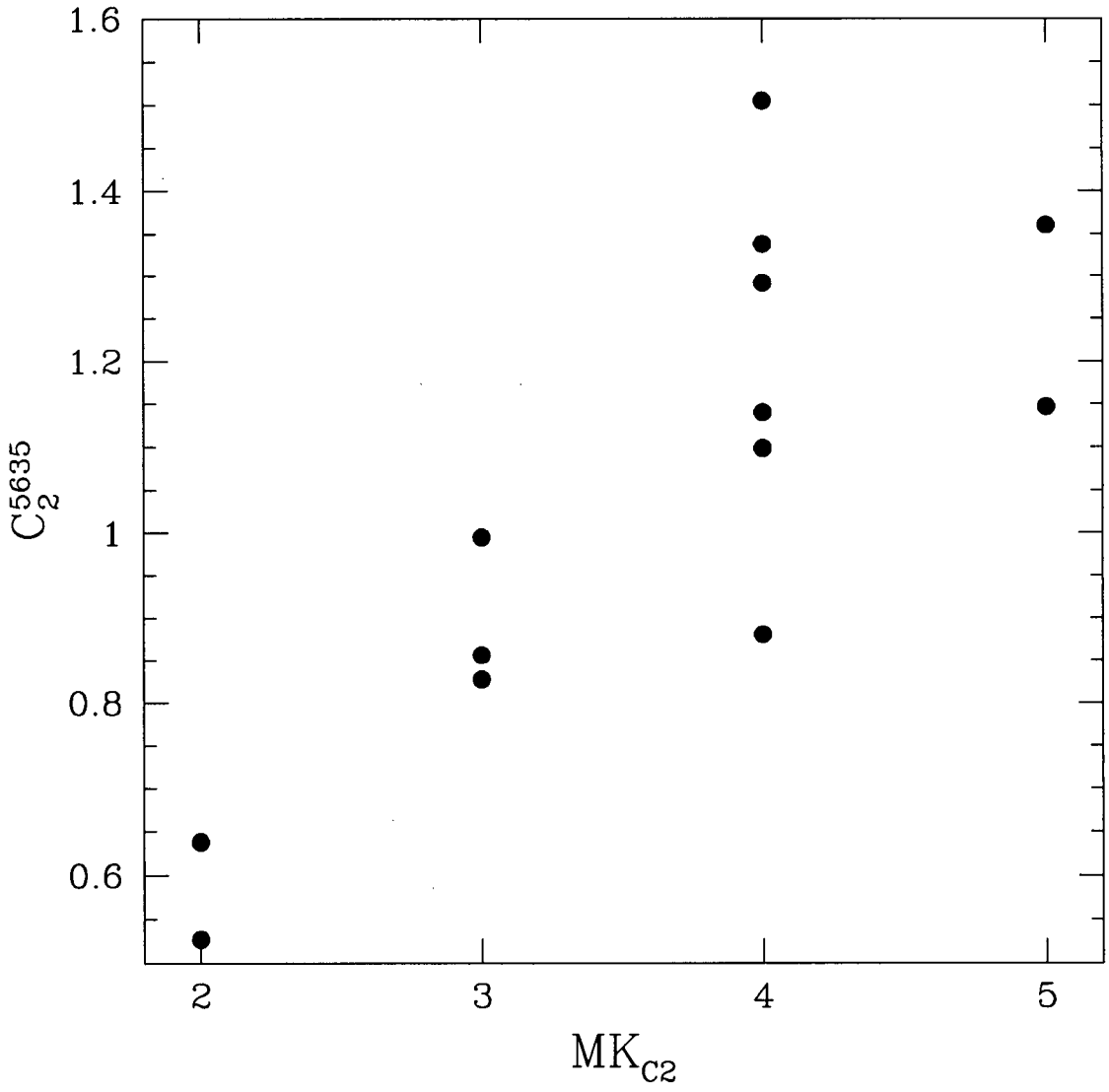

Figure 8.2: In this diagram I plot the KM C_2 band measurement (as given by Yamashita 1972, 1975) against the value of C_2^{5635} (measured as outlined in §8.1) for the Galactic C-stars.

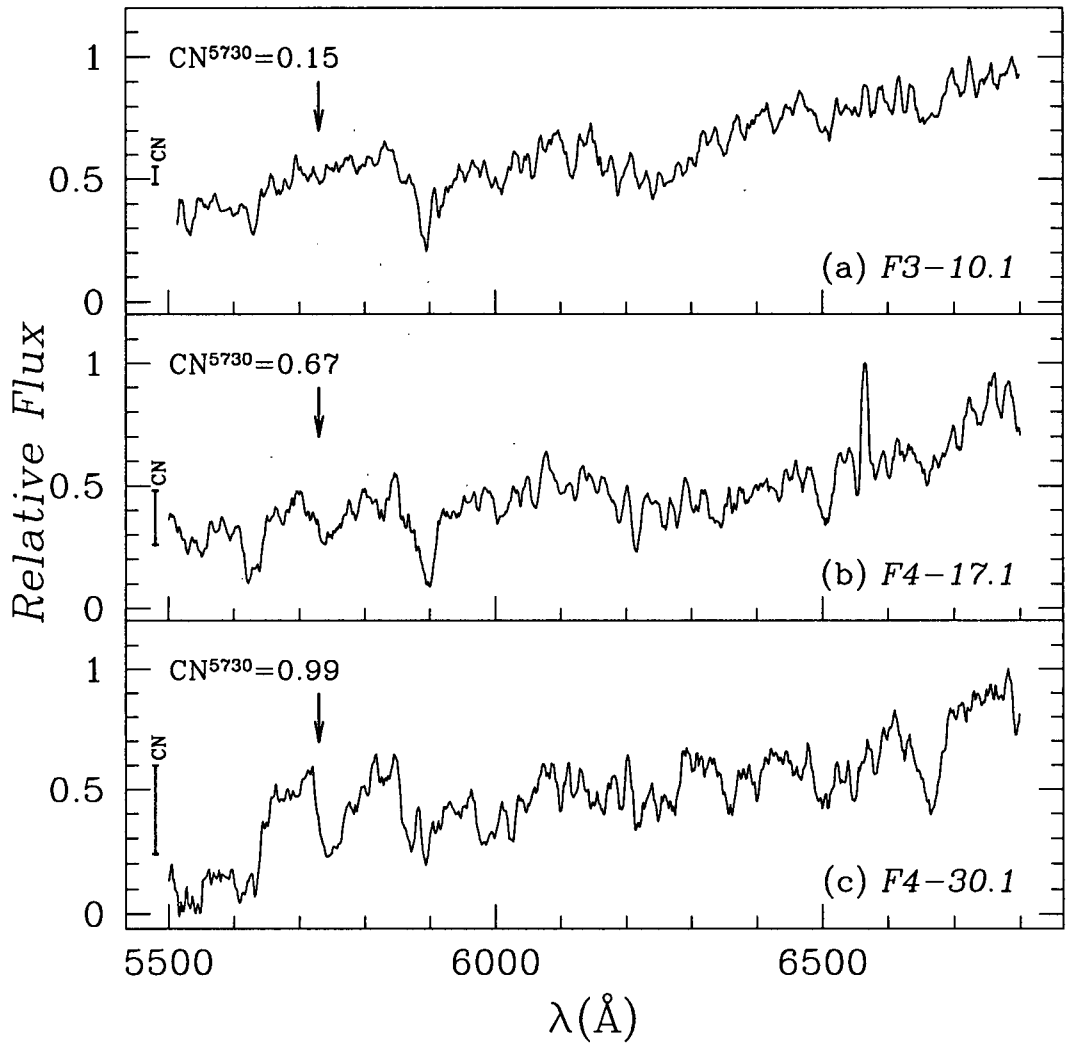

Figure 8.3: From top to bottom, the three panels contain spectra of M31 C-stars which show progressively stronger CN^{5730} bands. Included in each panel is: (1) a vertical arrow showing the wavelength of the band head; (2) an "error bar" indicating where I measured the red and blue side of the CN^{5730} band to lie; and (3) the value of CN^{5730}, as defined in §8.2. All three spectra have been wavelength shifted to lie in a zero velocity frame (see §6.2.5) and smoothed using a bin size of 7 pixels.

8.3 Recognition of J-Stars

A J-star is a C-star in which the $^{13}C/^{12}C$ ratio is greatly increased over the ratio expected from the third dredge-up mechanism alone. Spectroscopically, a J-star is recognized by its strong isotopic bands of ^{13}C. In their selection of J-stars, ROW79 restricted their sample to stars whose ^{13}CN band at 6260Å was as strong as its isotopic band at 6206Å, and similarly for the $^{12}C^{13}C$ band at 6168Å compared with $^{12}C^{12}C$ at 6191Å. The criterion I adopt is simply that the $^{12}C^{13}C$ band at 6168Å has to be as strong as the $^{12}C^{12}C$ band at 6191Å. In Fig. 8.4a I present the spectrum of Y-CVn, a Galactic J-star, while in Figs. 8.4b and 8.4c I present spectra of an M31 J-star and, in contrast, an M31 non J-star. The C-stars I found to have ^{13}C features that met my J-star criterion are indicated by a tick in column 10 of Tables 6.1 and 6.2, while a colon indicates those C-stars which exhibited isotopic features of ^{13}C, but failed to meet my criterion to be J-stars (henceforth referred to as marginal J-stars). Of the 48 C-stars, I classified 7 (15%) as J-stars, while noting that 8 (17%) of the C-stars exhibited enhanced ^{13}C features but failed to meet my J-star criterion.

8.4 Recognition of Emission-Line Stars

The spectral signature of emission-line stars is Hα emission at 6563Å. Of the 48 C-stars, I found 2 (4%) with strong Hα emission, while 13 (27%) had Hα emission at a (relatively) reduced level. In Fig. 8.5a-c I present spectra of F4–17.1 (an M31 C-star exhibiting strong Hα emission), F4–25.2 (an M31 C-star with weak Hα emission), and V-Oph (a known Galactic emission-line C-star). The two M31 C-stars with strong Hα emission are noted in Tables 6.1 and 6.2 by a tick in column 11, while those I considered to exhibit Hα at a reduced level (henceforth referred to as marginal Hα) are indicated by a colon.

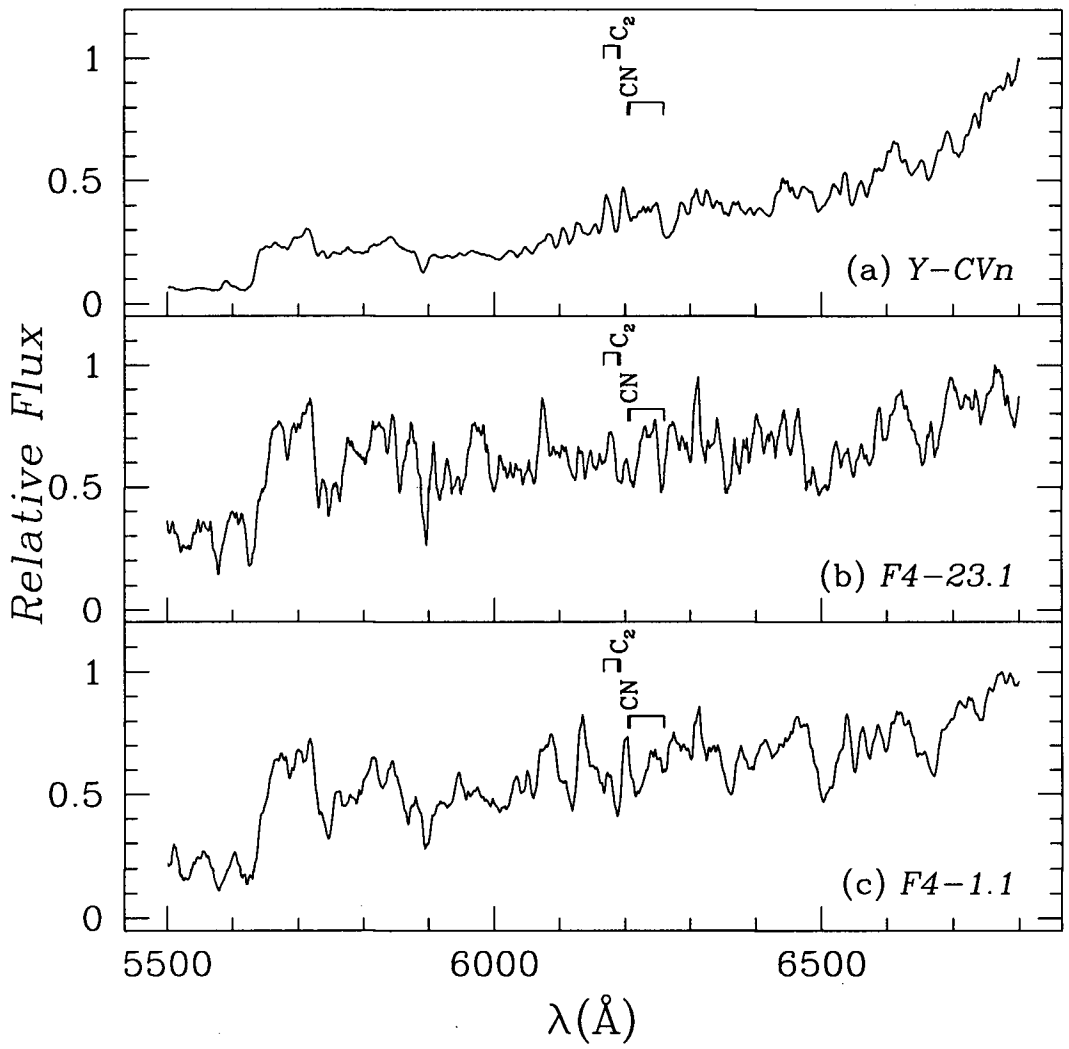

Figure 8.4: In the upper panel I show the spectrum of Y-CVn, a Galactic C-star classed as C5,5J on the Okayama system (Yamashita 1972). The middle panel shows F4–23.1, one of the 7 M31 C-stars classed as J-stars using my criterion described in §8.3. The spectrum of F4–23.1 can be contrasted with that of F4–1.1 which is an M31 C-star that does not exhibit enhanced ^{13}C isotopic bands. Included on all three panels are marks showing the C_2 band at 6191Å, along with its isotopic band at 6168Å and the CN band at 6206Å, along with its isotopic band at 6260Å. The lower two spectra have been wavelength shifted to lie in a zero velocity frame (see §6.2.5) while all three spectra have been smoothed using a bin size of 7 pixels.

Table 8.1: Hα-emission and Lithium Star Candidates in M31.

ID	λ_{obs} (Å)[a]	λ_0 (Å)[b]	W_λ (Å)
	———Hα———		
F3–4.1	6550.3	6562.2	–7.2
F4–17.1	6552.0	6563.9	–10.6
	———Lithium———		
F3–7.1	6693.8	6706.0	4.8
F4–11.1	6699.8	6712.0	4.1
F4–28.2	6695.8	6708.0	7.6

[a]Observed central wavelength.
[b]Corrected for a radial velocity of –545 km/s.

In the upper part of Table 8.1 I give the equivalent widths and central wavelengths (both corrected and uncorrected for radial velocity) of the Hα emission lines measured in the two C-stars with strong Hα emission. The central wavelengths (after correction for radial velocity) show good agreement with the expected wavelength of Hα emission. The equivalent widths of Hα in the marginal Hα stars were typically a few angstroms (for example, I measured stars F3–8.2, F3–10.1, and F3–19.1 as having equivalent widths of –3.3Å, –1.8Å, and –2.8Å respectively).

The spectroscopic signature of a Mira star is Hα in emission, while photometrically they can be recognized by their variability. Are the emission-line stars Miras? I note that of the variable stars from Baade & Swope (1965) which I was able to re-identify in Field 3, none were C-stars. I believe that this is due to the insensitivity of Baade & Swope's (1965) survey to these very red stars. Without evidence of photometric variability, I class my emission-line stars simply as "possible Miras".

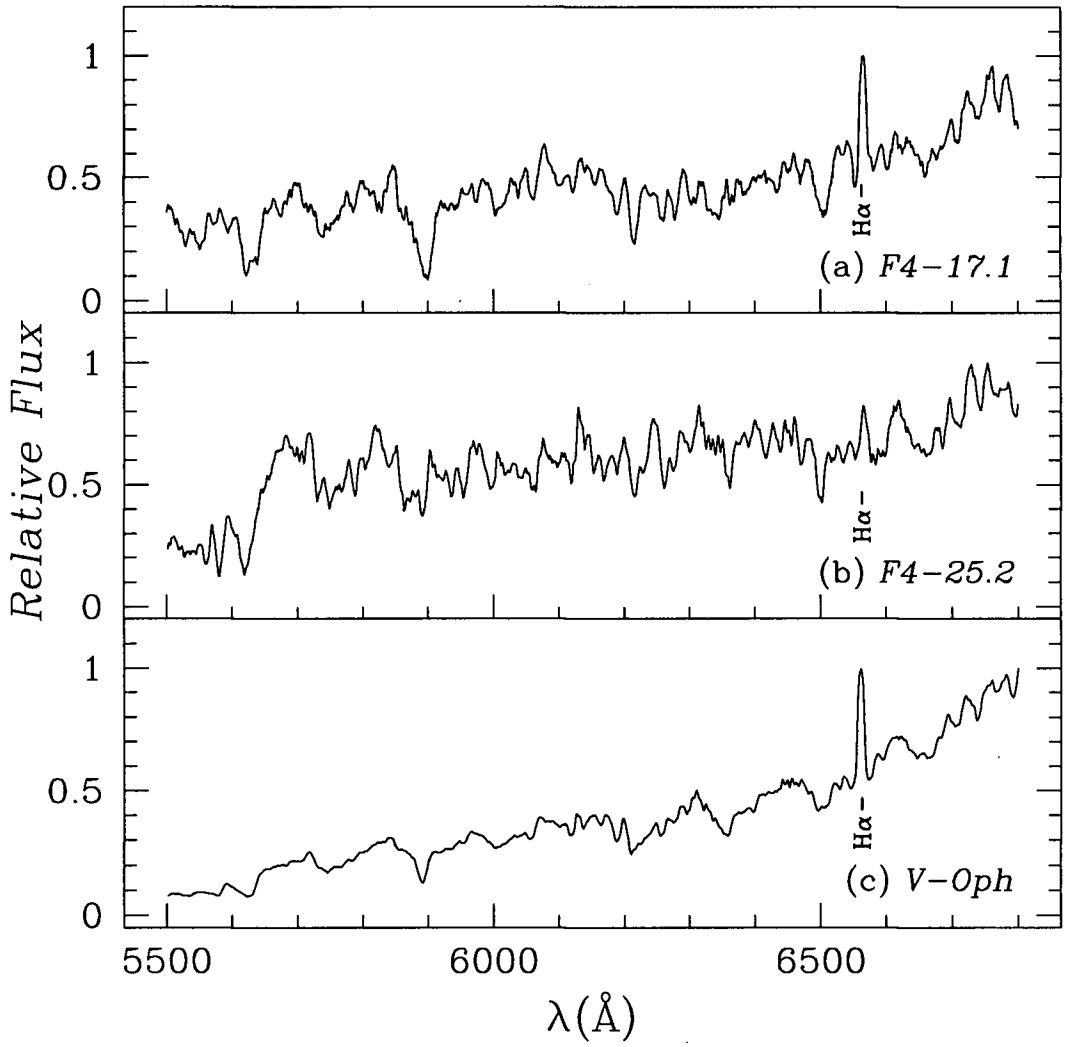

Figure 8.5: In the upper panel I show the spectrum of F4–17.1, one of the two M31 C-stars that exhibited strong Hα emission. The middle panel is the spectrum of F4–25.2, a C-star in M31 that I classed as having marginal Hα emission. For comparison, I have included the spectrum of V-Oph, a Galactic C-star classed as an emission-line star. Included on all three panels is a mark at 6563Å showing the expected wavelength of the Hα emission line. The upper two spectra have been wavelength shifted to lie in a zero velocity frame (see §6.2.5) while all three spectra have been smoothed using a bin size of 7 pixels.

8.5 Recognition of Superrich Lithium Stars

Observationally, superrich Li (SRL) stars are recognized by the resonance doublet of neutral ^{7}Li at 6708Å, with an equivalent width of $W_\lambda \sim 8$Å (Abia *et al.* 1993). The spectrum of a SRL C-star, WZ Cas, is presented in Fig. 1 of Yamashita (1972).

Of the 48 C-star spectra, I found 3 (6%) with a ^{7}Li absorption feature at $\sim$ 6708Å. These stars are listed in the lower part of Table 8.1, along with the equivalent width of the Li absorption line, the measured central wavelength of the feature, and the wavelength of the absorption line after correction for a radial velocity of –545 km/s. The equivalent width is relative to the local continuum (the true continuum is heavily blanketed) and is only a guide to the strength of the Li line in these stars. Each of these spectra were inspected for defects at 6708Å and none were found. Inspection of Table 8.1 shows that F3–7.1 and F4–11.1 have Li lines which are substantially weaker than $W_\lambda = 8$Å and central wavelengths which deviate slightly from 6708Å. For these reasons, I class the stars F3–7.1 and F4–11.1 as marginal SRL, while reserving the title of SRL for F4–28.2 alone. These classifications are contained in column 12 of Tables 6.1 and 6.2, while I present spectra of all three stars in Fig. 8.6. Included in Fig. 8.6 are the C_2 and CN bandheads shown in Fig. 8.4. I note that using my criterion from §8.3, I classify all three of the Li-stars as J-stars.

Considering only F4–28.2, it is seen that there is only 1 SRL star in my sample of 48 C-stars. The proportion of SRL stars in my sample is consistent with the work of Abia *et al.* (1993) who found three SRL stars out of a sample of 161 Galactic C-stars.

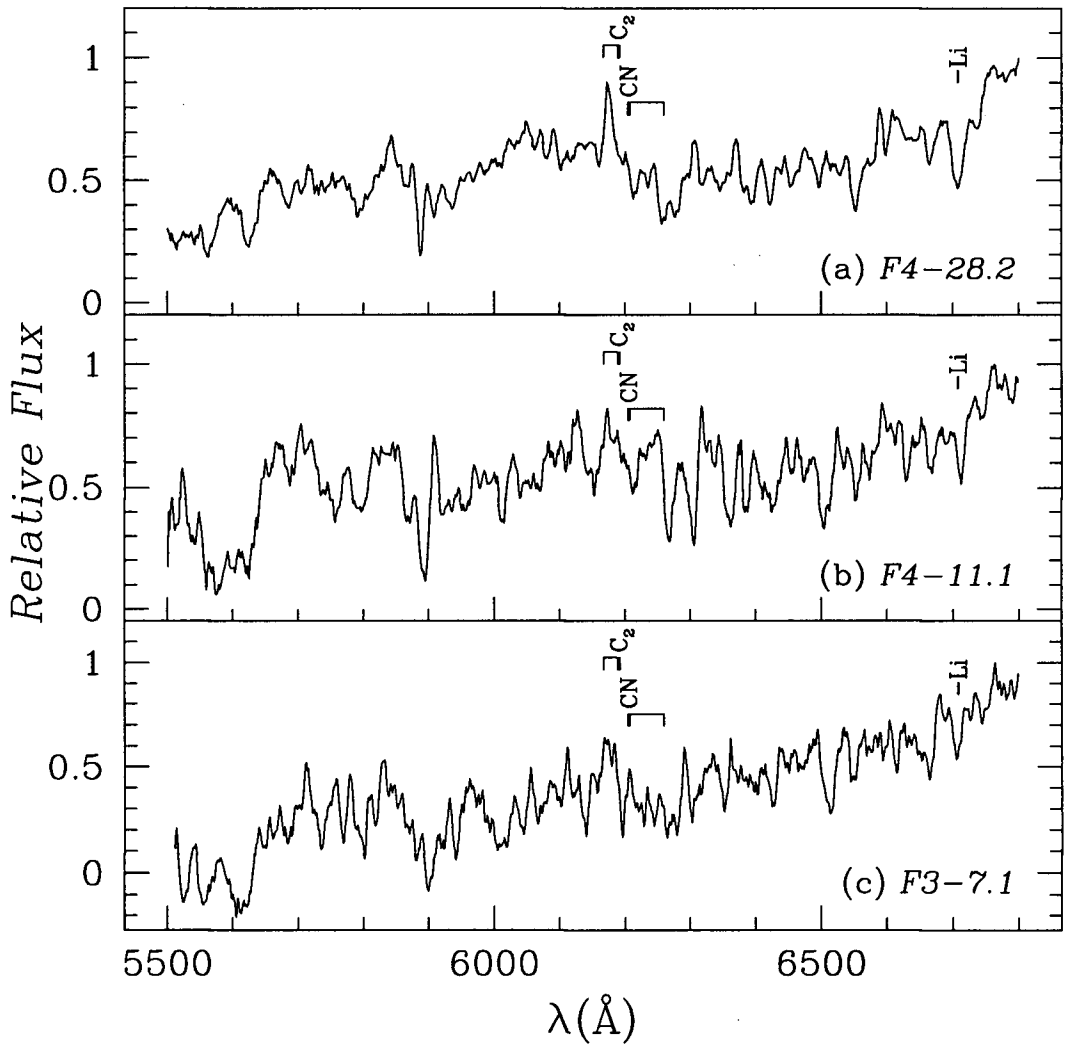

Figure 8.6: In the upper panel I show the spectrum of F4–28.2, my SRL C-star. The lower two panels show the spectra of F4–11.1 and F3–7.1, the two C-stars which each have a Li absorption line, but neither of which is strong enough for either star to be classed as a SRL C-star. As well as a mark at 6708Å to indicate the Li, I have included marks in all three panels showing the C_2 band at 6191Å and the CN band at 6206Å, along with their isotopic bands at 6168Å and 6260Å respectively. Using my criterion described in §8.3 I classed all three stars as J-stars. All three spectra have been wavelength shifted to lie in a zero velocity frame (see §6.2.5) and smoothed using a bin size of 7 pixels.

8.6 Recognition of S-Type Stars

The photometric criteria used to define the regions in a $(CN-TiO,\ V-I)$ TCD in which C-, S- and M-stars are likely to fall were discussed in §7.2. These criteria suggest that two of my stars, F3–24.2 and F3–36.2, are likely to be S-type stars. In Fig. 8.7a-c I present spectra of an M-star (F3–26.1), F3–24.2, and a C-star (F3–1.1) respectively. The difference between the three spectra is immediately obvious, and it is seen that F3–24.2 clearly shows the strong (0,0) bandhead at 6474Å of the γ system of ZrO which is the unmistakable signature of an S-type star. From a comparison with spectra in TTCB it is hard to obtain a subtype for F3–24.2, although I note that it looks similar to WX Cam (S5/5) and to BB Tau (SC6/7). In subsequent discussion, I simply refer to F3–24.2 as 'S-type'. I note that star F3–24.2 is *the first S-type star to be discovered in M31* and also *the most distant S-star known.*

The other S-star candidate, F3–36.2, is somewhat more problematic. The spectrum appears to have a ZrO band at 6474Å, though is generally dissimilar to the spectrum of F3–24.2. Until a better spectrum of this star can be obtained, I leave its classification open.

Several S-type stars have been discovered in the Magellanic Clouds using objective prism methods, the first being an SC-type star discovered by Richer & Frogel (1980). The Magellanic Clouds aside, the only other extra-Galactic S-star known was discovered in NGC 6822 by Aaronson *et al.* (1985). In common with this thesis, Aaronson *et al.* (1985) made the preliminary identification of the star using an FBPS.

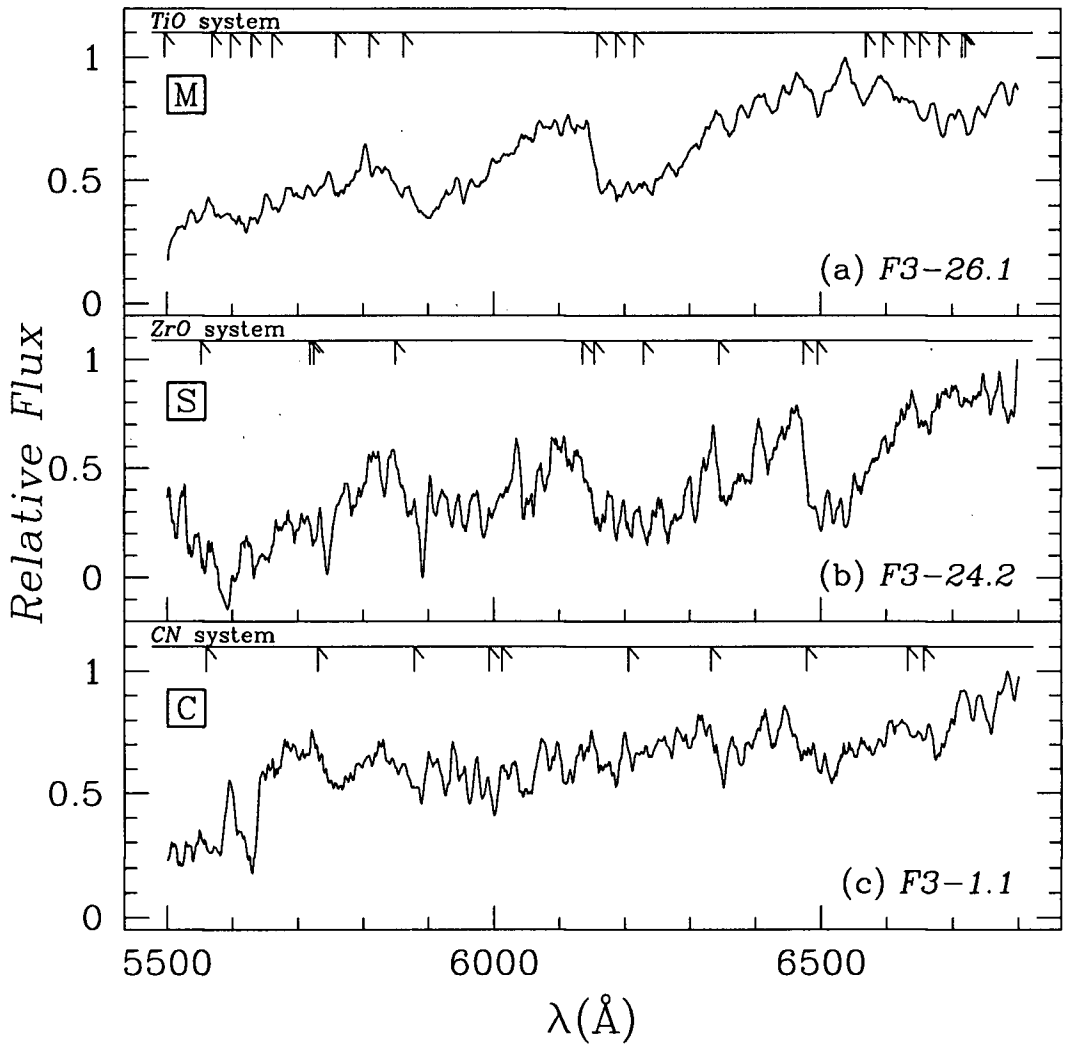

Figure 8.7: In the upper panel I show the spectrum of an M31 M-star (F3–26.1) along with bandheads of the TiO system. The middle panel shows *the first spectroscopically identified S-star in M31.* I include in the middle panel the bandheads of ZrO, especially prominent in this spectrum is the ZrO band at 6474Å. In the lower panel I show the spectrum of an M31 C-star (F3–1.1), and include on this diagram the bandheads of CN. Comparing the three spectra, one can see the strong differences that the C/O ratio in these stars has on the resulting spectrum. All three spectra have been wavelength shifted to lie in a zero velocity frame (see §6.2.5) and smoothed using a bin size of 7 pixels.

Chapter 9

EVOLUTION OF SPECTRAL CHARACTERISTICS

"Errors using inadequate data are much less than those using no data at all."

Charles Babbage (1792 – 1871)

9.1 Overview

As an AGB star evolves, both its luminosity and the temperature at the base of its convective envelope (T_{ce}) increase.[1] The nuclear processes responsible for C-star spectral peculiarities depend on T_{ce}, and so it is expected that certain processes operate only at certain (bolometric) magnitudes. Sackmann & Boothroyd (1992) and Boothroyd *et al.* (1993) modeled the evolution of TPAGB stars and predict values of M_{bol} at which C-stars may be expected to develop peculiarities in their spectra. For this reason, it is of great interest to have values of M_{bol} for my sample of C-stars so as to be able to compare my observations with model predictions.

Models of AGB evolution predict values for M_{bol}, and these are easily compared to observations. On the other hand, T_{eff} is difficult to predict as it depends on the treatment of convection and on the poorly-known molecular and grain opacities. If model values of T_{eff} are to be compared with observations, there is the additional problem of transforming T_{eff} into the observers plane. Consequently I only compare the observed and predicted values of M_{bol} in this chapter.

As I am interested in seeing how peculiarities evolve in the CMD, it is interesting to

[1]Though note that: (1) TPAGB stars will undergo interflash dips in luminosity; and (2) stars which undergo HBCE burning deviate from the core mass-luminosity relation and rapidly reach higher luminosities (see Sackmann & Boothroyd 1992 and references therein).

ask how well the C-stars for which I have spectra sample the C-star population of Fields 3 and 4 as a whole. In Figs. 9.1 and 9.2 I have plotted ($M_{\rm bol}$, $V-I)_0$ CMDs of the C-stars from Fields 3 and 4 that meet the colour and magnitude criteria (described in §4.2) to be C-stars. These stars are plotted as smaller solid points, while the C-stars for which a spectrum was obtained are plotted as large open points. In addition to this, I have labelled those C-stars for which I obtained spectra. Figures 9.1 and 9.2 demonstrate that I achieved the goal, mentioned in §6.2.2, of sampling the magnitude range of C-stars in the two fields.

9.2 Bolometric Corrections

The flux from C-stars is mainly in the infrared. To obtain accurate values of $M_{\rm bol}$, I need measurements of this flux. As I made no measurements of infrared flux for my C-stars, I instead apply a bolometric correction (BC) to the (Cousins) I_0 magnitude (which I previously defined as BC_{I_C}). The only such BC_{I_C} in terms of $(V-I)_0$ in the literature of which I am aware is that of Reid & Mould (1985) who give

$$\mathrm{BC}_{I_C} = 1.9 - 0.7(V-I)_0 \tag{9.1}$$

for LMC C-stars. The sense of eq. 9.1 is such that

$$m_{bol} = I_c + \mathrm{BC}_{I_C}. \tag{9.2}$$

Reid & Mould (1985) derived their expression for BC_{I_C} from the work of Cohen *et al.* (1981), who obtained an expression for the BC to LMC C-stars in terms of $(R-I)_0$, and the VRI observations of Blanco & Richer (1979) of C-stars in NGC 419, a compact SMC cluster. It appears that eq. 9.1 might be inappropriate as: (1) it is assumed that the relationship between $(R-I)_0$ and $(V-I)_0$ for SMC C-stars holds for LMC C-stars;

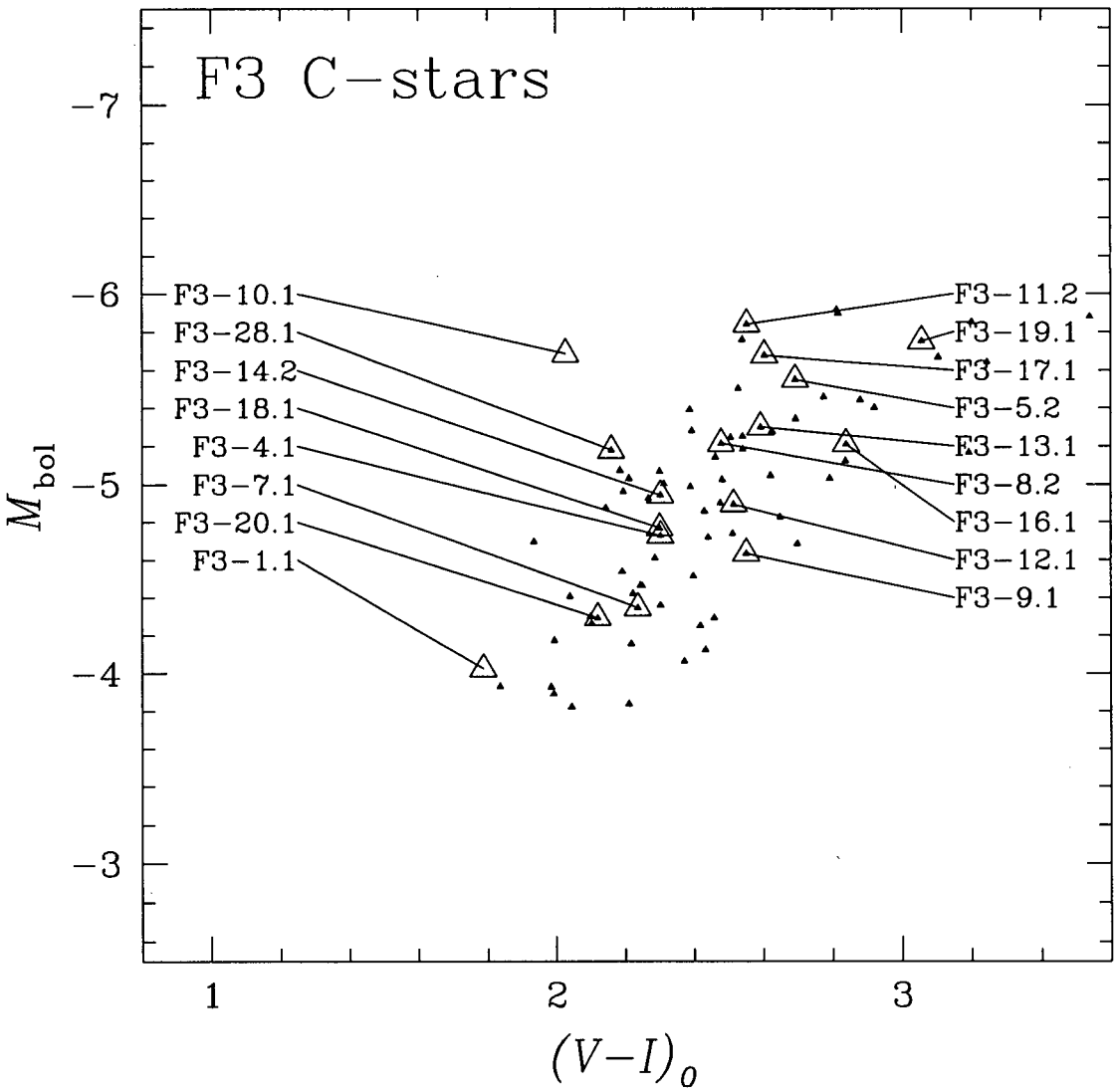

Figure 9.1: In the above diagram I plot as small solid triangles the stars from Field 3 that met the photometric criteria (described in §4.2) to be C-stars. Plotted as large open triangles are those stars spectroscopically confirmed as C-stars. Two of the spectroscopically confirmed C-stars (F3–1.1 and F3–10.1) failed to meet the photometric criteria to be classed as C-stars, and are the empty open triangles.

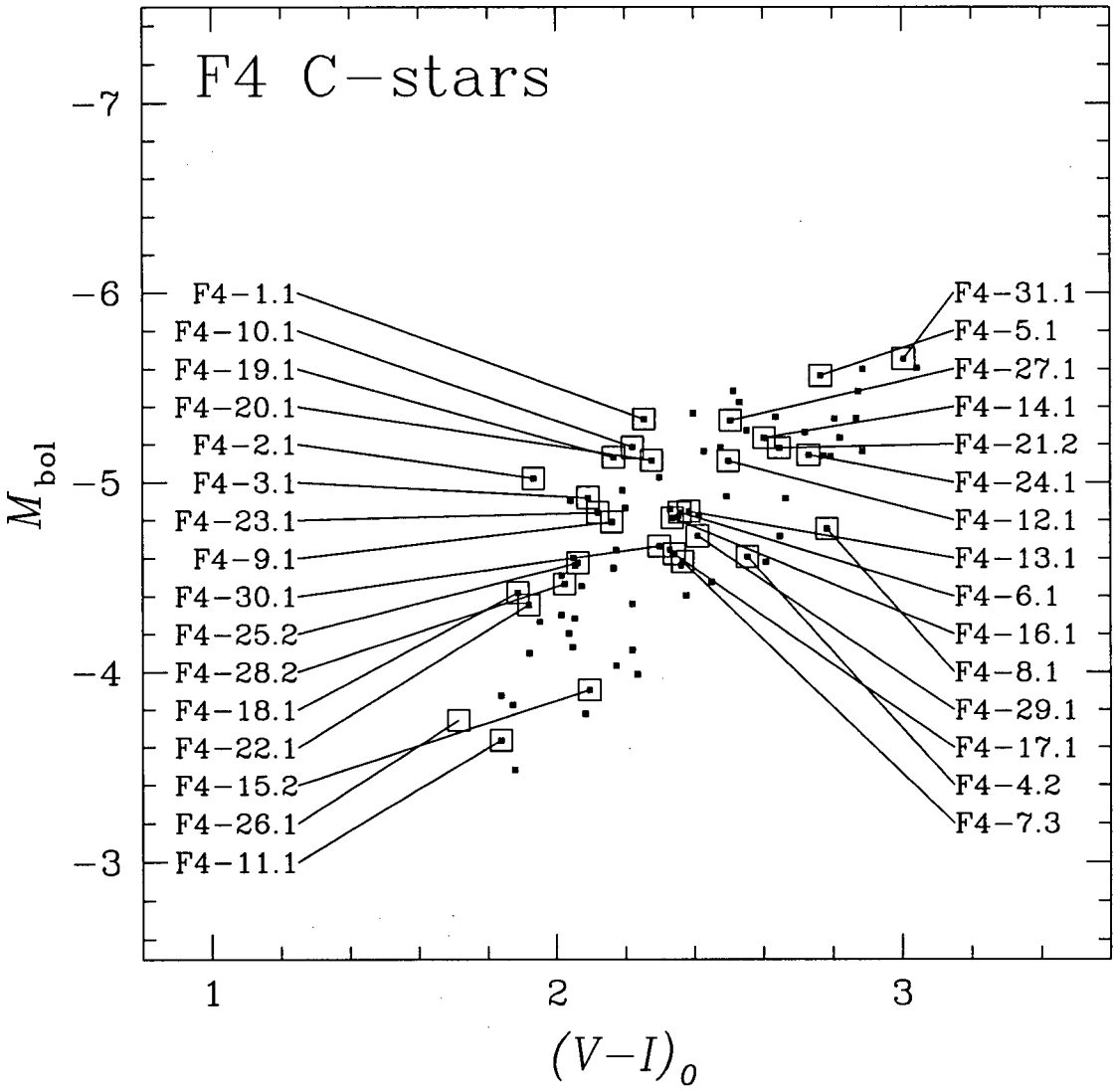

Figure 9.2: In the above diagram I plot as small solid squares the stars from Field 4 that met the photometric criteria (described in §4.2) to be C-stars. Plotted as large open squares are those stars spectroscopically confirmed as C-stars. One of the spectroscopically confirmed C-stars (F4–26.1) failed to meet the photometric criteria to be classed as C-stars, and is the empty open square.

(2) Reid & Mould (1985) neither allowed for reddening or differing filter systems in making their substitution of $(R-I)_0$ in eq. 1b of Cohen *et al.* (1981); and (3) Cohen *et al.* (1981) state that the LMC data on which the BC was based exhibited a large scatter (indeed, using their data I calculated a value of 0.23 for the correlation coefficient between $m_{I_0} - m_{bol}$ and $(R-I)_0$). Given the caveats associated with eq. 9.1, I drop it from further consideration.

In Fig. 1 of Bessell & Wood (1984) BC_{I_C} is plotted as a function of $(V-I)_0$ colour for stars in the solar neighbourhood as well as stars from the SMC, LMC, and 47 Tuc. The figure shows no variation of BC_{I_C} with metallicity for the oxygen-rich (M-type) stars, and Bessell & Wood (1984) defined a *single* relationship between BC_{I_C} and $(V-I)_0$ for these stars. The sample of stars in Fig. 1 of Bessell & Wood (1984) contains only 4 C-stars, and no attempt is made to fit these data. I, on the other hand, performed a least-squares fit on these four data points and obtained

$$BC_{I_C} = 2.52 - 1.06(V-I)_0, \tag{9.3}$$

where the sense of BC_{I_C} is as in eq. 9.2. I note that: (1) whereas fitting a line to four data points is a poor man's approach to obtaining BC_{I_C}, it is an improvement on eq. 9.1; and (2) the relationship for oxygen-rich stars (Bessell & Wood 1984, Fig. 1) appeared to be insensitive to metallicity, suggesting that the same may hold for C-stars and that I am consequently justified in using eq. 9.3 for my sample of C-stars. For the rest of this paper I use the BC_{I_C} given in eq. 9.3 to obtain the bolometric magnitudes of the C-stars.

In Fig. 9.3a I plot: (1) as a dashed line, the BC_{I_C} from Reid & Mould (1985), given in eq. 9.1; (2) as a dotted line, the BC_{I_C} from Bessell & Wood (1984), given in eq. 3.2, which is applicable to oxygen-rich stars; and (3) as a solid line, the BC_{I_C}, given in eq. 9.3 which I derived from the data of Bessell & Wood (1984). In the lower panel of Fig. 9.3

I have plotted a histogram of the colour distribution of all the C-stars in Fields 3 and 4 (solid lines) and the C-stars for which I obtained spectra (shaded histogram). I note that: (1) for stars redder than $(V-I)_0 = 1.8$ (which will be all of the C-stars identified by the FBPS) eq. 9.3 gives the largest BC_{I_C}; (2) the difference between using eq. 9.1 (dashed line) and eq. 9.3 (solid line) is minimal (a few tenths of a magnitude) for most of the C-stars in my sample; and (3) the reddest C-stars are bolometrically 1 magnitude brighter than M-stars with the same I magnitude and $(V-I)$ colour. What error should be associated with the BC_{I_C} given in eq. 9.3? The data from which eq. 9.3 was derived showed that BC_{I_C} was greater for C-stars than M-stars. Consequently, I can say that BC_{I_C} will not be less than that given by eq. 3.2. As I have insufficient data to address the question of whether BC_{I_C} is larger than that given by eq. 9.3, I leave this question unanswered.

Before applying the BC_{I_C} I need first to correct for interstellar reddening and absorption. This I do using the reddening values along with the relationships given in §3.2. Finally, to obtain the absolute bolometric magnitude I use a true distance modulus of 24.41 (§3.3.1) for M31.

9.3 C_2 Band at 5635Å

The C_2 bandstrengths of AGB stars from a coeval population (i.e. a population in which all stars currently ascending the AGB are of approximately the same mass) might be expected to initially increase with luminosity. With all other parameters being the same, the C_2 bandstrength will depend on the abundance of C_2, and this will increase as a star ascends the AGB and undergoes third dredge-up. If the coeval stars are so massive that they undergo HBCE burning, C_2 is destroyed and the C_2 bandstrength will weaken. Consequently, it might be expected that at some luminosity, an *inverse* correlation will

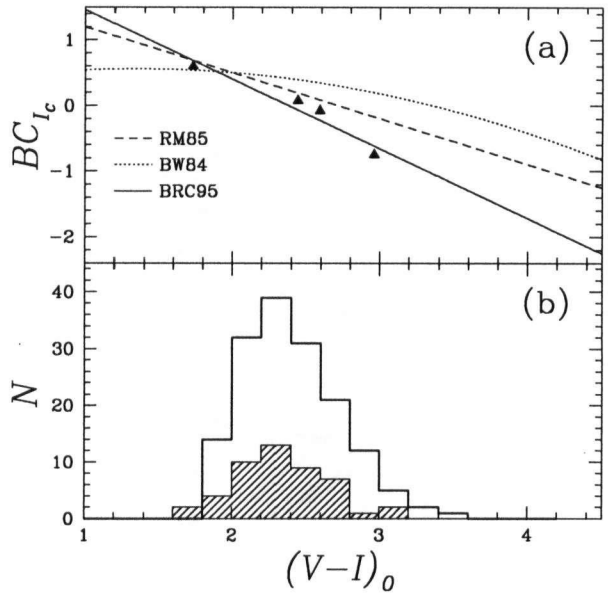

Figure 9.3: In the upper panel I have plotted: (1) the BC_{I_C} given by Reid & Mould (1985, see eq. 9.1); (2) the BC_{I_C} from Bessell & Wood (1984, see eq. 3.2); and (3) the BC_{I_C} which I derived from the data (shown as solid triangles) of Bessell & Wood (1984, see eq. 9.3). A legend is given in the upper panel to distinguish between the three BC_{I_C}. The lower panel is a colour histogram for all the C-stars in Fields 3 and 4 (thick line) and the C-stars from Fields 3 and 4 for which spectra were obtained (thin line and shaded).

exist between the C_2 bandstrength and luminosity. Scalo *et al.* (1975) state that there is some evidence that the C_2 bandstrengths of C-stars decreases with luminosity, and note that gravity cannot be responsible for this. Indeed, ROW79 suggested that there was a weak inverse correlation between C_2 bandstrength and luminosity in their survey of LMC C-stars.

In Fig. 9.4 I plot C_2^{5635} measured for the M31 C-stars (see §8.1) as a function of position in an ($M_{\rm bol}$, $V-I)_0$ CMD. In this CMD, I have scaled the point size to the C_2^{5635} bandstrength. Figure 9.4 shows no correlation between either C_2^{5635} and $M_{\rm bol}$ (correlation coefficient of 0.07) or C_2^{5635} and $(V-I)_0$ (correlation coefficient of 0.11). Superficially, the stars with the strongest C_2^{5635} appear at brighter magnitudes, though I note that there is

a higher frequency of stars in this part of the CMD, and many of these have weak C_2^{5635} bands. I suggest that the lack of a correlation between C_2^{5635} and luminosity is due to the stars in Fields 3 and 4 not being coeval. Consequently, the stars would have different envelope masses, and different C_2^{5635} evolution.

9.4 CN Band at 5730Å

In Fig. 9.5 I plot CN^{5730} measured for the M31 C-stars (see §8.2) as a function of position in an (M_{bol}, $V-I)_0$ CMD. In this CMD, I have scaled the point size to the CN^{5730} bandstrength. As with Fig. 9.4, Fig. 9.5 shows a lack of any correlation between either CN^{5730} and M_{bol} (correlation coefficient of –0.07) or CN^{5730} and $(V-I)_0$ (correlation coefficient of 0.25). Keenan (1993) mentions that the CN bands show a positive luminosity effect in C-stars (this effect is well known for M-stars) though does not specify which CN bands. My data clearly show that the CN^{5730} band is *not* a luminosity indicator. I attribute the lack of a correlation between CN^{5730} and luminosity to the same reason that no correlation was found for C_2^{5635} and luminosity, namely that the C-stars on the AGB are not coeval, and have differing envelope masses.

9.5 J-Stars

When the helium shell in a TPAGB star ignites, ^{4}He is burnt to ^{12}C by the triple-α process. The ^{12}C can be brought to the surface by the third dredge-up mechanism, the consequence of which is an increase in the $^{12}C/^{13}C$ ratio. In J-stars the ratio of $^{12}C/^{13}C$ is *lower* than the ratio at the onset of the TPAGB. These unusual isotopic ratios can be explained by hot bottom convective envelope (HBCE) burning, in which the CN cycle converts ^{12}C to ^{13}C and ^{14}N and reduces the $^{12}C/^{13}C$ ratio to the CN cycle equilibrium

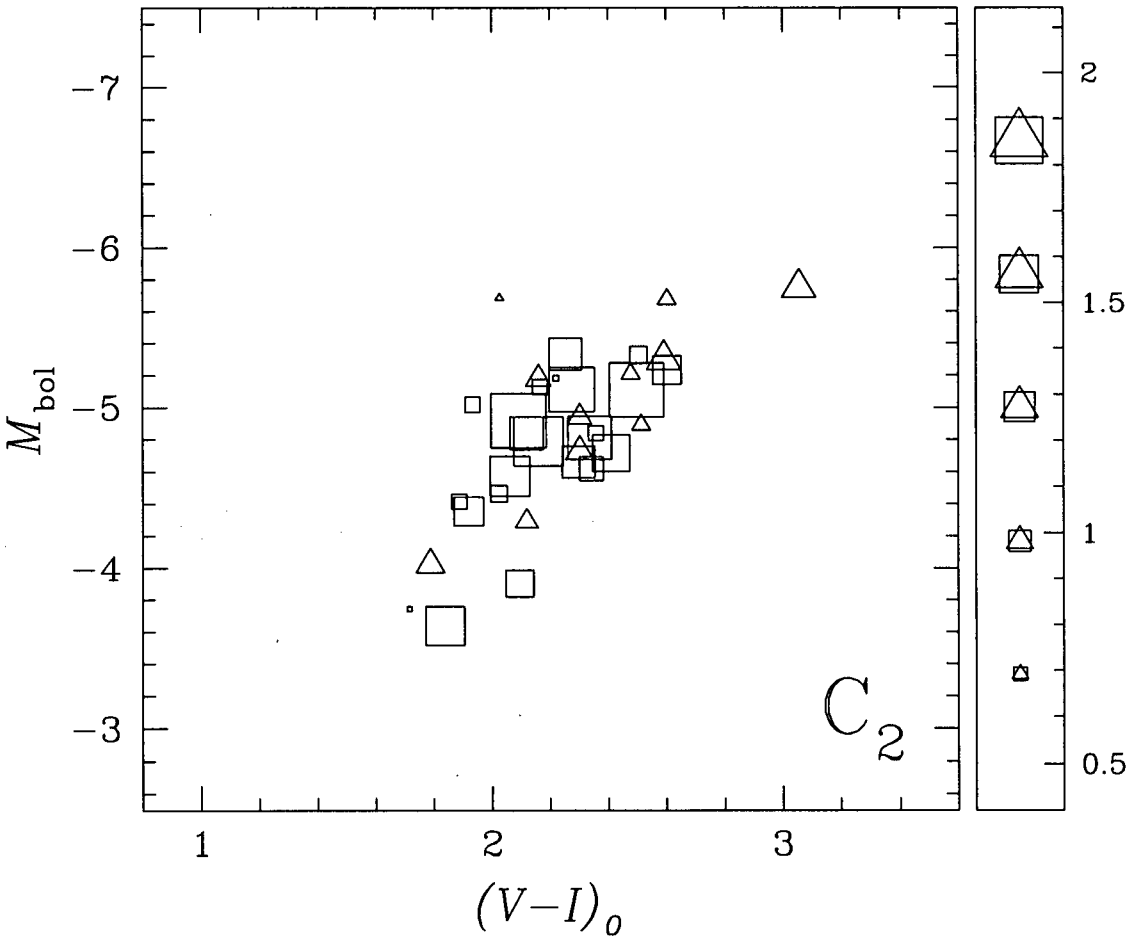

Figure 9.4: An (M_{bol}, $V-I)_0$ CMD for stars which I spectroscopically confirmed as C-stars. Excluded from this figure are those stars which had a negative flux level (see §6.2.5), as well as two stars with poor spectra. Triangles represent stars from Field 3, while squares are stars from Field 4. In this diagram, I have scaled the point size to the strength of the C_2 band at 5635Å (C_2^{5635}, the measurement of which is described in §8.1). The legend on the right of the diagram shows the scaling used between point size and C_2^{5635}.

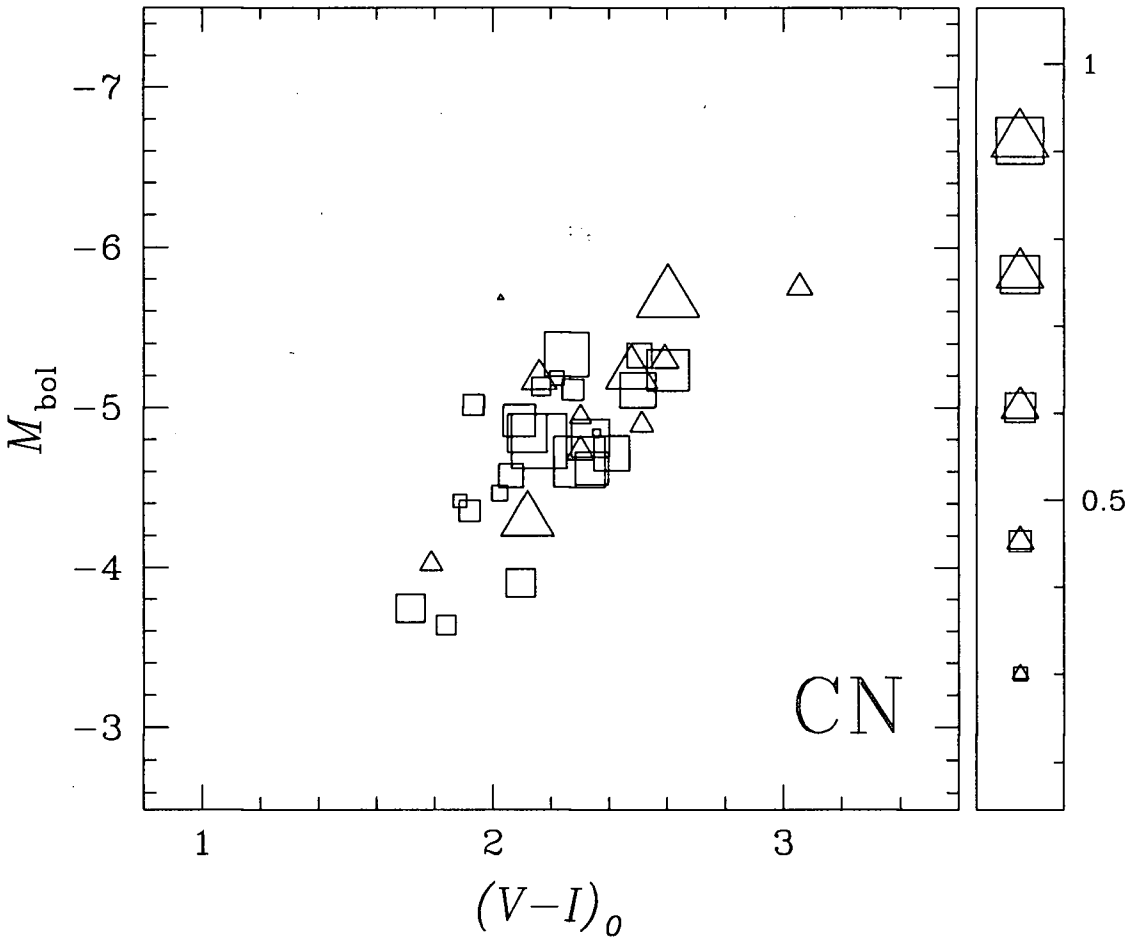

Figure 9.5: An $(M_{bol}, V-I)_0$ CMD for stars which I spectroscopically confirmed as C-stars. Excluded from this figure are those stars which had a negative flux level (see §6.2.5), as well as two stars with poor spectra. Triangles represent stars from Field 3, while squares are stars from Field 4. In this diagram, I have scaled the point size to the strength of the CN band at 5730Å (CN^{5730}, the measurement of which is described in §8.2). The legend on the right of the diagram shows the scaling used between point size and CN^{5730}.

value of ~3.

Boothroyd *et al.* (1993) modeled 4, 5, and $6\mathcal{M}_{\odot}$ AGB stars with both Z = 0.02 (Population I) and Z = 0.001 (Population II) abundances, investigating the effects of HBCE burning on their CNO abundances. From their models, Boothroyd *et al.* (1993) predict the existence of two C-star luminosity boundaries. The first boundary, at $M_{\rm bol}^{\rm C} = -6.4$, is the maximum magnitude at which C-stars can exist. Any AGB stars brighter than $M_{\rm bol}^{\rm C}$ will have undergone HBCE burning, destroyed ^{12}C, and reduced their C/O ratios to less than 1. Boothroyd *et al.* (1993) mention that this is in good agreement with observations of the Magellanic Clouds, and I can state that *I see no C-stars brighter than* $M_{\rm bol}^{\rm C}$ *in M31.* However, the C-star LF terminates *before* this limit, at a magnitude of $M_{\rm bol} \sim -6$ (this is shown in the lower panel of Fig. 9.9, which shall be described more fully in §9.7). The second boundary, at $M_{\rm bol}^{\rm C13} = -6.3$, divides the C-stars from J-stars. The stellar models have ^{12}C/^{13}C ratios of ~ 14 to 18 when they reach the AGB. At magnitudes fainter than $M_{\rm bol}^{\rm C13}$ the ^{12}C/^{13}C ratios are increased by third dredge-up (recall, the dredged up carbon was formed by triple-α burning and is ^{12}C), whereas at magnitudes brighter than $M_{\rm bol}^{\rm C13}$ the ratio is reduced by HBCE burning, eventually reaching the CN cycle equilibrium value of ~3.

The $4\mathcal{M}_{\odot}$ AGB models (both compositions) of Boothroyd *et al.* (1993) showed no significant HBCE burning of carbon up to the point where the model was terminated due to numerical problems. I (crudely) interpret this as saying that only stars more massive than $4\mathcal{M}_{\odot}$ evolve into J-stars. The stronger blue component seen in the Field 3 CMD over the Field 4 CMD (see Fig. 6.2) suggests that I am more likely to find J-stars in Field 3. The ratio of J-stars to C-stars in Field 3 is 2/17, while in Field 4 it is 5/30. Although the statistics are poor, the similarity in the ratios suggests that the two fields, despite their star formation differences, have a similar population of (presumably more massive)

J-star progenitors.

The J-stars I identified have been plotted in an ($M_{\rm bol}$, $V-I)_0$ CMD in Fig. 9.6. In Fig. 9.6 the J-star candidates are plotted as solid points, whereas those stars which exhibited ^{13}C isotopic features, but failed to satisfy the criterion from §8.3, are shown as open points with crosses. The models of Boothroyd *et al.* (1993) suggest that J-stars should be brighter than $M_{\rm bol}^{\rm C13}$, though fainter than $M_{\rm bol}^{\rm C}$. Figure 9.6 shows this is clearly not the case. Indeed, I find (with one exception) the J-stars to be among the fainter C-stars. Are there other observations of J-stars fainter than $M_{\rm bol}^{\rm C13}$? In their spectroscopic survey of the LMC, ROW79 identified eight J-stars of which three (115, 131, and 12–1) were substantially fainter than $M_{\rm bol}^{\rm C13}$. However, the other 5 J-stars found by ROW79 were brighter than $M_{\rm bol}^{\rm C13}$, and 4 of them were brighter than $M_{\rm bol}^{\rm C}$! Provided the estimates of $M_{\rm bol}$ from the two surveys are comparable, might the difference between us finding the J-stars to be generally fainter and ROW79 finding J-stars to be generally brighter be related to the abundance difference between the LMC and M31? Clearly, more work is needed by both observers and theoreticians if there is to be convergence between observations and models.

9.6 Emission-Line Stars

Balmer line emission is always present in very late C-stars (Reimers & Groote 1983) and is indicative of a high mass-loss rate at the terminal phases of AGB evolution. Consequently, I expect the C-stars with Hα emission to be generally redder and more luminous than the other C-stars. In Fig. 9.7 I plot an ($M_{\rm bol}$, $V-I)_0$ CMD and include as open points the C-stars for which spectra were obtained, as solid points those C-stars with Hα emission, and as crosses those C-stars with marginal Hα emission. The C-stars

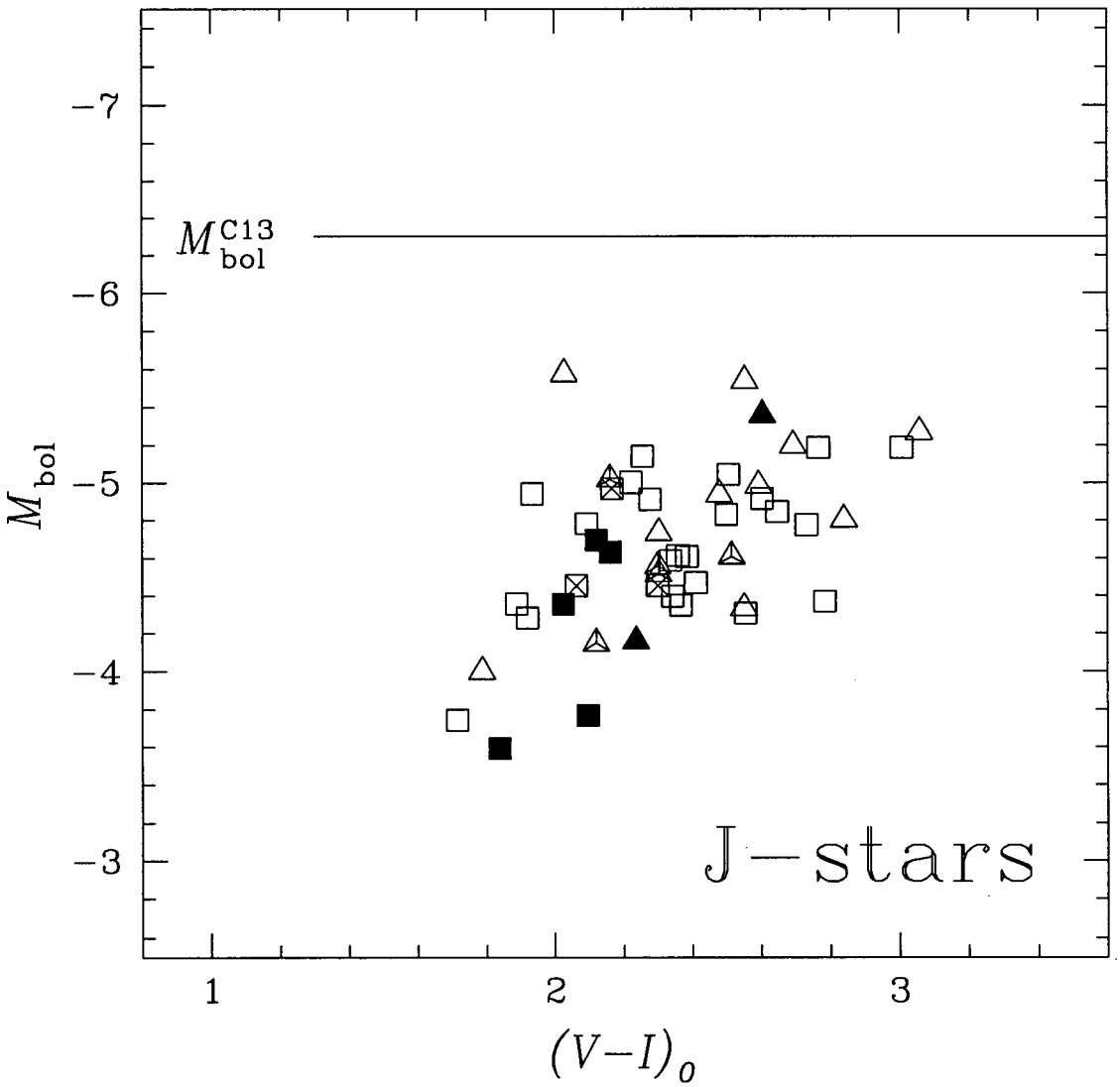

Figure 9.6: An (M_{bol}, $V-I)_0$ CMD for all the stars which I spectroscopically confirmed as C-stars. Triangles represent Field 3 C-stars, while squares are Field 4 C-stars. In this diagram the solid points represent stars which I found to be J-stars using the criterion described in §8.3, while points which encase crosses represent those stars which exhibited isotopic features but failed to meet my J-star criterion (the marginal J-stars). The horizontal line represents the magnitude at which the models of Boothroyd *et al.* (1993) predict C-stars will evolve into J-stars as they ascend the AGB.

in which I found marginal Hα emission are fairly evenly distributed, while the two C-stars with strong Hα emission are among the redder C-stars. ROW79 similarly found that C-stars with Hα emission were among the redder of the C-stars in their survey. I note that the C-stars exhibiting Hα found by ROW79 span nearly the entire range of their C-star magnitudes, a finding with which I concur if I consider stars with both weak and strong Hα emission.

In passing, I note that a hot white dwarf companion could lead to Hα emission from a C-star by exciting its wind. A white dwarf companion is one of the explanations forwarded by Reimers & Groote (1983) for the presence of hydrogen emission lines in the spectrum of UV Aur.

9.7 Superrich Lithium Stars

The existence of Galactic SRL C-stars has been known for some time. An explanation for the enhanced Li abundances found in these stars was forwarded by Cameron (1955) and Cameron & Fowler (1971). They suggested that ^{7}Be is produced in the reaction ^{3}He(^{4}He,γ)^{7}Be during the He shell flash of a TPAGB star and is subsequently transported to a cooler region of the star where it undergoes electron capture (^{7}Be(e^-,ν)^{7}Li) to form ^{7}Li. The key to this mechanism is the transportation of ^{7}Be to a cooler region; if the ^{7}Be underwent electron capture in a hot region, the ^{7}Li produced would be immediately destroyed by proton capture.

To model the surface abundance of Li produced in the Cameron/Fowler scenario, Sackmann & Boothroyd (1992) combined a time-dependent convective diffusion algorithm for HBCE burning with a fully self-consistent evolutionary sequence. Sackmann & Boothroyd (1992) explored models of 3, 4, 5, 6, and 7$\mathcal{M}_\odot$ for metallicities of Z = 0.02

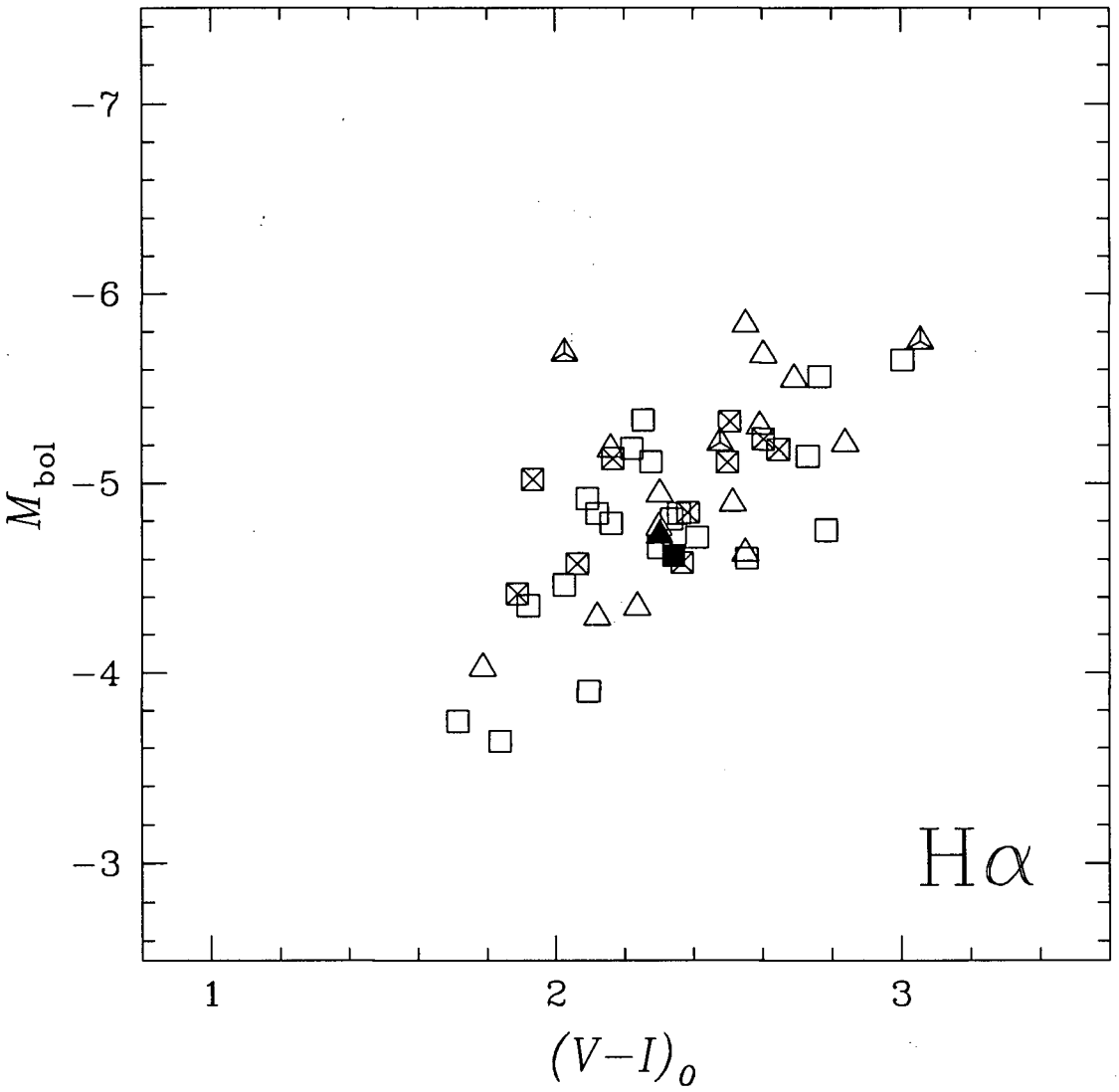

Figure 9.7: An $(M_{\rm bol},\ V-I)_0$ CMD for all the stars which I spectroscopically confirmed as C-stars. Triangles represent Field 3 C-stars, while squares are Field 4 C-stars. In this diagram the solid points represent stars for which I found strong Hα emission, while points which encase crosses represent those stars for which I found marginal Hα emission (see §9.6).

(Population I) and Z = 0.001 (Population II). In both the Population I and Population II $3\mathcal{M}_\odot$ stars, the base of the convective envelope failed to attain a high enough temperature for the production of Li, while in the $7\mathcal{M}_\odot$ models (both metallicities) carbon ignited in the core before they evolved into AGB stars with HBCE burning. The population I $4\mathcal{M}_\odot$ model showed no sign of producing detectable Li abundances, while the Population II $4\mathcal{M}_\odot$ model looked as though it might. The $5\mathcal{M}_\odot$ and $6\mathcal{M}_\odot$ models (both metallicities) became SRL stars. From their models, Sackmann & Boothroyd (1992) predict that SRL stars lie in the range $M_{\rm bol}\sim$ –6.2 to –6.8 (For Population I, this range may be be extended to brighter magnitudes by stars more massive than $6\mathcal{M}_\odot$).

In Fig. 9.8 I plot the position of my SRL star and the two marginal SRL stars in an ($M_{\rm bol}$, $V-I)_0$ CMD. In this diagram I have shaded the range of $M_{\rm bol}$ at which Sackmann & Boothroyd (1992) predict SRL stars will occur. As can be clearly seen, all of the stars which have an enhanced Li line at 6708Å are *much* fainter than predicted by the models. Indeed, my Li-stars are among the fainter C-stars in my sample!

This conflict between observation and theory has been noted before. Smith *et al.* (1995) conducted a spectroscopic search for Li-stars in the Magellanic Clouds. They found 6 C-stars with detectable Li I, which spanned the luminosity range $-5.7 \lesssim M_{\rm bol} \lesssim -4.6$. Of the six, they gave three (two of which had been previously identified) the title of SRL. The three SRL C-stars were found to lie in the magnitude range $M_{\rm bol} = -5.5$ to –5.7. At a magnitude of $M_{\rm bol}\sim$ –4.5, my SRL star is considerable fainter than these.

Is the SRL C-star a pathological case? I believe not, and back up this claim with Fig. 9.9. In the upper panel of Fig. 9.9 I reproduce the upper panel of Fig. 8 from Smith *et al.* (1995) which shows the fraction of C- and S-stars they found to be Li-rich in their survey of the Magellanic Clouds. In the middle panel of Fig. 9.9 I show the magnitude range at which Sackmann & Boothroyd (1992) predict SRL stars will occur and also the

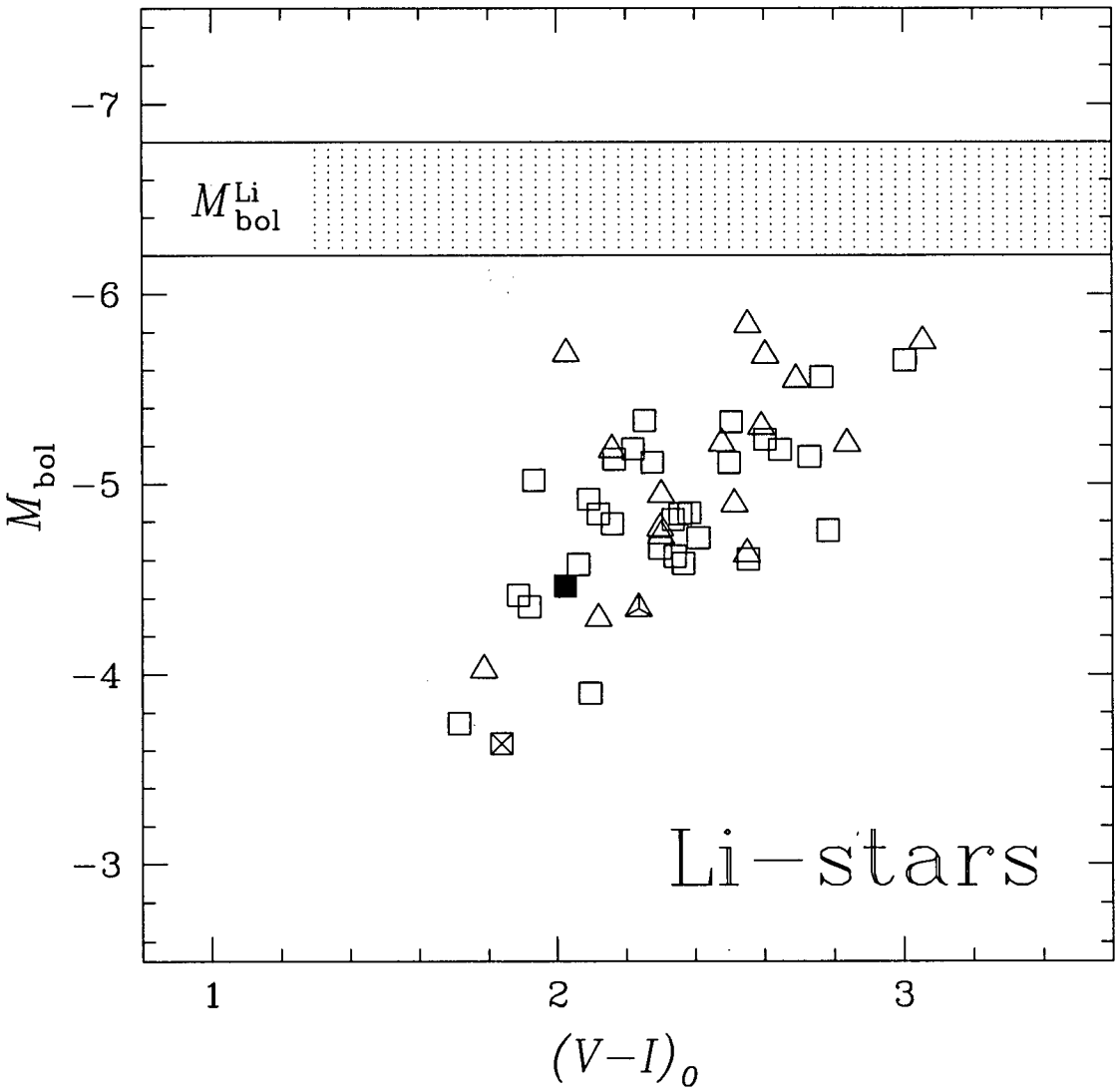

Figure 9.8: An ($M_{\rm bol}$, $V-I)_0$ CMD for stars which I spectroscopically confirmed as C-stars. Triangles represent Field 3 C-stars, while squares are Field 4 C-stars. In this diagram the solid point is F4–28.2, my SRL C-star. The two points which encase crosses are stars F3–7.1 and F4–11.1 which are marginal SRL C-stars (see §8.5). The shaded region in this diagram shows the magnitude range at which the models of Sackmann & Boothroyd (1992) predict Li-stars will occur.

magnitude of my SRL star (solid point) and marginal SRL stars (open points). The lower panel of Fig. 9.9 (which I shall discuss further in §9.8) shows the LFs of the C-stars in Fields 3 and 4 (solid line) and those C-stars for which I obtained spectra (hatched).

What can be learnt from Fig. 9.9? The upper histogram shows that the magnitude range of Li-stars extends to considerably fainter magnitudes than predicted by the models of Sackmann & Boothroyd (1992). Smith *et al.* (1995) suggest that additions to the models of HBCE burning may be needed to explain the fainter Li-stars. I note that whereas Smith *et al.* (1995) found no Li-stars as faint as ours, it seems conceivable that the tail of the distribution in the upper panel of Fig. 9.9 may extend to fainter magnitudes (indeed, the faintest magnitude bin of Smith *et al.* (1995) had only 7 stars which, with a low Li-star frequency, may have led to them finding no Li-stars in this bin). Taking this into account, along with my dubious bolometric magnitudes, I conclude that I am seeing a population of faint Li-stars in M31 similar to those seen by Smith *et al.* (1995) in the Magellanic Clouds.

In summary, I have found stars with enhanced Li abundances at magnitudes considerable fainter than predicted by theory. *It appears that the faint Li-stars I observed have undergone HBCE burning, as they constitute a subset of the J-stars.* I agree with the opinion of Smith *et al.* (1995) that the lower luminosity Li-rich stars remain an enigma, and may require additions to the models of HBCE burning.

9.8 An S-Type Star

What is the bolometric magnitude of F3–24.2, the S-star in my sample? In §9.2 I adopted a BC_{I_C} for C-stars by fitting data from Bessell & Wood (1984, see eq. 9.3). Applying this BC to the S-star gives $M_{\rm bol} = -6.2$. However, Reid & Mould (1985) used the BC_{I_C} (applicable to K- and M-types) of Bessell & Wood (1984, see eq. 3.2) for S-stars, and

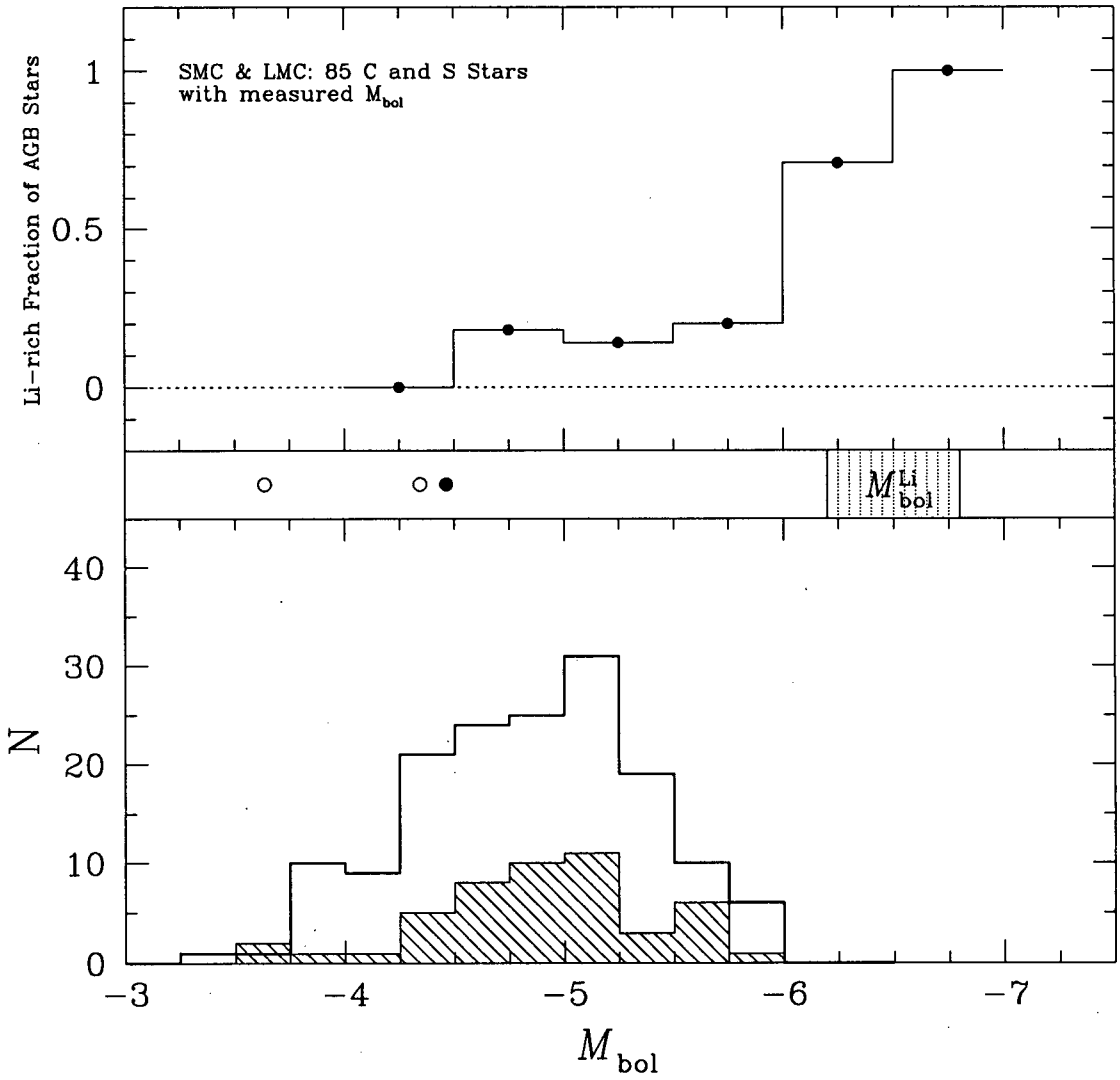

Figure 9.9: The upper panel is reproduced from Fig. 8 of Smith *et al.* (1995) and shows the fraction of C- and S-stars that they surveyed in the Magellanic Clouds that exhibited enhanced Li abundances. The shaded region in the middle panel shows the luminosity range in which the models of Sackmann & Boothroyd (1992) predict enhanced Li abundances should occur, while the solid point shows the magnitude of my SRL star, and the open points the magnitudes of the marginal SRL stars. The solid line histogram in the lower panel shows the LF of all the C-stars in Fields 3 and 4, while the hatched histogram is the LF of the C-stars for which spectra were obtained.

using this gives $M_{\rm bol} = -5.32$ for F3–24.2. Without obtaining IR photometry of this star, I conclude that the true value of $M_{\rm bol}$ lies somewhere in the range of these two estimates. In Fig. 9.10 I plot up the position of the S-star in an $(M_{\rm bol},\ V-I)_0$ CMD, adopting a value of –6.2 for $M_{\rm bol}$.

The most noticeable feature of Fig. 9.10 is that the S-star is (virtually) the brightest and reddest star in the diagram. What does this tell us about the evolutionary status of F3–24.2? While on the TPAGB, third dredge-up increases the abundance of ^{12}C in a star's atmosphere and under the right circumstances can change a star's spectral type from M to S, and finally to C. Given this picture of abundance evolution, it seems that M-, S- and C-stars should form a sequence of increasing luminosity, and indeed Bessell *et al.* (1983) have shown that S-stars on the AGBs of Magellanic Cloud clusters lie in the transition region between M- and C-stars. There is more to the story though. The LFs of C-stars are known to have an upper luminosity limit of $M_{\rm bol}\sim$ –6 (LMC: Richer 1981b, Cohen *et al.* 1981; M31: lower panel of Fig. 9.9), even though the AGB magnitude limit is $M_{\rm bol}\sim$ –7.1. Does this mean that the AGB terminates before the core mass has reached the Chandrasekhar limit? If a star undergoes HBCE burning then it can make another chameleon-like change by converting ^{12}C to ^{14}N and ^{13}C, thus reducing its C/O ratio and evolving back to an S- or even M-star. Consequently, provided it is not mass loss that terminates the C-star LFs, I may expect to find S- and M-type TPAGB stars beyond the C-star LF cut-off.

In Fig. 8 of Smith *et al.* (1995), a comparison is made between the LMC C-star LF and a histogram (which I reproduced in the upper panel of Fig. 9.9) that shows the proportion of C- and S-stars found to have enhanced Li. Smith *et al.* (1995) suggest that the lack of C-stars brighter than $M_{\rm bol} = -6$ is due to their conversion to S-stars by HBCE burning, and that HBCE burning provides an explanation for the S-stars with

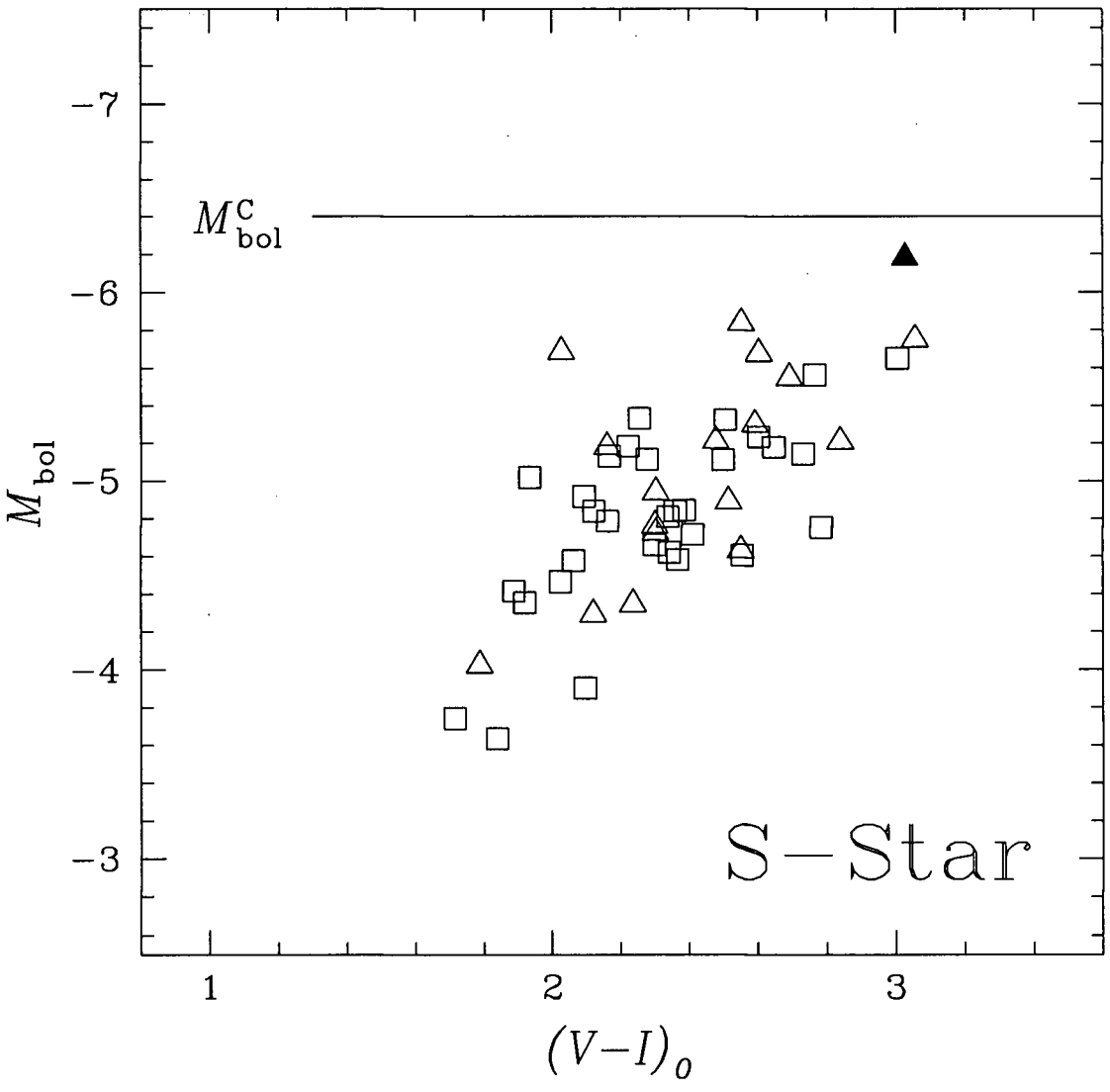

Figure 9.10: An (M_{bol}, $V-I)_0$ CMD for stars which I spectroscopically confirmed as C-stars. Triangles represent Field 3 C-stars, while squares are Field 4 C-stars. In addition to the C-stars, I show as a solid point F3–24.2, the spectroscopically confirmed S-star. The bolometric magnitude of the S-star was derived using eq. 9.3. The horizontal line shows the magnitude at which star C-star formation is prevented by HBCE burning (Boothroyd *et al.* 1993).

enhanced Li they see at $M_{\rm bol} < -6$. This suggests, at least for the more massive stars, that it is HBCE burning which terminates the C-star LF at $M_{\rm bol}\sim$ –6 and *not mass loss.*

Can the same conclusion be drawn about M31's C-star LF? I note that the LMC C-star LF presented in Fig. 8 of Smith *et al.* (1995) is similar to the C-star LF from Fields 3 and 4 (lower panel of Fig. 9.9). However, as demonstrated by their very different C/M ratios, differences do exist between the AGB populations of M31 and the Magellanic Clouds. The C/M ratio has been shown to be inversely correlated with metallicity, and a possible explanation for this may lie in the dependence of mass-loss rate on metallicity. Provided the C-star LF cut-off in M31 is due to HBCE burning and not mass-loss, a possibility yet to be ruled out, then it seems likely that F3–24.2 has undergone HBCE burning.

As pointed out by Wood *et al.* (1983) another possible evolutionary path for bright S-stars exists: more massive stars may dredge up insufficient carbon to drive C > O before the termination of the AGB. Consequently, the star may appear as an S-star at magnitudes brighter than the C-stars. These two possibilities (HBCE burning and insufficient dredge-up of carbon) can be distinguished as HBCE burning would lead to S-stars with high ^{14}N abundances and low ^{12}C/^{13}C ratios.

The above suggests that F3–24.2 has either: (1) evolved through the C-star phase, and has become an S-star by HBCE burning; or (2) has a large envelope mass in which insufficient dredge up has occurred to drive C > O. I include on Fig. 9.10 $M_{\rm bol}^{\rm C}$, the magnitude at which HBCE burning will occur (From Boothroyd *et al.* 1993, see §9.5). The S-star is fainter than this limit, which would initially suggest the latter evolutionary path. I point out however that I have found evidence for HBCE burning at fainter magnitudes: the J-stars I identified (§9.5) were fainter than this limit. In conclusion, further observations are needed to distinguish between these two evolutionary scenarios.

Chapter 10

CONCLUSIONS

"As the births of living creatures at first are ill-shapen, so are all innovations, which are the births of time."

Sir Francis Bacon (1561 – 1626)

On page 4 I mentioned that one of the aims of this thesis was to take a "census" of AGB stars in fields along the SW semi-major axis of M31 and study the interplay between properties of M31's AGB population, such as C-star LFs and C- to M-star ratios, and differences in local properties, such as metallicity and star-forming history. I have fulfilled this goal by using a four-band photometric system (FBPS) to identify the C- and M-stars. My main findings from the photometric data are as follows.

1. Using previously identified Cepheids, I obtained a true distance modulus for M31 of $(m-M)_0 = 24.42 \pm 0.05$ which is consistent with a value that FM90 derived from Cepheids.

2. The measured $(V-I)$ widths of the RGBs show that:

   - in all but Field 1, the RGB width is wider than expected from metallicity dispersion alone.
   - much of the RGB width can be accounted for if stars of varying mass are "funnelling" onto the RGB.
   - the contribution from differential reddening remains unknown, though is unlikely to account for the entire width of the RGBs.

3. The AGB LF gradients of Fields 1 and 2 were similar, though significantly different to the AGB LFs in Fields 3 and 4 (which were also similar). This indicated that differences in star forming history exist between the fields.

4. A distance modulus was derived using C-stars in Fields 2, 3 and 4, and found to be in good agreement with the distance modulus derived from the Cepheids. I further found that despite differences in the star-forming history and metallicity in Fields 2, 3 and 4, the mean magnitudes of the C-stars were, within observational error, the same.

5. The ratio of C- to M-stars (C/M) was shown to increase with galactocentric distance in M31. Completeness tests on the data showed this result to be independent of the crowding conditions in the fields.

6. Under the assumption that the C/M ratio is a metallicity indicator, I derived metallicity values for the fields using previous observations as a guide. I then showed that there was good agreement between my data and measurements from H II regions and that my data indicate a flattening of the metallicity gradient in M31 beyond $R_{\rm M31} = 15$ kpc.

7. I considered the impact that a varying C/M ratio would have on the ISM. The main conclusions that I arrived at here were that there is evidence that the extinction law in M31 is compatible with what would be caused by the observed C/M ratio gradient, and that a fruitful area of future research may be to look for a correlation between the ratio of DIB strength and reddening against Galactocentric distance.

Having identified AGB stars in the 5 M31 fields, I then proceeded to obtain spectra of a sample of these stars from Fields 3 and 4. As mentioned on page 4, the motivation

for making the spectral observations came from a desire to make a comparison between observation and theory. Such a comparison will help us better understand the nuclear processes occurring in these stars. My main findings from the spectroscopic data are as follows.

8. The FBPS works in crowded fields, and performed admirably in separating the C-, S-, and M-type stars. I found only C-stars in the C-star region, and of the 48 C-stars I spectroscopically identified, only three failed my photometric criteria to be C-stars.

9. Neither the strength of the C_2 band at 5635Å or the CN band at 5730Å correlates with either $M_{\rm bol}$ or $(V-I)_0$.

10. The J-stars in my sample, unlike the J-stars identified by ROW79 in the LMC, tend not to lie at brighter magnitudes.

11. The Hα emission stars in my sample tend to lie to the red in an ($M_{\rm bol}$, $V-I)_0$ CMD, suggesting that these stars are losing mass and will soon terminate their evolution on the AGB.

12. I have identified the first SRL C-star in M31 as well as two other stars with enhanced Li absorption. I found all three of these stars to be J-stars, and all to be less luminous than predicted by the models of Sackmann & Boothroyd (1992).

13. I have identified the first S-type star in M31, and suggested that either HBCE burning is responsible for its evolutionary status, or that it is a massive star which has dredged up insufficient carbon to evolve into a C-star.

My spectral observations strongly suggest that HBCE burning occurs *at fainter magnitudes than AGB models predict.* There is now evidence for this in both the LMC

(ROW79, Smith *et al.* 1995) and M31 (this study). It appears that modifications to existing theory must be made, and I await with interest future developments of AGB models. Another possible explanation for the disagreement between observation and theory lies in BC_{I_C}. Could it be that some of the C-stars I observed (presumably the more evolved, and consequently those showing evidence of HBCE burning) are evolving into infrared C-stars and require larger bolometric corrections than I applied? I strongly suggest that future observers undertaking similar spectroscopic surveys obtain infrared photometry. Such photometry will put $M_{\rm bol}$ on a secure footing, and allow sturdier comparison with model predictions.

Chapter 11

DESIDERATA

"All is flux, nothing is stationary."

Heracleitus (fl. 513 B.C.E.)

In the best of scientific traditions, this thesis has raised new questions to be addressed. In this brief chapter I discuss some ideas for future studies which will help shed additional light on some aspects of this thesis, as well as some ideas for related projects.

11.1 An FBPS Survey of M33

In Table 11.1 I provide a summary of properties of M31 and M33 to demonstrate that M33 is a ripe target for the FBPS, it providing a good contrast to the FBPS survey of M31. As can be seen, M33 is a substantially more metal-poor system and so many more C-stars are expected. In addition, M33 has a steeper metallicity gradient than M31, meaning that its C/M ratio should vary *dramatically.* As M33 and M31 have similar distance moduli, and the crowding in M33 is less severe, there is no observational reason why a study of M33 could not be made. The (optical) size of M33 on the sky is $53' \times 83'$ (see van den Bergh 1991a) and with the new generation of mosaic CCD cameras (such as CFHT's MOCAM camera which has a field size of $14' \times 14'$) contiguous fields could easily be observed that spanned along M33's *entire* southern semi-major axis. Cook *et al.* (1986) have previously observed a *single* $1\farcm5 \times 2\farcm5$ field in M33 using an FBPS similar to the one described in §2.1. Aaronson *et al.* (1986) found 14 C-stars which, from scaling arguments, suggests that in a field the size of the MOCAM field, there will be around

800 C-stars. With this many C-stars, the statistics will allow an accurate determination of $\langle I \rangle$ as well as a comparison with other C-star LFs and synthetic models. I believe observations of M33 will help answer some of the following questions:

- Does the C/M ratio in M33 track the metallicity gradient in both arm and interarm fields? In M31 it appeared that the C/M ratio was independent of the star forming history of the field. Observations of M33 will help confirm this result as its southern arm is the best-defined spiral structure in the Local Group (van den Bergh 1991a) and, using a detector with a large field size, it will be easy to observe both arm and interarm fields as a function of galactocentric distance. Unlike my M31 observations where the C/M ratio was only *sampled* along the axis, in M33 it will be relatively easy to obtain *entire coverage* of its axis. There is no problem in making a comparison with M33's metallicity gradient as a measurement of this has been made (Smith *et al.* 1993).

- Does the C/M ratio in M33 flatten out with increasing galactocentric distance, like I suspect it does in M31? If differences are found in the "evolution" of the C/M ratios between M31 and M33, and the differences are due purely to a metallicity effect, then the difference may be attributable to the different morphological types of these galaxies. The differences will help place constraints on the formation models of these two different types of spiral galaxy.

- In §5.2 I found that differences in the extinction law appeared to correlate with the C/M ratio in M31. This strongly suggests that the C/M ratio affects the composition of the ISM (presumably by altering the ratio of carbonaceous to siliceous grains). As an understanding of extinction laws is fundamental to many branches of astronomy, confirmation of this result would be of great interest.

Table 11.1: A Comparison Between the Physical Properties of M31 and M33.

Property	M31	Ref.	M33	Ref.
Distance modulus, true	24.3	1	24.5	2
Foreground reddening	0.08	1	0.07	2
Angle of plane to line of sight	12°.5	1	56°	2
Hubble type	SbI-II	3	Sc(s)II-III	3
$M_{B_T}^{0,i}$	–21.61	3	–19.07	3
[Fe/H] (dex)	0	4	–0.6	5
Abundance gradient (dex/kpc)	–0.035	4	–0.1	5

References: (1) Hodge (1992), and references therein; (2) van den Bergh (1991a), and references therein; (3) Sandage & Tammann (1987); (4) BKC82; (5) Smith *et al.* (1993).

- In M31 I found that the mean luminosity of C-stars appeared to be independent of galactocentric distance (see §4.3). Observations of M33 will further help assess the impact of star formation history (comparison of arm and interarm fields) and metallicity (comparison of fields at differing galactocentric distances) on the C-star LF.

- How smoothly does the C/M ratio change with galactocentric distance? Using a detector with a large field size will allow the C/M ratio to be measured along the axis *uninterrupted* in a reasonable amount of time.

11.2 Zenith Surveys for C-stars

As mentioned earlier, the FBPS is suited to surveys of C-stars. The present limit on the FBPS is the small detector size available and the willingness of time allocation committees to assign large amounts of observing time. Dr. Paul Hickson at the University of British Columbia faced similar problems for a proposed multi-band survey of galaxies. The

solution that Hickson found was to build a cheap large-aperture telescope that would be dedicated to his survey. Normally the phrase "cheap large-aperture telescope" would be considered an oxymoron, but Hickson has proven this not to be the case by building a 2.7m liquid mirror telescope (LMT). Basically, the LMT is a large dish of mercury that when rotated forms a near-perfect paraboloid mirror. Naturally, the dish must remain level, and so the LMT always points at the zenith. In lieu of tracking, the CCD detector is read out at the sidereal rate and a continuous strip of sky is imaged. Readers interested in more than this brief summary are referred to Hickson *et al.* (1994) and references therein.

The LMT would work ideally with the FBPS as a survey instrument for C-stars. One of the possible uses of such a survey would be to constrain estimates of halo kinematics and structure, as was done by Green *et al.* (1994).

11.3 Magellanic Stream

With the advent of large mosaics of CCD detectors, the FBPS may be used to find C-stars in the Magellanic Stream. This is of interest as follow up spectra of these stars would yield radial velocities. When the radial velocity measurements are combined with proper motion measurements (measured over a period of time), a value for the mass of the Galaxy can be obtained. The northern tip of the Magellanic Stream is visible from Mauna Kea, making this a viable CFHT project.

11.4 Sagittarius Galaxy

The galaxy in Sagittarius recently discovered by Ibata *et al.* (1994) was found by them to contain C-stars. Because of their strong spectra and the relatively low levels of foreground

contamination from Galactic C-stars, the Sagittarius galaxy C-stars make ideal dynamic probes for the system, and will allow an estimate of its mass to be made. Dynamic probes aside, the presence of C-stars (which are generally a few Gyr old) in the Sagittarius galaxy raises the interesting question of where the gas that formed these stars came from. If the Sagittarius galaxy is on an orbit that takes it through the plane of the Milky Way, the gas it contains would have been stripped long ago, leaving it unable to form new stars. It may be that the galaxy is making its first pass through the disk, in which case we might expect it to have a C/M ratio similar to that seen in Fornax and Sculptor. Alternatively, it may have acquired enough gas during its orbit around the Milky Way (either from red giants or the Galactic halo) to be able to form these stars. In this case its C/M ratio can be expected to be quite different from those seen in Fornax and Sculptor.

11.5 Determination of H_0

The FBPS used here is limited by seeing and crowding conditions; enough positive identifications of C-stars are needed to build an LF to allow a reasonable estimate of the mean to be obtained. For example, the innermost field in this study is of no use for determining the distance modulus of M31 as the crowding produces errors in the photometry which cause many misidentifications and a deviant C-star LF. Taking this effect into account, I estimate that the FBPS (possibly modified to use $(R-I)$ as a temperature discriminator instead of $(V-I)$) may be workable out to the Virgo cluster galaxies from superb ground-based sites such as CFHT (and in the future Gemini) with the use of adaptive optics. I back up this claim by noting that the C-stars are as bright as the Cepheids in I, and that Cepheids have recently been identified in the Virgo cluster with both ground-based (Pierce *et al.* 1994) and HST (Freedman *et al.* 1994) observations.

11.6 Infrared Photometry

As mentioned in Chapter 9, most of the flux from C-stars is in the infrared, and to obtain accurate values of $M_{\rm bol}$, measurements of this flux is needed. The recent rapid advances in detector technology (in the past decade infrared astronomy has gone from using single element photometers to using sensitive array detectors) means that obtaining photometry in crowded fields, such as my M31 fields, is now feasible. In the future I hope to obtain infrared photometry of the stars in Chapter 9 which showed spectral features expected only in brighter stars.

FIN

References

Aaronson, M., Blanco, V.M., Cook, K.H., & Schechter, P.L. 1989, ApJS, 70, 637

Aaronson, M., Da Costa, G. S., Hartigan, P., Mould, J., Norris, J., & Stockman, H.S. 1984, ApJ, 277, L9

Aaronson, M., & Mould, J. 1982, ApJS, 48, 161

Aaronson, M., Mould, J., & Cook, K.H. 1985, ApJ, 291, L41

Abia, C., Boffin, H.M.J., Isern, J., & Rebolo, R. 1993, A&A, 272, 455

Allen, C.W. 1976, Astrophysical Quantities (Athlone, London)

Anders, E., & Zinner, E. 1993, Meteoritics, 28, 490

Baade, W., & Swope, H. H. 1965, AJ, 70, 212

Barnbaum, C. 1994, ApJS, 90, 317

Bertelli, G., Bressan, A., Chiosi, C., Fagotto, F., & Nasi, E. 1994, A&AS, 106, 275

Bessell, M.S. 1979, PASP, 91, 589

Bessell, M.S., & Brett, J.M. 1988, PASP, 100, 1134

Bessell, M.S., & Wood, P.R. 1984, PASP, 96, 247

Bessell, M.S., Wood, P.R., & Lloyd Evans, T. 1983, MNRAS, 202, 59

Blaauw, A. 1965, in Stars and Stellar Systems. Vol. 5: Galactic Structure, edited by A. Blaauw and M. Schmidt (University of Chicago Press, Chicago), p. 435

Blair, W.P., & Kirshner, R.P. 1981, ApJ, 247, 879

Blair, W.P., Kirshner, R.P., & Chevalier, R.A. 1982, ApJ, 254, 50 (BKC82)

Blanco, B.M., Blanco, V.M., & McCarthy, M.F. 1978, Nature, 271, 638

Blanco, V.M. 1965, in Stars and Stellar Systems. Vol. 5: Galactic Structure, edited by A. Blaauw and M. Schmidt (University of Chicago Press, Chicago), p. 241

Blanco, V.M., & McCarthy, M.F. 1981, in Physical Processes in Red Giants, edited by I. Iben Jr. and A. Renzini (Reidel, Holland), p. 147

Blanco, V.M., McCarthy, M.F., & Blanco, B.M. 1980, ApJ, 242, 938

Blanco, V.M., & Richer, H.B. 1979, PASP, 91, 659

Bohlin, R.C., Cornett, R.H., Hill, J.K., Hill, R.S., Stecher, T.P. 1988, ApJ, 334, 657

Bolte, M., 1989, ApJ, 341, 168

Boothroyd, A.I., Sackmann, I.-J., & Ahern, S.C. 1993, ApJ, 416, 762

Brewer, J.P., Fahlman, G.G., Richer, H.B., Searle, L., & Thompson, I. 1993, AJ, 105, 2158

Burstein, P., & Heiles, C. 1984, ApJS, 54, 33

Cameron, A.G.W. 1955, ApJ, 212, 144

Cameron, A.G.W., & Fowler, W.A. 1971, ApJ, 164, 111

Cameron, L.M. 1987, A&A, 147, 39

Cardelli, J. 1994, private communication

Cohen, J.G., Frogel, J.A., Persson, S.E., & Elias, J.H. 1981, ApJ, 249, 481

Cook, K.H. 1987, Ph.D. thesis (Department of Astronomy, University of Arizona

Cook, K.H. 1993, private communication

Cook, K.H., Aaronson, M., & Norris, J. 1986, ApJ, 305, 634

Da Costa, G.S, & Armandroff, T.E. 1990, AJ, 100, 162

Davis, L. 1994, private communication

Dennefeld, M., & Kunth, D. 1981, AJ, 86, 989

de Vaucouleurs, G. 1958, ApJ, 128, 465

Dinerstein, H.L. 1990, in The Interstellar Medium in Galaxies, edited by H.A. Thronson, Jr. and J.M. Shull (Kluwer, Holland), p. 257

Draine, B.T., & Lee, H.M. 1984, ApJ, 285, 89

Drukier, G.A., Fahlman, G.G., Richer, H.B., & VandenBerg, D.A. 1988, AJ, 95, 1415

Ford, H.C., & Jacoby, G.H. 1978, ApJS, 38, 351

Freedman, W.L., *et al.* 1994, ApJ, 427, 628

Freedman, W.L., & Madore, B.F. 1990, ApJ, 365, 186 (FM90)

Frogel, J.A., & Richer, H.B. 1983, ApJ, 275, 84

Gaposchkin, S. 1962, AJ, 67, 334

Green, P.J. 1992, PASP, 104, 977

Green, P.J., Margon, B., Anderson, S.F., & Cook, K.H. 1994, ApJ, 434, 319

Herbig, G.H. 1995, ARA&A, 33, 19

Hickson, P., Borra, E.F., Cabanac, R., Content, R., Gibson, B.K., & Walker, G.A.H. 1994, ApJ, 436, L201

Hodge, P. 1979, AJ, 84, 744

Hodge, P. 1981, Atlas of the Andromeda Galaxy (University of Washington Press, Seattle)

Hodge, P. 1992, The Andromeda Galaxy (Kluwer, Dordrecht)

Hodge, P., & Lee, M.G. 1988, ApJ, 329, 651

Hudon, J.D., Richer, H.B., Pritchet, C.J., Crabtree, D.R., Christian, C.A., & Jones, J. 1989, AJ, 98, 1265

Hutchings, J. 1995, private communication

Ibata, R.A., Gilmore, G., & Irwin, M.J. 1994, Nature, 370, 194

Iben, I., Jr. 1975, ApJ, 196, 525

Iben, I., Jr. 1981, ApJ, 246, 278

Iben, I., Jr. 1995, Physics Reports, 250, 1

Iben, I., Jr., & Renzini, A. 1983, ARA&A, 21, 271 (IR83)

Iben, I., Jr., & Truran, J.W. 1978, ApJ, 220, 980

Jacoby, G.H. 1994, private communication

Jørgensen, U.G. 1992, in Newsletter of Chemically Peculiar Red Giant Stars, Number 13, edited by S. Yorka (Ohio State University Astronomy Department, Ohio), p. 3

Keenan, P.C. 1993, PASP, 105, 905

Keenan, P.C., & Morgan, W.W. 1941, ApJ, 94, 501

Kingsburgh, R.L., & Barlow, M.J. 1994, MNRAS, 271, 257 (KB94)

Knapp, G.R. 1991, in Frontiers of Stellar Evolution, ASP Conference Series, Vol. 20, edited by D.L. Lambert (ASP, San Francisco), p. 229

Kraft, R.P. 1963, in Stars and Stellar Systems. Vol. 3: Basic Astronomical Data, edited by K.A. Strand (University of Chicago Press, Chicago), p. 421

Krisciunas, K. 1994, private communication

Kron, G.E., & Mayall, N.U. 1960, AJ, 65, 581

Landolt, A.U. 1992, AJ, 104, 340

Lee, M.G., Freedman, W.L., & Madore, B.F. 1993, ApJ, 417, 553

Lee, T.L. 1970, ApJ, 162, 217

Le Fèvre, O., Crampton, D., Lilly, S.J., Hammer, F., & Tresse, L. 1995, ApJ, 455, 60

Lilly, S.J. 1987, MNRAS, 229, 589

Maciel, W.J., & Köppen, J. 1994, A&A, 282, 436

Madore, B.F., & Freedman, W.L. 1991, PASP, 103, 933 (MF91)

Massey, P., Valdes, F., & Barnes, J. 1992, A User's Guide to Reducing Slit Spectra with IRAF (Kitt Peak National Observatory, Tucson)

Mould, J., & Aaronson, M. 1979, ApJ, 232, 421

Mould, J., & Aaronson, M. 1986, ApJ, 303, 10

Pagel, B.E.J., & Edmunds, M.G. 1981, ARA&A, 19, 77

Pagel, B.E.J., Edmunds, M.G., Fosbury, R.A.E, & Webster, B.L. 1978, MNRAS, 184, 569

Palmer, L.G., & Wing, R.F. 1982, AJ, 87, 1739

Peimbert, M. 1995, in Highlights in Astronomy, Vol. 10, edited by I. Appenzeller (Kluwer, Dordrecht), (in press)

Pierce, M.J., Welch, D.L., McClure, R.D., van den Bergh, S., Racine, R., & Stetson, P.B. 1994, Nature, 371, 385

Pritchet, C.J., Richer, H.B., Schade, D., Crabtree, D.R., & Yee, H.K.C 1987, ApJ, 323, 79

Reid, N., & Mould, J. 1984, ApJ, 284, 98

Reid, N., & Mould, J. 1985, ApJ, 299, 236

Reimers, D., & Groote, D. 1983, A&A, 123, 257

Renzini, A. 1977, in Advanced Stages of Stellar Evolution, edited by P. Bouvier and A. Maeder (Geneva Observatory, Geneva), p. 149

Renzini, A. 1981, Ann. Phys. (Paris) 6, 87

Renzini, A., & Voli, M. 1981, A&A, 94, 175

Richer, H.B. 1981a, ApJ, 243, 744

Richer, H.B. 1981b, in Physical Processes in Red Giants, edited by I. Iben Jr. and A. Renzini (Reidel, Holland), p. 153

Richer, H.B., & Crabtree, D.R. 1985, ApJ, 298, L13 (RC85)

Richer, H.B., Crabtree, D.R., & Pritchet, C.J. 1984, ApJ, 287, 138 (RCP84)

Richer, H.B., Crabtree, D.R., & Pritchet, C.J. 1990, ApJ, 355, 448 (RCP90)

Richer, H.B., & Frogel, J.A. 1980, ApJ, 242, L9

Richer, H.B., Olander, N., & Westerlund, B.E. 1979, ApJ, 230, 724 (ROW79)

Richer, H.B., Pritchet, C.J., & Crabtree, D.R. 1985, ApJ, 298, 240

Rubin, V.C., & Ford, W.K. 1970, ApJ, 159, 379

Sackmann, I.-J., & Boothroyd, A.I. 1992, ApJ, 392, L71

Sandage, A., & Tammann, G.A. 1987, A Revised Shapley-Ames Catalog of Bright Galaxies (Carnegie Institute of Washington, Washington D.C.)

Savage, B.D. & Mathis, J.S. 1979, ARA&A, 17, 73

Scalo, J.M. 1981, in Physical Processes in Red Giants, edited by I. Iben Jr. and A. Renzini (Reidel, Holland), p. 77

Scalo, J.M., Despain, K.H., & Ulrich, R.K. 1975, ApJ, 196, 805

Scalo, J.M., & Miller, G.E. 1979, ApJ, 233, 596

Schwarzschild, M., & Härm, R. 1965, ApJ, 142, 855

Searle, L. 1982, in Carnegie Year Book, pp. 622-624

Searle, L., & Thompson, I. 1985, in Carnegie Year Book, pp. 68-69

Sharpless, S.L. 1956, ApJ, 124, 342

Smith, R.C., Kirshner, R.P., Blair, W.P., Long, K.S., & Winkler, P.F. 1993, ApJ, 407, 564

Smith, V.V., Plez, B., & Lambert, D.L. 1995, ApJ, 441, 735

Snow, T.P., Jr., York, D.G., & Welty, D.E. 1977, AJ, 82, 113

Stetson, P.B. 1987, PASP, 99, 191

Stetson, P.B. 1990, PASP, 102, 932

Stetson, P.B. 1992, in Astronomical Data Analysis Software and Systems I, ASP Conference Series, Vol. 25, edited by D.M. Worrall, C. Biemesderfer, and J. Barnes (ASP, San Francisco), p. 297

Stetson, P.B. 1993, in Stellar Photometry – Current Techniques and Future Developments, IAU Coll. 136, edited by C.J. Butler and I. Elliot (Cambridge University Press, Cambridge), p. 291

Stetson, P.B., Davis, L.E., & Crabtree, D.R. 1990, in CCDs in Astronomy, ASP Conference Series, Vol. 8, edited by G.H. Jacoby (ASP, San Francisco), p. 289

Stetson, P.B., & Harris, W.E. 1988, AJ, 96, 909

Thronson, H.A., Latter, W.B., Black, J.H., Bally, J., & Hacking, P. 1987, ApJ, 322, 770

Turnshek, D.E., Turnshek, D.A., Craine, E.R., & Boeshaar, P.C. 1985, An Atlas of Digital Spectra of Cool Stars (Western Research Company, Arizona) (TTCB)

van den Bergh, S. 1968, Observatory, 88, 168

van den Bergh, S. 1991a, PASP, 103, 609

van den Bergh, S. 1991b, PASP, 103, 1053

Walker, G.A.H. 1963, MNRAS, 125, 141

Walterbos, R.A.M., & Kennicutt, R.C., Jr. 1988, A&A, 198, 61

Welch, D.L., McAlary, C.W., McLaren, R.A., & Madore, B.F. 1986, ApJ, 305, 583

Wells, D.C., Greisen, E.W., & Harten, R.A. 1981, A&AS, 44, 363

Westerlund, B.E. 1965, MNRAS, 130, 45

Wood, P.R., Bessell, M.S., & Fox, M.W. 1983, ApJ, 272, 99

Yamashita, Y. 1972, Tokyo Obs. Ann., (2) 13, 169

Yamashita, Y. 1975, Tokyo Obs. Ann., (2) 14, 47

Zaritsky, D. 1992, ApJ, 390, L73

Appendix A

M31 SPECTRA

In this appendix I present the spectra obtained at the CFHT. As mentioned in §§6.2.4 and 6.2.5, the spectra were first wavelength calibrated and then shifted such that they lie in a zero velocity frame. The spectra have also been divided by their maximum flux level. Included on all the plots are: (1) marks showing the position of the three telluric lines which often subtracted poorly (due to the wavelength shift applied to the spectra, these are not at their rest wavelengths); (2) the star's ID (lower right); (3) my classification of the spectrum (upper left); (4) on most of the C-star spectra two "error bars" which show my estimates of where the red and blue side of the CN (5730Å) and C_2 (5635Å) bandheads lie; (5) the expected positions of certain bandheads and atomic features which are associated with M-, S-, and C-stars; and finally (6) in some panels I provide comments.

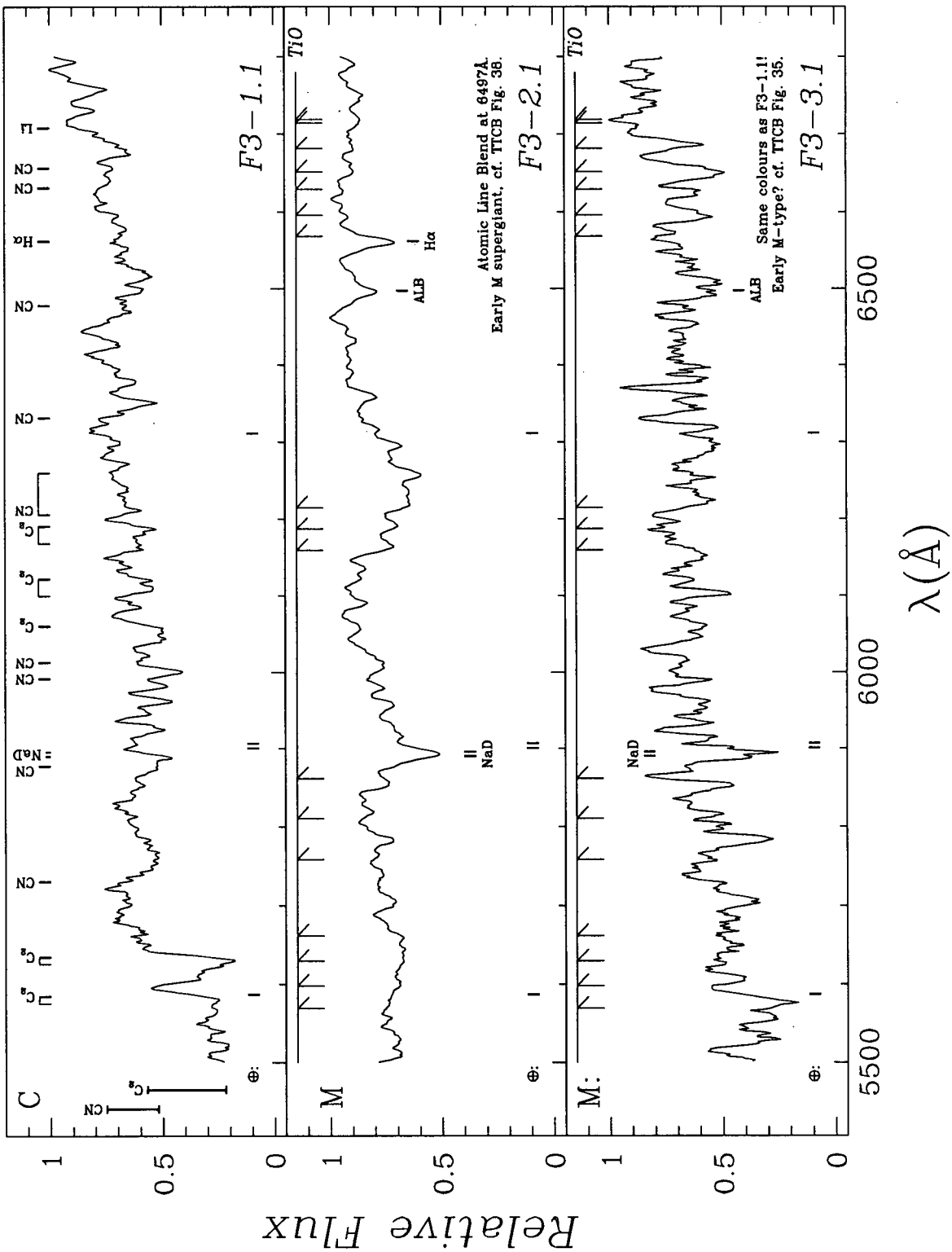

Figure A.1: Spectra of M31 stars. The above spectra have been: (1) wavelength calibrated; (2) shifted to lie in a zero velocity frame (see §6.2.5); and (3) smoothed using a bin size of 7 pixels.

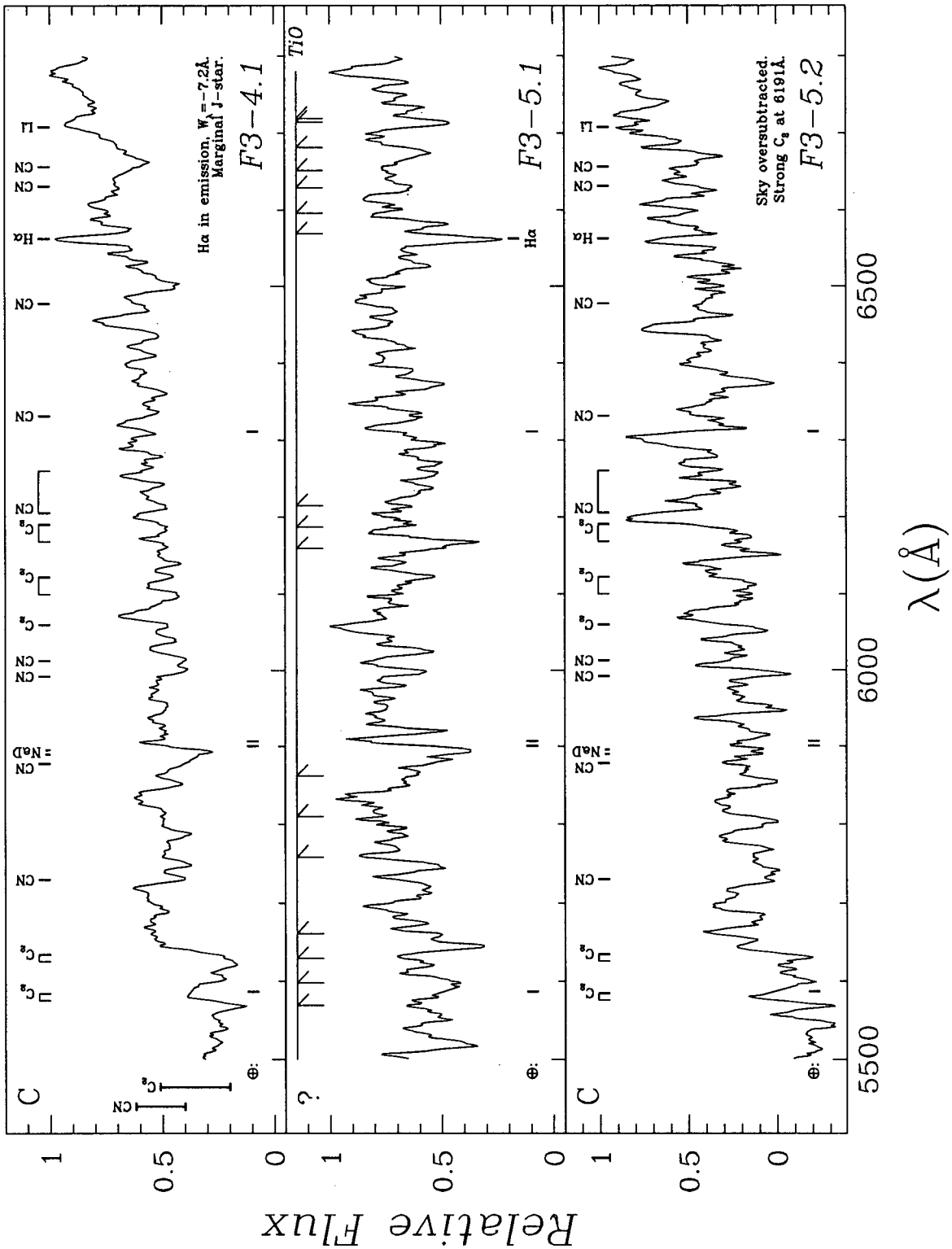

Figure A.1 (continued): Spectra of M31 stars. The above spectra have been: (1) wavelength calibrated; (2) shifted to lie in a zero velocity frame (see §6.2.5); and (3) smoothed using a bin size of 7 pixels.

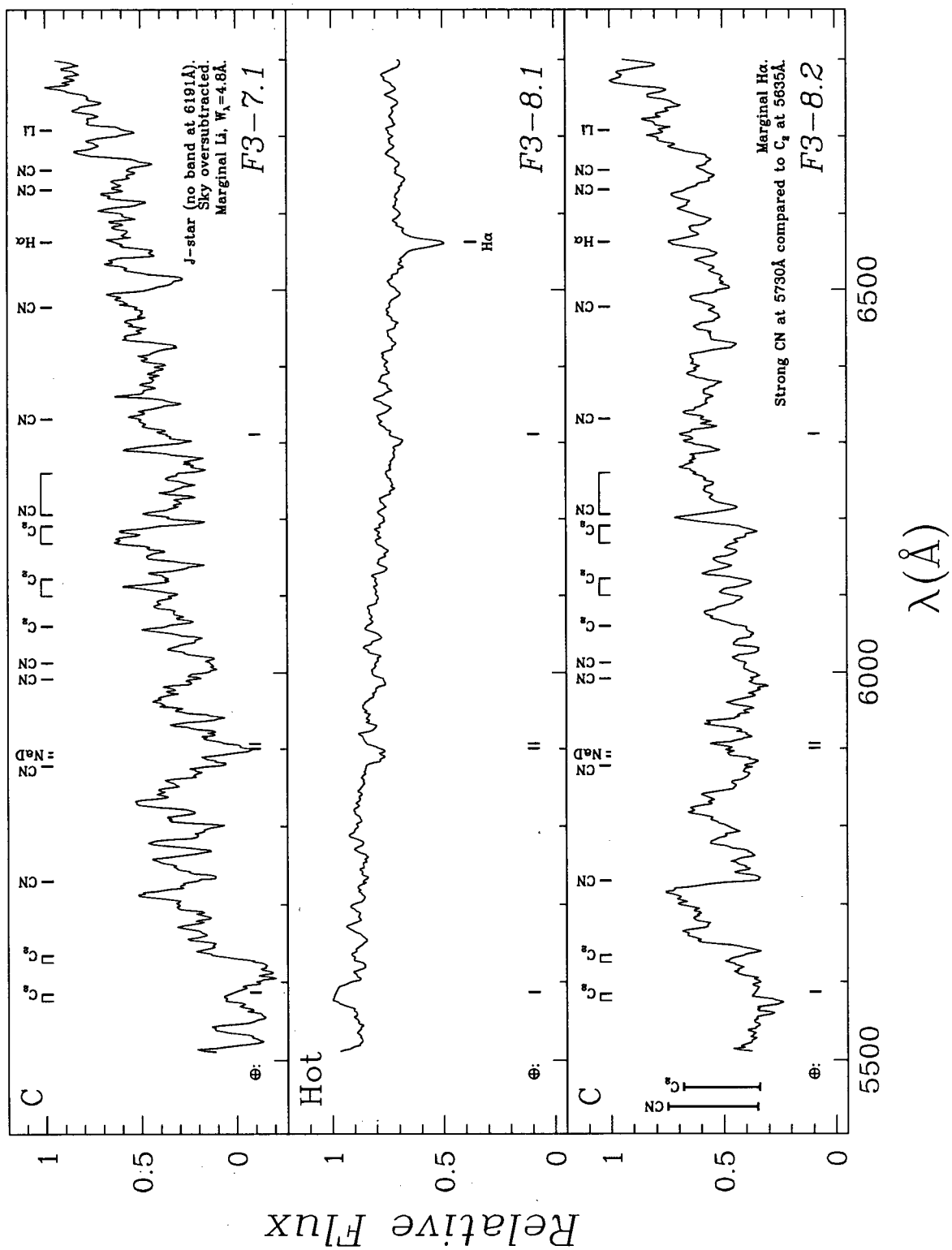

Figure A.1 (continued): Spectra of M31 stars. The above spectra have been: (1) wavelength calibrated; (2) shifted to lie in a zero velocity frame (see §6.2.5); and (3) smoothed using a bin size of 7 pixels.

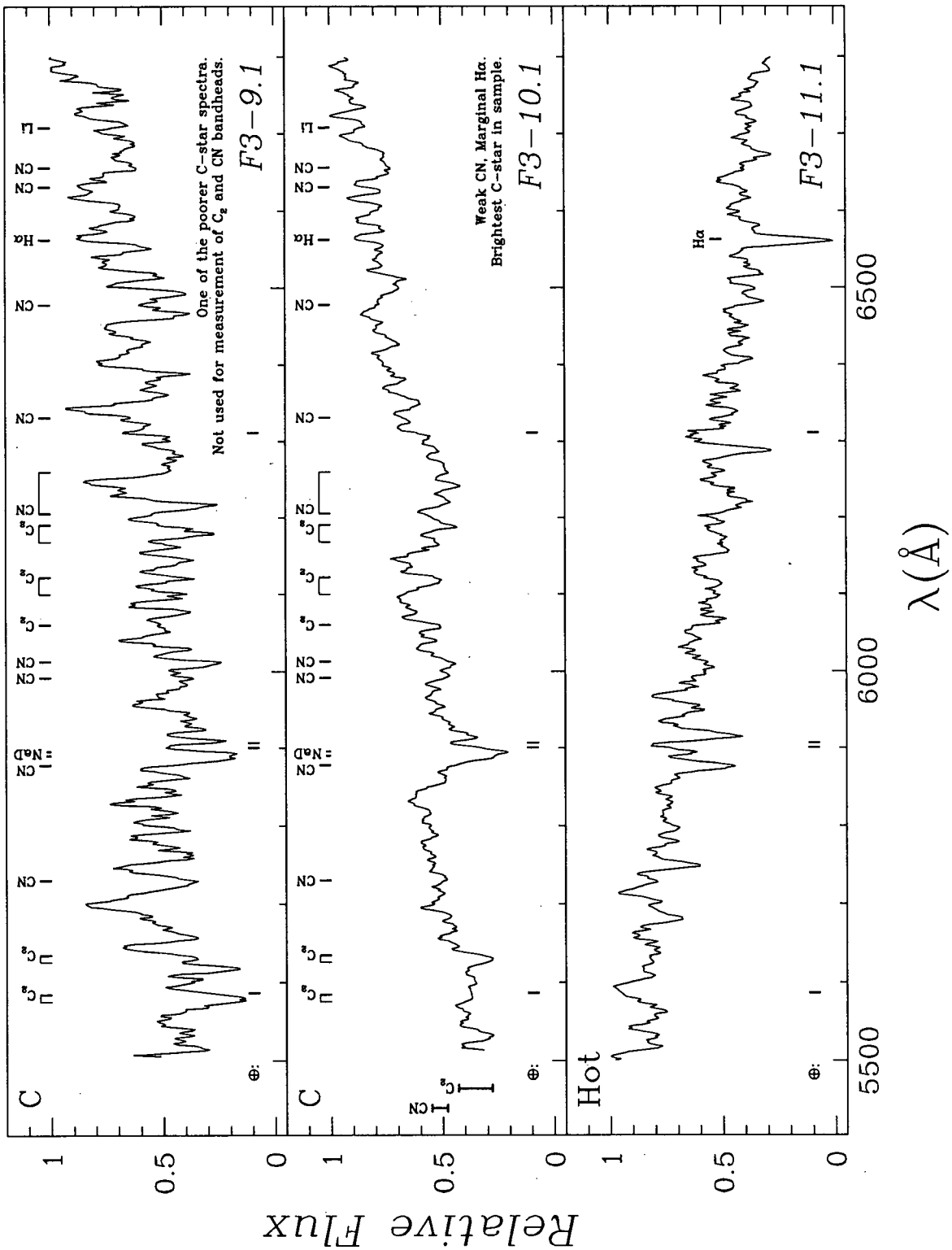

Figure A.1 (continued): Spectra of M31 stars. The above spectra have been: (1) wavelength calibrated; (2) shifted to lie in a zero velocity frame (see §6.2.5); and (3) smoothed using a bin size of 7 pixels.

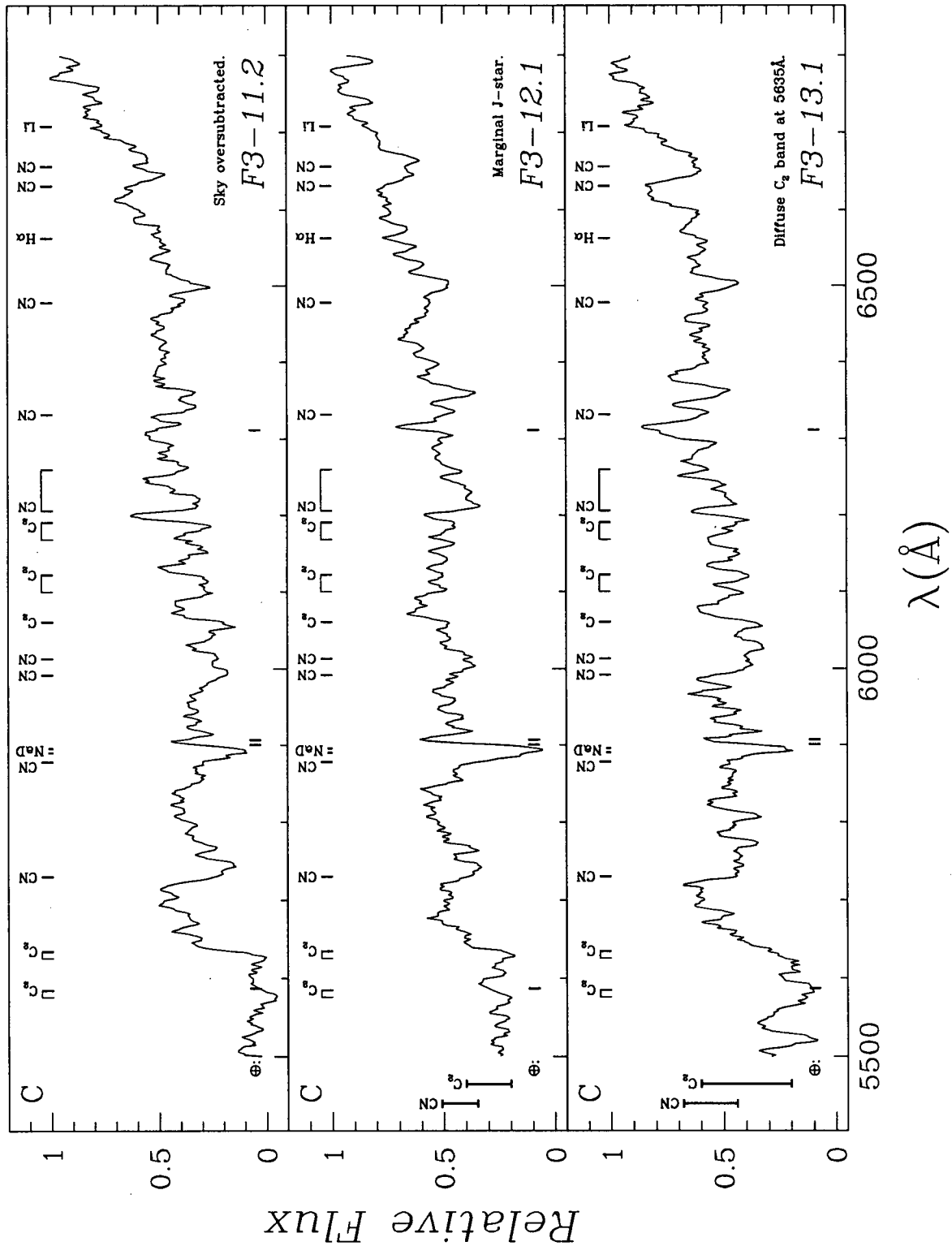

Figure A.1 (continued): Spectra of M31 stars. The above spectra have been: (1) wavelength calibrated; (2) shifted to lie in a zero velocity frame (see §6.2.5); and (3) smoothed using a bin size of 7 pixels.

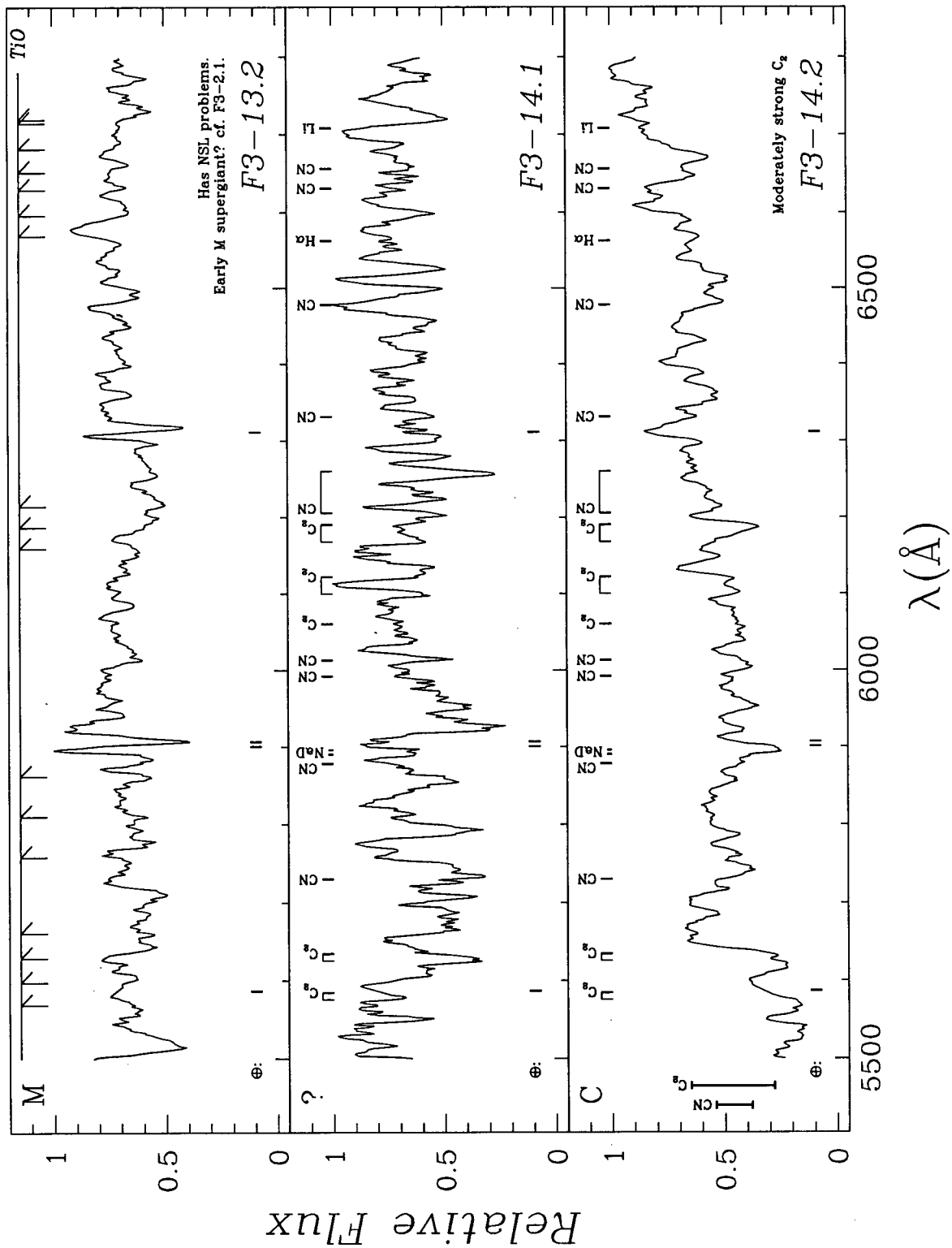

Figure A.1 (continued): Spectra of M31 stars. The above spectra have been: (1) wavelength calibrated; (2) shifted to lie in a zero velocity frame (see §6.2.5); and (3) smoothed using a bin size of 7 pixels.

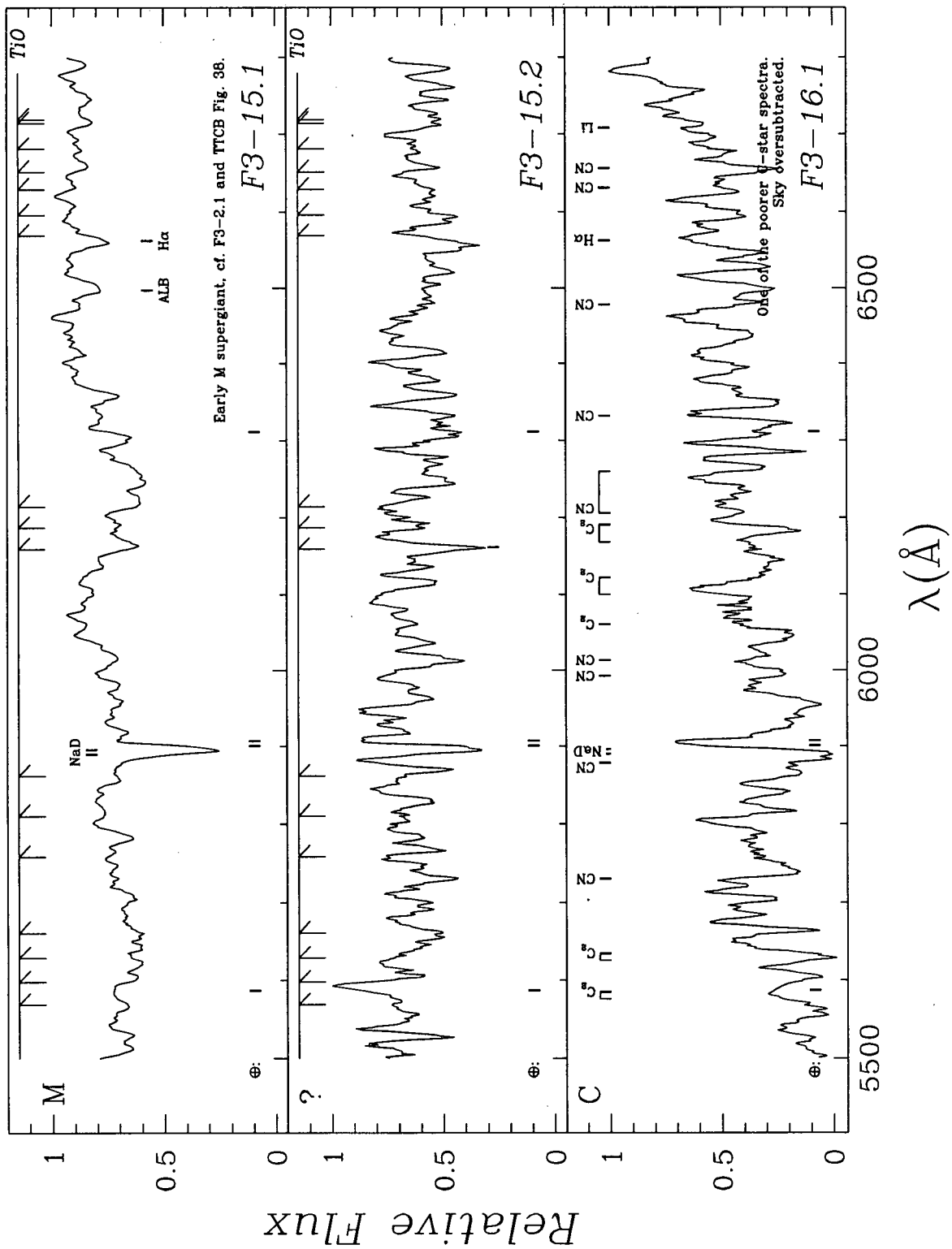

Figure A.1 (continued): Spectra of M31 stars. The above spectra have been: (1) wavelength calibrated; (2) shifted to lie in a zero velocity frame (see §6.2.5); and (3) smoothed using a bin size of 7 pixels.

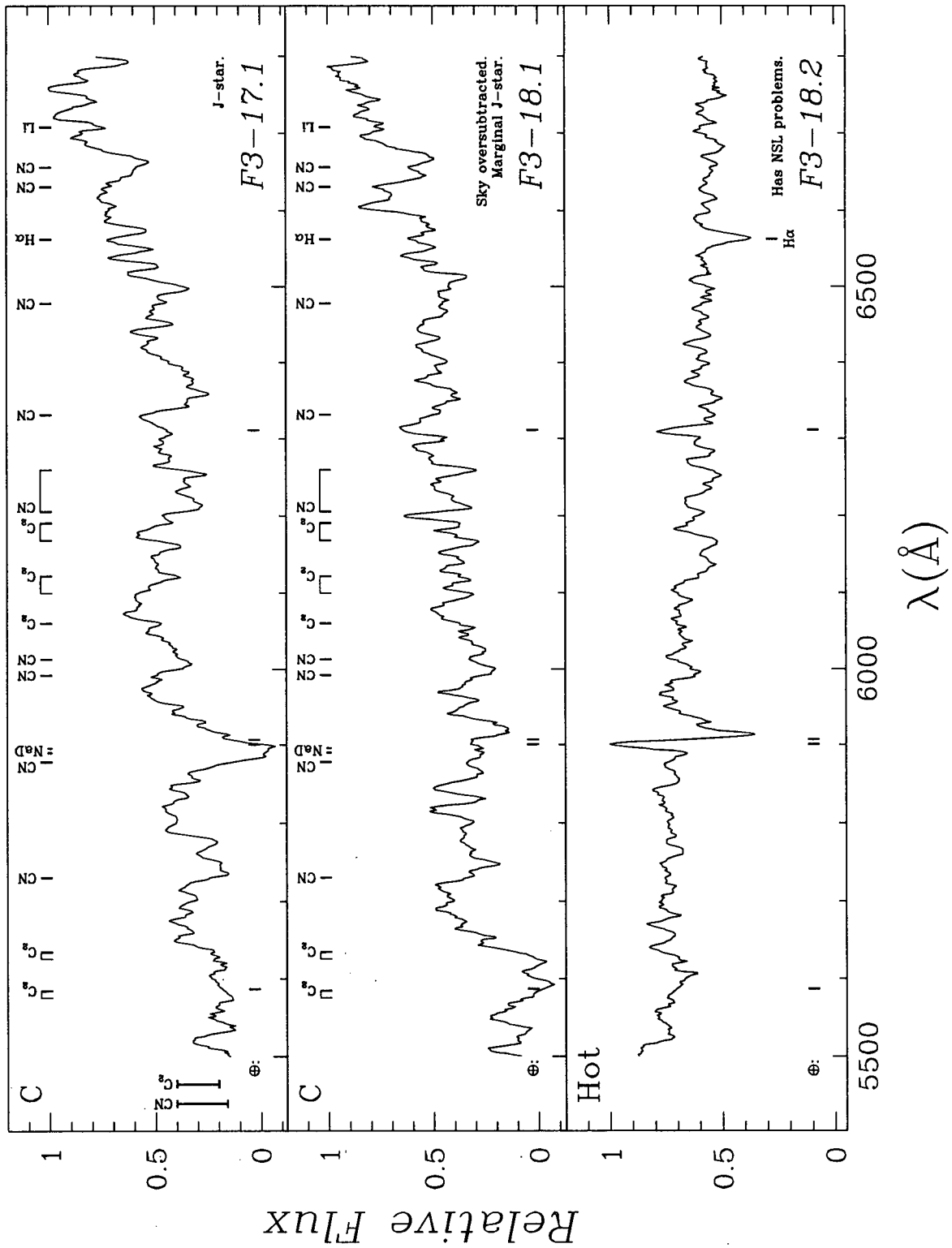

Figure A.1 (continued): Spectra of M31 stars. The above spectra have been: (1) wavelength calibrated; (2) shifted to lie in a zero velocity frame (see §6.2.5); and (3) smoothed using a bin size of 7 pixels.

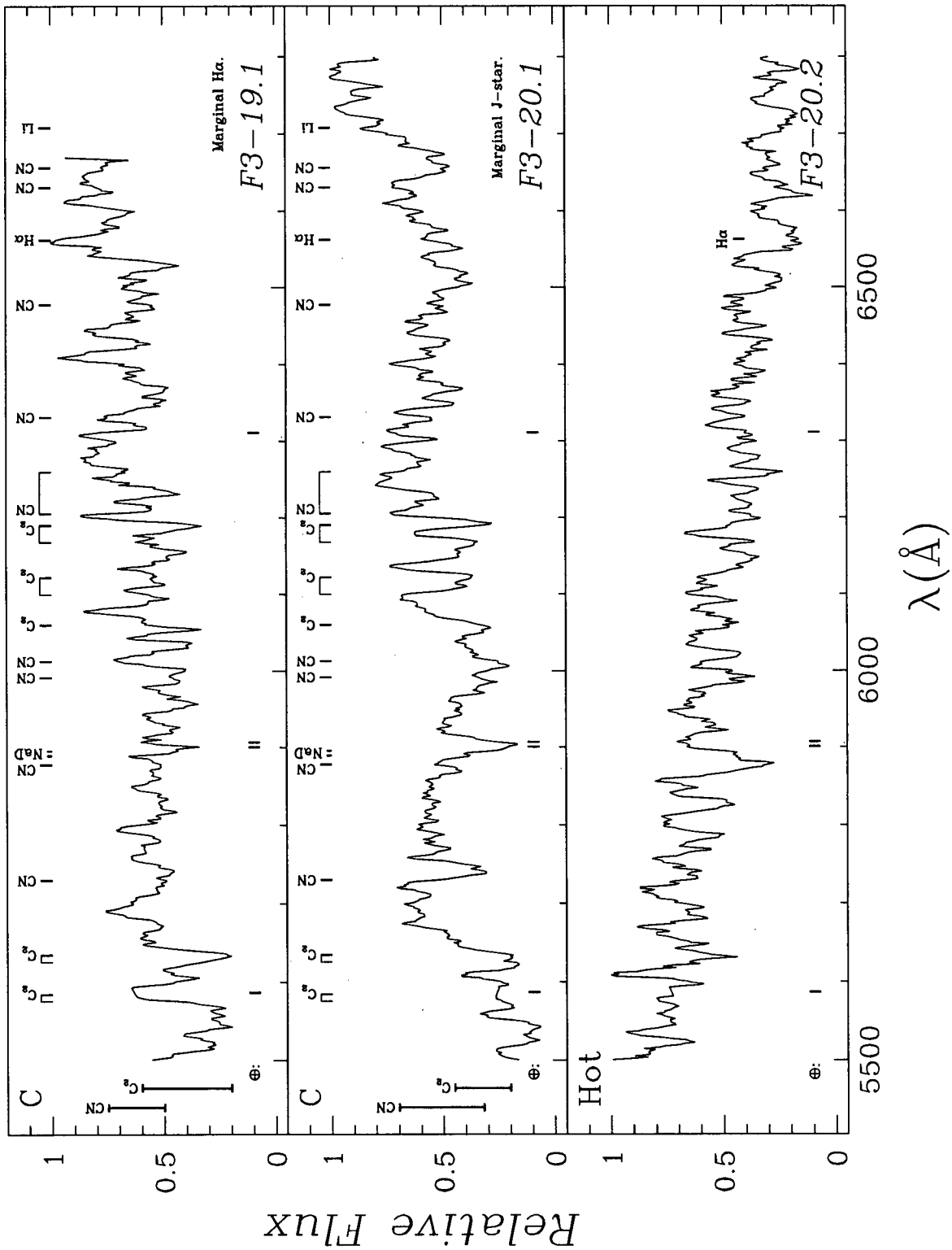

Figure A.1 (continued): Spectra of M31 stars. The above spectra have been: (1) wavelength calibrated; (2) shifted to lie in a zero velocity frame (see §6.2.5); and (3) smoothed using a bin size of 7 pixels.

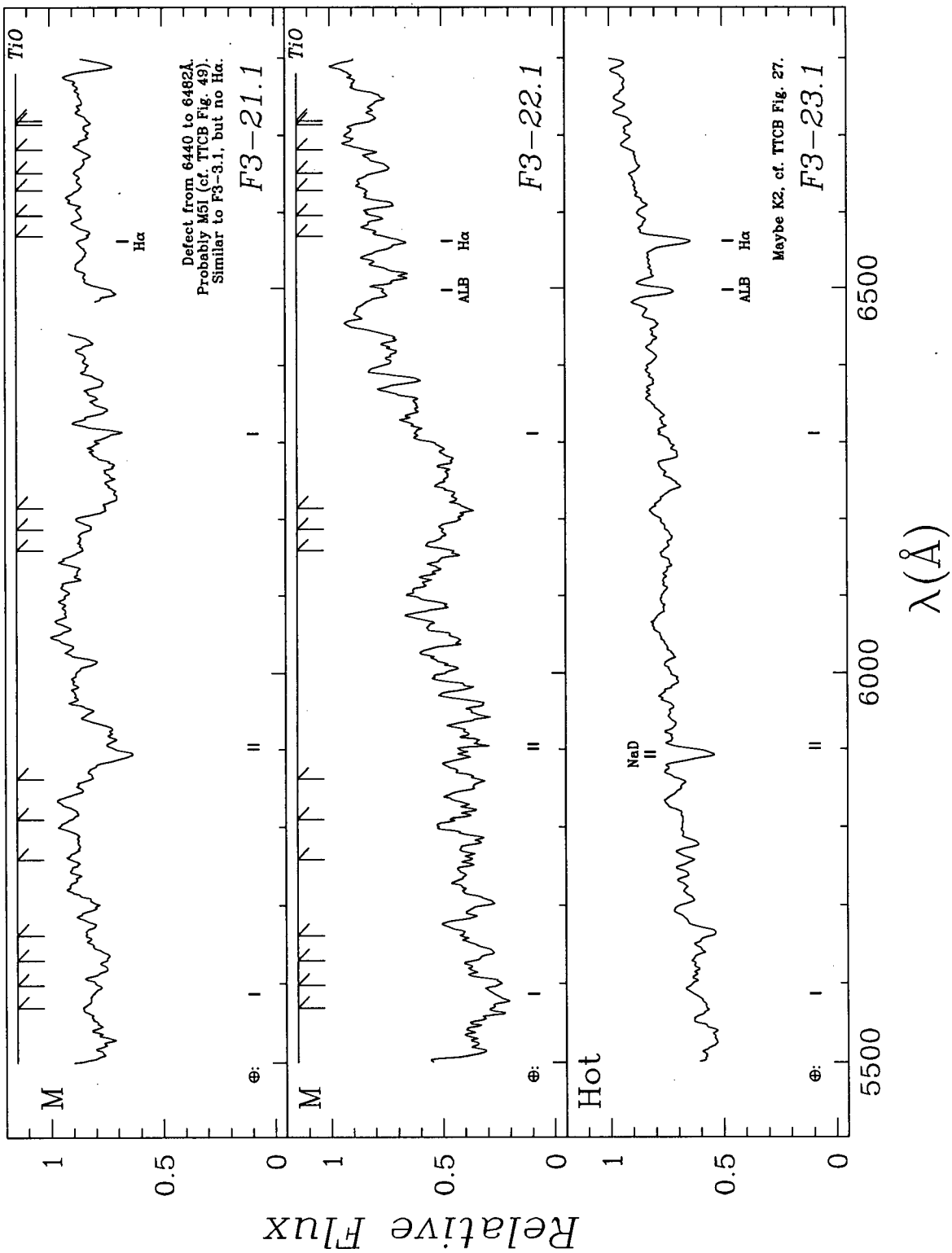

Figure A.1 (continued): Spectra of M31 stars. The above spectra have been: (1) wavelength calibrated; (2) shifted to lie in a zero velocity frame (see §6.2.5); and (3) smoothed using a bin size of 7 pixels.

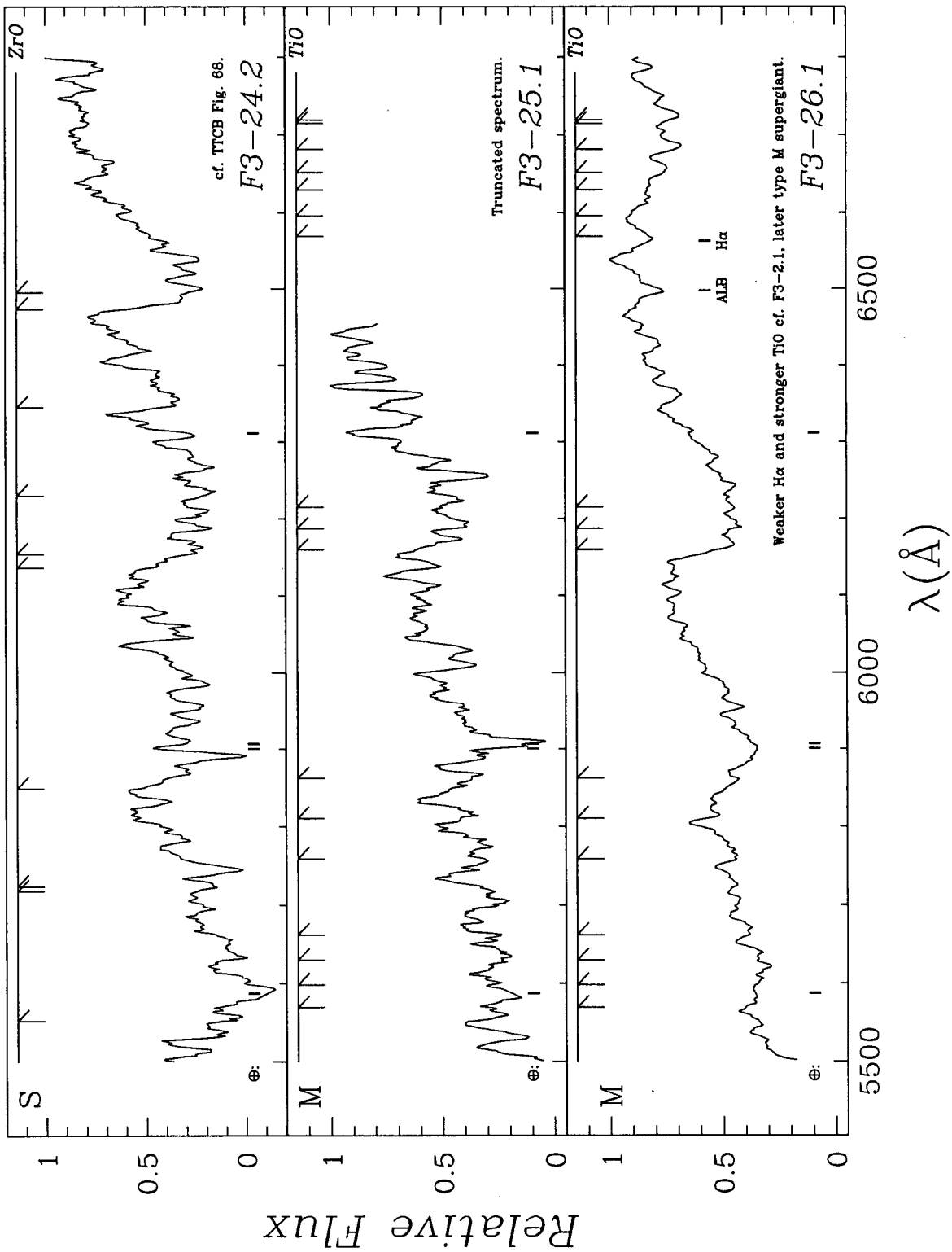

Figure A.1 (continued): Spectra of M31 stars. The above spectra have been: (1) wavelength calibrated; (2) shifted to lie in a zero velocity frame (see §6.2.5); and (3) smoothed using a bin size of 7 pixels.

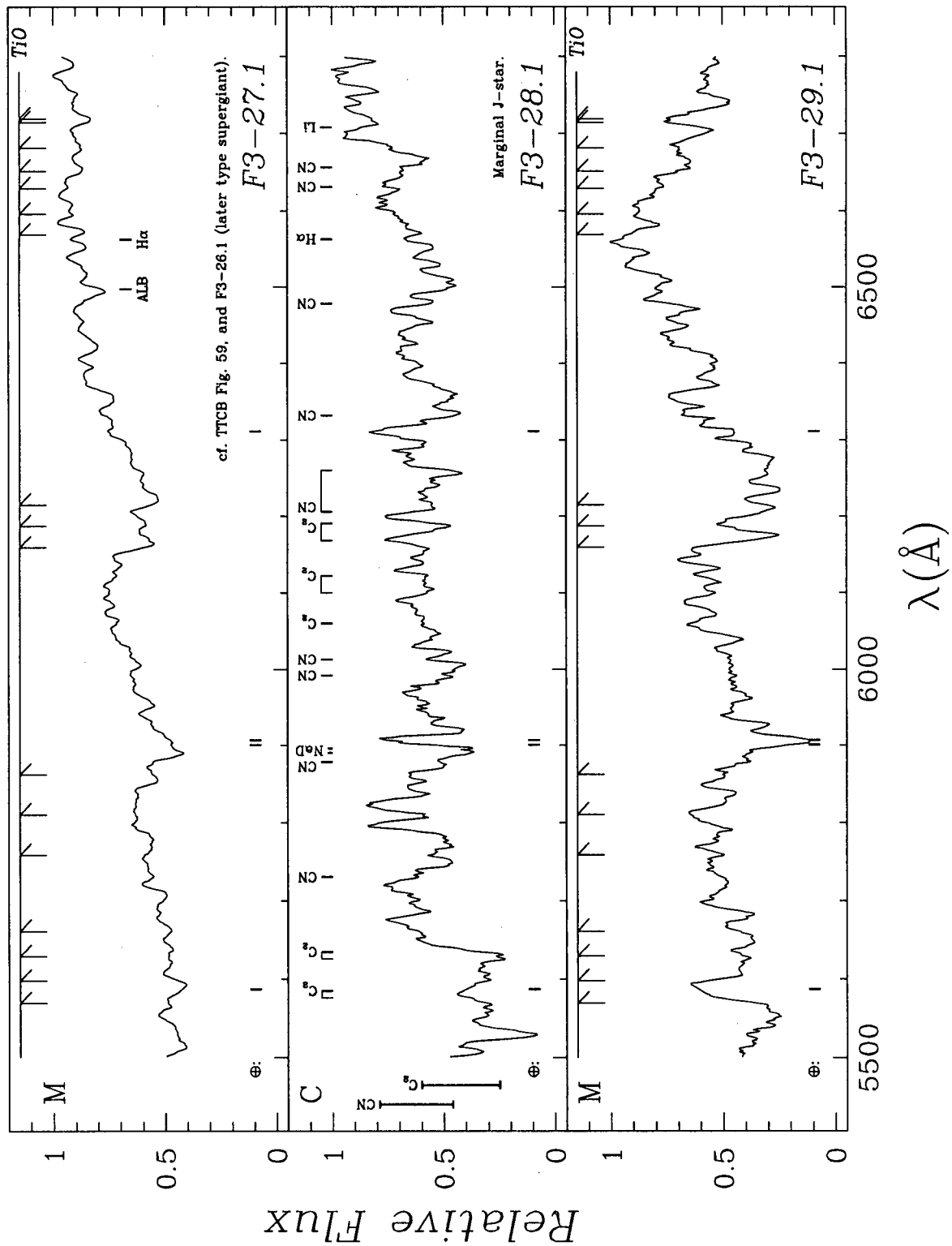

Figure A.1 (continued): Spectra of M31 stars. The above spectra have been: (1) wavelength calibrated; (2) shifted to lie in a zero velocity frame (see §6.2.5); and (3) smoothed using a bin size of 7 pixels.

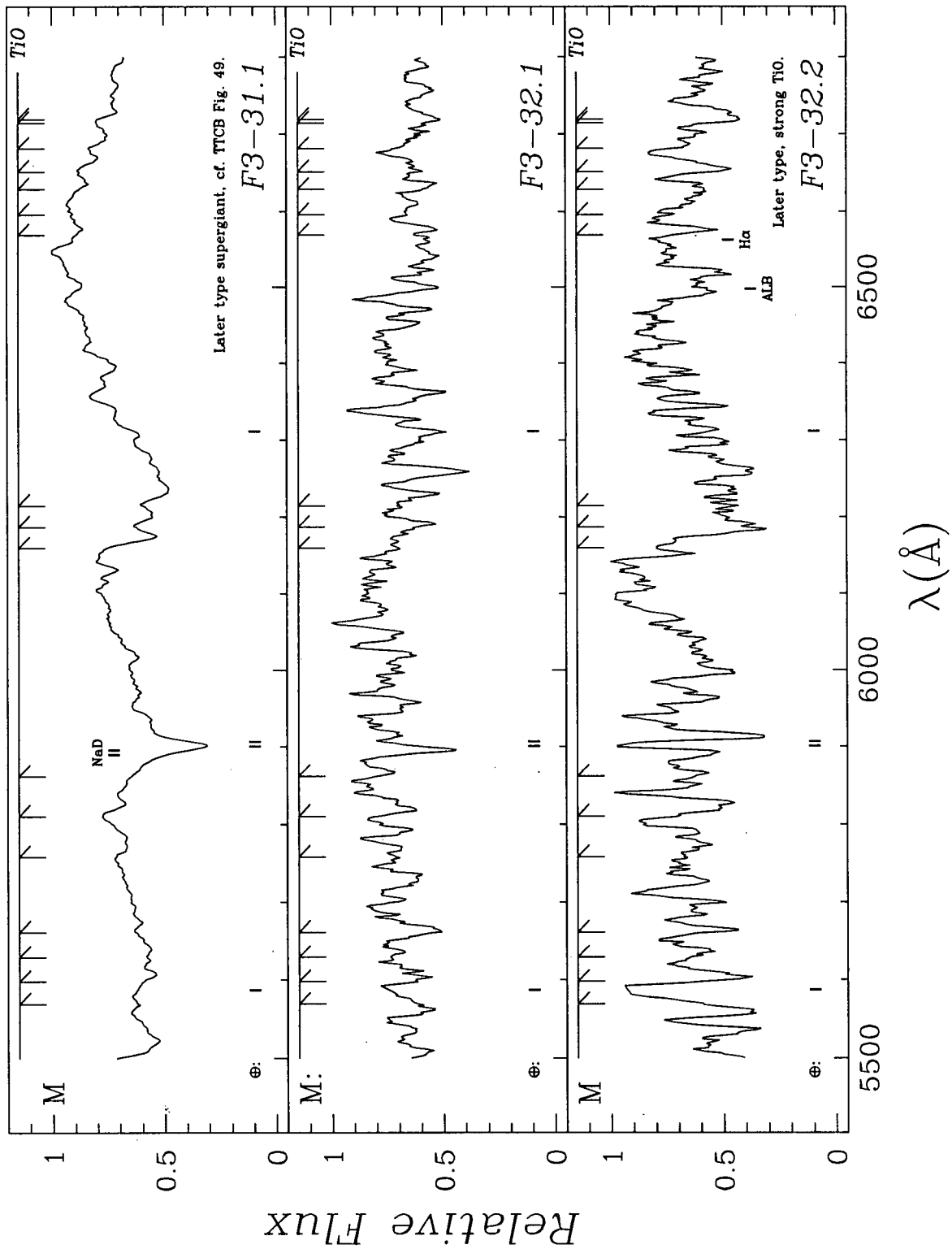

Figure A.1 (continued): Spectra of M31 stars. The above spectra have been: (1) wavelength calibrated; (2) shifted to lie in a zero velocity frame (see §6.2.5); and (3) smoothed using a bin size of 7 pixels.

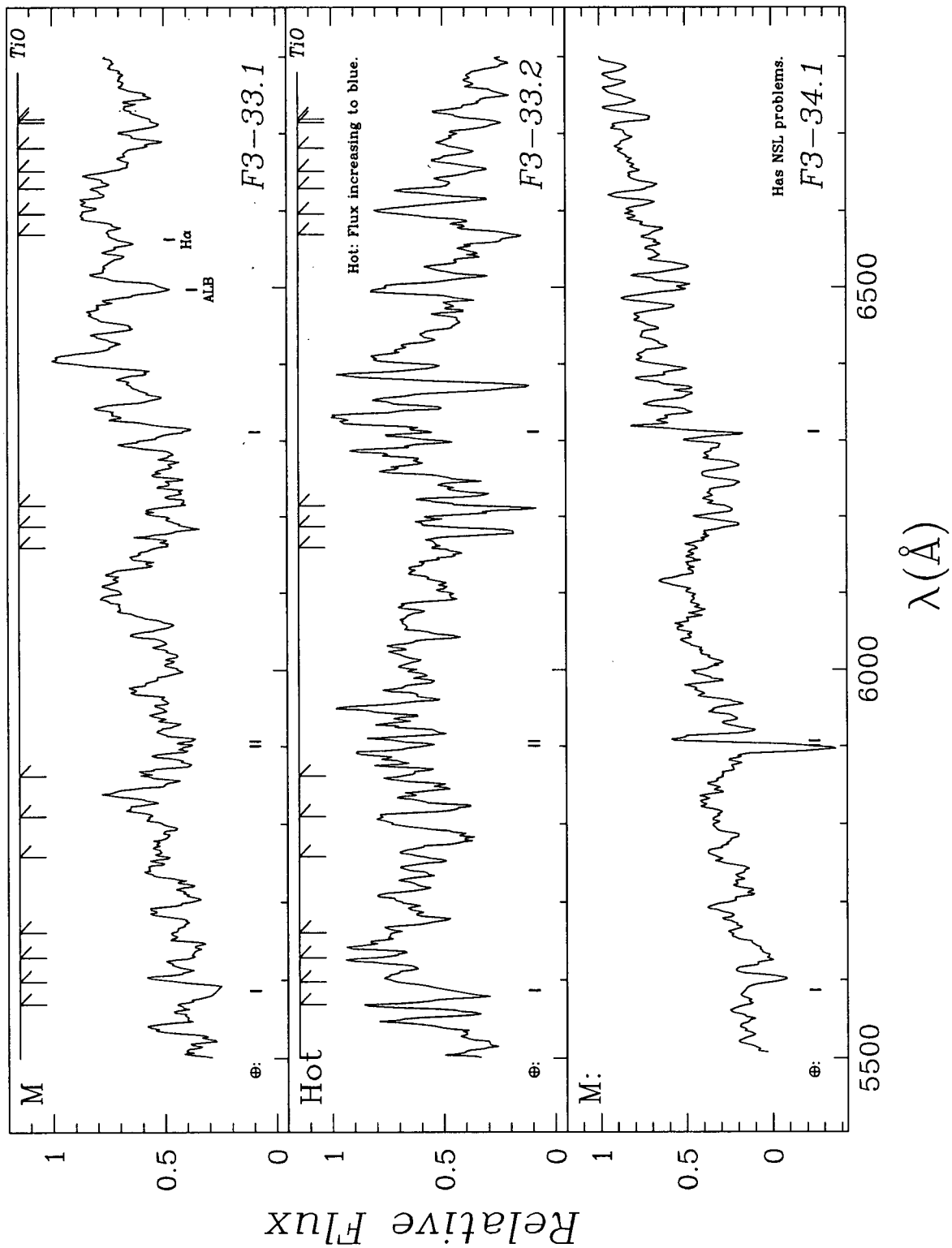

Figure A.1 (continued): Spectra of M31 stars. The above spectra have been: (1) wavelength calibrated; (2) shifted to lie in a zero velocity frame (see §6.2.5); and (3) smoothed using a bin size of 7 pixels.

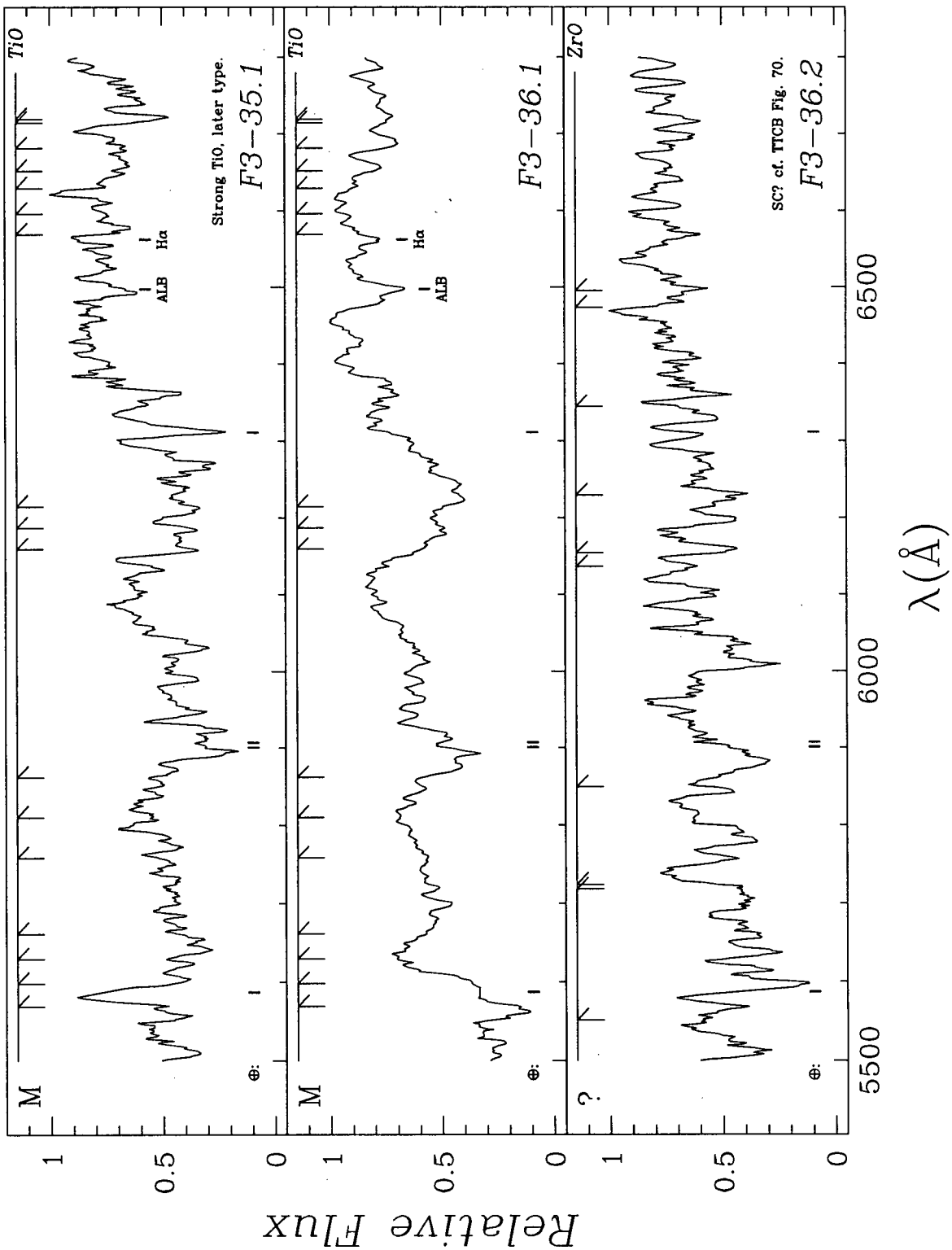

Figure A.1 (continued): Spectra of M31 stars. The above spectra have been: (1) wavelength calibrated; (2) shifted to lie in a zero velocity frame (see §6.2.5); and (3) smoothed using a bin size of 7 pixels.

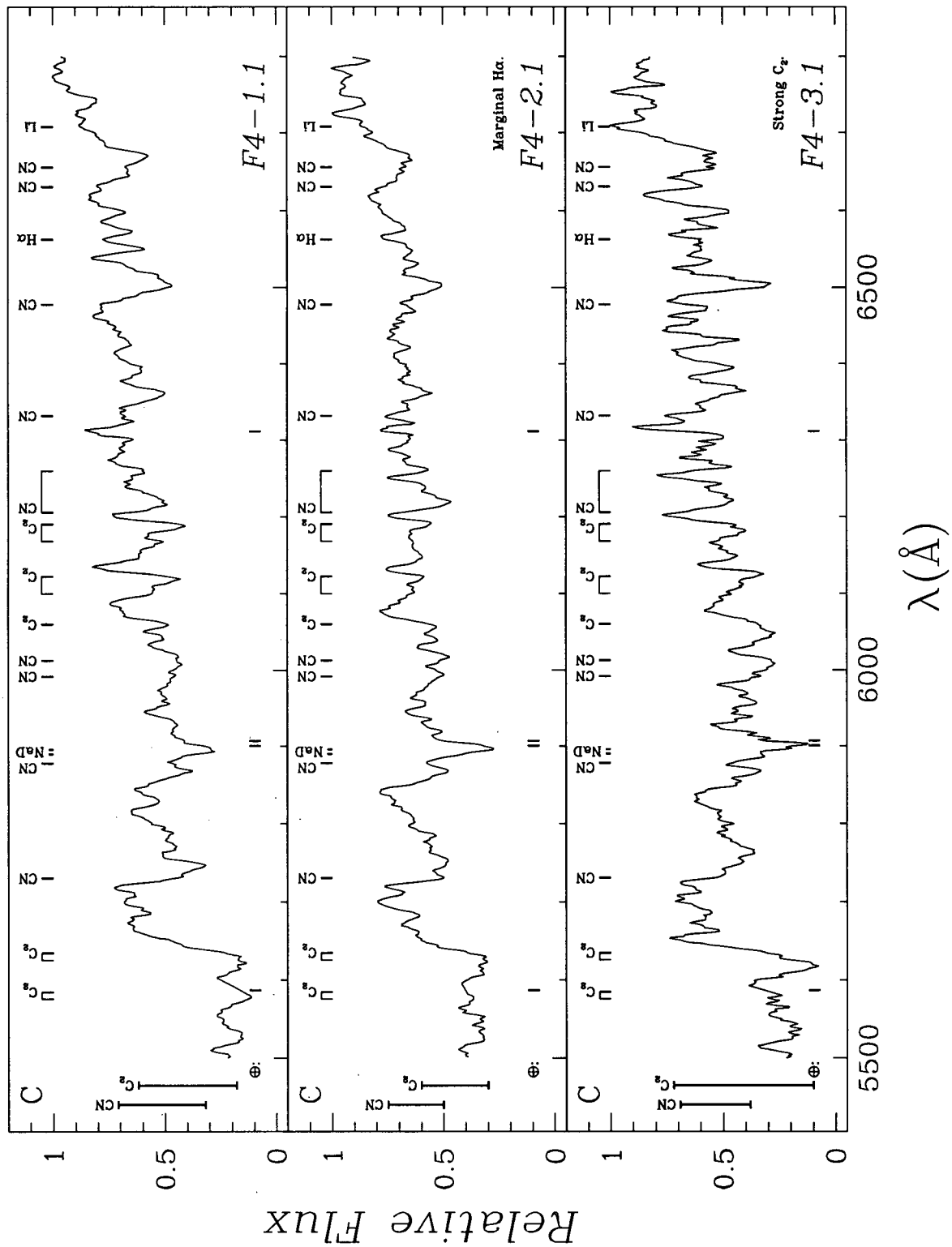

Figure A.1 (continued): Spectra of M31 stars. The above spectra have been: (1) wavelength calibrated; (2) shifted to lie in a zero velocity frame (see §6.2.5); and (3) smoothed using a bin size of 7 pixels.

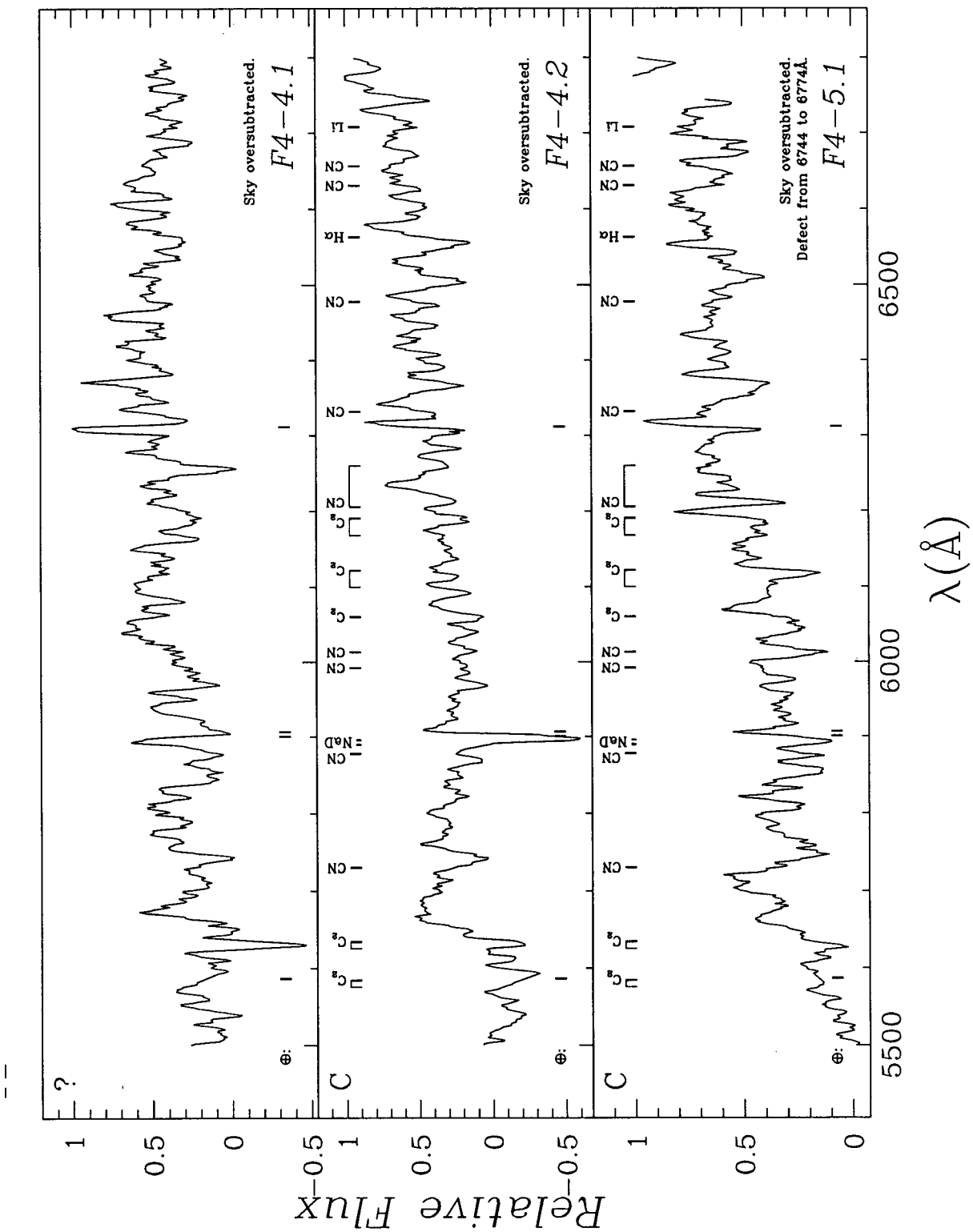

Figure A.1 (continued): Spectra of M31 stars. The above spectra have been: (1) wavelength calibrated; (2) shifted to lie in a zero velocity frame (see §6.2.5); and (3) smoothed using a bin size of 7 pixels.

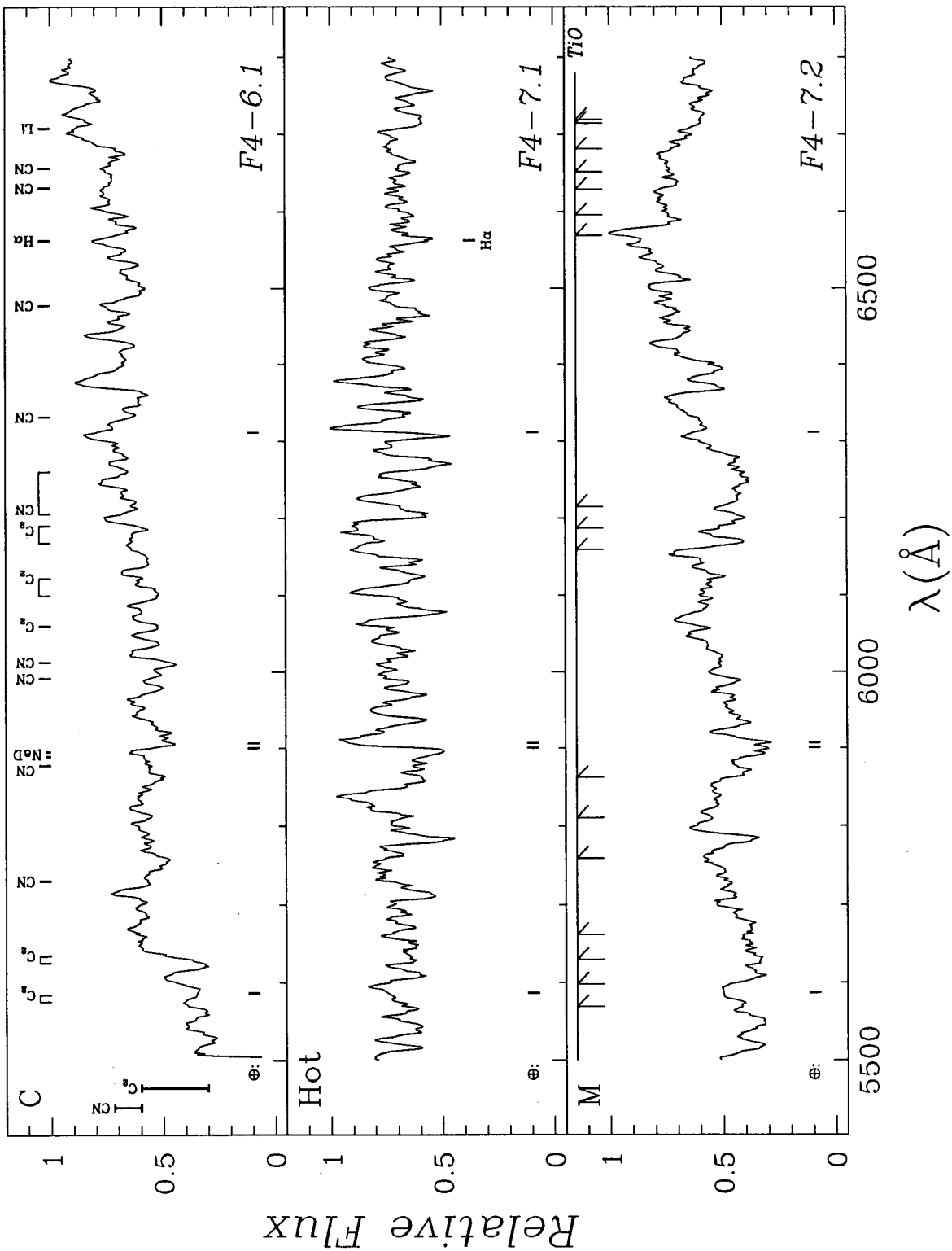

Figure A.1 (continued): Spectra of M31 stars. The above spectra have been: (1) wavelength calibrated; (2) shifted to lie in a zero velocity frame (see §6.2.5); and (3) smoothed using a bin size of 7 pixels.

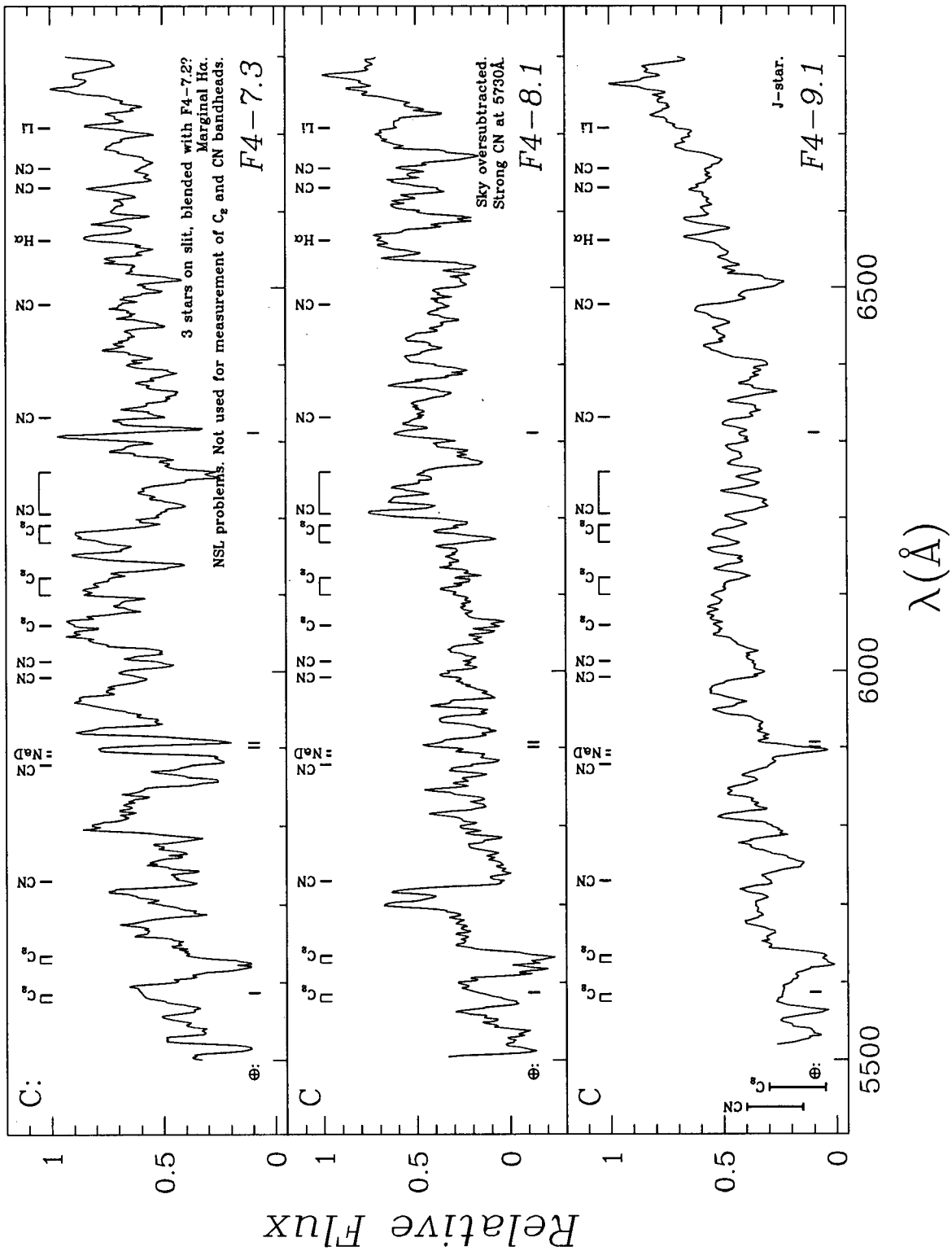

Figure A.1 (continued): Spectra of M31 stars. The above spectra have been: (1) wavelength calibrated; (2) shifted to lie in a zero velocity frame (see §6.2.5); and (3) smoothed using a bin size of 7 pixels.

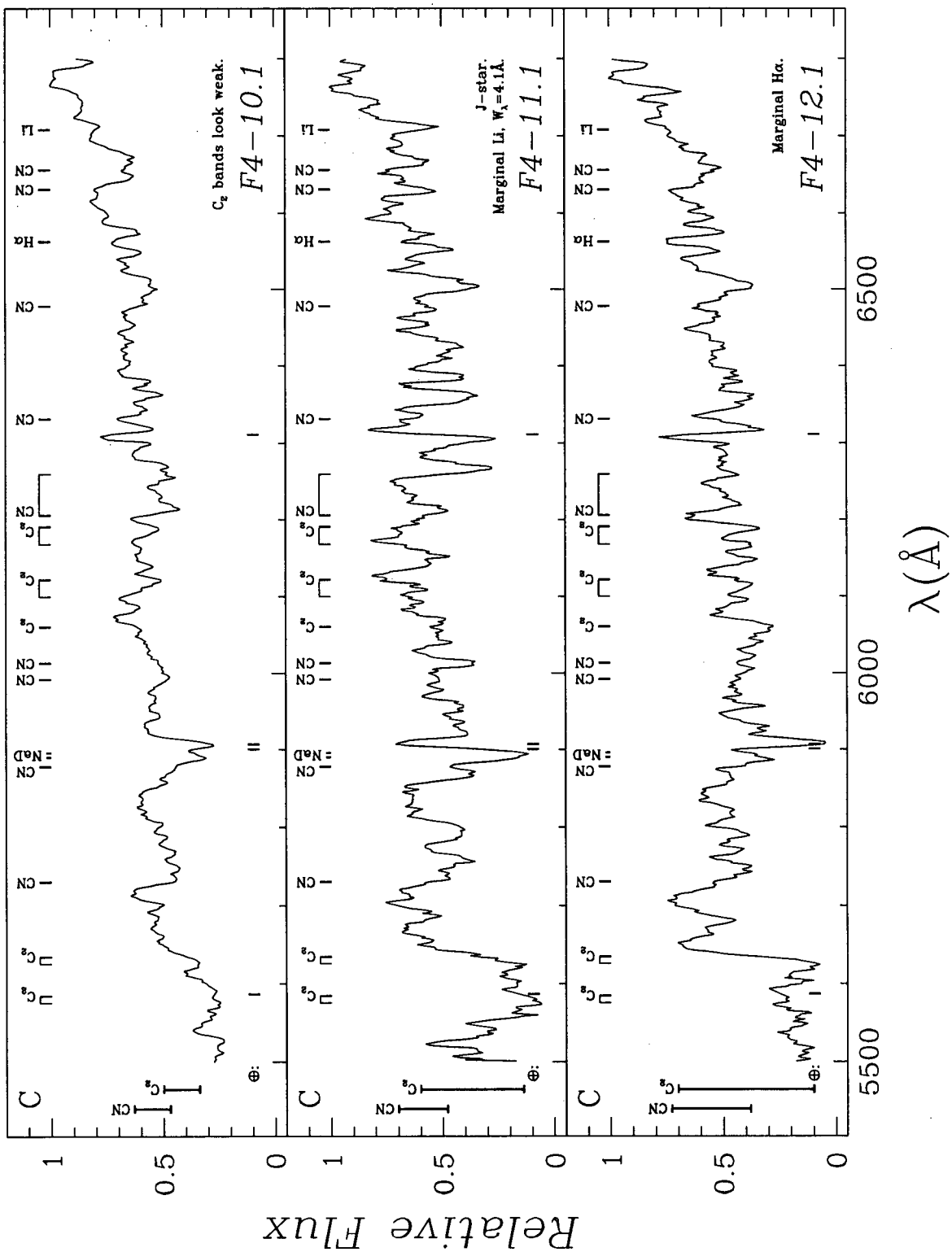

Figure A.1 (continued): Spectra of M31 stars. The above spectra have been: (1) wavelength calibrated; (2) shifted to lie in a zero velocity frame (see §6.2.5); and (3) smoothed using a bin size of 7 pixels.

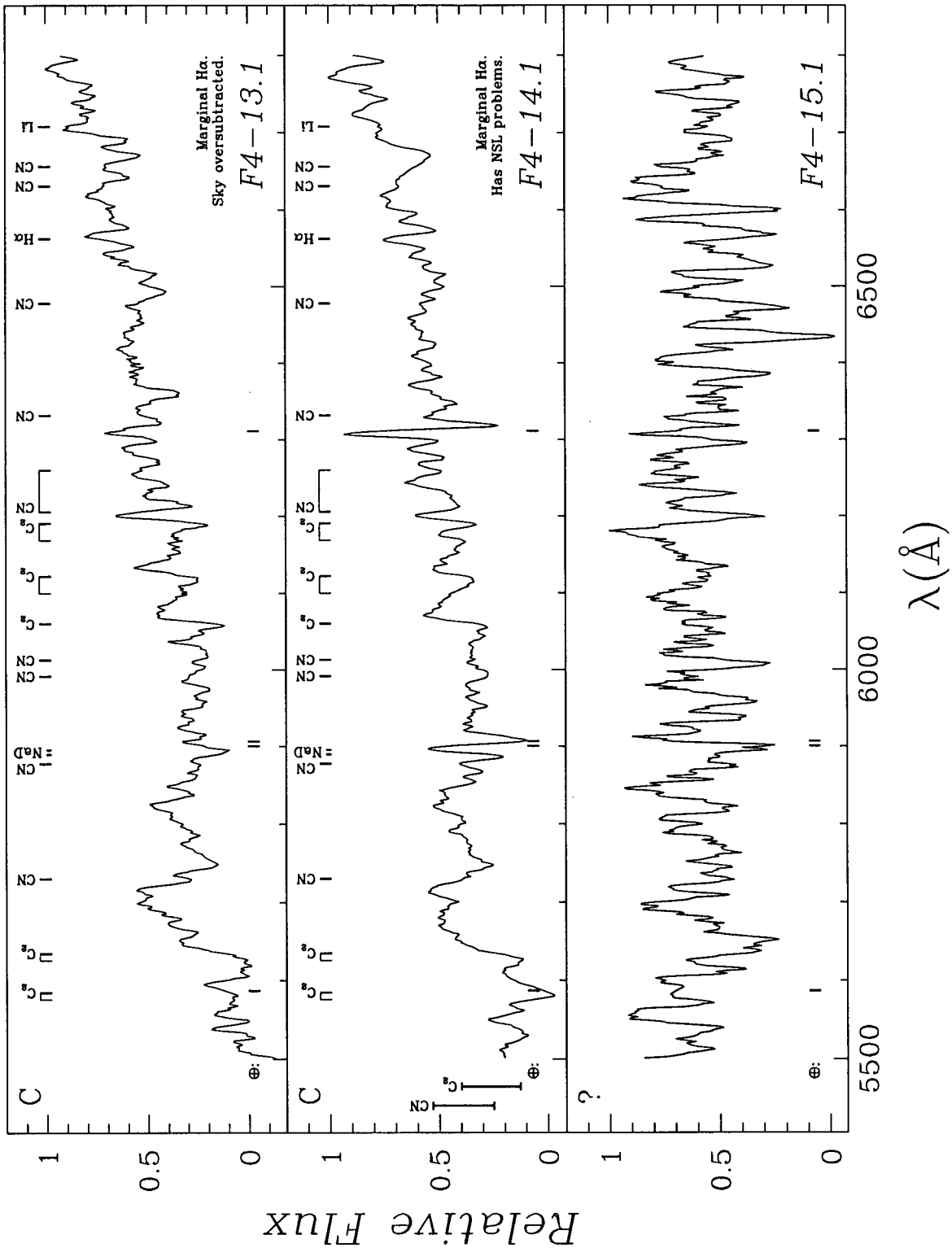

Figure A.1 (continued): Spectra of M31 stars. The above spectra have been: (1) wavelength calibrated; (2) shifted to lie in a zero velocity frame (see §6.2.5); and (3) smoothed using a bin size of 7 pixels.

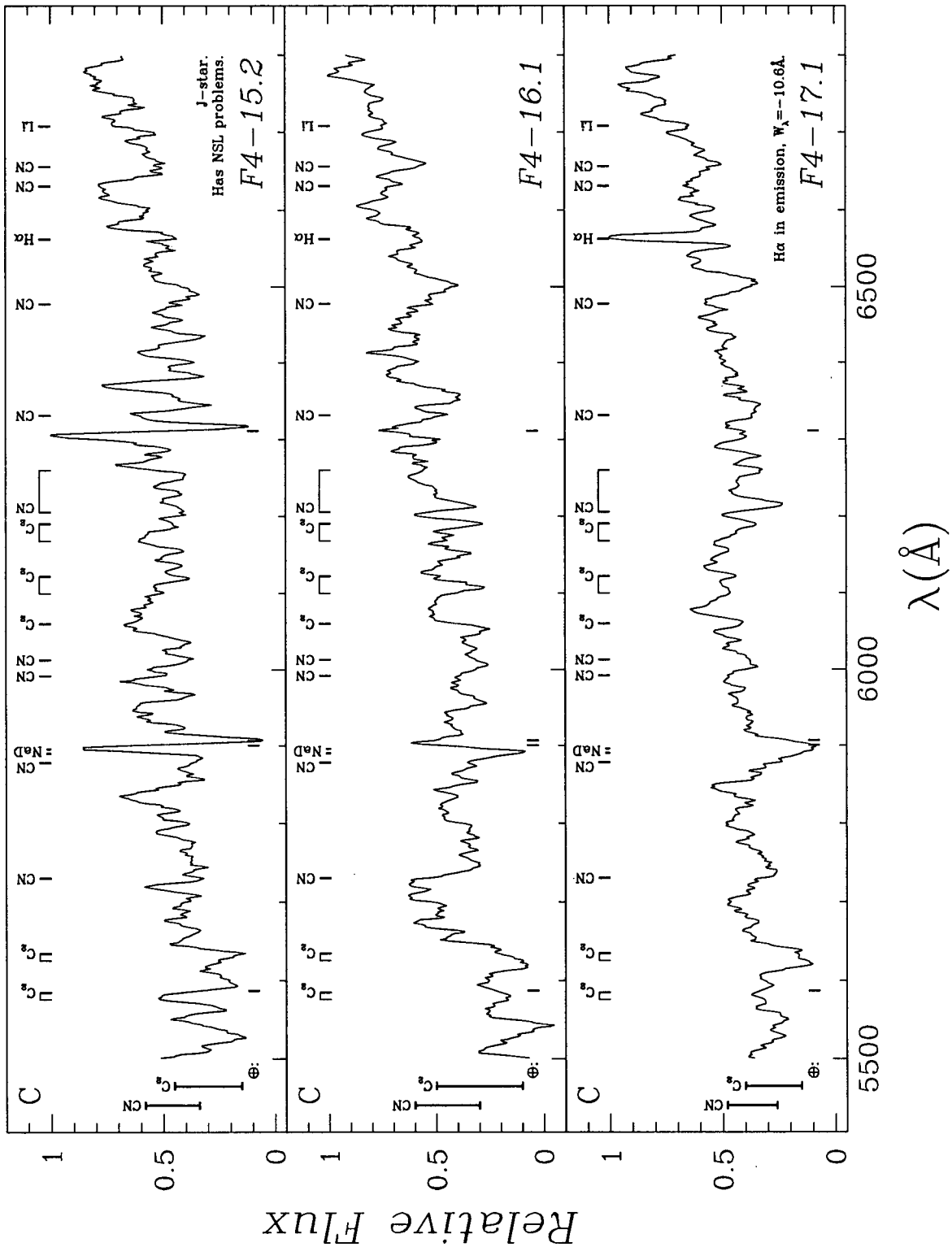

Figure A.1 (continued): Spectra of M31 stars. The above spectra have been: (1) wavelength calibrated; (2) shifted to lie in a zero velocity frame (see §6.2.5); and (3) smoothed using a bin size of 7 pixels.

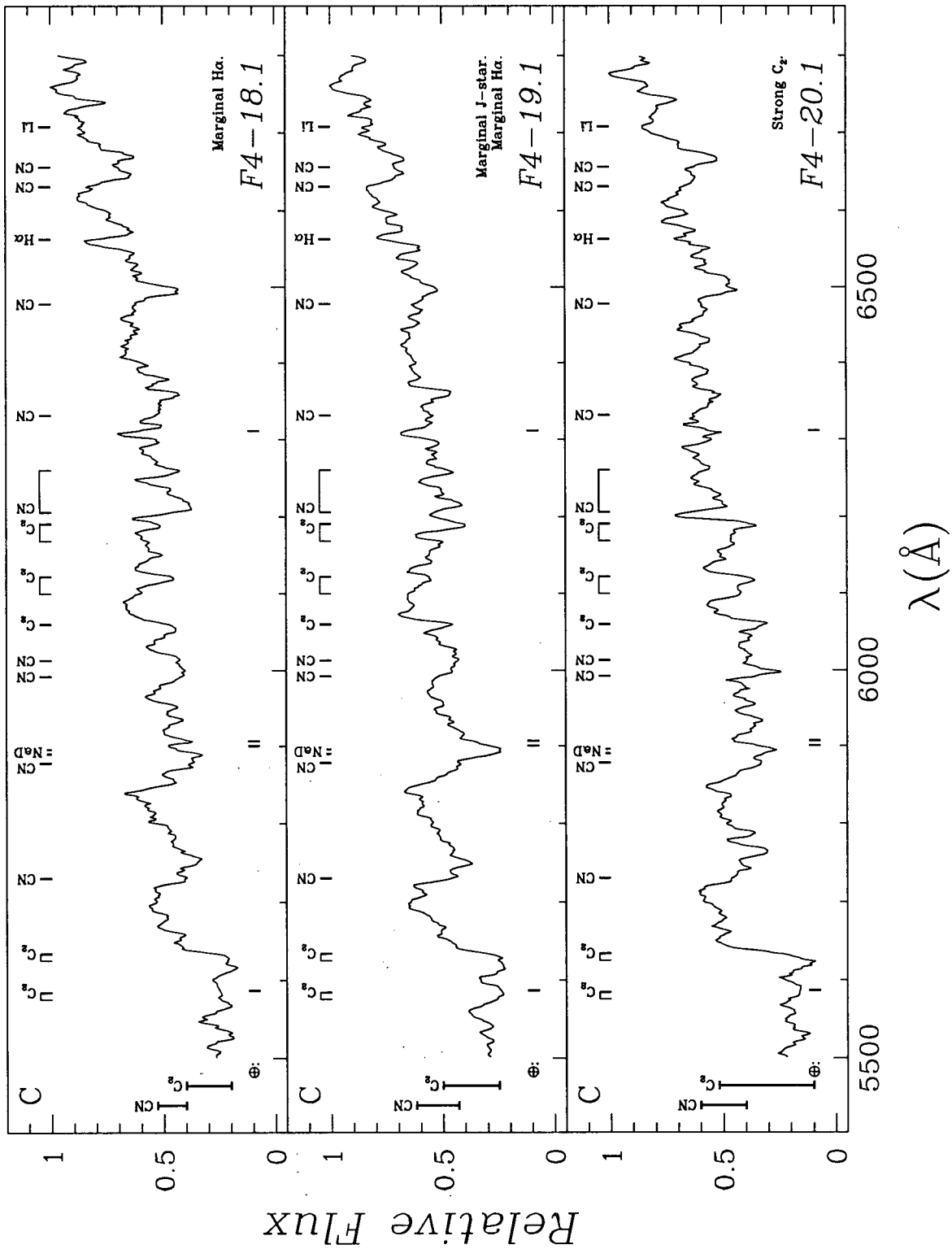

Figure A.1 (continued): Spectra of M31 stars. The above spectra have been: (1) wavelength calibrated; (2) shifted to lie in a zero velocity frame (see §6.2.5); and (3) smoothed using a bin size of 7 pixels.

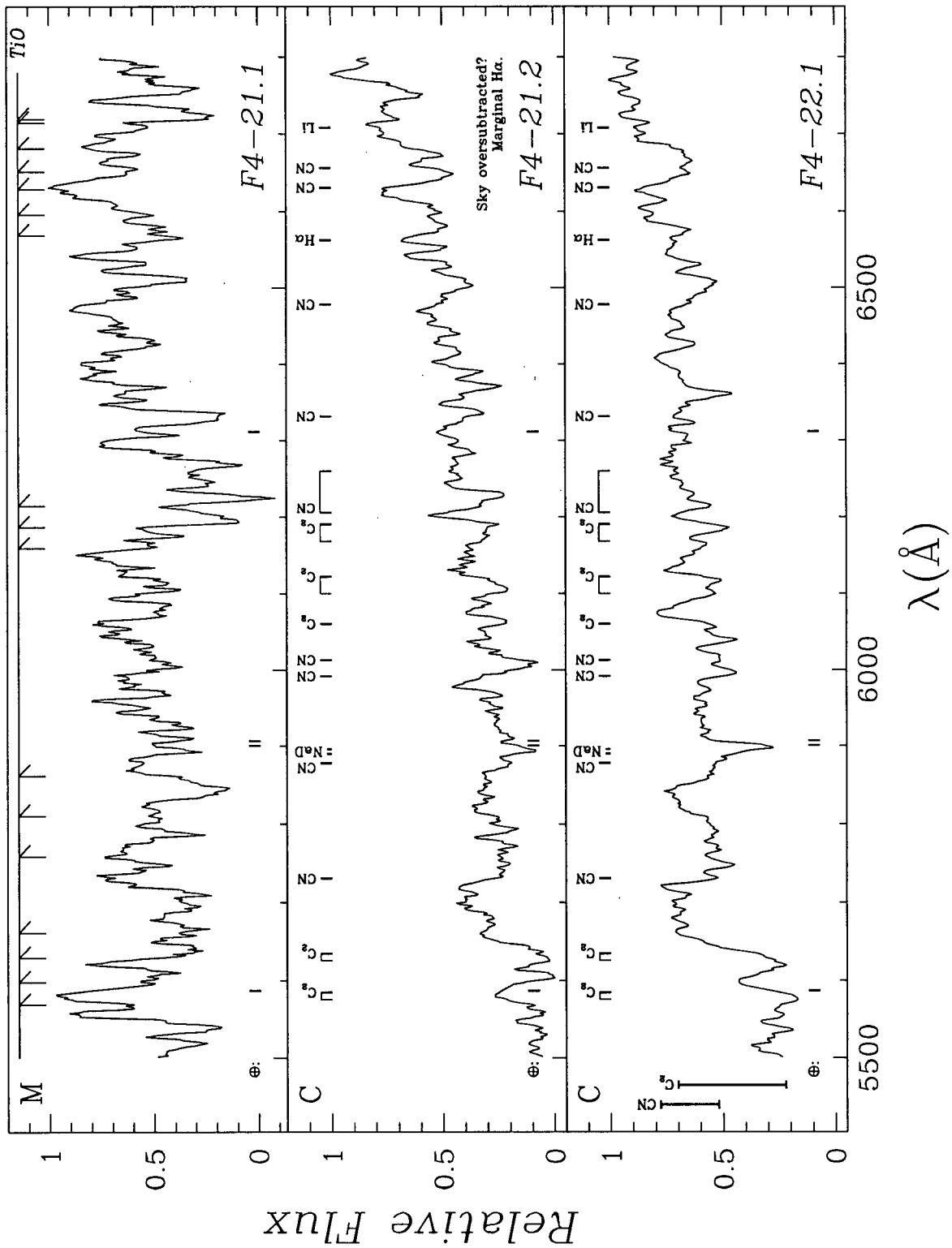

Figure A.1 (continued): Spectra of M31 stars. The above spectra have been: (1) wavelength calibrated; (2) shifted to lie in a zero velocity frame (see §6.2.5); and (3) smoothed using a bin size of 7 pixels.

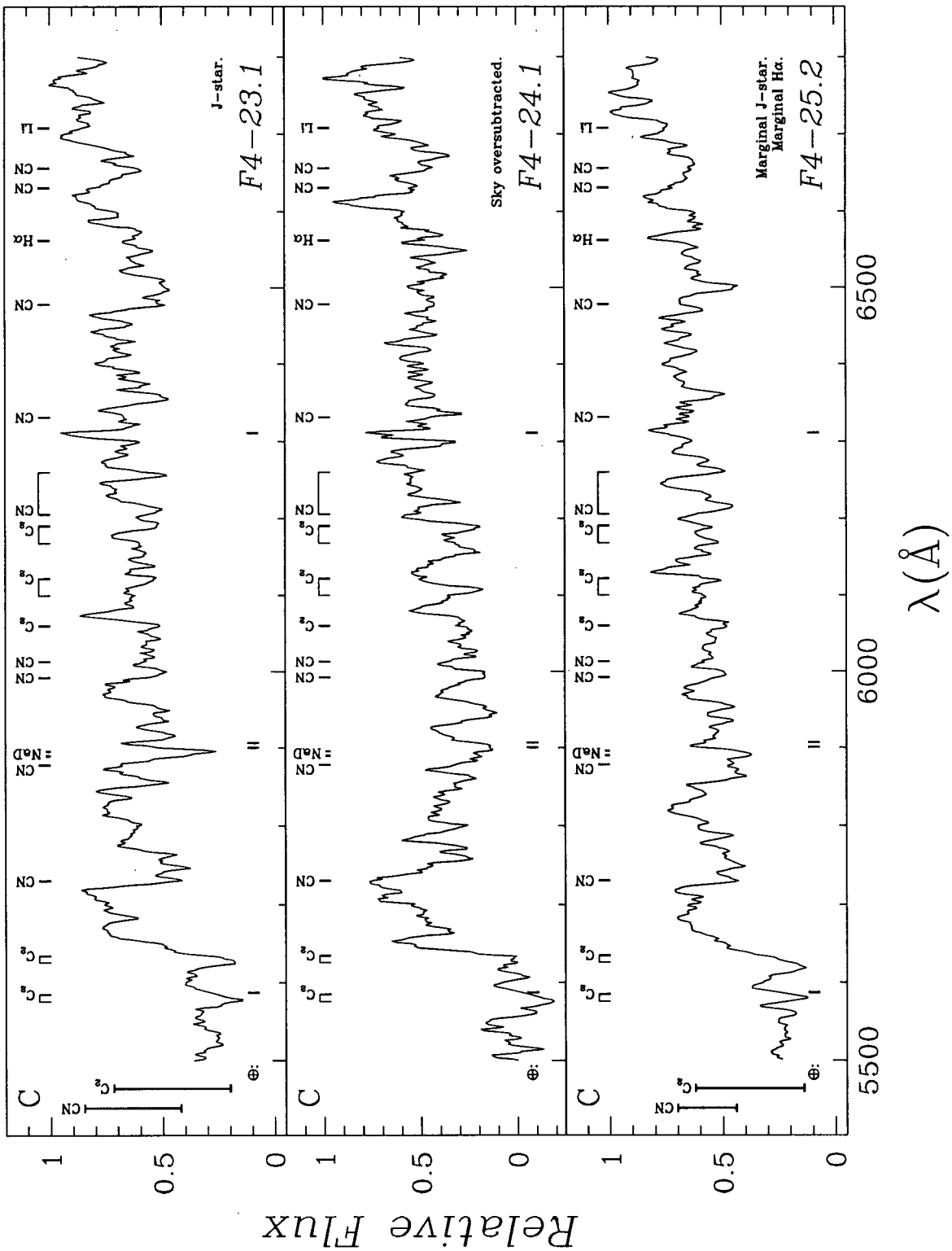

Figure A.1 (continued): Spectra of M31 stars. The above spectra have been: (1) wavelength calibrated; (2) shifted to lie in a zero velocity frame (see §6.2.5); and (3) smoothed using a bin size of 7 pixels.

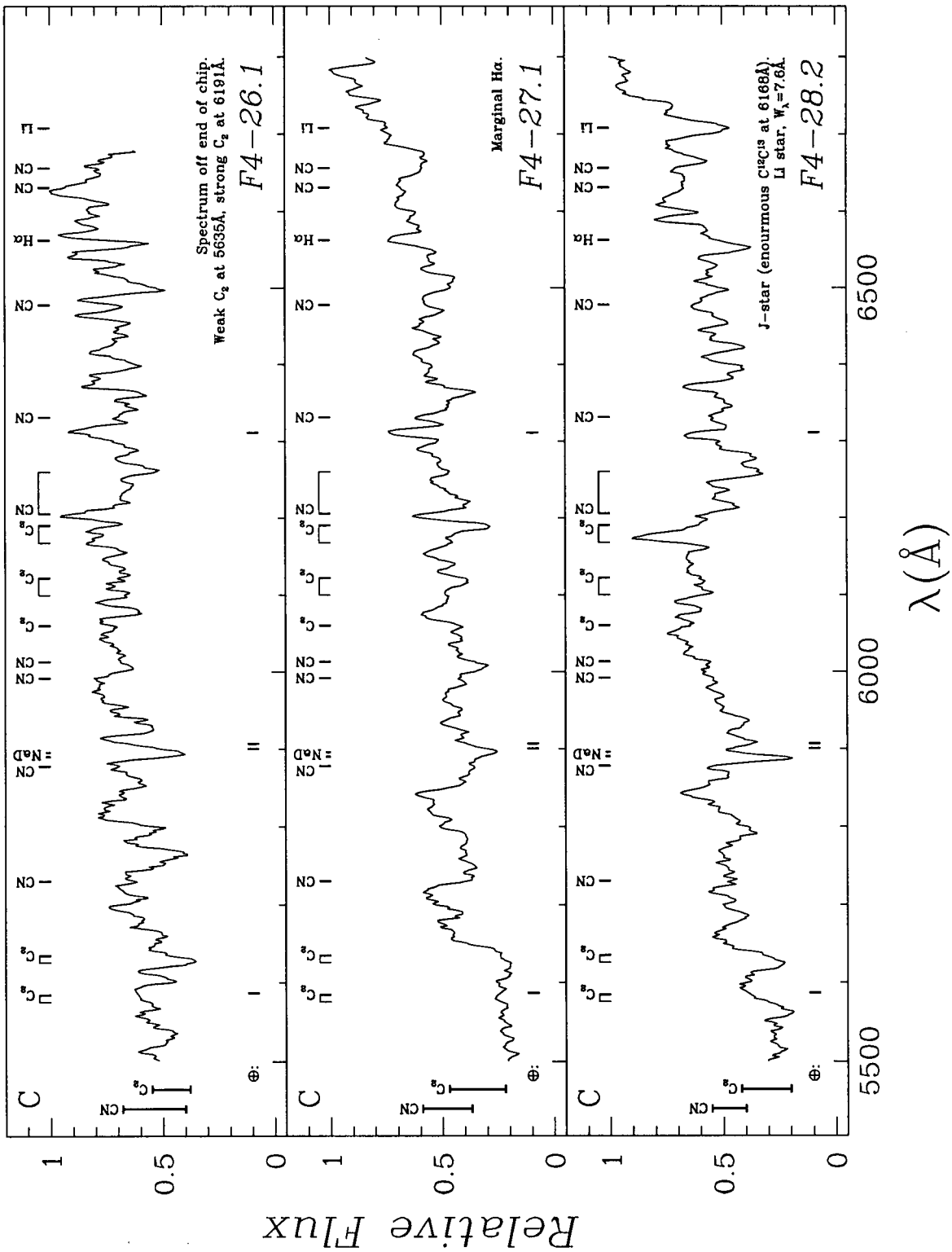

Figure A.1 (continued): Spectra of M31 stars. The above spectra have been: (1) wavelength calibrated; (2) shifted to lie in a zero velocity frame (see §6.2.5); and (3) smoothed using a bin size of 7 pixels.

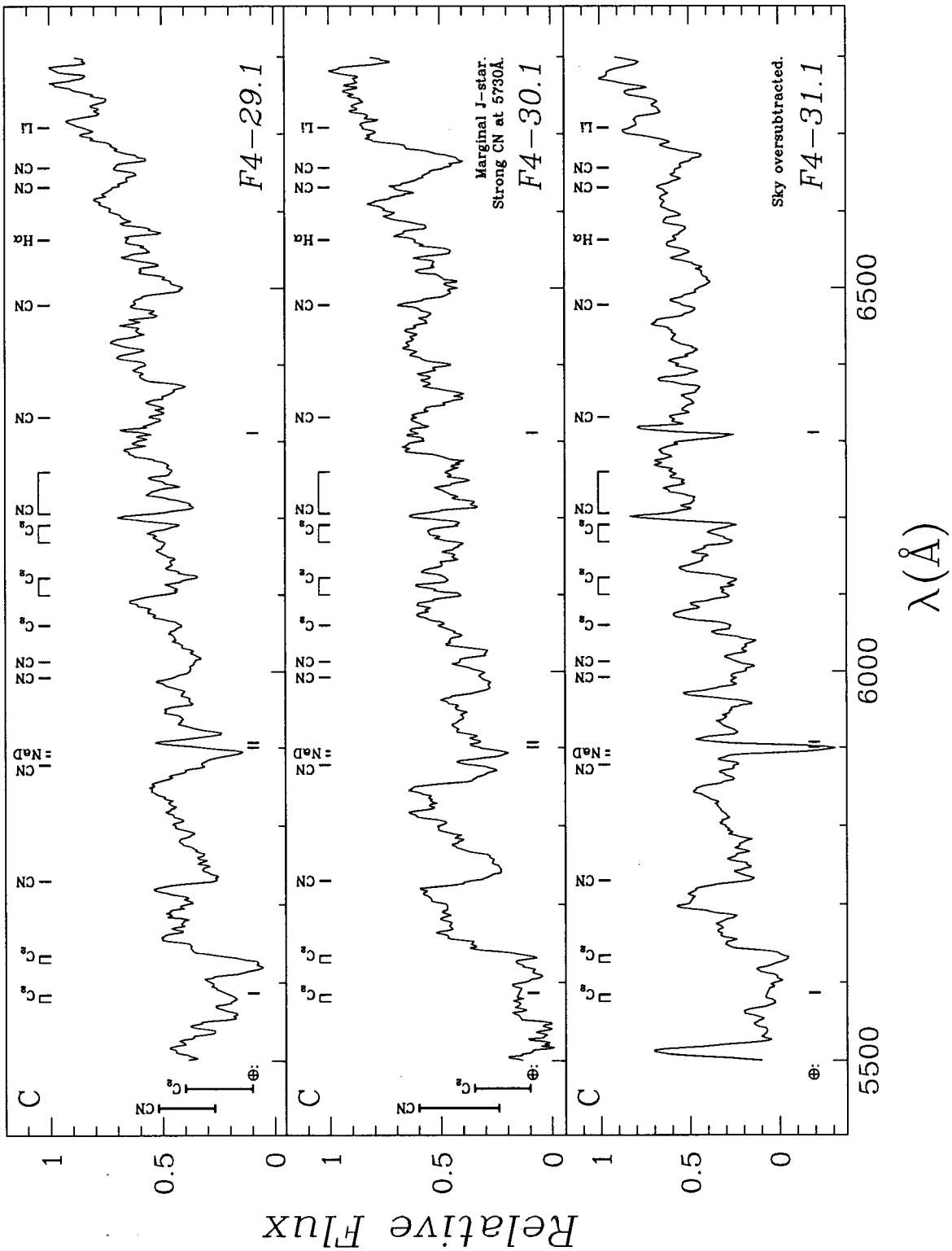

Figure A.1 (continued): Spectra of M31 stars. The above spectra have been: (1) wavelength calibrated; (2) shifted to lie in a zero velocity frame (see §6.2.5); and (3) smoothed using a bin size of 7 pixels.

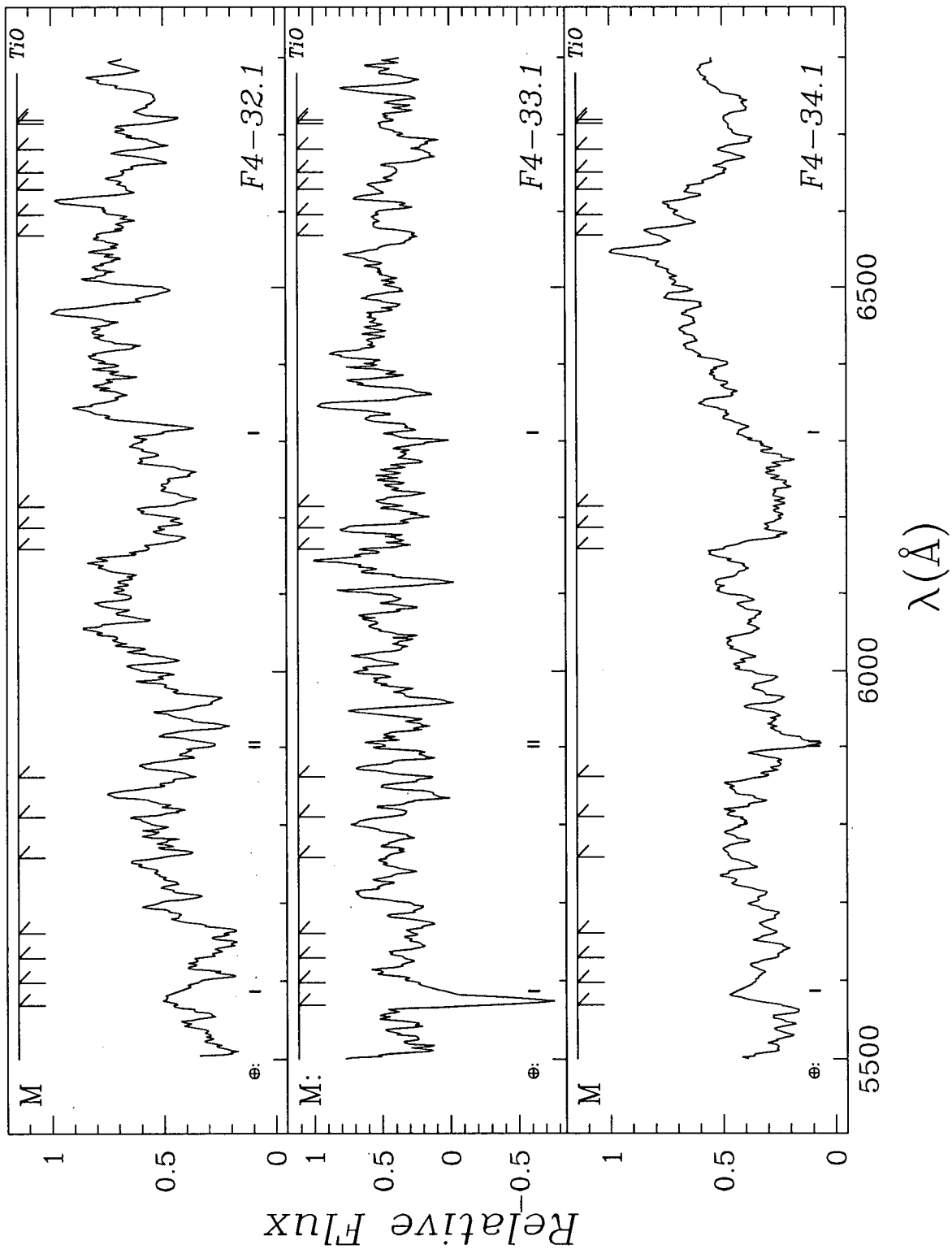

Figure A.1 (continued): Spectra of M31 stars. The above spectra have been: (1) wavelength calibrated; (2) shifted to lie in a zero velocity frame (see §6.2.5); and (3) smoothed using a bin size of 7 pixels.

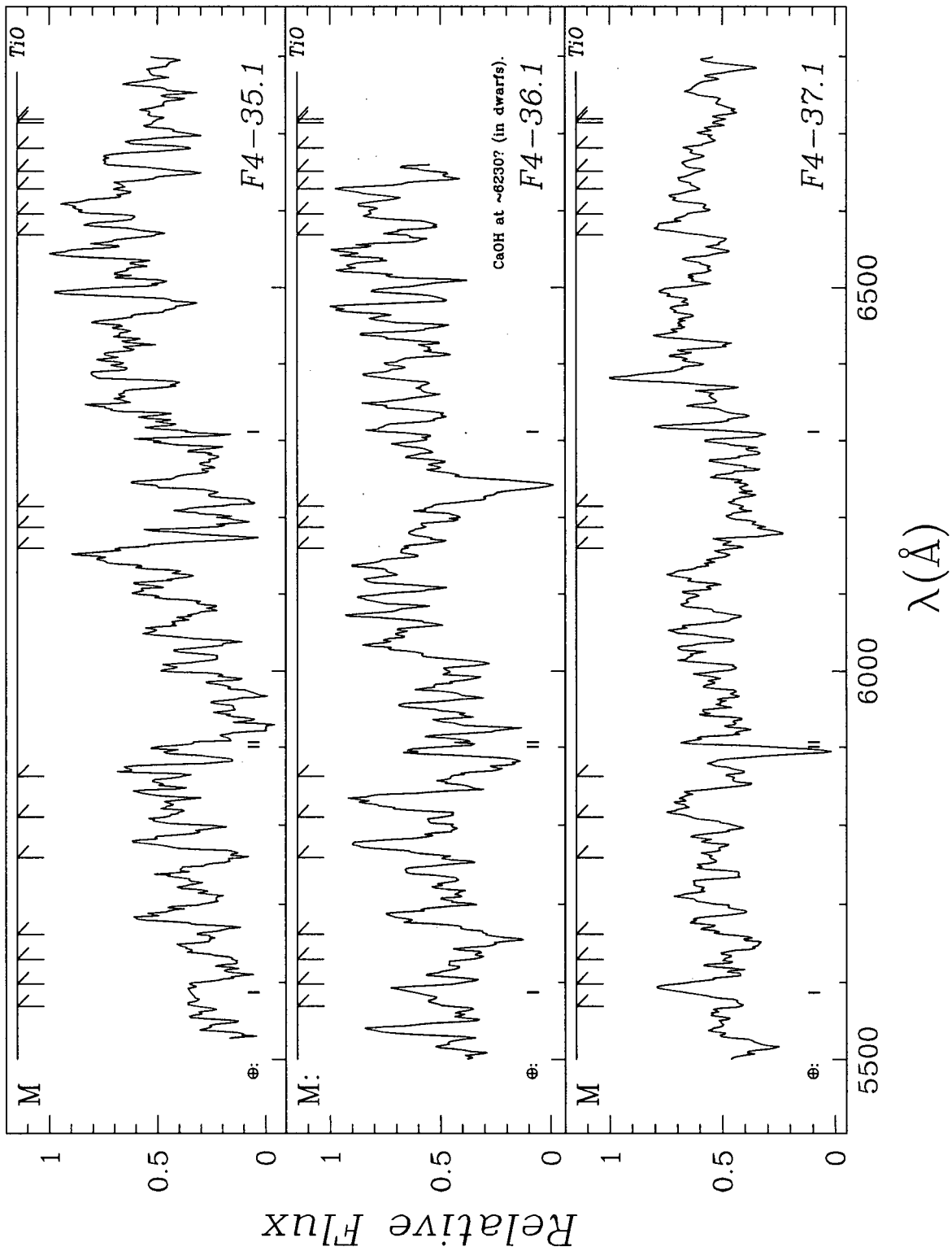

Figure A.1 (continued): Spectra of M31 stars. The above spectra have been: (1) wavelength calibrated; (2) shifted to lie in a zero velocity frame (see §6.2.5); and (3) smoothed using a bin size of 7 pixels.

Appendix B

GALACTIC C-STAR SPECTRA

In this appendix I present spectra of Galactic C-stars obtained at the DAO. As mentioned in §§6.3.4 and 6.3.5, the spectra are wavelength calibrated and have been divided by their maximum flux level. No wavelength shift has been applied to these spectra. Included on the spectra are two "error bars" which show my estimates of where the red and blue sides of the CN (5730Å) and C_2 (5635Å) bandheads lie. Included on each spectrum is the star's name along with its classification on the KM system; above this I give the star's classification on the Okayama system. Finally, I plot the positions of some bandheads and atomic features expected to be seen in C-stars.

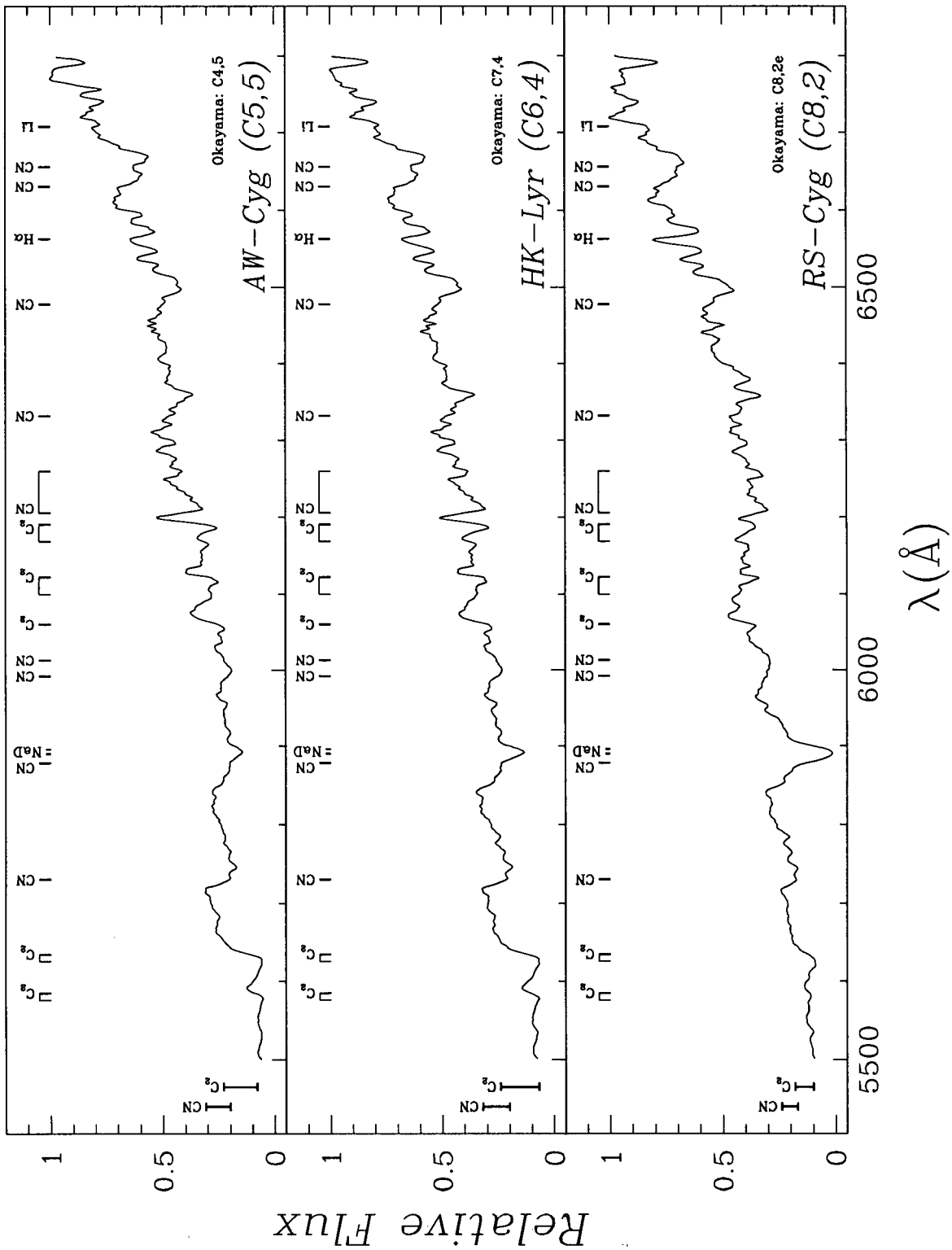

Figure B.1: Spectra of Galactic C-stars obtained at the DAO. The spectra have been wavelength calibrated and smoothed using a bin size of 7 pixels.

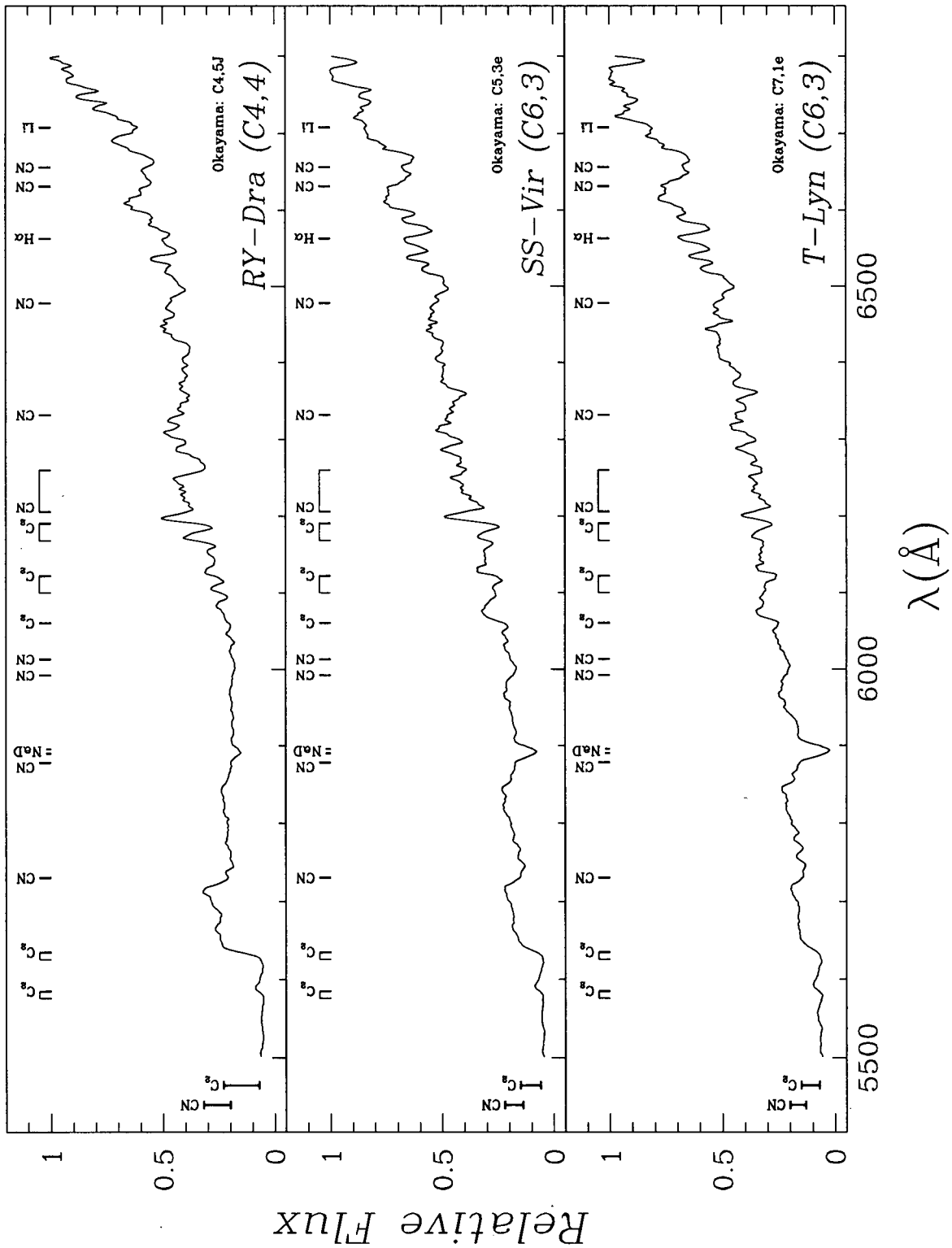

Figure B.1 (continued): Spectra of Galactic C-stars obtained at the DAO. The spectra have been wavelength calibrated and smoothed using a bin size of 7 pixels.

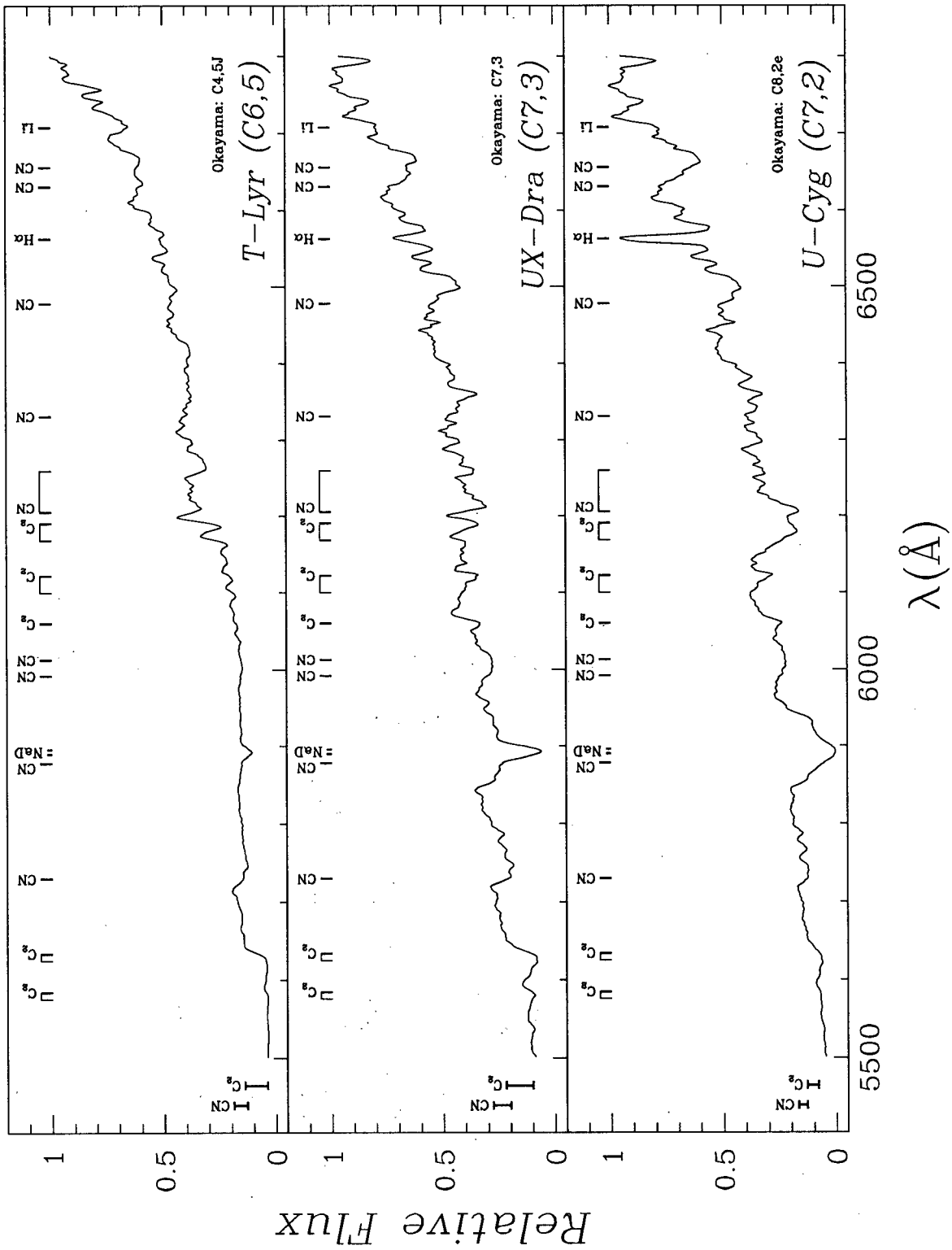

Figure B.1 (continued): Spectra of Galactic C-stars obtained at the DAO. The spectra have been wavelength calibrated and smoothed using a bin size of 7 pixels.

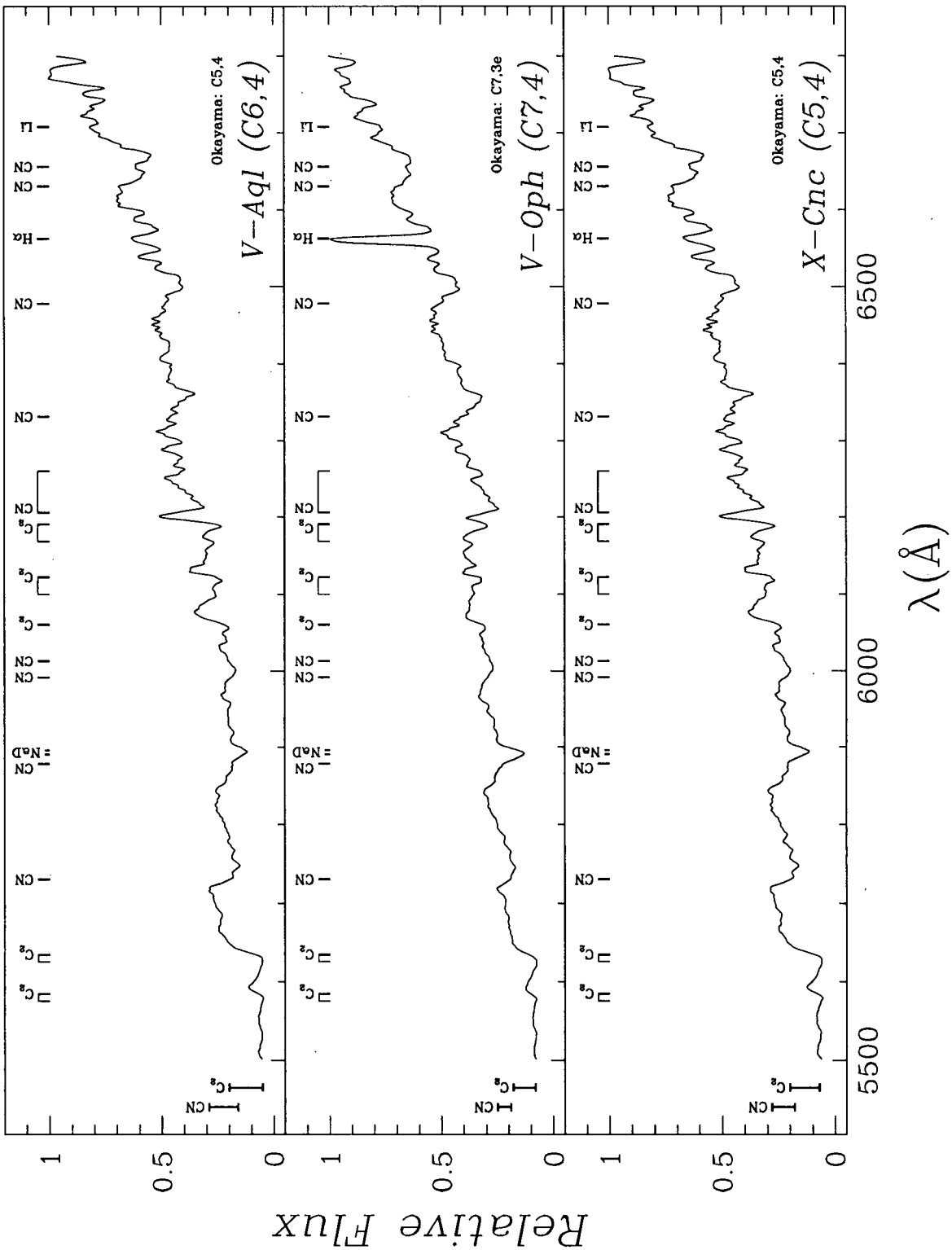

Figure B.1 (continued): Spectra of Galactic C-stars obtained at the DAO. The spectra have been wavelength calibrated and smoothed using a bin size of 7 pixels.

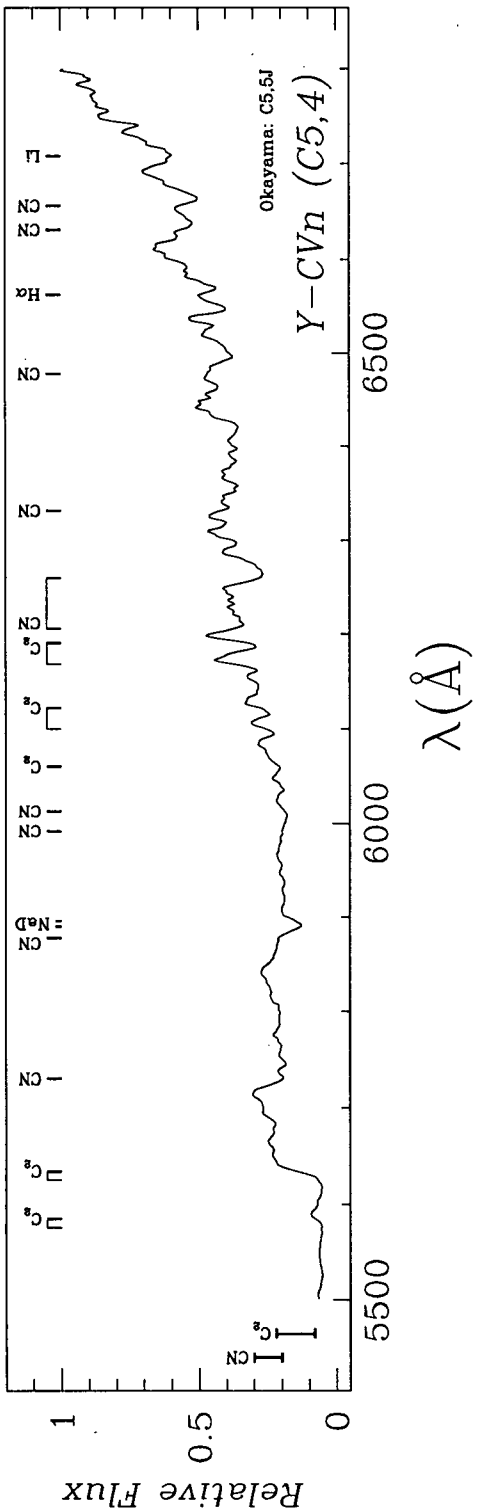

Figure B.1 (continued): Spectra of Galactic C-stars obtained at the DAO. The spectra have been wavelength calibrated and smoothed using a bin size of 7 pixels.